

Microcircuit remodeling processes underlying learning in the adult

Inauguraldissertation

zur

Erlangung der Würde eines Doktors der Philosophie

vorgelegt der

Philosophisch-Naturwissenschaftlichen Fakultät

der Universität Basel

von

Flavio Donato

von Italia

Basel, 2013

Originaldokument gespeichert auf dem Dokumentenserver der Universität Basel
edoc.unibas.ch



Dieses Werk ist unter dem Vertrag „Creative Commons Namensnennung-Keine kommerzielle Nutzung-Keine Bearbeitung 2.5 Schweiz“ lizenziert. Die vollständige Lizenz kann unter **creativecommons.org/licences/by-nc-nd/2.5/ch** eingesehen werden.

Genehmigt von der Philosophisch-Naturwissenschaftlichen Fakultät auf Antrag von

Prof. Dr. Pico Caroni

(Dissertationsleiter)

Prof. Dr. Silvia Arber

(Korreferent)

Basel, den 11. 12. 2012

Prof. Dr. Jörg Schibler

(Dekan)

Index:

1. Summary;

2. Preface and overview of the thesis;

3. Introduction;

3.1 Structure and function of cortical microcircuits;

3.1.1 An interplay between excitation and inhibition;

3.1.2 A plethora of inhibitory neurons subpopulations;

3.1.3 Dendritic and perisomatic inhibition;

3.1.4 Interneurons regulation of critical periods;

3.2 The Hippocampal formation;

3.2.1 Hippocampal Function;

3.2.2 Hippocampal connectivity;

3.2.3 The mossy fiber projection;

3.2.4 Developmental origin;

3.2.5 Neuronal diversity;

3.3 Structural plasticity upon learning: regulations and functions;

3.3.1 Molecular mechanisms of synapse remodeling;

3.3.2 Synapse turnover specificity *in vivo*;

3.3.3 Distribution of structural plasticity;

3.3.4 Plasticity regulation;

3.3.5 From structural plasticity to memories;

3.3.6 Synapse remodeling and mental health;

3.3.7 Outlook: network structure-function;

3.3.8 Bibliography of the section.

4. Results

4.1 A microcircuit module to regulate plasticity and learning in the adult;

4.1.1 Summary;

4.1.2 Introduction;

4.1.3 Results;

4.1.4 Discussion;

4.1.5 Supplementary material;

4.2 Goal-oriented searching mediated by ventral hippocampus early in trial-and-error learning;

4.2.1 Summary

4.2.2 Introduction;

- 4.2.3 Results;
- 4.2.4 Discussion;
- 4.2.5 Supplementary materials;
- 4.2.6 Materials and methods;
- 4.2.7 Bibliography;

4.3 Temporally matched subpopulations of selectively interconnected principal neurons in the Hippocampus;

- 4.3.1 Summary;
- 4.3.2 Introduction;
- 4.3.3 Results;
- 4.3.4 Discussion;
- 4.3.5 Supplementary materials;
- 4.3.6 Materials and methods;
- 4.3.7 Bibliography.

4.4 A critical period for cognitive enhancement during hippocampal development;

- 4.4.1 Summary;
- 4.4.2 Introduction;
- 4.4.3 Results;
- 4.4.4 Discussion and future directions;
- 4.4.5 Supplementary material;

4.5 A network mechanism underlying age-related cognitive decline in the hippocampus;

- 4.5.1 Summary;

4.5.2 Introduction;

4.5.3 Results;

4.5.4 Discussion and future directions;

4.5.5 Supplementary material;

5. General Discussion and Outlook;

6. Material and methods;

7. Abbreviations;

8. Bibliography;

9. Acknowledgements.

1. Summary

One of the most intriguing discoveries in neuroscience of the past decades has been showing that experience is able to induce structural modifications in cortical microcircuit that might underlie the formation of memories upon learning (for a review, see Caroni, Donato and Muller 2012). Hence, learning induces phases of synapse formation and elimination that are strictly regulated by a variety of mechanisms, which impact on cortical microcircuits affecting both excitatory and inhibitory neurons. Nevertheless, the extent to which specific configurations might be implemented to support specific phases of learning, as well as the impact of experience-induced structural modifications on further learning, is still largely unknown.

Here, I explore how the remodeling of identified microcircuits in the mouse hippocampus and neocortex supports learning in the adult.

In the first part, I identify a microcircuit module engaging VIP and Parvalbumin (PV) positive interneurons to regulate the state of the PV+ network upon experience. This defines states of enhanced or reduced structural plasticity and learning based on the distribution of PV intensity in the network.

In the second part, I demonstrate how specific hippocampal subdivisions are exploited to learn subtasks of trial-and-errors forms of learning via the deployment of increasingly precise searching strategies, and sequential recruitment of ventral, intermediate, and dorsal hippocampus.

In the third part, I highlight the existence of genetically matched subpopulations of principal cells in the hippocampus, which achieve selective connectivity across hippocampal subdivisions via matched windows of neurogenesis and synaptogenesis during development.

In the fourth part, I investigate the maturation of microcircuits mediating feedforward inhibition in the hippocampus, and highlight windows during development for the establishment of the proper baseline configuration in the adult. Moreover, I identify a critical window for cognitive enhancement during hippocampal development.

In the fifth part, I study how ageing affects the PV network in hippocampal CA3, providing evidence for which age related neuronal loss correlates to reduced incidental learning performances in old mice. Therefore, by manipulating the PV network early during life, I provide strategies to modulate cognitive decline.

2. Preface and Overview of the thesis

Cortical microcircuits represent the substrate on which our brain exerts its complex functions, ranging from exhibiting conditional reflexes to specific stimuli (for example, the startle reflex to an unexpected tone), to performing abstract reasoning about ethics and morality or addressing complex scientific questions about neuronal computation and function. Moreover, they constitute the system that, by performing association between sensory perceived stimuli and physical or abstract concepts, allows learning about the environment and producing memories of these associations. And yet, cortical microcircuits are not only active when contingencies require their abilities, but they are likely in a state of perpetual activation, even in the absence of environmental or body-derived stimuli. When these stimuli come into play, they likely create perturbations from these internally generated programs, perturbations that are absolutely essential to adapt the brain's internal operations to perform its computation (Buzsaki, 2006). Hence, it would be reasonable to hypothesize that the baseline state of a brain microcircuit might be able to influence the efficiency to which its computation is executed upon external recruitment: in other words, we could imagine the existence of particular microcircuit configurations in which processing of newly perceived stimuli is enhanced, as opposed to configurations that instead support the processing of learned associations but impinge a higher filter to the learning of new stimuli. Moreover, a broad body of scientific literature has clearly demonstrated that experience is able to act on cortical microcircuits to change their properties at a functional or structural level, thereby allowing the brain to exert the aforementioned functions of learning and memory. In particular, experience supports a rewiring of cortical microcircuits which is required for learning, and the extent to which this rewiring takes place is a function of the complexity of the task as well as the particular period during life when learning takes place (for review, see Hensch T, 2005; Holtmaat and Svoboda, 2009; Caroni et al., 2012).

If we could know all the connections and wiring patterns of the brain of an individual, could we understand how he/she thinks, feels, and gives rise to behavior? The answer is debatable, although many labs are now involved in such a daunting task as mapping all the connections in brains ranging from simple to more complex organisms. Nevertheless, we can turn the question around and provide an answer to which many neuroscientists will agree, that is that we can never understand brain computation without elucidating the basic principles of its connectivity, and how this is shaped (again, functionally or structurally) by experience. Building such knowledge is not only necessary, but perhaps mandatory to understand how perception gives rise, through learning, to the expression of a memory, which most likely predicts the behavior that a person is going to enact in the future. Moreover, it requires a combined effort at a triple level: first, we need to uncover the rules governing the basic wiring of cortical microcircuits; second, we need to uncover the rules

governing interactions among neurons and neuronal systems; third, we need to uncover the rules by which specific behaviors impinge on defined microcircuit modules, or specific systems in the brain.

The latter three levels of investigation are conceptually at the basis of my work of thesis. I explored each of them individually or in combination by focusing on a model organism (the mouse) that is simple enough to provide a starting point for study, yet evolutionary complex to allow me to aim at generalizing my findings. At first I focused my attention to microcircuits in the hippocampus due to the fact that its connectivity principles and cell types are fairly conserved when looking at higher order areas in the brain (i.e., neocortex) and yet organized in such a way that allowed me to distinguish and study separately how specific inputs behave upon experience at a structural level; in addition, its involvement in specific learning paradigms and behavior is well established since many years (although with some caveats, see the Introduction), which makes it an attractive model to study how learning underlies plasticity, and vice versa.

In the first part of my thesis, I have investigated the possible existence of microcircuit configurations that underlie states of enhanced or reduced plasticity and learning (Flavio Donato and Pico Caroni, in preparation). Following the observation that environmental enrichment and contextual fear conditioning induce opposite modulations of structural plasticity in the CA3 area of the hippocampus (fast and lower synaptic turnover, respectively), and opposite performance in a further hippocampal dependent task (Novel object recognition: enhanced performances for enrichment, reduced for conditioning), I define “Plastic” or “Crystallized” states relying on prevalence of Low or High expressing parvalbumin interneurons, respectively, which causally modulate plasticity and learning. After characterizing structural and functional properties of these two categories of interneurons, I elucidated the mechanisms that impinge on single interneurons to modulate the composition of the PV network, which relies on enhancement of the excitatory or inhibitory drive onto these interneurons by means of increase density of feedforward inhibitory or disinhibitory synapses as results of experience. Then, I investigated if incremental forms of learning exploit different configurations to support defined aspect of the learning process. The morris water maze (a hippocampal dependent incremental learning paradigm) implements a Plastic configuration early during learning, to shift to a Crystallized state upon learning completion. Although the overall mechanisms mediating state transitions was coincident with the one elucidated before, I described a higher degree of input specificity in the structural plasticity underlying configurations, describing a dedicated

microcircuit module based on the enhancement of disinhibition provided by VIP+ interneurons onto PV+ interneurons early during learning, followed by enhancement of FFI mediated by the large mossy fiber terminals in CA3 upon learning completion. Lastly, I confirmed that the transition through a VIP-mediated plastic state was necessary for learning, and that the same microcircuit module described in the hippocampus could be responsible of other forms of incremental learning in neocortex, with particular focus on Primary Motor cortex upon Rotarod learning.

In the second part of my thesis, I have focused my attention to understanding how the same basic microcircuit might be used to learn specific aspects of a learning task in a manner that is dependent from the neuronal system where the microcircuit is located (Sarah Ruediger*, Dominique Spirig*, Flavio Donato* and Pico Caroni, *Nature Neuroscience* 2012). Therefore, I exploited how different regions of the hippocampus along the dorsoventral axis might be recruited to learn different aspects of the morris water maze task. Although each region (defined as Dorsal, Intermediate and Ventral based on gene expression, spatial distribution, extrinsic connectivity, and functional recruitment: Bannerman et al., 2002; Czerniawski et al., 2009; Fanselow, 2000; Lee and Kesner, 2004; Moser et al., 1993; Moser et al., 1995; Pothuizen et al., 2004; Bannerman et al., 2003; Kjelstrup et al., 2002) would host the same organizational principles (Anderson et al., 1971), and display increase in FFI upon learning completion, we showed by means of structural, functional and lesion experiments that their recruitment upon learning followed a marked ventral-to-dorsal directionality, with ventral hippocampus being recruited early during learning, followed by intermediate and dorsal at later time points. Moreover, recruitment of each region would underlie different aspect of the task, with the ventral hippocampus being tuned to both spatial and reward-based signals and thus mediating task-specific goal-oriented searching, and dorsal being instead tuned specifically to spatial computation. In addition, although performance and strategy deployment progressed continuously at the population level, single mice showed discrete learning phases, each characterized by particular searching habits and implemented by each specific region, for which targeted lesions of each region would disrupt defined habits. Therefore, we could conclude that trial-and-error navigational learning processes in naïve mice involve a stereotype sequence of increasingly precise subtask learned through distinct hippocampal subdivision.

In the third part of my thesis, I shifted the focus to structural aspects of microcircuit investigation by exploiting to what extent excitatory microcircuits in the hippocampus are equivalent in terms of cell diversity and connectivity, or rather if genetically and

developmentally identified principal neurons subpopulations might connect selectively across hippocampal subdivision (Yuichi Deguchi*, Flavio Donato*, Ivan Galimberti*, Erik Cabuy and Pico Caroni, Nature Neuroscience 2011). Therefore, I took advantage of sparse reporters mice lines created in the lab (Thy1.2 driven, Lsi1 and 2 mice lines) which express membrane-targeted GFP in a subset of neurons of each subdivision in the hippocampus. Previous works in the lab had already shown that granule cells expressing membrane-bound GFP in these two lines behaved differently in terms of intrinsic plasticity of their mossy fiber terminals, hosting one (Lsi1 Mouse line) or more (Lsi2 mouse line) “terminal arborizations” (TAs), which in the Lsi1 would follow a topographic arrangement along the CA3 projection based on cell body position and developmental instructive signals (Ivan Galimberti*, Ewa Bednarek*, Flavio Donato and Pico Caroni, Neuron 2010). Thus, we showed that cells highlighted by GFP expression in the same mouse line could indeed be considered as distinguishable subpopulations, since they would exhibit a unique and matched pattern of gene expression profiles across hippocampal subdivisions, shared distinct neurogenesis and synaptogenesis time windows, and selective connectivity at dentate gyrus-to-CA3 and CA3-to-CA1 synapses. The mechanisms underlying selective connectivity would effectively rely on the matched time of synaptogenesis between pre- and post-synaptic partners belonging to the same subpopulations, since in heterochronic co-cultures we were able to force cross-subpopulation connectivity by playing with the explants age. Therefore, we conclude that the hippocampus contains parallel connectivity channels assembled from distinct principal neuron subpopulations through matched schedules of synaptogenesis.

The specific interplay between excitation and inhibition which gives rise in the adult to complex phenomena like selective tuning of cells to preferred stimuli (see introduction), or creates states of enhanced or reduced plasticity and learning upon experience (see part1 of results), is a distinguishable feature of microcircuits even during development, and regulates the occurrence of “critical periods” in sensory cortices. Therefore, in the fourth part of my thesis I have studied how the feed-forward inhibitory component would be integrated upon development in hippocampal microcircuits, by studying the maturation of parvalbumin interneurons and their connectivity in the CA3 area of the hippocampus (Flavio Donato and Pico Caroni, unpublished results). Thereby, I could demonstrate that the maturation of FFI connectivity from mossy fiber terminals upon PV interneurons constituted the driving force for the expression of the protein Parvalbumin in CA3, which is usually taken as an indicator of interneuron maturation in the neocortex (Sugiyama et al., 2008). Moreover, Lsi1 and 2 subpopulations participated differently to the process, with the first exhibiting a counterhomeostatic response to MFT release modulation (thereby trying to compensate for

the delay in PV maturation), and the latter responding homeostatically to it. Interestingly, developmental intervention that modulated PV maturation selectively in an Lsi1 or Lsi2 responsive windows, elicited long-lasting consequences upon baseline CA3 microcircuits that extend further into adulthood, with features associated to the “Plastic” or “Crystallized” state respectively (prevalence of High or Low PV interneurons, modulation of active zone turnover at mossy fiber terminals, enhanced or reduced performances in the novel object recognition task, modulation of learning in the morris water maze task). We hypothesize that the integration of Parvalbumin interneurons in hippocampal microcircuits defines critical window in which basic properties of these interneurons are established. Hence, the correct subpopulation-based maturation of the PV network produces the proper balanced configuration that will constitute the baseline state of cortical microcircuit in the adult; nevertheless, perturbations of this process might set the system in an incorrect configuration which is usually achieved upon experience. Moreover, we provide developmental temporal windows of pharmacological treatments that produce cognitive enhancement in the adult.

Last but not least, in the fifth part of my thesis, I focused my attention on how ageing impinge on cortical microcircuits to produce declining performances in incidental learning tasks underlying episodic memory (Flavio Donato and Pico Caroni, unpublished results). Therefore, I have followed the evolution of the PV network in CA3 upon physiological ageing, and analyzed if changes in the network might underlie the decline in incidental learning performances occurring with age, since it causally regulates performance in the Plastic or Crystallized state (see Part1). In CA3, ageing was correlated with a decrease in the absolute number of PV expressing interneurons, which produced a marked shift toward the Low PV component of the network. Moreover, incidental learning in single mice correlated to the extent of survival of PV interneurons, which would predict with high probability the behavioral performance of the mouse. High PV interneurons showed a higher vulnerability toward age related neuronal loss, producing the highest decrease in old mice: therefore, I tried to modulate this process by applying strategies that reduce or increase the PV context in a large cohort of interneurons via remote experience or developmental manipulation. Both strategies resulted effective in preserving cognitive performances to levels of younger individuals, by reducing the extent of neuronal loss among PV interneurons. Therefore, we propose new strategies to mitigate or even abolish the cognitive decline in episodic memory that is usually occurring with ageing by promoting survival of PV+ interneurons in CA3.

3. Introduction

3.1 Structure and function of cortical microcircuits

3.1.1 An interplay between excitation and inhibition

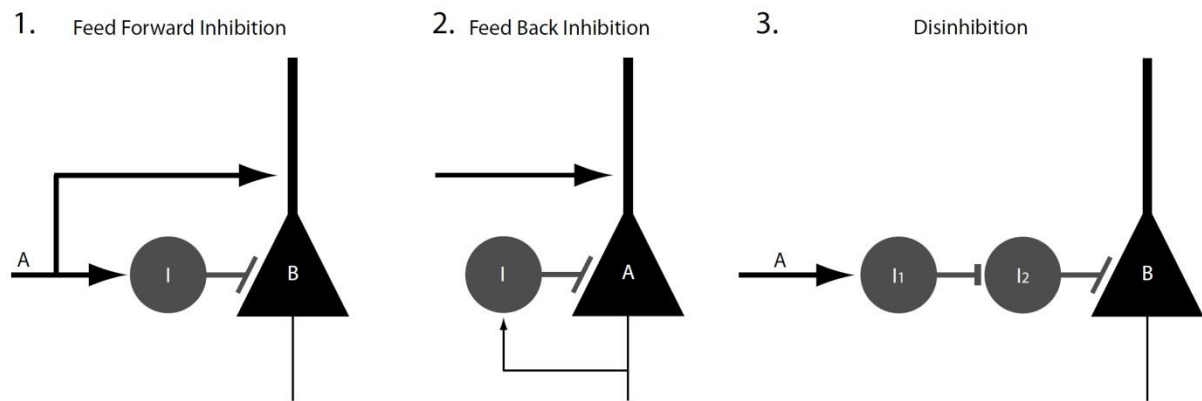
Synaptic processing reflects the interplay between cortical excitation and cortical inhibition: even the most simple sensory stimuli, like deflecting a whisker (Okun and Lampl, 2008; Swadlow, 2003; Wilent and Contreras, 2005), a brief tone (Tan et al., 2004; Wehr and Zador, 2003; Wu et al., 2008), an odor (Poo and Isaacson, 2009), or an oriented bar in the visual field (Anderson et al., 2000; Monier et al., 2003) lead to the concomitant occurrence of excitation and inhibition in sensory cortices (for review, see Isaacson and Scanziani, 2011). Moreover, this co-occurrence of excitation and inhibition is not limited to sensory experience, but underlies spontaneous activity, spontaneous oscillations or up and down states during cortical processing (Isaacson and Scanziani, 2011).

Therefore, cortical microcircuits have to be structured in a way to make this interplay possible, without ending up with an excess of excitation or inhibition, which may both underlie pathological states. Inhibition in the cortex is exerted by neurons that release the transmitter GABA, and comprise roughly around 20% of the cortical neuronal population (Meinecke and Peters, 1987). In contrast to their excitatory counterpart, they usually do not form long range connections (although important exceptions have been pointed out recently, see Melyer et al., 2012), and for this reason they have collectively acquired the name of interneurons (Ascoli et al., 2008; Freund and Buzsaki, 1996).

The connectivity patterns by which inhibition can be incorporated in excitatory cortical microcircuits can have multiple shapes, which assume different names based on the net physiological result, and differ in the way in which excitatory and inhibitory neurons interact (Schema 1) (Kullmann 2011):

- Feed-Forward Inhibition (FFI, Schema 1, 1): the discharge from an excitatory neuron A produces the activation of a postsynaptic excitatory cell B and of an interneuron I whose synapses influence the activity of the same postsynaptic cell B. This can substantially increase the temporal precision of firing (Buzsaki 1984), as well as narrowing the window of non-zero probability of discharging (Pouille and Scanziani, 2001);

- Feed-Back Inhibition (FBI, Schema 1, 2): the discharge from an excitatory neuron A produces the activation of an interneuron I whose synapses influence the same presynaptic neuron A. An extreme case of this wiring diagram is represented by lateral inhibition, where the activation of an interneuron I from a principal cell A suppresses the activity of surrounding principal cells (N, N+1, ...);
- Disinhibition (Dis, Schema 1, 3): this peculiar wiring diagram takes place when a principal cell A activates an interneuron I1, which in turn suppress the activity in a second interneuron I2 thereby limiting its inhibitory influence on a second principal cell B which is post-synaptic to I2.



Schema 1: Connectivity patterns mediating inhibition in cortical microcircuits.

The schematics shows the wiring diagrams by which inhibitory neurons can exert inhibition in cortical microcircuits. Note that while the first two arrangements (feedforward inhibition, feedback inhibition and lateral suppression) result in a net increase in inhibition on pyramidal cells, the third, by means of inhibition of inhibitory neurons, actually increase excitability of target pyramidal cells.

Through the recruitment of FFI and FBI, inhibition in cortical microcircuit is somehow proportional to the incoming excitation: it has been observed, for example, that a sensory stimulus lead to concomitant changes in the strength of both (Anderson et al., 2000; Poo and Isaacson, 2009; Wehr and Zador, 2003; Wilent and Contreras, 2004; Zhang et al., 2003). Furthermore, manipulation of cortical microcircuit that decouple E and I shift cortical activity toward a hyperexcitable (epileptiform) or silent (comatose) state (Dudek and Sutula, 2007): thereby, the proper “balance” (although not literal, Isaacson and Scanziani, 2011) between these two forces seems to be necessary for keeping a proper physiological function of cortical microcircuits, that otherwise deviate toward pathological states (Turrigiano, 2011).

The physiological functions of inhibition seem to be vast: from gain and dynamic range control (Pouille et al., 2009; Shadlen and Newsome, 1998), to sharpening of tuning (Katzner et al., 2011, Wu et al., 2008, Poo and Isaacson, 2009, Liu et al., 2011), and pacing of cortical oscillations especially in the “gamma” frequency range (Atallah and Scanziani, 2009; Cardin et al., 2009; Hasenstaub et al., 2005; Sohal et al., 2009; Traub et al., 1996, 1997; Wang and Buzsaki, 1996).

3.1.2 A plethora of inhibitory neurons subpopulations

With such a complex repertoire of functions performed by cortical microcircuits, it is perhaps not surprising that there is a wide variety of subpopulations of interneurons defined by physiological and structural features (Ascoli et al., 2008; Somogyi and Klausberger, 2008). Here, I'll try to describe three criteria to define diversity among interneurons in relation to their function, considering that often one class can span transversally multiple criteria, and that even interneurons that fulfill the same requisites (e.g., targeting the perisomatic region of excitatory cells) can have different roles as a function of their intrinsic properties (e.g., Parvalbumin and CCK expressing Basket cells). Moreover, I will focus on hippocampal area CA1, since it is the most studied in terms of interneuron variety

1. Expression of Markers.

Cortical interneurons can be divided in classes according to the expression of a series of marker that belong to different categories. For example, they can be classified according to the expression of Calcium binding proteins, like Parvalbumin (PV), Calretinin (CR), or Calbindin (CB) (Kosaka et al., 1987; Katsumaru et al., 1988); neuropeptides, like Cholecystokinin (CCK), Somatostatin (SOM), VIP or NPY (Danglot, Triller and Marty, 2007; Freund and Buzsaki 1996); or by the expression of specific receptors, like CB1 or 5HT3A (Fishell and Rudy, 2012). The expression of specific proteins is sometimes sufficient to confer defined physiological features to a subpopulation of interneurons: it is the case, for example, with the expression of the protein Parvalbumin and the characteristic “fast spiking” profile of basket and Chandelier cells (Contreras, 2004: although exceptions can be observed, see Freund and Katona 2007).

2. Developmental origin.

Interneurons originate largely in the subpallium, from where they migrate toward their specific locations using a combination of radial and tangential migration (Anderson et al., 1997; Pleasure et al., 2000, Marin et al., 2000). Different proliferative regions of the subpallium give rise to different classes of interneurons, which populate specific structures: the Medial Ganglionic Eminence produces exclusively PV+ and SOM+ Interneurons, with a small fraction of CR+ being produced as well (Wichterle et al., 2001); by contrast, the Caudal Ganglionic Eminence (CGE) produces largely the CR+ or VIP+ interneurons (Fishell, 2007). Other classes of neurons (NPY, CB, etc) are produced in both regions (for review, see Danglot, Triller and Marty, 2007). Fast Spiking cells seem to be produced exclusively in the MGE (Fishell, 2007).

3. Specificity of innervation.

The specialization in stratification of axonal and dendritic ramification is another distinguish feature of cortical interneurons. Dendrites can stratify in specific layers of the hippocampal formation (OLM cells, neurogliaform cells), or be largely unspecific in their ramifications (Ivy cells, bistratified cells) (for a comprehensive review, see Freund and Buzsaki 1996, Klausberger and Somogyi 2008). This organization is reflected on the input that an interneuron receives, which in the hippocampus largely coincide with the region where dendrites stratify. From an axonal point of view, interneurons can be distinguished based on the dendritic territory that they innervate: therefore, interneurons can innervate the dendrites (most of the classes of interneurons), the soma and proximal dendrites (basket cells), or the axon initial segment (chandelier cells) of principal neurons. Moreover, even among the same compartment, interneurons can show a great deal of specificity in the region targeted: for example, OLM neurons are defined in this way because they receive input exclusively in stratum Oriens (where their dendrites ramify), and extend their axonal projections selectively to the portion of the principal neurons dendrites that is located in stratum Lacunosum-Moleculare, parallel to entorhinal cortex inputs (hence their name, Oriens-Lacunosum Moleculare neurons) (Leao RN et al., 2012). Last, a small portion of interneurons specifically innervates other interneurons (Acsady et al., 1996 a and b). These neurons selectively express either VIP or Calretinin, and present different properties in term of receptors (can express 5HT3A) or specificity in the input source (polarized or multipolar in dendritic ramifications) (Acsady et al., 1996 a and b). These interneurons selectively mediate disinhibition.

An overall view on the classes of interneurons present in the CA1 area of the hippocampus is provided in Figure 1 (modified from Klausberger and Somogyi, 2008).

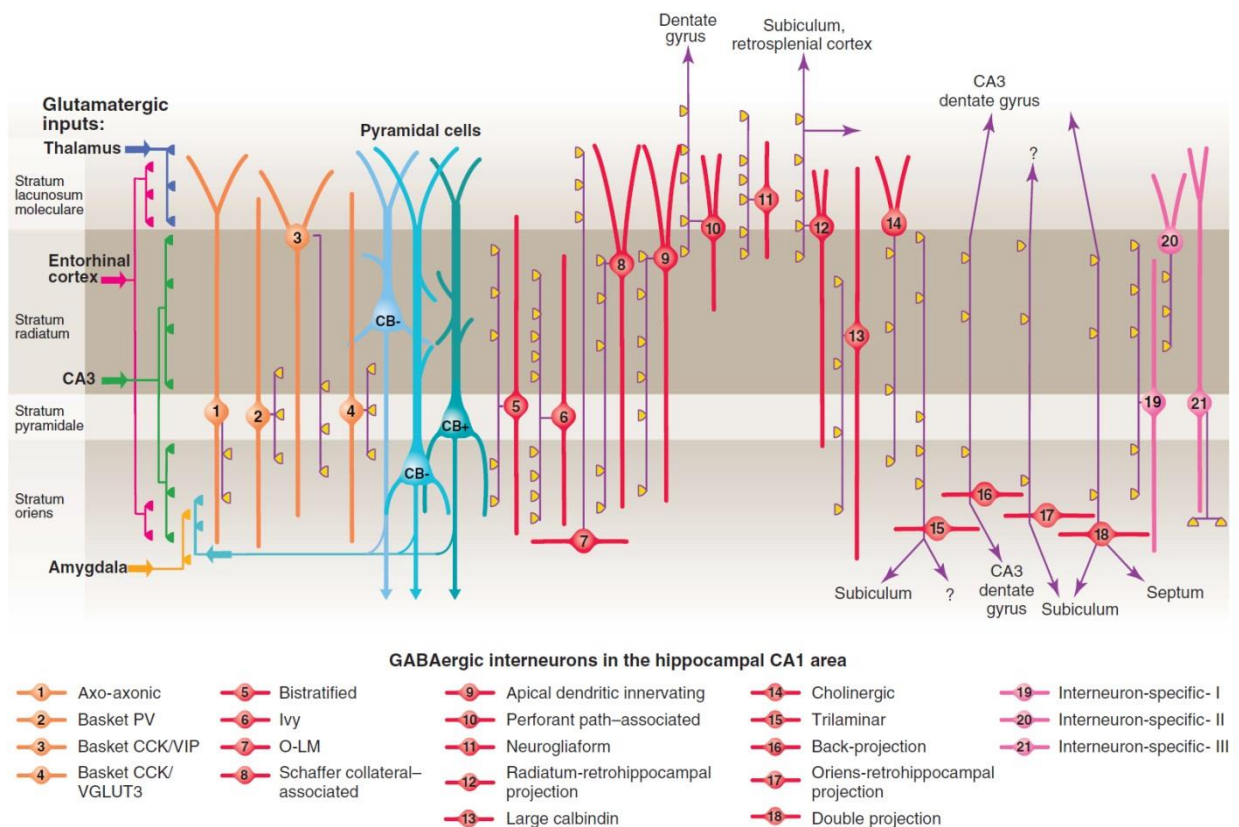


Figure 1: Interneurons classes in CA1

This schema summarizes the identified classes of interneurons that have been characterized via the three principles enumerated before. In my work, I will pay particular attention to the Basket PV (class 2), Basket CCK/CGLUT3 (class 4), and Interneurons specific VIP expressing (multipolar, class 19, or polarized, class 20).

3.1.3 Dendritic and Perisomatic inhibition

The specificity in innervation of subcellular domains in principal cells has profound consequences on the function that interneurons exert in cortical microcircuits (Miles et al., 1996). Dendritic inhibitory innervation likely controls the membrane potential around the region of innervation, and produces small and slow IPSC at the soma due to the fact that the reversal potential of Cl^- is close to the resting potential of the membrane, and therefore gives low driving force. Nevertheless, a major effect of Cl^- channel activation is ‘shunting inhibition.’ If the conductance is large, shunting inhibition can be very effective. When positive charge from an activated excitatory synapse arrives at the inhibitory synapse, it attracts Cl^- ions through the activated Cl^- channels, thus reducing the EPSP (Spruston N,

2009). Therefore, Interneurons that innervate pyramidal cell dendrites are responsible for the control of the efficacy and plasticity of glutamatergic inputs from specific sources (Freund and Katona, 2007).

On the other hand, sitting at a region where dendritic inputs get integrated and action potential are generated (Megias et al., 2001; Papp et al., 2001), interneurons impinging on the soma-equivalent region (soma, proximal dendrites and axon initial segment) are likely to control the output of principal cells, most notably the synchrony of action potentials of large populations of cells (Cobb et al., 1995; Miles et al., 1996). These interneurons are largely constituted of Basket cells (which can be divided in two classes according to the expression of the protein Parvalbumin and CCK, and form synapses on the soma and proximal dendrites), and Chandelier cells (which target the axon initial segment of principal cells, thereby likely controlling the action potential initiation) (figure 2).

Basket cells expressing Parvalbumin and CCK differ for a great variety of properties. PV+ Basket cells are fast-spiking (Connors and Gutnick 1990, McCormick et al. 1985), have only a few receptor types for subcortical modulatory signals, but are efficiently and faithfully driven by local principal cells, as expected from an “oscillator” (Freund, 2003), and participate in the production and maintenance of fast oscillations in the Gamma band (Traub et al., 2004; Bartos et al., 2007; Cardin et al., 2009). CCK+ basket cells, on the other hand, are regular-spiking, modulate synchronous ensemble activities as a function of subcortical inputs that carry information about motivation, emotions, and the autonomic state of the animal (the “inner world”; Buzsaki, 1996) due to the expression of 5HT₃ and nicotinic receptors (Freund and Katona, 2007), and likely mediate the anxiolytic effect of benzodiazepines since they act specifically on postsynaptic GABA receptors containing the subunit A α 2. Most importantly, due to their low time constant, PV Interneurons are sought to mediate specifically FFI, while CCK interneurons have longer time constant that give them the unique ability to summate feedforward and feedback inputs, and to get activated only when local pyramidal cells are also activated (Glickfeld and Scanziani, 2006) (figure 2, panel C).

A clear example of the dichotomy between these two populations of perisomatic innervating interneurons comes from Gamma (30-80 Hz) oscillation production and regulation. Indeed, an elegant work of Sohal et al (Sohal et al, 2009) has demonstrated that direct excitatory activation of PV interneurons is sufficient to generate gamma-frequency oscillation and enhance information transmission in the neocortex, while inhibition of these interneurons disrupt underlying gamma rhythms. On the other hand, CCK positive neurons can be recruited only transiently by repetitive stimulation (Glickfeld and Scanziani, 2006); moreover,

activation of CB1 cannabinoid receptors, which are present in CCK but not PV basket cells, markedly reduces the power of gamma oscillation (Hajos et al., 2000). Therefore, we might conclude that the overall clockwork that control rhythmic populations activity reside in the PV In network, while CCK interneurons would carry on the fine-tuning of normal network operations to respond to subcortical modulatory signal about the “state” of the system. Pathology comes in support of this division of labor: in epilepsy, which is known to be a disorder of abnormal rhythmical activity in cortical networks, PV interneurons seem to be critically involved (Cossart et al., 2005; Magloczky and Freund, 2005; Ogiwara et al., 2007), unlike CCK-containing interneurons (Monory et al., 2006); on the other hand, at least six different receptors that are implicated in anxiety (5-HT₃, nicotinic α_7 and α_4 , CB1, GABA_A enriched in α_2 subunit, estrogen α) converge onto the CCK-containing cells, but are absent or expressed at very low levels in PV cells (Freund, 2003).

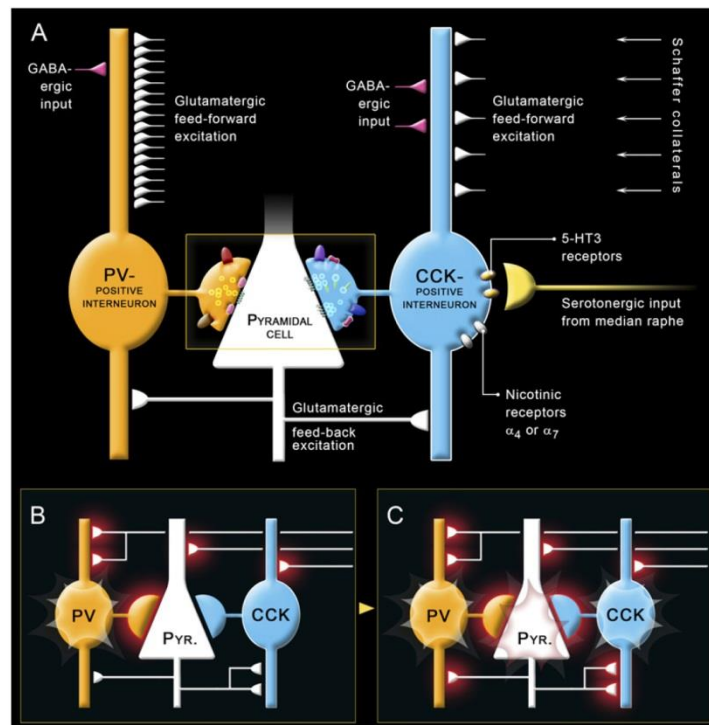


Figure 2: perisomatic inhibition

Schematic expressing peculiar properties of the two classes of basket cells, which can be differentiated by their preferential role in FFI (PV basket cells, panel B) or both feedforward and feedback inhibition (CCK basket cells, Panel B), being active when the pyramidal cells are activated. From Freund and Katona, 2007

3.1.4 Interneurons and regulation of critical periods

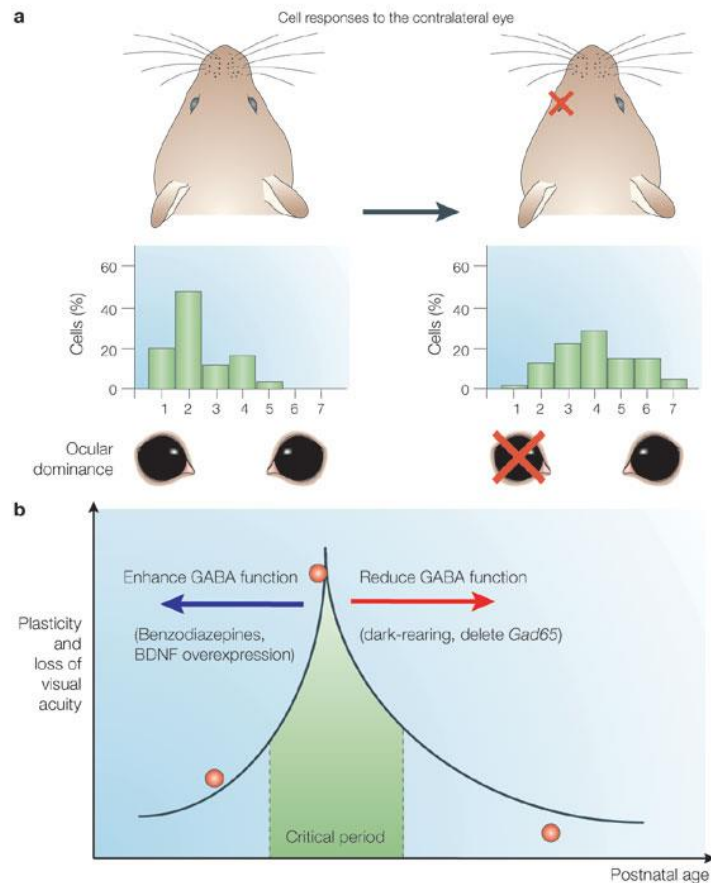
Recently, a lot of attention has been paid to interneurons as regulators of windows of enhanced plasticity during development, that are generally known as “critical periods”.

Critical periods are best (and longest) studied in sensory systems, where over 40 years of study have revealed their presence and part of the mechanisms responsible of these windows of opportunity. Indeed, during a brief period of postnatal life whose extent and timing depend on the structure analyzed (Hensch 2005), an external perturbation of the proper sensory experience like the occlusion of one eye, the shaving of a whisker, or a white noise, can produce long-lasting rearrangements in the microcircuits that underlies that sensory modality. Therefore, in the binocular visual cortex, inputs from the spared eye in the case of monocular deprivation can invade the territory normally occupied by the other eye, in an attempt to overcome the external insult (Wiesel and Hubel 1963 a to d, Hubel et al, 1976, Shatz C and Stryker, 1978). This great degree of plasticity present during development seem to be lost in adulthood, where monocular deprivation cause little to no rearrangements of cortical microcircuits, although during the years it has been shown that many interventions are able to restore to a certain extent a high degree of plasticity even in the adults (Pizzorusso T et al., 2002; Vetencourt et al., 2008).

In the last decade, many studies have implicated the development of the inhibitory component of cortical microcircuits in the regulation of the opening or closure of critical periods (for review, see Hensch 2005). Therefore, in mice that lack the enzyme GAD-65 (which is critically involved in the synthesis of GABA, Tian N et al, 1999) ocular dominance plasticity is suppressed until the proper level of inhibition is restored by infusion of Diazepam (GABA_A2 agonist, Hensch et al 1998). Conversely, the onset of critical periods can be accelerated if GABA transmission is enhanced (Fagiolini et al, 2000 and 2004), or GABA neurons maturation is accelerated (for example via BDNF overexpression, Huang et al 1999, Hanover et al 1999). Moreover, in an elegant study in 2010, Southwell et al. implicated causally the development of interneurons in the opening of critical periods: when they transplanted immature neurons (in a mixed populations composed of PV, CR, NPY and SOM) into a more mature cortex, they were able to observe the opening of an additional period of enhanced plasticity that correlated with a specific window during interneurons development (Southwell et al., 2010). This topic will be treated further in the third part of this introduction.

Figure 3: Critical period regulation via maturation of inhibition in cortical microcircuits

During cortical microcircuit development, the maturation of inhibition exerted by define interneuron classes (in particular, PV+ interneurons providing perisomatic inhibition), is responsible for regulation of plasticity defining “critical periods”. Indeed, interventions that impinge on inhibitory development (Benzodiazepines, BDNF, Dark rearing, GAD deletion) can modulate the timing and the extent of the critical period. Modified from Takao Hensch, Nature review neuroscience 2005



Copyright © 2005 Nature Publishing Group
Nature Reviews | Neuroscience

The extent to which all the subpopulations of interneurons would contribute with the same importance to the opening and closure of critical period has then been immediately addressed by targeted experiments. In birdsongs, it has been shown that critical period for song learning coincide with perineuronal nets formation around PV interneurons in HVC, which is where song learning take place, and that failure in learning is mirrored by failure in developing proper PNNs (Balmer et al, 2009). When it became clear that restoring plasticity in the adult could be achieved by specifically shaving the prineuronal nets in the extracellular

matrix that form around Parvalbumin expressing interneurons (Pizzorusso et al., 2002), this class of interneuron was immediately under investigation to elucidate their contribution to the developmental critical periods. In their 2008 study, Sugiyama et al. demonstrated that during development, experience is instrumental in inducing the synthesis of the homeobox transcription factor Otx2 in early sensory areas (retina and Lateral geniculate nucleus), and promoting the transport of this protein to the visual cortex where, through local concentration induced by the formation of PNNs, it accumulates in PV+ interneurons thereby regulating their maturation and concomitantly critical period timing (Sugiyama et al. 2008).

Therefore, the state of the interneuron network (and in particular that of PV interneurons) regulates the extent of plasticity during development, establishing those window of opportunity that are generally observed in sensory areas. Moreover, it might also be defining states that support learning in defined windows, as for song learning in zebra finches. Nevertheless, the possibility that this regulation mechanisms holds even in adult microcircuits, as well as the modalities by which it is implemented by experience, are still open questions in neurobiology. Moreover, the forces regulating the development of the inhibitory component in cortical microcircuits that lies further away from sensory experience remains to be elucidated.

3.2 The Hippocampal Formation

3.2.1 Hippocampal Function

Sitting underneath the cortical surface in the medial temporal lobe, the Hippocampus is one of the structures in the brain that has gained an overwhelming attention due to its involvement in learning and memory. Indeed, since the studies about the patient H.M, it is largely accepted that damages to the hippocampus (and other structures of the hippocampal formation, and more in general the medial temporal lobe) produce anterograde amnesia as well as temporally graded retrograde amnesia: both spare the ability to recall remote memories, but impair the ability to form new one or retrieve recent memories, respectively. In this prospect, the hippocampus is thought to play a role in consolidating information from short-term to long-term memories, which are dependent on neostriatal structures (Squire, 2004).

Specifically, the Hippocampus is involved in the formation of episodic memory, which consists in the ability to remember personal past experiences; this is achieved by creating a relational representation of various aspect of experience (the “what, where and when” components) that can be later recalled by partial input cues (Eichenbaum, 1999; Greene, 2001). The ability to form representations without obvious reinforcers is known as “incidental learning”, as opposed to the other forms of learning producing “semantic memory” which refers to the ability to acquire general knowledge without being specifically related to personal experience. Both forms of memory are known as “declarative”, due to the deliberate and conscious effort made to recall that information, which is usually about factual knowledge of people, places or events which bear a meaning attached to them (Kandel, 2000): the Hippocampus is well known to play a role in both (Rosenbaum et al., 2000; Tulving, 2002).

Moreover, the Hippocampus has long been studied for its contribution to spatial memory and navigation. Many neurons in the hippocampus possess the ability to fire action potentials when the animal passes through a specific part of the environment, a peculiar property that has led to the definition of these cells as “place cells” (O’Keefe and Conway, 1978; O’Keefe and Dostrovsky, 1971; O’Keefe and Nadel, 1978). Based on this peculiar property, it has been hypothesized that the hippocampus mediates memory for spatial relations among objects in an environment (O’Keefe and Nadel, 1978, McNaughton et al., 2006; Moser et al.,

2008), thereby providing a representation of the external world known as “cognitive map” (O’Keefe and Nadel, 1978). To do so, place cells in the hippocampus likely work in close correlation with Grid cells (that fire action potentials in defined positions in the environment thereby describing regular grids of hexagonal form which can be distinguished by spacing and orientation, Hafting T et al., 2005), Head direction cells (which fire action potentials depending on the orientation of the animals, Sargolini F et al., 2006), and border cells (which fire action potentials in close proximity to a physical border, Solstad T et al., 2008) in the Medial Entorhinal Cortex.

Therefore, although its contribution to learning and memory is widely accepted, the specific modality by which the Hippocampus participates in different forms of learning is still under debate. Experimental evidence for both concepts has been provided. For example, *in vivo* recordings have identified hippocampal cells that solely encode spatial or non-spatial information (Okeefe and Dostrovs.J 1971; Hampson, Simeral et al. 1999; Lee, Griffin et al. 2006; Royer, Sirota et al. 2010). In addition, a population of hippocampal neurons has been reported to encode both non-spatial as well as spatial information (Hampson, Simeral et al. 1999; Wood, Dudchenko et al. 2000; Lee, Griffin et al. 2006). Therefore, place cells might contribute to episodic memory as a component of contextual representation (Smith and Mizumori 2006 a and b), but at the same time the hippocampus might extract common features across episodes and therefore play a critical role in semantic memory as well (O’Reilly and Rudy, 2001), thereby binding all kind of stimuli into a unitary representation that can later be recalled from partial input cues (Eichenbaum et al, 1999; O’Reilly and Rudy, 2001).

3.2.2 Hippocampal Connectivity

The hippocampal formation in rodents is a C-shaped structure composed of three distinct subregions, which are populated by different types of excitatory cells: the Dentate Gyrus (DG), which comprises the granular layer and the Hilus, is where the Granule and Mossy cell bodies are located; The Cornu Ammonis, divided in Area 3, 2 and 1 (CA3, CA2 and CA1, respectively), hosts the somas of the Pyramidal cells; the Subiculum (Sub, to which are associated the presubiculum and parasubiculum) connects the hippocampus proper to the Entorhinal cortex by its own Pyramidal cells.

This anatomical division is instrumental in understanding the unidirectional flow relaying information from the Entorhinal cortex to the hippocampus, and then back to the entorhinal cortex itself, which constitute the trisynaptic circuitry of the hippocampus proper (Figure 1). Hence, Cortical inputs from layer two entorhinal cortex enter the hippocampus to engage synapses with the DG Granule cells, whose axons are sent via the mossy fiber pathway to CA3 pyramidal neurons; by means of their Schaffer collateral, these neurons project to CA1 pyramidal cells, whom, in turn, project back to the EC directly or via the subiculum. Moreover, extensive axon ramifications from CA3 pyramidal cells innervate other pyramidal cells in the CA3 area itself, thereby creating an intricate recurrent connection. Although this closed loop constitutes the main route of information flow in the hippocampus, the entorhinal cortex projection (called Perforant Path, PP) can project directly to every area in the hippocampus proper. Therefore, input arising in Layer 2 EC can project to the DG or directly to CA3 pyramidal neurons, while inputs originating in Layer3 EC project directly to the pyramidal cells in CA1. Moreover, the Entorhinal cortex can be divided anatomically in Medial (MEC) and Lateral (LEC), which convey different spatial and emotional information, and which project both to the Dentate gyrus and the hippocampus proper.

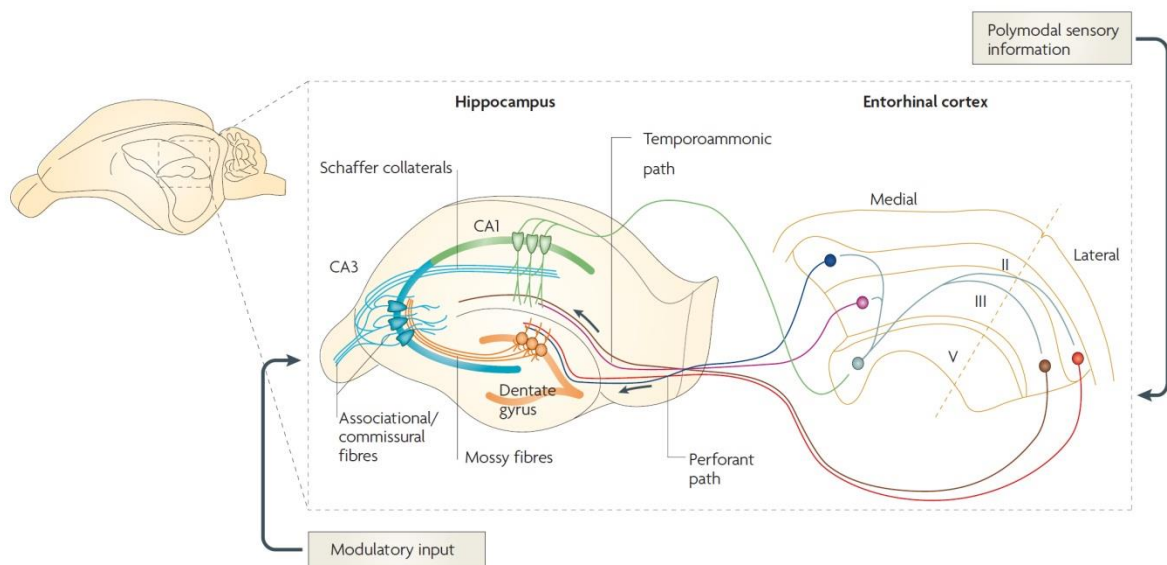


Figure 1: basic anatomy of the Hippocampus

From Neves et al., 2008. Here, the projection relaying the entorhinal cortex to the hippocampus proper is highlighted as main source of incoming information to the hippocampus. To organize its inputs, the trisynaptic hippocampal circuit relaying granule cells to pyramidal cells in CA3, which in turn project to pyramidal cells in CA1, shows a high degree of lamination along the dendrites of its neurons.

Such an intricate network of connectivity is structured in laminated fashion for which inputs that share their presynaptic origin stratify at different levels along the postsynaptic cell dendrites. Hence, inputs to the dendrites of granule and pyramidal cells can be analyzed according to position, which defines strata in each subdivision.

In the dentate gyrus, the dendrites of granule cells extend from the granular layer (where cell bodies are located) to the molecular layer, without any ramification toward the Hilus (hilar dendrites are present during development but retracted in a later time point). Hence, the region closest to the cell body is defined “inner molecular layer”, where inputs from the hilar mossy cells constituting the commissural/association fibres stratify (Blackstad, T. W, 1956 and 1958). The outer molecular layer is occupied by inputs arising from L2 entorhinal cortex, that again stratify according to their origin: the inner part of the layer is occupied by inputs arising in the MEC, while the outer part hosts inputs coming from LEC.

In CA3, pyramidal cells receive synapses onto both basal and apical dendrites. Basal dendrites are present in the Stratum Oriens, which receives inputs from the septal fibers and the commissural fibers from the contralateral hippocampus. Immediately above the Stratum Pyramidale, where the cell bodies of pyramidal cells are located, the lamination of the mossy fibers defines the Stratum Lucidum, where the large mossy fiber terminals relay information from the granule to the pyramidal cells. Further above, the Stratum Radiatum contains the ramification from the Schaffer Collaterals, which relay pyramidal cells in CA3 to each other, thereby forming the intricate recurrent innervation typical of this region. Stratum Lacunosum-Moleculare defines the most apical stratum where inputs from L II Entorhinal cortex synapse directly upon CA3 Pyramidal cells.

In CA1, the division in strata is somehow similar to the CA3 subregion; nevertheless, since CA1 misses entirely the inputs from granule cells, no Stratum Lucidum can be distinguished, and its position is occupied by a larger Stratum Radiatum where inputs from the CA3 Schaffer collaterals stratify.

3.2.3 The mossy fiber projection

Making synapses on the apical tract of the CA3 pyramidal cells dendrites, the mossy fiber projection consists of unmyelinated axons arising from granule cells, running in the Stratum Lucidum of CA3, and exhibiting a strict lamellar organization parallel to the transversal

hippocampal axis (Gaarskjaer, 1986; Henze et al., 2000). Mossy fiber axons exhibit three morphologically distinct presynaptic specializations: large 'giant' boutons (large mossy fiber terminals, LMTs) that are thought to represent the main bodies of mossy fibers (Galimberti et al., 2006), small *en passant* varicosities, and filopodial extensions emerging from the LMT core (Amaral and Dent, 1981) (Figure 2). LMTs are large (> 2.5 μm in diameter) and potent presynaptic terminals that innervate complex clusters of dendritic spines called *thorny excrescences* (or *thorns*) on CA3 pyramidal neurons (Blackstad and Kjaerheim, 1961; Hamlyn, 1962; Rollenhagen et al., 2007). The mossy fiber synapses made by LMTs are very powerful and are also known as "detonator synapses", due to their ability to generate large postsynaptic currents and potentials in CA3 pyramidal neurons under conditions of high activation (Henze et al., 2002; Lawrence et al., 2004; Maccaferri et al., 1998). Moreover, they present most of the features that are attributed to "driver" synapses (The Pasquale et al., 2011). LMTs can exhibit "satellites", or terminal appendices that are connected to the main core through 10 – 200 μm processes (Galimberti et al., 2006) (Figure 2). Like core LMTs, satellites are larger than 2.5 μm in diameter, exhibit filopodia and establish excitatory contacts onto distinct postsynaptic pyramidal neurons, thereby mediating feed-forward excitation (FFE) (figure 2). Furthermore, LMTs have been shown to exhibit structural plasticity as a consequence of age, experience and learning (De Paola et al., 2003; Galimberti et al., 2006; Ruediger et al., 2011). As opposed to these powerful excitatory connections, mossy fibres establish synapses with inhibitory GABAergic interneurons in the hilus and *stratum lucidum* via *en passant* varicosities and LMT filopodial extensions (Acsady et al., 1998; Szabadics and Soltesz, 2009). In turn, these interneurons make inhibitory synapses on CA3 pyramidal neurons, thereby mediating feed-forward inhibition (FFI. Figure 2). At low-frequency firing, FFI dominates over CA3 pyramidal neuron excitation (Acsady et al., 1998), providing powerful regulatory control over CA3 principal cell excitability and timing of action potential generation (Lawrence and McBain, 2003 and 2004).

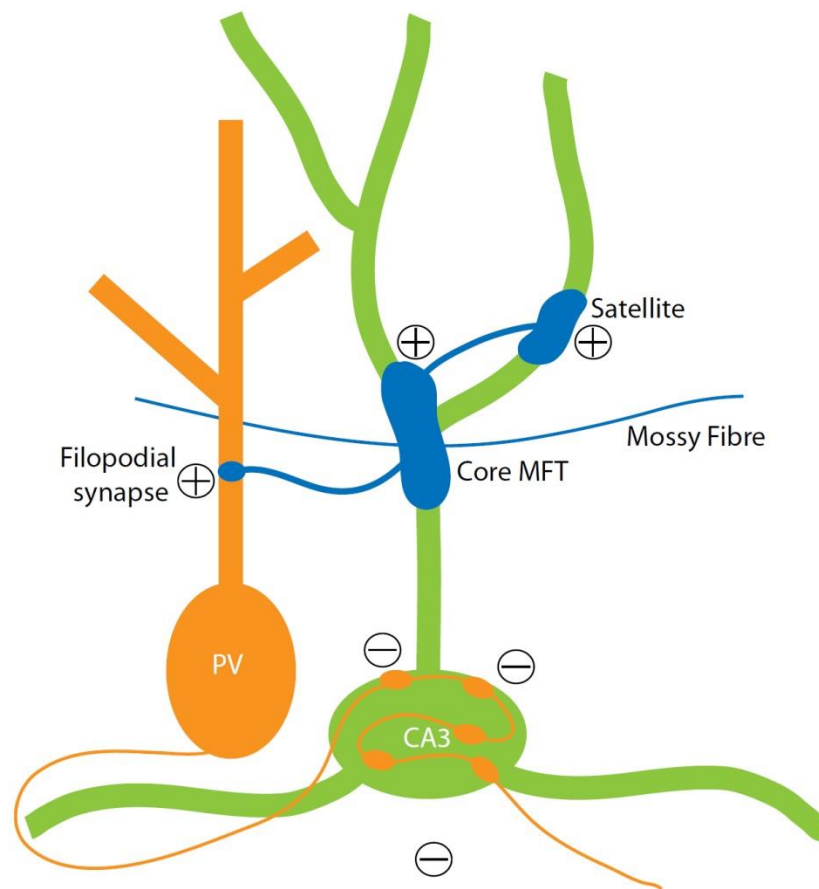


Figure 2: Connectivity of the Mossy Fiber pathway in CA3

Schematic of connectivity in CA3. The large mossy fiber terminals are able to mediate both feedforward excitation via excitatory synapses onto excitatory cells (Core and satellites LMTs on CA3 pyramidal cells), and Feedforward inhibition via Parvalbumin (PV) positive interneurons recruitment largely mediated by filopodial synapses.

3.2.4 Developmental origin

The developmental origin of the hippocampus proper lies in the subpallial region of the developing brain called hippocampal neuroepithelium (Altman and Bayer, 1990 a, b and c), in close proximity to the cortical Hem. Here, a continuous sheet of Nestin+ progenitor cells (radial glia-like) facing the wall of the ventricular formation undergo a final asymmetric cell division to give rise to both Pyramidal cells of areas CA3 and CA1, as well as granule cells of the dentate gyrus: hence, the hippocampal neuroepithelium can be segmented in ammonic neuroepithelium, primary dentate neuroepithelium, and fimbrial gliopithelium, according to their increasing proximity to the Hem (Altman and Mayer, 1990; Li and Pleasure, 2005 and

2007). This latter structures is known to produce many of the morphogens that are required for cells specification and maturation in the hippocampus, including WNT3a (Grove EA et al, 1998; Mangale VS et al, 2008) which lies upstream of a cascade of transcription factor that define hippocampal fate (like Lef1, Emx2 and Lhx5, Li Q et al., 2011).

During the course of the second week of the mouse embryonic development, the hippocampus neurepithelium undergoes a sustained period of cell division (Altman and Bayer, 1990), which produces postmitotic pyramidal cells and a mixed population of postmitotic granule cells as well as a larger fraction of granule cells progenitors (Altman and Bayer, 1990 b). The postmitotic pyramidal cells , which are overall produced in a time window spanning from E10.5 to E18.5 in the mouse (Danglot, Triller and Marty 2007), start then their path of radial migration toward their final destination in stratum pyramidale of the cornu ammonis, where they settle in the classical cortical inside-out order with older cells in the outer layer. Granule cells, on the other hand, are produced in two waves: a first, pioneer subset of postmitotic granule cells start to migrate to the final territory of the dentate gyrus as early as E 10.5, thereby settling in the outer layer of stratum granulare (Altman and Bayer, 1990); a second, larger cohort of granule cells will instead be produced postnatally from the pool of progenitors that had previously settled in the hilar region, in a window that comprises the first ten days of postnatal life. Nevertheless, a small portion of progenitors will be retained in the subgranular zone for the whole life of the animal, giving rise to the adult born granule cells (Kempermann et al., 2000).

This early period of neurogenesis is followed by an extensive period of synaptogenesis in which all the synaptic connection in the hippocampus are formed, in a marked temporal order which favors inputs closer the soma as early established, followed by the other inputs in a centrifugal manner. The recognition between pre and postsynaptic partners seem to be favored by selective interaction of adhesion molecules, like synCAMs (Forgel AI et al., 2007). Moreover, the program establishing a correct lamination of inputs in the hippocampus seems to rely entirely on genetic factors, with little influence from activity (Forter, Zhao and Frotscher 2006).

3.2.5 Neuronal diversity

The extent to which, in cortical mircorcuits, excitatory cells of the same type can be considered as a homogeneous population or divided according to some specific properties is

still an open question in neurobiology. In the hippocampus, this has led many researchers to try to understand if all pyramidal and granule cells share the same properties in the adult microcircuits. It has been already pointed out that most, but not all the pyramidal cells in CA3 and CA1 exhibit “place cells” properties in vivo, thereby creating a first functional difference among hippocampal cells (O’Keefe J., 1976). More recently, Kenji Mizuseki and Yuri Buzsaki have demonstrated that pyramidal cells in CA1 can be distinguished base on their physiological properties and position in deeper or superficial layers: deep pyramidal cells fired at higher rates, bursted more frequently, were more likely to have place field and were more strongly modulated by slow oscillations during sleep (Mizuseki et al., 2011). This might suggest that pyramidal cells in CA1 might form functional distinguishable subclasses that might go beyond the intrinsic morphological and physiological difference observed in CA3 (Bilkey DK et al, 1990).

Moreover, at the genetic level, Thompson et al., have demonstrated the existence of a robust cohort of transcripts that show a strong, regionalized expression in the hippocampus. This thereby defines a complex molecular parcellation into a relatively coherent set of nine expression domains in the septal/temporal and proximal/distal axes in CA3, with reciprocal, nonoverlapping boundaries (Thompson et al, 2008). The extensive presence of adhesion molecules among those transcripts suggests that the underlying rule defining this parcellation might reside in differential connectivity, as demonstrated to connectivity toward the lateral septum.

Nevertheless, the extent to which a group of cells might share similar genetic and physiological properties in a defined subregion, and find a correlate in groups belonging to other subregions (thereby defining horizontal subpopulations across DG, CA3 and CA1), is not yet known. Moreover, the possibility that connectivity might be organized differently among cells belonging to the same subpopulation as opposed to different ones, and the rules governing the achievement of this selective connectivity, might highlight the existence of parallel microcircuits in the hippocampus whose function would remain to be determined.

3.3 Structural plasticity upon learning: regulations and functions

Published Review:

Pico Caroni, Flavio Donato, Dominique Muller.

Nature Review Neuroscience 2012 Jun 20; 13(7) 478-90

The contributions of brain networks to information processing and learning and memory are classically interpreted within the framework of Hebbian plasticity and the notion that synaptic weights can be modified by specific patterns of activity. However, accumulating evidence over the past decade indicates that synaptic networks are also structurally plastic, and that connectivity is remodeled throughout life, through mechanisms of synapse formation, stabilization and elimination¹. This has led to the concept of structural plasticity, which can encompass a variety of morphological changes that have functional consequences. These include on the one hand structural rearrangements at pre-existing synapses, and on the other hand the formation or loss of synapses, of neuronal processes that form synapses or of neurons. In this Review we focus on plasticity that involves gains and/or losses of synapses. Its key potential implication for learning and memory is to physically alter circuit connectivity, thus providing long-lasting memory traces that can be recruited at subsequent retrieval. Detecting this form of plasticity and relating it to its possible functions poses unique challenges, which are in part due to our still limited understanding of how structure relates to function in the nervous systems.

We review recent studies that relate the structural plasticity of neuronal circuits to behavioral learning and memory and discuss conceptual and mechanistic advances, as well as future challenges. The studies establish a number of strong links between specific behavioral learning processes and the assembly and loss of specific synapses. Further areas of substantial progress include molecular and cellular mechanisms that regulate synapse dynamics in response to alterations in synaptic activity, the specific spatial distribution of the synaptic changes among identified neurons and dendrites and the relative roles of excitation and inhibition in regulating structural plasticity.

The new findings provide exciting early vistas of how learning and memory may be implemented at the level of structural circuit plasticity. At the same time, they highlight major gaps in our understanding of plasticity regulation at the cellular, circuit and systems levels. Accordingly, achieving a better mechanistic understanding of learning and memory

processes is likely to depend on the development of more effective techniques and models to investigate ensembles of identified synapses longitudinally, both functionally and structurally.

3.3.1 Molecular mechanisms of synapse remodeling

A remarkable feature of excitatory and inhibitory synapses is their high level of structural variability² and the fact that their morphologies and stabilities change over time³. This phenomenon is regulated by activity, and the size of spine heads correlates with synaptic strength⁴, presynaptic properties⁵ and the long-term stability of the synapse⁶. The morphological characteristics of synapses thus reveal important features of their function and stability. Most importantly, there is a continuity of regulatory processes relating synaptic activity to the strength, shape and long-term retention of existing synapses.

Synapse restructuring. Early electron microscopy studies provided the first evidence that the induction of synaptic plasticity could affect the size and shape of dendritic spines⁷. Later, two photon glutamate uncaging and imaging experiments demonstrated a close association between increased synaptic strength and an enlargement of the spine head⁴. The significance of this enlargement could reflect several important functional modifications of the synapse. It could be linked to the changes in receptor expression that are thought to account for the increase in synaptic strength at many synapses⁸. It could also result from the mobilization of subcellular resources to potentiated synapses, such as ribosomes or additional cytoskeleton-associated proteins⁹. In addition, this restructuring could be part of a more global set of changes that promote the stabilization of the synapse¹⁰. Several recent studies have indeed highlighted the importance of synapse stabilization as a defined feature associated with behavioural learning. Novel sensory experience was shown to promote the stabilization of a new set of persistent spines in the somatosensory cortex in vivo⁶. Similarly, in motor skill learning experiments, new spines that grow on selective populations of neurons are preferentially stabilized during subsequent training, with the spines persisting long after training has stopped^{11,12}.

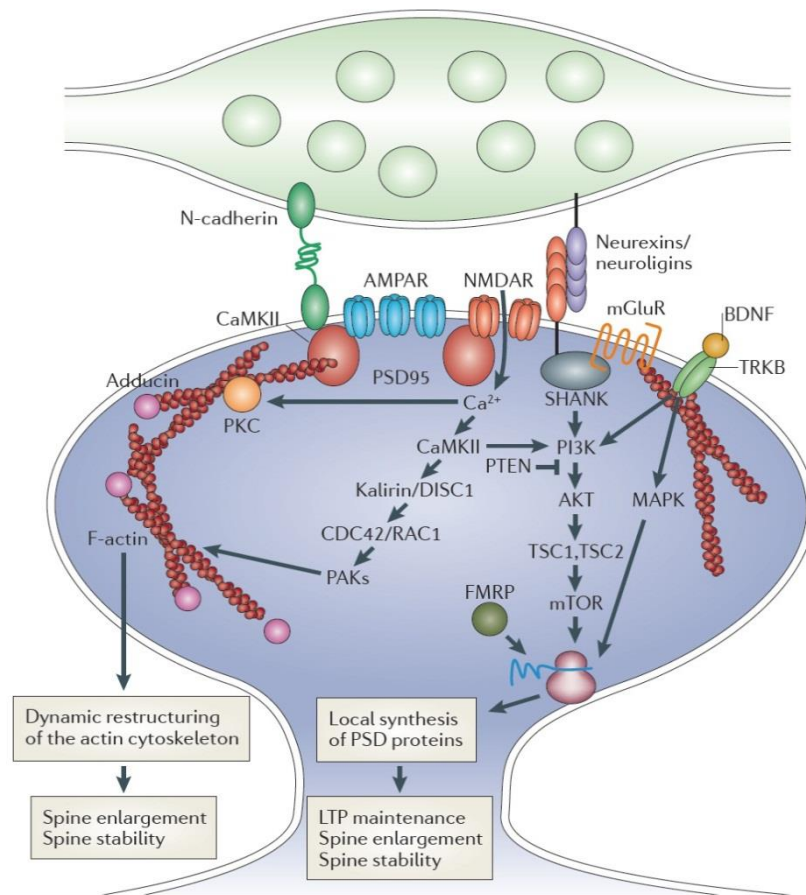


Figure 1: Molecular mechanisms regulating activity-mediated stabilization of dendritic spines.

Induction of synaptic plasticity at individual synapses is associated with a rapid enlargement of the spine head, an increase in synaptic efficacy and a switch in the stability of the synapse that could make them persistent. Recent findings implicate an important role of protein kinases (such as PKC (protein kinase C) and CaMKII (calcium/ calmodulin protein kinase II)) contributing to long-term potentiation (LTP) maintenance, spine enlargement and in vivo spine stability (for PKC). In addition, local protein synthesis (for example of BDNF (brain-derived neurotrophic factor), TRKB (tyrosine kinase B), MAPK (mitogen-activated protein kinase), PI3K, (phosphoinositide 3-kinase), PTEN (phosphatase and tensin homologue), AKT, TSC1 (tuberous sclerosis 1), TSC2, mTOR (mammalian target of rapamycin) and FMRP (fragile X mental retardation protein)) contributes to LTP maintenance, spine enlargement and spine stability. Proteins implicated in the regulation of the actin cytoskeleton (such as DISC1 (disrupted in schizophrenia 1), CDC42 (cell division control protein 42), RAC1 (Ras-related C3 botulinum toxin substrate 1), PAKs (p21-activated kinases) and adducin) contribute to LTP maintenance and spine enlargement (and spine stability for PAK3). The actin cytoskeleton is indicated as F-actin. Moreover, adhesion molecules and molecules of the postsynaptic density (including PSD95 (postsynaptic density protein of 95 kDa), SHANKs (SH3 and multiple ankyrin repeat domains proteins), neuroligins, N-cadherins, AMPA receptors (AMPA receptors) and NMDA receptors (NMDARs)) are implicated in LTP maintenance, spine enlargement and spine stability.

In birds, song learning by imitation during a juvenile sensitive period leads to a rapid stabilization and enlargement of dendritic spines that is correlated with an enhancement of synaptic activity¹³. These different studies support the idea that the stabilization of selective subpopulations of spines could represent a structural basis for memory storage. Although this stabilization process is often associated with the induction of plasticity, several important issues remain to be addressed. How does this stabilization relate to changes in synaptic strength or spine size? Are changes in synaptic strength required for the stabilization of a synapse? How stable is this mechanism? A recent study suggests that reconditioning

following a procedure of conditioning and extinction preferentially eliminates dendritic spines formed and stabilized by extinction¹⁴. Accordingly, stabilization may be considered as a key reversible property of individual synapses that is linked to the induction of plasticity.

Molecular mechanisms of synapse stabilization. The molecular mechanisms accounting for synapse stabilization are likely to implicate a variety of factors, which have often been inferred from indirect analyses of either mechanisms contributing to long-term potentiation (LTP) maintenance or mechanisms implicated in activity-mediated spine enlargement. Relatively few studies have examined molecular mechanisms contributing to spine stabilization by directly measuring the persistence of dendritic spines in vivo. Current evidence, however, suggests that there is a significant overlap between the molecular pathways implicated in these different aspects of stability (FIG. 1), emphasizing the close link existing between induction of plasticity and synapse stability.

First, an important part is likely to be played by phosphorylation mechanisms. Both calcium/calmodulin-dependent protein kinase II (CaMKII) and protein kinase C (PKC) have been directly implicated in LTP maintenance and behavioural learning^{15,16}. CaMKII activity is required for activity-mediated spine enlargement¹⁷, and PKC contributes to in vivo spine stabilization¹⁸. Another central mechanism for spine stabilization involves the local regulation of protein synthesis, which includes the signaling cascades (such as the mitogen-activated protein kinase (MAPK) and phosphoinositide 3 kinase (PI3K) pathways) downstream of receptor tyrosine kinase B (TRKB; also known as NTRK2) activation, the mammalian target of rapamycin (mTOR) signalling complex and the translation of mRNAs that encode proteins such as ARC or CaMKII. Interference with this signaling, with protein synthesis or with ARC translation have been strongly implicated in LTP maintenance and in spine enlargement^{19–23}, whereas in vivo blockade of protein synthesis results in synapse destabilization¹⁸. A third set of molecular factors critical for spine stabilization includes the various signaling pathways and actin-regulatory proteins that control the spine actin cytoskeleton. Interference with actin polymerization impairs LTP maintenance and changes in spine size^{23–25}. Furthermore, phosphorylation of the cytoskeleton-stabilizing protein β -adducin through PKC is required for the stabilization of populations of synapses induced by environmental enrichment¹⁸. Additional evidence supporting a role of the cytoskeleton in spine stabilization comes from the implications of Rho GTPases and several upstream or downstream modulators of this pathway, such as kalirin 7, DISC1 (disrupted in schizophrenia 1) or PAKs (p21 activated kinases). Interference with this signaling affects LTP mechanisms and the capacity of spines to enlarge^{26,27}. Finally, one important mechanism through which synapse stability could be improved is by changes in the organization of the postsynaptic density (PSD) that promote trans-synaptic adhesion and contact. Expression of PSD95 and/or AMPA receptors

enhances synaptic strength and synapse stability^{28,29}. Several adhesion molecule systems have also been linked to spine stability, including neuroligin 1^{29,30} and N cadherin. Activity-mediated expression of N cadherin correlates with, and is required for, the long-term stabilization of spines activated by theta-burst stimulation³¹. Secreted members of the C1q family have also been shown to rapidly induce changes in synapse numbers by, for example, stabilizing synapses in the mature cerebellum in vivo through the formation of trans-synaptic complexes³². Taken together, these data highlight how spine stabilization is regulated by a multiplicity of molecular mechanisms, probably reflecting the importance and complexity of the phenomenon.

3.3.2 Synapse turnover specificity in vivo

A comparatively small but significant fraction of synapses in the adult in vivo undergo a continuous turnover process, which may allow a continuous adaptation of synaptic networks to experience¹. The magnitude of this turnover process varies strongly during development, decreasing significantly in adult brain^{6,33,34}, but a substantial capacity for circuit rewiring is maintained throughout life and can be reactivated by lesions¹. As discussed below, processes known to involve enhanced plasticity also enhance the fraction of synapses that undergo turnover in the adult.

Remodelling of connectivity. An important feature of synapse turnover is its regulation by activity and sensory experience³³. Whereas initial in vitro experiments mainly focused on spine growth and synapse formation in response to neuronal activation^{34–36}, more recent experiments have shown that activity also destabilizes existing synapses^{10,35}. Under in vivo conditions, training in motor skill learning tasks results in a rapid rewiring through the formation and elimination of spines in the primary motor cortex, affecting different sets of synapses for different motor skills^{11,12}. Spine elimination and formation caused by fear conditioning and extinction, respectively, occur in a cue- and location-specific manner¹⁴. Similarly, a major correlate of environmental enrichment is a marked increase in synapse remodeling, including synapse formation and destabilization¹⁸.

An interesting feature of activity-mediated spine dynamics is that it might be regulated locally: evidence suggests that induction of plasticity is facilitated in the vicinity of potentiated spines and that new spines preferentially form close to activated spines^{10,37}. Two recent studies further support these results. Using a repetitive motor learning task, it has been shown that new spines formed during the acquisition of learning emerge in clusters as neighbouring spine pairs that are more likely to persist than non-clustered spines³⁸. Another study carried out during development by monitoring synaptic activity through calcium imaging shows that neighbouring synapses are more likely to be co active than synapses

farther from each other³⁹. Local regulation of spine dynamics may thus be an important mechanism to promote such clustering activity.

A different aspect of the regulation of spine turnover is that, in some cases, the effect may be more global and differentially affect spine formation and elimination, resulting in actual changes in spine density⁴⁰. In the motor learning task experiments, the increase in spine formation and spine loss roughly cancelled each other out, resulting in no marked changes in spine density^{11,12}. By contrast, the enriched environment protocols greatly promoted spine growth, leading to an increase in the absolute numbers of spines¹⁸. Regulation of spine dynamics thus not only promotes rewiring but also controls the level of connectivity of the network. Taken together, these observations suggest that the rewiring observed under behavioural learning conditions represents a structural correlate of learning (FIG. 2).

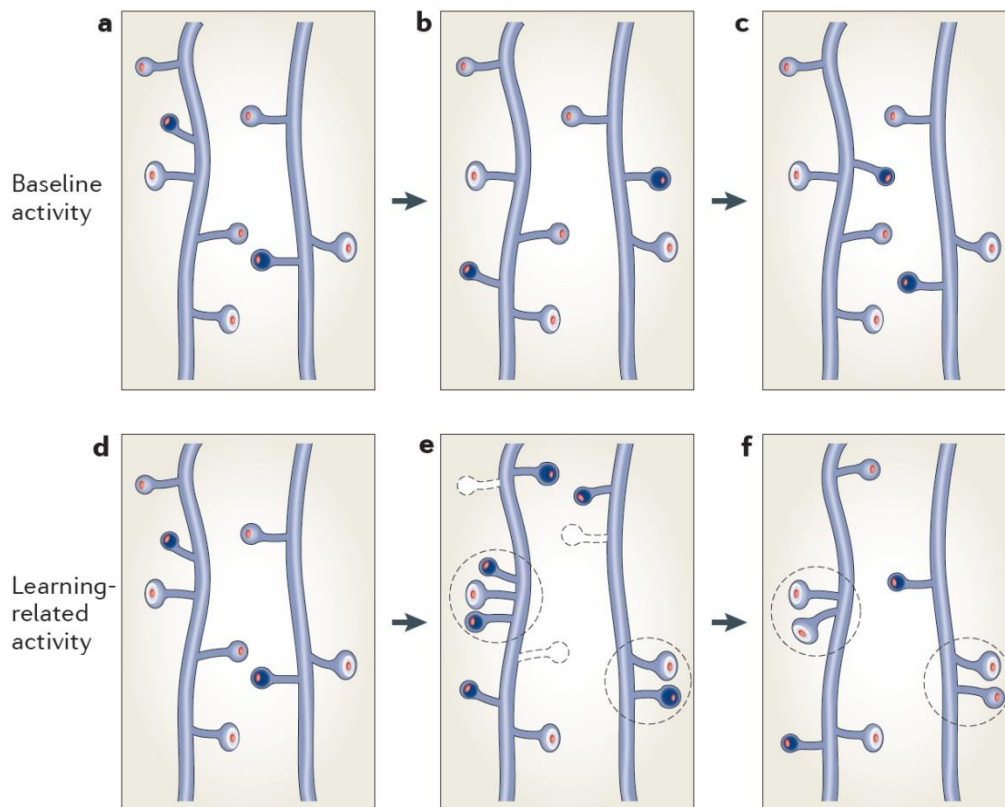


Figure2: Learning-induced structural rewiring of synaptic networks.

a-c. Schematic showing a characteristic spine turnover sequence under baseline activity conditions, which includes both loss of existing spines and gain of new ones, and affects a small subpopulation of transient spines (small dark spines), leaving a larger population of more stable, persistent spines unaffected. d-f | Under conditions of behavioural learning, this turnover is markedly enhanced, leading to the formation of additional new spines (small dark spines), and the elimination of pre-existing spines (dashed spines). Although connectivity is modified, spine density can remain unchanged. The new spines formed following learning tend to occur in clusters (encircled areas) and exhibit a higher probability to become stabilized as persistent spines, introducing a lasting modification of the synaptic network.

Regulation of spine and synapse turnover. One important factor controlling synapse turnover appears to be the balance between excitation and inhibition. Alterations of this balance during critical (or sensitive) periods — that is, developmental time windows of enhanced plasticity — strongly affect the capacity for structural plasticity⁴¹. Furthermore, several recent studies have shown that manipulations that reduce inhibition in adulthood are able to restore visual plasticity to levels comparable to those observed during development^{42,43}. Although it remains unclear how exactly modulation of the excitatory–inhibitory balance can promote or reduce cortical plasticity, part of the effect could implicate changes in synapse dynamics. Consistent with this possibility, spine changes correlate with the capacity for visual plasticity in vivo⁴⁴ and, during development, short-term anaesthesia or administration of drugs that enhance GABAergic inhibition results in rapid and marked changes in spine growth and synapse gain⁴⁵.

Several additional molecular mechanisms have also been reported to modify spine numbers and dynamics. Estrogens, for example, can rapidly shift the balance of spine turnover towards increased growth and stabilization, thus leading to an increase in spine density in the hippocampus^{46,47}. The effect is reversible and probably accounts for the variations in spine density reported during the estrous cycle. Brain-derived nerve growth factor (BDNF) also affects spine formation mechanisms by enhancing both destabilization of spines and spine formation in the cortex and hippocampus, and could thus contribute to some of the activity-dependent regulations of synapse dynamics^{48,49}. The mechanisms through which BDNF influences spine growth are as yet unclear, but could be linked to a regulation of protein synthesis. Thus, PI3K, which interacts with AKT and has functional links with mTOR signaling, also regulates spinogenesis⁵⁰. Furthermore, protein synthesis, mTOR signaling and spine turnover are affected in fragile X mental retardation protein (FMRP) knockout mice, a mouse model of fragile X syndrome⁵¹. A further group of molecular mechanisms affecting spine growth includes proteins implicated in the regulation of the cytoskeleton, such as Rho GTPases and their regulatory proteins. The extent to which some of these factors can diffuse locally could account for the mechanisms of clustered spinogenesis^{52,53}. Notably, RAS, which is activated by LTP induction, has been shown to diffuse locally and promote plasticity in neighbouring spines³⁷. Through its activation of the MAPK pathway and its effects on protein synthesis, it could also locally modulate spine growth. Although substantial progress has been made recently, more work will be needed in order to better understand how precisely these molecular mechanisms control spine turnover.

3.3.3 Distribution of the structural plasticity

Circuit rearrangements can be confined to the neurons involved in the particular learning process, or to neuronal subpopulations within systems involved in the learning process. However, under different circumstances, structural rearrangements can also be induced in a broad range of systems in the brain (for example, upon environmental enrichment, see below). An issue that arises is whether the differences in plasticity distribution reflect different roles of structural plasticity or whether a common logic may underlie these distinct phenomena. In this context, it is useful to take into account that synapse gains and losses related to a particular learning process are mostly specified subsequent to the initial learning event. Accordingly, if memory consolidation upon learning involves the selective stabilization and strengthening of some synapses combined with the weakening and loss of other synapses, the different spatial scales of the structural plasticity may involve the distinction between the potential substrates of memory consolidation, which may be distributed locally or broadly, and the actual substrates of the consolidation, which may be specifically associated with the neurons involved in the particular learning process. Consequently, two crucial issues concern the specificity of the structural changes at the local level and whether more global structural alterations may serve as potential substrates for specific local modifications.

Plasticity within local microcircuits. A remarkable aspect of the recent studies relating learning to changes in dendritic spines and axon terminals is that the structural plasticity could be detected readily using sparse labeling approaches *in vivo*, provided that cortical areas relevant to the particular form of learning were analyzed repeatedly during an appropriate time window. One might expect that changes in synapse numbers that correlate with new learning may only affect a very small fraction of the synapses within a relevant network, and for that reason methods that only sample 0.1–1% of the neurons of a given kind^{1,6,35} may not be adequate to detect such changes. The dramatic detection sensitivity of these structural plasticity studies is probably owing to the fact that these experiments have involved longitudinal analysis of the same large ensembles of synaptic structures, an approach that is far superior to comparisons of synapse groups, which tend to underestimate the extent of the structural plasticity. In addition, the detection of structural changes was probably facilitated by the fact that behavioral learning initially increases the dynamics of a fraction of spine synapses that is larger than the fraction ultimately retained as a structural trace of learning^{11,12,40}. Nevertheless, the detection of synapse remodeling events did not reflect a lack of specificity in the circuit elements involved in the structural plasticity. For

example, in agreement with behavioral observations, structural plasticity in the motor cortex upon learning of a grasping movement was specifically confined to projection neurons driving distal limb muscles and did not affect those driving proximal muscles⁵⁴. The specificity was particularly remarkable considering that the different projection neurons are locally inter-mingled within the primary motor cortex. Notably, the extent of the structural plasticity was correlated with the magnitude of the learned movement⁵⁴. Evidence for specificity was also provided in experiments in which sensory deprivation in the adult produced specific patterns of growth and retraction in cortical axons and dendrites^{55,56}.

In support of the notion that the local structural plasticity was specifically associated with learning, re learning the same task or a second occurrence of the same kind of sensory deprivation did not elicit further plasticity in the same neurons^{11,12,40}. These findings suggest that learning-induced structural plasticity can initially affect a substantial fraction of the neurons involved in the learning, and that less abundant but more persistent alterations reflect 'lasting structural traces' of learning⁴⁰. The number of structural traces of learning that become long lasting may depend on intrinsic processes that regulate plasticity and on the amount of repeated training that triggers memory consolidation and reconsolidation processes. Elucidating the extent to which the new synapses may truly mediate the encoding of memories (that is, whether they represent 'engrams') will require more sophisticated methods to combine structural and functional imaging of synapses in vivo⁵⁷ (see below). Nevertheless, two recent studies have provided some evidence that there may indeed be a direct correspondence between new synapses and engrams in learning. In one study, fear learning and its extinction affected the formation and disappearance of spines within two microns of distance on the same dendrites, suggesting that opposite changes in the numbers of spatially closely related synapses are associated with opposite behavioral outcomes¹⁴. Evidence for specificity was provided by the observation that learning–extinction cycles for different tones, which produced separate regulation behaviorally, were associated with distinct stretches of dendrites¹⁴. In a second study, new spines assembled upon repeated motor learning had a high probability to appear in the close vicinity of spines that had appeared at previous days during the same motor learning process, suggesting a striking correspondence between the gradual encoding of specific new memories and the spatial position of new spines along particular dendrites³⁸.

In addition to alterations at subsets of neurons and synapses, behavioral learning can produce more global alterations in the numbers of specific types of synapses within systems involved in the particular learning. For example, different forms of behavioral learning can lead to up to a doubling in the numbers of excitatory synapses onto fast-spiking inhibitory interneurons in the hippocampus and/or cerebellar cortex (feedforward inhibitory (FFI)

growth)⁵⁸. Using targeted virus-mediated rescue experiments in a β -adducin mutant background deficient in learning-induced synaptogenesis, the same study provided causal evidence that this plasticity is critically important for the behavioural precision of the memory, but not for the memory of the learned association itself⁵⁸. Although the high level of local prevalence of the FFI growth might suggest a lower circuit level specificity for this form of structural plasticity, this may in fact not be the case. Thus, fast-spiking interneurons are thought to detect local levels of circuit excitation through the convergence of large numbers of weak excitatory synapses onto them and to broadcast that signal to most excitatory neurons within their local environment. Accordingly, the broad FFI growth plasticity may be specifically adjusted to the connectivity properties of fast-spiking feedforward excitation targeting cell bodies and proximal dendrites. Whether learning produces additional broadly distributed alterations in defined elements of neuronal circuits remains to be determined.

Plasticity affecting multiple systems and neurons. Several factors have been shown to influence future learning and behavioral outputs by inducing major modifications in the numbers, arrangements and dynamics of synaptic connections. For example, environmental enrichment and estrogen both produce large increases in synapse turnover and synapse numbers at multiple neuronal systems^{18,46,47}. Conversely, stress can reduce synapse numbers in some systems (for example, in the hippocampus), while increasing them in other systems (for example, in the amygdala)⁵⁹. Synapse dynamics and numbers are further influenced by seasonal changes and developmental age⁶⁰. For environmental enrichment, the increased synapse turnover has been causally related to improved learning¹⁸. Common to these influences of external and internal contingencies on structural plasticity is the fact that they do not involve specific learning processes. The structural alterations related to experience, hormones and age are not confined to a few neuronal systems, but their distribution has not yet been investigated in sufficient detail to extract possible patterns. It is possible that these alterations may reflect the properties of the signals that induced them, such as the distribution of hormone receptors and the ways through which novel sensory experience influences circuit function.

Widespread dynamics followed by confined consolidation. How can the presence of broadly distributed structural alterations upon experience and learning be reconciled with the specificity necessary for the structural modifications to selectively reflect learned relationships? It is possible that some of the broad changes in circuit structure affect function in ways that are unrelated to mechanisms of learning. However, many of the alterations as a result of experience, hormones and ageing are likely to affect learning and memory by acting on the same cellular and molecular processes. As discussed in previous sections, LTP and learning are accompanied by enhanced rates of synapse assembly and disassembly

events^{10,61}. Several studies of learning-related synapse dynamics in vivo have provided strong evidence that enhanced dynamics is specifically correlated with new learning in intact birds, rodents and primates, and with recovery after stroke in the human adult^{13,44,59,62,63}. Similar studies have further shown that a subpopulation of new synapses is subsequently stabilized during a process depending on repeated training, which lasts for many days and even weeks^{11-13,63}. A study of how zebra finches learn to sing from a tutor provides a particularly compelling case for the relationship between behavioural learning and synapse turnover¹³. Thus, at the appropriate developmental stage, enhanced spine turnover was detected on sensorimotor neurons involved in the learning, and the learning experience stabilized some of these spines. An age-related decline in spine dynamics was delayed if the birds were raised without a tutor¹³. Furthermore, enhanced learning upon environmental enrichment was dependent on increased gains and losses of synapses¹⁸. These were, in part, provided by the population of additional dynamic synapses that were induced upon enrichment¹⁸. Similar principles seem to apply to the increase in labile synapses induced by oestrogen^{46,47}. It is likely that several types of signals, some acting locally and directly related to new learning, and others acting more globally and related to experience, hormones and age, may all produce alterations in synapse turnover and in the numbers of dynamic synapses that provide potential substrates for learning. The presence of larger numbers of dynamic synapses before learning may facilitate learning, whereas the selective stabilization of small subsets of dynamic synapses upon repeated learning may provide structural traces of learning (FIG. 3). As enhanced learning upon environmental enrichment also depends on synapse loss¹⁸, it is likely that learning also involves the selective elimination of synapse subpopulations.

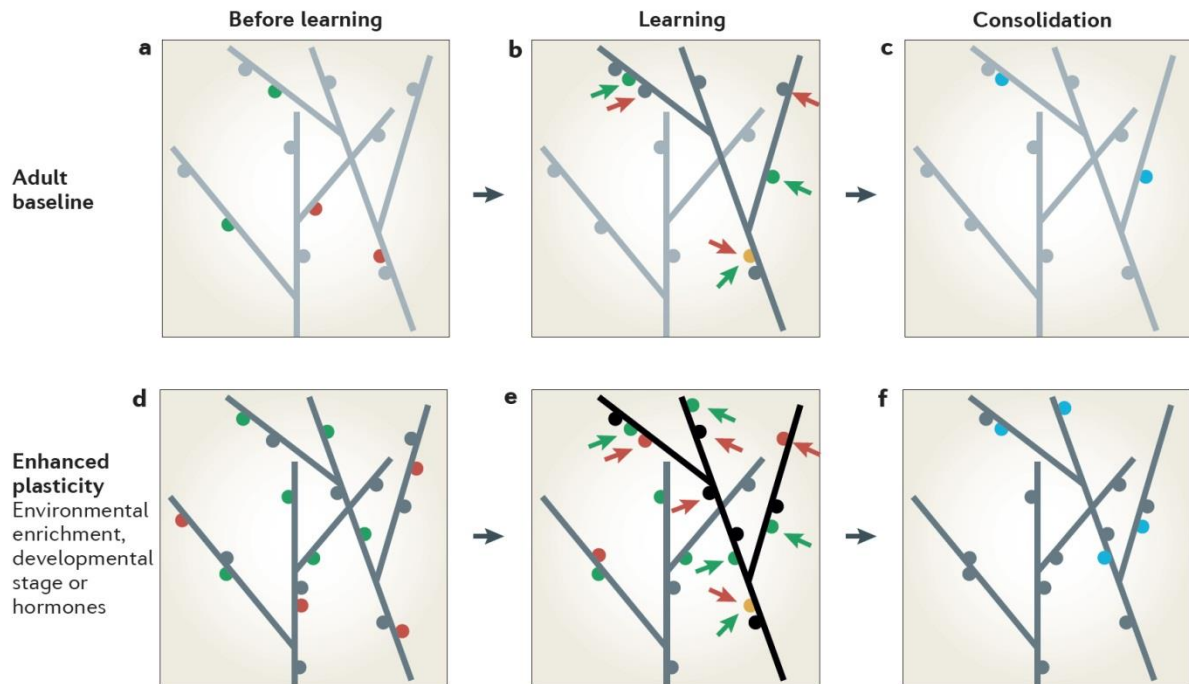


Figure 3: Global and local synapse turnover regulation processes affecting learning and memory.

The schematics represent dendrites of two excitatory neurons and their spine synapses. Increasing plasticity is represented as darker grey tones. Dynamic spines are green (gains) and red (losses); spine changes upon learning are indicated by green and red arrows; orange spines appear upon learning, but do not persist during consolidation; and structural traces of learning upon consolidation include spine gains (blue) and spine losses. a–c | Learning-induced structural plasticity enhances the turnover of subpopulations of new and pre-existing synapses specifically in excitatory neurons involved in the learning (a versus b), and leads to the selective stabilization of some learning-induced spines (c). d–f | Enhanced baseline levels of synapse turnover as a consequence of enrichment, developmental stage or hormones (d versus a) may augment the magnitude of learning-induced spine gains and losses (e versus b), and may lead to more robust structural traces of learning (f versus c). The enhanced structural plasticity baseline levels underlie improved behavioural learning upon enrichment¹⁸, and improved song learning in the presence of a tutor during zebra finch development¹³.

It is conceivable that learning and memory, under a regime of previously enhanced (for example, after environmental enrichment) or reduced widespread synapse dynamics, might be subject to regulation that differs, in part, from that involving synapse dynamics specifically induced during learning. That may, for example, involve distinct molecular compositions and stabilization mechanisms at synapses involved in learning. Such differences could have important implications for how experience (for example, stress) influences internal states and learning, but an adequate investigation of these phenomena will probably depend on the establishment of more sensitive experimental paradigms to study specific relationships between the structure and function of neuronal networks in living animals (see below).

3.3.4 Plasticity regulation

What mechanisms regulate the potential for structural plasticity (metaplasticity) in the brain? Much of the current knowledge and concepts about plasticity regulation are derived from studies of juvenile animals in which time windows of enhanced plasticity facilitate adjustments that are important for adult function^{41,42,64–66}. Whereas most of the studies have investigated plasticity to adjust for malformations such as strabismus or monocular deprivation, a recent study revealed that within the binocular visual cortex, critical period plasticity produces a matching of the orientation preferences of individual neurons in response to each eye⁶⁷. Critical period studies in the visual and auditory system have provided evidence for profound structural plasticity during learning, including the assembly and long-term retention of alternative extra circuits that can be recruited in the adult under appropriate conditions^{64,65,67–69}. Studies in barn owls have revealed that the additional learned circuits that had been assembled during a sensitive period in juvenile birds were turned on and off in the adult through mechanisms distinct from those that turn innate natural circuits on and off (disinhibition versus AMPA/NMDA ratios for the innate and learned circuits, respectively), suggesting that innate and acquired circuit arrangements can be distinguished functionally^{64,65}. At the mechanistic level, the studies of critical periods have uncovered a major role for the maturation of inhibitory circuits, and in particular those established by parvalbumin-positive (PV+) fast-spiking interneurons, in opening and closing plasticity windows^{41,66,70}. Recent findings suggest that similar mechanisms may regulate plasticity in the adult, and that the regulatory mechanisms may in part involve structural plasticity at inhibitory interneurons.

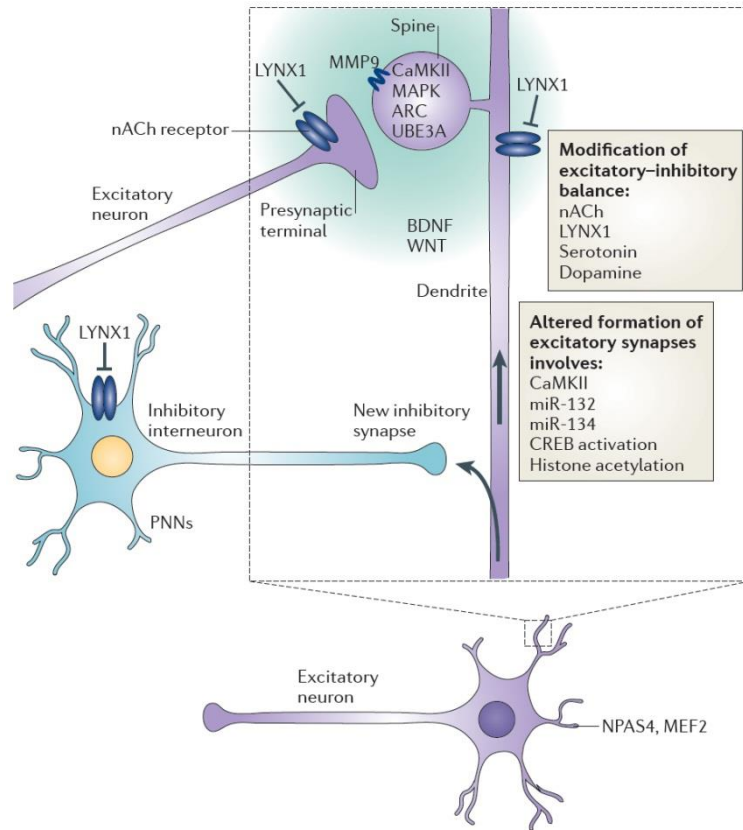


Figure 4: Mechanisms of structural metaplasticity regulation.

The capacity for structural plasticity can be regulated at various levels. Alterations in expression of certain genes in target neurons (shown in purple) and their transport into dendrites and to synapses (straight arrow) results in structural plasticity by mechanisms that may enhance the formation of excitatory synapses (such as calcium/calmodulin kinases (CaMKs), miR-132, CREB (cAMP response element-binding), UBE3A (ubiquitin protein ligase E3A) and histone acetylation) or reduce the formation of such synapses (such as MEF2 (myocyte enhancer factor 2) and miR-134). Expression of the transcription factor NPAS4 (neuronal PAS domain-containing protein 4) promotes the formation of inhibitory synapses (indicated by a curved arrow). Structural plasticity can result from neuromodulatory modifications of the excitatory–inhibitory balance (including the cholinergic system, LYNX1 (Ly-6/neurotoxin-like protein 1), serotonin and dopamine). LYNX1 inhibits nicotinic acetylcholine (nACh) receptors, which can be found presynaptically, on dendrites and around somas. Furthermore, structural plasticity can be achieved through diffusible factors (including brain-derived neurotrophic factor (BDNF) and WNT, indicated by the green shading) that can affect synaptic signalling pathways (such as CaMKII, MAPK (mitogen-activated protein kinase), ARC and UBE3A) or through alterations of the extracellular matrix (matrix metalloprotease 9 (MMP9) and perineuronal nets (PNNs)).

Factors promoting and inhibiting plasticity. Some of the molecular pathways known to regulate plasticity are illustrated in FIG. 4. In most cases, plasticity regulation involves signalling pathways relating neuronal activity to the expression of key activity-regulated genes^{71–73}. Consistent with its central roles in mediating signalling downstream of synaptic activity, calcium has prominent roles in activity-regulated gene expression. One of the genes regulated by calcium is the transcription factor MEF2 (myocyte enhancer factor 2), which reduces excitatory synapse numbers. Genes regulated through MEF2 include the synaptic components ARC and HOMER1, and the neurotrophin BDNF, which augments inhibitory synapse numbers⁷¹. Although many growth factors can enhance plasticity when applied to

cultured neurons or in vivo, only a few of them, particularly BDNF, have been related conclusively to endogenous plasticity regulation under physiological conditions⁷⁴. Strong evidence supports the notion that BDNF signalling has a key role in promoting plasticity, and that this signaling pathway is recruited upon enhanced excitation^{48,49}. Intracellular signaling molecules and pathways relating excitation and BDNF signaling to plasticity include: ARC, MAPK, CaMK, CREB (cAMP response element-binding) activation, histone acetylation and the microRNA miR-132 (REFS 19, 75–82). Mechanisms through which age influences plasticity regulation can involve chromatin remodeling pathways⁸¹. Extracellular factors that facilitate plasticity include the proteases matrix metalloprotease 9 and urokinase-type plasminogen activator⁸³. In addition, WNT signaling can enhance synapse numbers⁸⁴. Further important signaling molecules with a major role in regulating plasticity include the neuromodulators acetylcholine, noradrenaline, serotonin and dopamine. Among them, a particularly strong case has been made for a link between nicotinic cholinergic transmission and enhanced plasticity. Thus, cholinergic transmission is critically important for skill learning and for functional recovery after brain injury^{85–87}.

In addition to enhanced excitation, reduced inhibition augments plasticity under a number of different conditions, including environmental enrichment, the effects of fluoxetine treatments and the reduction of perineuronal nets around the cell body and proximal dendrites of PV+ interneurons^{41,88–90}. Several lines of evidence have directly related reduced inhibition to enhanced plasticity during critical periods and in the adult in rodents^{41,62,90}.

Finally, important recent studies have introduced the notion that the potential for plasticity in the adult may be as robust as that detected in juvenile animals, but that adult plasticity is effectively prevented through ‘brake’ mechanisms⁶². The reduced plasticity in the adult may prevent aberrant plasticity after the formation of lesions and may ensure the transmission of adaptive behaviors learned from conspecifics across generations. In addition to perineuronal nets and myelin-associated inhibitors, which may in part have structural roles, LYNX1 (Ly 6/neurotoxin-like protein 1) has been identified as a specific inhibitor of nicotinic cholinergic signaling that suppresses plasticity in the presence of widespread cholinergic innervation in the adult⁴³. An important transcriptional pathway involving NPAS4 (neuronal PAS domain-containing protein 4) also specifically links excitation to the establishment of a higher number of inhibitory synapses onto activated neurons⁹¹. Furthermore, miR 134 has been identified as a major negative post-transcriptional regulator of plasticity downstream of SIRT1 (NAD-dependent protein deacetylase sirtuin 1) and upstream of CREB⁹².

Inhibitory circuit rearrangements. Whereas most studies of structural plasticity initially focused on excitatory neurons, several recent studies have revealed that structural plasticity

by inhibitory neurons⁹³ precedes that by excitatory neurons and may have a critical role in regulating plasticity during learning. An initial series of studies documented structural plasticity of dendritic tips by GABAergic neurons in adult mouse cortex, with most of the plasticity contained within a superficial strip of layer 2/3 (REFS 94–96). A subsequent study documented pronounced structural plasticity of inhibitory axons upon sensory deprivation, which preceded sprouting by excitatory axons, and several-fold enhanced spine and axonal bouton turnover^{55,56}. Changes in structural plasticity were detected within hours following peripheral lesions, suggesting that they might account for rapid changes in functional plasticity of receptive fields. Furthermore, dramatic changes in structural plasticity by fast-spiking striatal inhibitory neuron axons that specifically target the indirect striatal pathway were detected following lesions that result in dopamine deprivation⁹⁷. Finally, two recent studies in sensory-deprived visual cortex provided evidence that regulation of structural plasticity by inhibitory interneurons may provide permissive conditions for subsequent plasticity by excitatory neurons. One study reported an early loss of spines, thus reducing excitatory inputs onto a subpopulation of inhibitory interneurons (mainly neuropeptide Y-positive), and a subsequent loss of axonal boutons, thus reducing inhibitory output by the same interneurons upon sensory deprivation⁹⁸. The second study reported a loss of excitatory inputs onto inhibitory neurons in layer 2/3 upon visual deprivation⁹⁹. Together, the studies suggest that early structural plasticity in sensory-deprived cortex may lead to a diminished excitatory drive onto inhibitory interneurons, suggesting a possible structural basis for disinhibition and enhanced excitation.

Is it inhibition or excitation? The recent discovery of early structural plasticity at inhibitory interneuron subpopulations preceding plasticity at excitatory neurons suggests a possible conceptual framework to account for how excitation–inhibition balances may regulate short- and long-term structural plasticity in the adult. The mechanisms involved appear to resemble those regulating plasticity during circuit maturation, consistent with the notion that plasticity is controlled in similar ways in young animals and in adults. Instead of focusing on excitatory or inhibitory neurotransmitter levels, or on global levels of excitation and inhibition, this emerging framework addresses plasticity regulation at the circuit level, thus offering possible mechanistic solutions to account for fine-tuned regulation and specificity in learning-related plasticity. Findings discussed in previous sections that may be particularly relevant are: at the level of individual neurons, structural plasticity is augmented by enhanced excitation; reducing inhibition is sufficient to enhance plasticity in the adult; and salient activity (for example, exposure to light after dark rearing) can produce disinhibition of excitatory neurons by activating ‘second layer’ (disinhibiting) inhibitory interneurons, partly through structural plasticity. Accordingly, signals that trigger plasticity may initially reduce the activation of

GABAergic neurons, such as PV+ interneurons that target excitatory neurons; depending on the extent of the plasticity, this may involve recruitment of disinhibitory interneurons and/ or structural plasticity to reduce the connectivity of PV+ interneurons, in turn leading to enhanced excitation and structural plasticity of excitatory neurons (FIG. 5). Targeting inhibitory neuron networks first might have a plasticity-facilitating effect at the network level. The enhanced potential for plasticity could then serve as a basis for more specific synapse remodeling processes at the level of individual excitatory neurons. The validity of the model, the identity of the particular interneuron subpopulations and the circuit mechanisms involved in short- and long-term plasticity regulation processes remain to be determined.

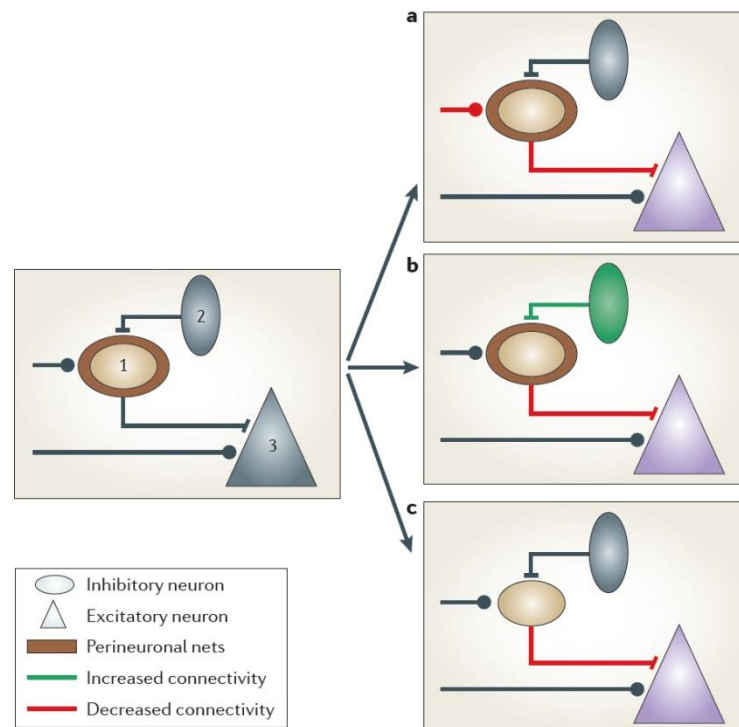


Figure 5: Circuit mechanisms of plasticity regulation.

Left: schematic representing a local circuit arrangement involving two inhibitory neurons (ovals 1 and 2, perisomatic and disinhibiting, respectively) impinging onto one excitatory cell (triangle 3). Circles: excitatory inputs; bars: inhibitory inputs. Right: circuit mechanisms leading to enhanced plasticity. Decreased connectivity (decreased synapse numbers (a,b) or decreased synapse function (c)) is represented by red colours; increased connectivity is represented by green colours. Structural plasticity in the excitatory cell is enhanced (shown in purple) under conditions of decreased excitatory connectivity (a), increased inhibitory connectivity (b) or perineuronal net reduction (c) on the perisomatic interneuron that directly inhibits the excitatory cell. Whereas the three scenarios involving structural plasticity at inhibitory interneurons lead to broad disinhibition of excitatory cells, a direct increase of the excitatory drive onto the excitatory neuron can also enhance plasticity.

3.3.5 From structural plasticity to memories

It is generally assumed that structural plasticity provides a mechanism for long-term storage of memory traces upon learning¹⁰⁰. However, the temporal sequences of events and the regulatory mechanisms relating learning and structural plasticity to long-term memory are still poorly understood. An important aspect involves the temporal delay between the early potentiation of pre-existing synapses, spine growth and synaptogenesis upon learning. Such delays may differ among learning protocols and systems involved. Thus, some studies have suggested that synapses involving new spines or filopodia are assembled within the first 1–3 hours after potentiation¹⁰¹, whereas other studies have provided evidence for delays of 12–18 hours¹⁰². The longer delays provide a potential mechanism to relate learning to the consolidation of memories, for example, during sleep. Such scenarios may enhance the specificity of synapse remodeling processes upon learning by uncoupling contingencies present during learning from the consolidation of new synapses and their integration into memory networks. Further structural plasticity may occur during longer lasting system-level consolidation processes, but experimental evidence for such plasticity is not available yet. Likewise, whether and how memory retrieval and reconsolidation processes involve structural plasticity remains to be determined. Addressing these fundamental issues in learning and memory at the structural level will require the development of more specific and sensitive approaches to investigate circuit and network remodeling processes in vivo, at the level of identified synapse ensembles.

Protein	Function	Synaptic contribution	Disease
ARHGEF6	RAC GEF, regulation of actin cytoskeleton	Synapse formation and maturation	Intellectual disability
CYFIP1	Protein synthesis	Unknown	Fragile X syndrome
DISC1	Scaffold protein	Synapse formation and maturation	Schizophrenia
EPAC2	RAP GEF	Spine maturation	ASD
ERBB4	Receptor tyrosine kinase	Regulation of excitatory transmission	Schizophrenia
FMRP	Protein synthesis	Synapse stabilization	Fragile X syndrome
GABRB3, GABRA5, GABRG3	GABA receptor subunits	Excitation–inhibition balance	ASD
IL1RAPL1	Scaffold protein	Synapse formation	Intellectual disability
Kalirin	RAC GEF, regulation of actin cytoskeleton	Synapse formation and maturation	Schizophrenia, ASD
LIMK1	Protein kinase, actin skeleton	Spine maturation	Williams syndrome, intellectual disability
MINT2	Presynaptic adaptor protein	Neurosecretion	ASD, schizophrenia
Neuregulin 1	Trans-synaptic modulator of ERBB4	Regulation of excitatory transmission	Schizophrenia
Neurexin 1	Presynaptic adhesion molecule	Synapse stabilization	ASD
Neurologin 3, neuroligin 4	Adhesion molecules	Synapse stabilization	ASD
Oligophrenin 1	RhoA GAP, regulation of receptor trafficking	Spine maturation	Intellectual disability
PAK3	Protein kinase, actin cytoskeleton	Synapse formation and stabilization	Intellectual disability
Protocadherins	Adhesion molecules	Unknown	ASD
PSD95	Scaffold protein	Synapse plasticity and stabilization	ASD, schizophrenia
PTEN	Tyrosine phosphatase, protein synthesis	Synapse stabilization	ASD, macrocephaly
RSK2	Protein kinase	Neurosecretion	Intellectual disability
SAP97	Scaffold protein	PSD protein trafficking	ASD, schizophrenia
SHANK2, SHANK3	Scaffold protein	Synapse stabilization	ASD
srGAP3	RAC1 GAP	Unknown	Intellectual disability
SSCAM (also known as MAGi2)	Scaffold protein	Receptor trafficking	Intellectual disability
SynGAP	RAS/RAP/RAC-GAP	Receptor trafficking and actin cytoskeleton	ASD, intellectual disability
TSC1, TSC2	Protein synthesis	Synapse stabilization	Intellectual disability
UBE3A	Protein degradation	Synapse formation	Angelman syndrome, intellectual disability

Table 1: Synaptic proteins with genetic defects that have been associated with developmental psychiatric disorders

Synaptic proteins for which genetic defects (single point mutations, deletions, translocations or copy number variations (CNVs)) have been associated with autism spectrum disorders (ASDs), intellectual disability or schizophrenia. Supporting references can be found in recent reviews^{72,103,114,115}. ARHGEF6, Rho guanine nucleotide exchange factor 6; CYFIP1, cytoplasmic FMR1-interacting protein 1; DISC1, disrupted in schizophrenia 1; EPAC2, Rap guanine nucleotide exchange factor 4; FMRP, fragile X mental retardation protein; IL1RAPL1, interleukin-1 receptor accessory protein-like 1; LIMK1, LIM domain kinase 1; MINT2, MUNC18-interacting protein 2; PAK3, p21-activated kinase 3; PSD, postsynaptic density; PTEN, phosphatase and tensin homologue; RSK2, ribosomal S6 kinase 2; SAP97, synapse-associated protein 97; SHANK, SH3 and multiple ankyrin repeat domains protein; srGAP3, SLIT-ROBO Rho GTPase-activating protein 3; SSCAM, membrane associated guanylate kinase, WW and PDZ domain containing 2; SynGAP, Ras GTPase-activating protein; TSC, tuberous sclerosis; UBE3A, ubiquitin protein ligase E3A.

3.3.6 Synapse remodeling and mental health

The important contribution of structural plasticity to various behavioral learning situations highlights the importance of connectivity remodeling and synapse stabilization as substrates for learning processes and memory retention. Accordingly, any defect in synapse dynamics can be expected to have a significant impact on the development, organization or specificity of synaptic networks. Indeed, the mechanisms regulating synapse dynamics have been implicated in several developmental psychiatric disorders as discussed below.

Synapse rearrangements in disease and upon lesions. Analyses of the synaptic defects associated with a number of synaptic proteins implicated in intellectual disability, autism spectrum disorders or schizophrenia show alterations of synapse structure or numbers (TABLE 1). Consistent with a key role for structural plasticity and the excitation–inhibition balance in controlling circuit maturation, many of the psychiatric conditions manifest during early life. SHANK3 (SH3 and multiple ankyrin repeat domains protein 3), PSD95, synapse-associated protein 97 and ubiquitin protein ligase E3A are involved in excitatory synapse stabilization. FMRP, PTEN (phosphatase and tensin homologue), TSC1 (tuberous sclerosis 1; also known as hamartin) and TSC2 (also known as tuberin) regulate local protein synthesis, possibly affecting mechanisms of synapse stabilization. Several molecules (such as DISC1, kalirin, EPAC2 (also known as RAPGEF4), PAK3 and ARHGAP6 (Rho guanine nucleotide exchange factor 6)) are implicated in signalling through Rho GTPases, and could perturb cytoskeletal functions that regulate spine and synapse dynamics. Finally, MECP2 (methyl-CpG-binding protein 2) and molecules of the neuroligin–neurexin complex appear to be important for regulating the balance between excitation and inhibition and could therefore interfere with spine formation and dynamics¹⁰³. All these observations point to the possibility that alterations of structural plasticity mechanisms may have an important role in these diseases. Consistent with this notion, defects in connectivity between layer 5 cortical neurons have been reported in a mouse model of Rett syndrome¹⁰⁴, and this is associated with important alterations of spine dynamics¹⁰⁵. Other recent evidence from in vivo imaging in a mouse model of fragile X syndrome suggests that synapse dynamics could be exaggerated, leading to an increased proportion of unstable synapses and an excessive remodelling of synaptic circuits^{106,107}. Similarly, mutation of the intellectual disability gene PAK3, which is an effector of the Rho GTPases RAC1 (Ras-related C3 botulinum toxin substrate 1) and CDC42 (cell division control protein 42 homologue), results in excessive spine growth and defects in activity-mediated spine stabilization⁵³. Alterations in synapse dynamics, either through excessive or insufficient rewiring or defects in synapse

stabilization, could perturb the specificity of the mechanisms through which learning shapes the formation of synaptic networks.

Structural plasticity is also important to restore function following lesions. Several recent studies have highlighted the extensive remodeling of both dendritic spines and axons in cortical tissue recovering from stroke or in the visual cortex following lesions^{55,98,108}. Synapse-restructuring-associated growth and pruning correlates with functional changes recapitulating the structural plasticity seen in early development.

3.3.7 Outlook: network structure–function

Studies of structural plasticity related to learning and memory have led to major advances during the past couple of years. First, specific synapse assembly and synapse loss processes have been related conclusively to animal learning, and to structural traces of the learning. How the new synapses contribute to memory is not yet clear⁵⁷, but the current evidence favors the notion that the new synapse arrangements do have specific roles in memory encoding. Second, causality relationships could be established between the new assembly of identified synapses upon learning and the behavioral expression of the learned memories. Third, important mechanisms and principles underlying the regulation of synapse remodeling upon enhanced synaptic activity and learning are being defined at the molecular and cellular level. Among them, an important new insight involves the assembly of new synapses in spatial clusters, suggesting mechanisms of local co regulation for synapses that may involve the same or connected learning-related memories. Finally, recent results suggest first conceptual frameworks to account for plasticity regulation mechanisms at the circuit level.

The emergence of structural plasticity as a growing research area in learning and memory raises new immediate and long-term challenges. Major unresolved mechanistic issues include: defining the relationships between gains and losses of identified individual synapses upon learning and the memory of what was learned at the microcircuit and systems level; identifying causal sequences of events that relate experience and learning to alterations in structural plasticity and the balance between excitation and inhibition, which includes elucidating how structural remodeling of identified inhibitory and excitatory neuron microcircuits impinge on long-term plasticity regulation during development, in the adult and in disease; and relating genes involved in psychiatric conditions to synapse and microcircuit

maturation and remodeling and to the functional consequences of these remodeling processes for system function and animal behaviour.

What will be the probable impact of these new findings for research in neuroscience? The recent advances suggest that structural plasticity processes may be integral components of most aspects of learning and memory. Accordingly, this field of research is likely to have an increasing impact on cognitive neuroscience. The main limitations going forward are of a technical nature. Although functional imaging techniques in intact animals are extremely valuable for uncovering volume alterations in grey matter or axonal projections upon learning or in disease models, they still lack the resolution required to detect structural plasticity at the microcircuit level. Nevertheless, future research will have to tackle network functions at the level of ensembles of individual identified synapses and neurons *in vivo*. Further progress will probably depend on the development of methods to image synapses and their molecular components with high sensitivity and spatiotemporal resolution *in situ*^{109–111}. Exciting recent developments mainly, but not exclusively, based on calcium imaging have achieved sufficient resolution to monitor function at the level of ensembles of spines in the neocortex^{112,113}. Combining such methods *in vivo* and in slice preparations should allow neuroscientists to bridge important gaps between the anatomy of microcircuits, their plasticity and their function. In parallel, modeling efforts will probably be important for the development of testable conceptual frameworks that take into account specific structural rearrangements within realistic neuronal networks. The addition of structural plasticity rules to current functional plasticity models may reveal new behaviors or properties that are important for learning capacity. Finally, targeted manipulations *in situ* — for example, through cellular, but possibly even subcellular, compartment-specific optogenetic methods — will be key in order to establish causal relationships between defined structural alterations in network architecture and network function in behaving animals. Combining cell- and synapse-specific imaging, modelling and optogenetic methods should allow neuroscientists to tackle learning, memory and cognition at the level of defined neuronal circuits.

3.3.8 Bibliography of

“Structural plasticity upon learning: regulations and functions”

1. Holtmaat, A. & Svoboda, K. Experience-dependent structural synaptic plasticity in the mammalian brain. *Nature Rev. Neurosci.* 10, 647–658 (2009).
2. Bourne, J. N. & Harris, K. M. Balancing structure and function at hippocampal dendritic spines. *Annu. Rev. Neurosci.* 31, 47–67 (2008).
3. Kasai, H. et al. Learning rules and persistence of dendritic spines. *Eur J. Neurosci.* 32, 241–249 (2010).
4. Matsuzaki, M., Honkura, N., Ellis-Davies, G. C. & Kasai, H. Structural basis of long-term potentiation in single dendritic spines. *Nature* 429, 761–766 (2004).
5. Tokuoka, H. & Goda, Y. Activity-dependent coordination of presynaptic release probability and postsynaptic GluR2 abundance at single synapses. *Proc. Natl Acad. Sci. USA* 105, 14656–14661 (2008).
6. Holtmaat, A. J. et al. Transient and persistent dendritic spines in the neocortex in vivo. *Neuron* 45, 279–291 (2005).
7. Yuste, R. & Bonhoeffer, T. Morphological changes in dendritic spines associated with long-term synaptic plasticity. *Annu. Rev. Neurosci.* 24, 1071–1089 (2001).
8. Malinow, R. & Malenka, R. C. AMPA receptor trafficking and synaptic plasticity. *Annu. Rev. Neurosci.* 25, 103–126 (2002).
9. Ostroff, L. E., Fiala, J. C., Allwardt, B. & Harris, K. M. Polyribosomes redistribute from dendritic shafts into spines with enlarged synapses during LTP in developing rat hippocampal slices. *Neuron* 35, 535–545 (2002).
10. De Roo, M., Klauser, P. & Muller, D. LTP promotes a selective long-term stabilization and clustering of dendritic spines. *PLoS Biol.* 6, e219 (2008).

This study provides evidence that new spines, upon LTP, tend to be established in clusters, providing a potential mechanism for clustered plasticity specifically upon learning.

11. Xu, T. et al. Rapid formation and selective stabilization of synapses for enduring motor memories. *Nature* 462, 915–919 (2009).

This study, and those in references 12, 13 and 40, show that new spine synapses assembled upon behavioural learning and were maintained for many months in the adult, providing long-lasting traces of learning.

12. Yang, G., Pan, F. & Gan, W. B. Stably maintained dendritic spines are associated with lifelong memories. *Nature* 462, 920–924 (2009).

See comments to reference 11.

13. Roberts, T. F., Tschida, K. A., Klein, M. E. & Mooney, R. Rapid spine stabilization and synaptic enhancement at the onset of behavioural learning. *Nature* 463, 948–952 (2010).

See comments to reference 11.

14. Lai, C. S., Franke, T. F. & Gan, W. B. Opposite effects of fear conditioning and extinction on dendritic spine remodelling. *Nature* 483, 87–91 (2012).

This study provides evidence that learning with opposite behavioural outcomes has opposite consequences on spines (for example, on their appearance and disappearance) within a short stretch of the same dendrite. This suggests a specific relationship between changes in spines and specific aspects of the learning.

15. Lisman, J., Yasuda, R. & Raghavachari, S. Mechanisms of CaMKII action in long-term potentiation. *Nature Rev. Neurosci.* 13, 169–182 (2012).

16. Sacktor, T. C. How does PKM ζ maintain long-term memory? *Nature Rev. Neurosci.* 12, 9–15 (2011).

17. Yamagata, Y. et al. Kinase-dead knock in mouse reveals an essential role of kinase activity of Ca²⁺/calmodulin-dependent protein kinase II α in dendritic spine enlargement, long-term potentiation, and learning. *J. Neurosci.* 29, 7607–7618 (2009).

18. Bednarek, E. & Caroni, P. β -Adducin is required for stable assembly of new synapses and improved memory upon environmental enrichment. *Neuron* 69, 1132–1146 (2011).

This paper provides evidence that enhanced learning upon environmental enrichment depends on both enhanced synapse assembly and disassembly processes.

19. Shepherd, J. D. & Bear, M. F. New views of Arc, a master regulator of synaptic plasticity. *Nature Neurosci.* 14, 279–284 (2011).

20. Costa-Mattioli, M., Sossin, W. S., Klann, E. & Sonenberg, N. Translational control of long-lasting synaptic plasticity and memory. *Neuron* 61, 10–26 (2009).

21. Tanaka, J. et al. Protein synthesis and neurotrophin-dependent structural plasticity of single dendritic spines. *Science* 319, 1683–1687 (2008).

22. Minichiello, L. TrkB signalling pathways in LTP and learning. *Nature Rev. Neurosci.* 10, 850–860 (2009).

23. Bramham, C. R. Local protein synthesis, actin dynamics, and LTP consolidation. *Curr. Opin. Neurobiol.* 18, 524–531 (2008).

24. Honkura, N., Matsuzaki, M., Noguchi, J., Ellis-Davies, G. C. & Kasai, H. The subspine organization of actin fibers regulates the structure and plasticity of dendritic spines. *Neuron* 57, 719–729 (2008).
 25. Cingolani, L. A. & Goda, Y. Actin in action: the interplay between the actin cytoskeleton and synaptic efficacy. *Nature Rev. Neurosci.* 9, 344–356 (2008).
 26. Hayashi-Takagi, A. et al. Disrupted-in Schizophrenia 1 (DISC1) regulates spines of the glutamate synapse via Rac1. *Nature Neurosci.* 13, 327–332 (2010).
 27. Xie, Z. et al. Kalirin 7 controls activity-dependent structural and functional plasticity of dendritic spines. *Neuron* 56, 640–656 (2007).
 28. Ehrlich, I., Klein, M., Rumpel, S. & Malinow, R. PSD 95 is required for activity-driven synapse stabilization. *Proc. Natl Acad. Sci. USA* 104, 4176–4181 (2007).
 29. Ripley, B., Otto, S., Tiglio, K., Williams, M. E. & Ghosh, A. Regulation of synaptic stability by AMPA receptor reverse signaling. *Proc. Natl Acad. Sci. USA* 108, 367–372 (2011).
 30. Wittenmayer, N. et al. Postsynaptic Neuroligin1 regulates presynaptic maturation. *Proc. Natl Acad. Sci. USA* 106, 13564–13569 (2009).
 31. Mendez, P., De Roo, M., Poglia, L., Klausner, P. & Muller, D. N cadherin mediates plasticity-induced long-term spine stabilization. *J. Cell Biol.* 189, 589–600 (2010).
 32. Yuzaki, M. Cbln1 and its family proteins in synapse formation and maintenance. *Curr. Opin. Neurobiol.* 21, 215–220 (2011).
 33. Trachtenberg, J. T. et al. Long-term in vivo imaging of experience-dependent synaptic plasticity in adult cortex. *Nature* 420, 788–794 (2002).
 34. Grutzendler, J., Kasthuri, N. & Gan, W. B. Long-term dendritic spine stability in the adult cortex. *Nature* 420, 812–816 (2002).
 35. Holtmaat, A., Wilbrecht, L., Knott, G. W., Welker, E. & Svoboda, K. Experience-dependent and cell-type-specific spine growth in the neocortex. *Nature* 441, 979–983 (2006).
- This study provides evidence for enhanced spine turnover and stabilization of some labile spines upon sensory deprivation in the mouse barrel cortex.**
36. Engert, F. & Bonhoeffer, T. Dendritic spine changes associated with hippocampal long-term synaptic plasticity. *Nature* 399, 66–70 (1999).
 37. Harvey, C. D., Yasuda, R., Zhong, H. & Svoboda, K. The spread of Ras activity triggered by activation of a single dendritic spine. *Science* 321, 136–140 (2008).
 38. Fu, M., Yu, X., Lu, J. & Zuo, Y. Repetitive motor learning induces coordinated formation of clustered dendritic spines in vivo. *Nature* 483, 92–95 (2012).

Repeated motor learning leads to the formation of new spines adjacent to spines that had formed during training on the same task. By contrast, ‘non-related spines’ avoid forming in the vicinity of

previous spines. Furthermore, spine neighbours are selectively stabilized. Like reference 14, this study supports the notion that spatially close spines encode functionally related memories.

39. Kleindienst, T. Winnubst, J., Roth-Alpermann, C., Bonhoeffer, T. & Lohmann, C. Activity-dependent clustering of functional synaptic inputs on developing hippocampal dendrites. *Neuron* 72, 1012–1024 (2011).

40. Hofer, S. B., Mrsic-Flogel, T. D., Bonhoeffer, T. & Hubener, M. Experience leaves a lasting structural trace in cortical circuits. *Nature* 457, 313–317 (2009).

See comments to reference 11.

41. Hensch, T. K. Critical period plasticity in local cortical circuits. *Nature Rev. Neurosci.* 6, 877–888 (2005).

42. Bavelier, D., Levi, D. M., Li, R. W., Dan, Y. & Hensch, T. K. Removing brakes on adult brain plasticity: from molecular to behavioral interventions. *J. Neurosci.* 30, 14964–14971(2010).

43. Morishita, H., Miwa, J. M., Heintz, N. & Hensch, T. K. Lynx1, a cholinergic brake, limits plasticity in adult visual cortex. *Science* 330, 1238–1240 (2010).

The endogenous negative regulator of nicotinic cholinergic transmission LYNX1 functions as an inhibitor of cortical plasticity in the adult.

44. Keck, T. et al. Massive restructuring of neuronal circuits during functional reorganization of adult visual cortex. *Nature Neurosci.* 11, 1162–1167 (2008).

This study provides evidence for a major enhancement of structural plasticity leading to replacement of most spine synapses during functional reorganization in a deprived visual cortex.

45. De Roo, M. et al. Anesthetics rapidly promote synaptogenesis during a critical period of brain development. *PLoS ONE* 4, e7043 (2009).

46. Kramar, E. A. et al. Cytoskeletal changes underlie estrogen's acute effects on synaptic transmission and plasticity. *J. Neurosci.* 29, 12982–12993 (2009).

47. Mendez, P., Garcia-Segura, L. M. & Muller, D. Estradiol promotes spine growth and synapse formation without affecting pre-established networks. *Hippocampus* 21, 1263–1267 (2010).

In hippocampal slice cultures, oestradiol reversibly promotes the assembly of new spine synapses without influencing the turnover of pre-existing synapses.

48. Horch, H. W., Kruttgen, A., Portbury, S. D. & Katz, L. C. Destabilization of cortical dendrites and spines by BDNF. *Neuron* 23, 353–364 (1999).

49. Horch, H. W. & Katz, L. C. BDNF release from single cells elicits local dendritic growth in nearby neurons. *Nature Neurosci.* 5, 1177–1184 (2002).

50. Cuesto, G. et al. Phosphoinositide-3 kinase activation controls synaptogenesis and spinogenesis in hippocampal neurons. *J. Neurosci.* 31, 2721–2733 (2011).

51. Sharma, A. et al. Dysregulation of mTOR signaling in fragile X syndrome. *J. Neurosci.* 30, 694–702 (2010).

52. Cerri, C. et al. Activation of rho GTPases triggers structural remodeling and functional plasticity in the adult rat visual cortex. *J. Neurosci.* 31, 15163–15172 (2011).

53. Dubos, A. et al. Alteration of synaptic network dynamics by the intellectual disability protein PAK3. *J. Neurosci.* 32, 519–527 (2012).

54. Wang, L., Conner, J. M., Rickert, J. & Tuszynski, M. H. Structural plasticity within highly specific neuronal populations identifies a unique parcellation of motor learning in the adult brain. *Proc. Natl Acad. Sci. USA* 108, 2545–2550 (2011).

Structural plasticity associated with learning of a forelimb skilled grasping task in adult rats is restricted to upper motor neurons controlling distal but not proximal forelimb musculature within the same area of the primary motor cortex.

55. Yamahachi, H., Marik, S. A., McManus, J. N., Denk, W. & Gilbert, C. D. Rapid axonal sprouting and pruning accompany functional reorganization in primary visual cortex. *Neuron* 64, 719–729 (2009).

56. Marik, S. A., Yamahachi, H., McManus, J. N., Szabo, G. & Gilbert, C. D. Axonal dynamics of excitatory and inhibitory neurons in somatosensory cortex. *PLoS Biol.* 8, e1000395 (2010).

Patterns of excitatory and inhibitory structural plasticity within deprived and non-deprived barrels upon whisker plucking in mice suggest a structural basis for topographic remapping upon sensory deprivation.

57. Hubener, M. & Bonhoeffer, T. Searching for engrams. *Neuron* 67, 363–371 (2010).

58. Ruediger, S. et al. Learning-related feedforward inhibitory connectivity growth required for memory precision. *Nature* 473, 514–518 (2011).

The study establishes a causal relationship between increased structural connectivity onto PV interneurons by mossy fibres in hippocampal CA3 and the precision of memory upon behavioural learning.

59. McEwen, B. S. The ever-changing brain: cellular and molecular mechanisms for the effects of stressful experiences. *Dev. Neurobiol.* 26 Aug 2011 (doi:10.1002/dneu.20968).

60. De Groof, G. et al. Structural changes between seasons in the songbird auditory forebrain. *J. Neurosci.* 29, 13557–13565 (2009).

61. Becker, N., Wierenga, C. J., Fonseca, R., Bonhoeffer, T. & Nagerl, U. V. LTD induction causes morphological changes of presynaptic boutons and reduces their contacts with spines. *Neuron* 60, 590–597 (2008).

62. Tropea, D., Majewska, A. K., Garcia, R. & Sur, M. Structural dynamics of synapses in vivo correlate with functional changes during experience-dependent plasticity in visual cortex. *J. Neurosci.* 30, 11086–11095 (2010).

63. Yu, X. & Zuo, Y. Spine plasticity in the motor cortex. *Curr. Opin. Neurobiol.* 21, 169–174 (2011).

64. Knudsen, E. I. Instructed learning in the auditory localization pathway of the barn owl. *Nature* 417, 322–328 (2002).

65. Knudsen, E. I. Sensitive periods in the development of the brain and behavior. *J. Cogn. Neurosci.* 16, 1412–1425 (2004).

66. Yazaki-Sugiyama, Y., Kang, S., Cateau, H., Fukai, T. & Hensch, T. K. Bidirectional plasticity in fast-spiking GABA circuits by visual experience. *Nature* 462, 218–221 (2009).

This study provides evidence for inhibitory circuit plasticity that is consistent with spike-time-dependent plasticity involving PV interneurons in the deprived visual cortex.

67. Wang, B. S., Sarnaik, R. & Cang, J. Critical period plasticity matches binocular orientation preference in the visual cortex. *Neuron* 65, 246–256 (2010).

This study provides evidence for a key role of critical period plasticity to adjust binocular receptive field properties in the visual cortex.

68. Linkenhoker, B. A., von der Ohe, C. G. & Knudsen, E. I. Anatomical traces of juvenile learning in the auditory system of adult barn owls. *Nature Neurosci.* 8, 93–98 (2005).

This study and the one in reference 69 provide evidence for the establishment and long-lasting retention of adaptive extra circuits upon juvenile learning in barn owls and mice.

69. Hofer, S. B., Mrcic-Flogel, T. D., Bonhoeffer, T. & Hubener, M. Prior experience enhances plasticity in adult visual cortex. *Nature Neurosci.* 9, 127–132 (2006).

See comments to reference 68.

70. Southwell, D. G., Froemke, R. C., Alvarez-Buylla, A., Stryker, M. P. & Gandhi, S. P. Cortical plasticity induced by inhibitory neuron transplantation. *Science* 327, 1145–1148 (2010).

Transplanted immature interneurons produce a second critical period window in the visual cortex of young mice, arguing for cell-intrinsic mechanisms of critical period regulation driven by interneuron maturation.

71. Flavell, S. E. & Greenberg, M. E. Signaling mechanisms linking neuronal activity to gene expression and plasticity in the nervous system. *Ann. Rev. Neurosci.* 31, 563–590 (2008).

72. West, A. E. & Greenberg, M. E. Neuronal activity-regulated gene transcription in synapse development and cognitive function. *Cold Spring Harb. Perspect. Biol.* 3, a005744 (2011).

73. Leslie, J. H. & Nedivi, E. Activity-regulated genes as mediators of neural circuit plasticity. *Prog. Neurobiol.* 94, 223–237 (2011).

74. Berardi, N., Pizzorusso, T., Ratto, G. M. & Maffei, L. Molecular basis of plasticity in the visual cortex. *Trends Neurosci.* 26, 369–378 (2003).

75. Dityatev, A. & Rusakov, D. A. Molecular signals of plasticity at the tetrapartite synapse. *Curr. Opin. Neurobiol.* 21, 353–359 (2011).
76. Jourdain, P., Fukunaga, K. & Muller, D. Calcium/ calmodulin-dependent protein kinase II contributes to activity-dependent filopodia growth and spine formation. *J. Neurosci.* 23, 10645–10649 (2003).
77. McCurry, C. L. et al. Loss of Arc renders the visual cortex impervious to the effects of sensory experience or deprivation. *Nature Neurosci.* 13, 450–457 (2010).
78. Mellios, N. et al. miR 132, an experience-dependent microRNA, is essential for visual cortex plasticity. *Nature Neurosci.* 14, 1240–1242 (2011).
79. Tognini, P., Putignano, E., Coatti, A. & Pizzorusso, T. Experience-dependent expression of miR 132 regulates ocular dominance plasticity. *Nature Neurosci.* 14, 1237–1239 (2011).
80. Peleg, S. et al. Altered histone acetylation is associated with age-dependent memory impairment in mice. *Science* 328, 753–756 (2010).
81. Putignano, E. et al. Developmental downregulation of histone posttranslational modifications regulates visual cortical plasticity. *Neuron* 53, 747–759 (2007).
82. Foscari, S. et al. Experience-dependent plasticity and modulation of growth regulatory molecules at central synapses. *PLoS ONE* 6, e16666 (2011).
83. Michaluk, P. et al. Matrix metalloproteinase 9 controls NMDA receptor surface diffusion through integrin β 1 signaling. *J. Neurosci.* 29, 6007–6012 (2009).
84. Gogolla, N., Galimberti, I., Deguchi, Y. & Caroni, P. Wnt signaling mediates experience-related regulation of synapse numbers and mossy fiber connectivities in the adult hippocampus. *Neuron* 62, 510–525 (2009).
85. Conner, J. M., Chiba, A. A. & Tuszynski, M. H. The basal forebrain cholinergic system is essential for cortical plasticity and functional recovery following brain injury. *Neuron* 46, 173–179 (2005).
86. Conner, J. M., Kulczycki, M. & Tuszynski, M. H. Unique contributions of distinct cholinergic projections to motor cortical plasticity and learning. *Cereb. Cortex* 20, 2739–2748 (2010).
87. Ramanathan, D., Tuszynski, M. H. & Conner, J. M. The basal forebrain cholinergic system is required specifically for behaviorally mediated cortical map plasticity. *J. Neurosci.* 29, 5992–6000 (2009).
88. Maffei, A., Lambo, M. E. & Turrigiano, G. G. Critical period for inhibitory plasticity in rodent binocular V1. *J. Neurosci.* 30, 3304–3309 (2010).
89. Maya Vetencourt, J. F. et al. The antidepressant fluoxetine restores plasticity in the adult visual cortex. *Science* 320, 385–388 (2008).
90. Sale, A. et al. Environmental enrichment in adulthood promotes amblyopia recovery through a reduction of intracortical inhibition. *Nature Neurosci.* 10, 679–681 (2007).

91. Lin, Y. et al. Activity-dependent regulation of inhibitory synapse development by Npas4. *Nature* 455, 1198–1204 (2008).

This study identifies the transcription factor NPAS4 as a key activity-dependent regulator of inhibitory synaptogenesis onto excitatory neurons.

92. Gao, J. et al. A novel pathway regulates memory and plasticity via SIRT1 and miR 134. *Nature* 466, 1105–1109 (2010).

93. Chen, J. L. & Nedivi, E. Neuronal structural remodeling: is it all about access? *Curr. Opin. Neurobiol.* 20, 557–562 (2010).

94. Lee, W. C. et al. Dynamic remodeling of dendritic arbors in GABAergic interneurons of adult visual cortex. *PLoS Biol.* 4, e29 (2006).

The first live imaging study of inhibitory dendritic arbor structural plasticity in the adult mouse visual cortex.

95. Lee, W. C. et al. A dynamic zone defines interneuron remodeling in the adult neocortex. *Proc. Natl Acad. Sci. USA* 105, 19968–19973 (2008).

96. Chen, J. L., Flanders, G. H., Lee, W. C., Lin, W. C. & Nedivi, E. Inhibitory dendrite dynamics as a general feature of the adult cortical microcircuit. *J. Neurosci.* 31, 12437–12443 (2011).

97. Gittis, A. H. et al. Rapid target-specific remodeling of fast-spiking inhibitory circuits after loss of dopamine. *Neuron* 71, 858–868 (2011).

See comment to reference 98.

98. Keck, T. et al. Loss of sensory input causes rapid structural changes of inhibitory neurons in adult mouse visual cortex. *Neuron* 71, 869–882 (2011).

This study, and the studies in references 97 and 99, provide evidence for rapid and pronounced structural plasticity of inhibitory circuitry upon deafferentation in the adult cortex and striatum.

99. Chen, J. L. et al. Structural basis for the role of inhibition in facilitating adult brain plasticity. *Nature Neurosci.* 14, 587–594 (2011).

See comment to reference 98.

100. Bailey, C. H. & Kandel, E. R. Synaptic remodeling, synaptic growth and the storage of long-term memory in Aplysia. *Prog. Brain Res.* 169, 179–198 (2008).

101. Zito, K., Scheuss, V., Knott, G., Hill, T. & Svoboda, K. Rapid functional maturation of nascent dendritic spines. *Neuron* 61, 247–258 (2009).

102. Nagerl, U. V., Kostinger, G., Anderson, J. C., Martin, K. A. & Bonhoeffer, T. Protracted synaptogenesis after activity-dependent spinogenesis in hippocampal neurons. *J. Neurosci.* 27, 8149–8156 (2007).

103. Penzes, P., Cahill, M. E., Jones, K. A., VanLeeuwen, J. E. & Woolfrey, K. M. Dendritic spine pathology in neuropsychiatric disorders. *Nature Neurosci.* 14, 285–293 (2011).
104. Dani, V. S. & Nelson, S. B. Intact long-term potentiation but reduced connectivity between neocortical layer 5 pyramidal neurons in a mouse model of Rett syndrome. *J. Neurosci.* 29, 11263–11270 (2009).
105. Landi, S. et al. The short-time structural plasticity of dendritic spines is altered in a model of Rett syndrome. *Sci. Rep.* 1, 45 (2011).
106. Pan, F., Aldridge, G. M., Greenough, W. T. & Gan, W. B. Dendritic spine instability and insensitivity to modulation by sensory experience in a mouse model of fragile X syndrome. *Proc. Natl Acad. Sci. USA* 107, 17768–17773 (2010).
107. Cruz-Martin, A., Crespo, M. & Portera-Cailliau, C. Delayed stabilization of dendritic spines in fragile X mice. *J. Neurosci.* 30, 7793–7803 (2010).
108. Brown, C. E., Li, P., Boyd, J. D., Delaney, K. R. & Murphy, T. H. Extensive turnover of dendritic spines and vascular remodeling in cortical tissues recovering from stroke. *J. Neurosci.* 27, 4101–4109 (2007).
109. Lang, S. B., Bonhoeffer, T. & Lohmann, C. Simultaneous imaging of morphological plasticity and calcium dynamics in dendrites. *Nature Protoc.* 1, 1859–1864 (2006).
110. Komiyama, T. et al. Learning-related fine-scale specificity imaged in motor cortex circuits of behaving mice. *Nature* 464, 1182–1186 (2010).
111. Brown, C. E., Aminoltejadi, K., Erb, H., Winship, I. R. & Murphy, T. H. In vivo voltage-sensitive dye imaging in adult mice reveals that somatosensory maps lost to stroke are replaced over weeks by new structural and functional circuits with prolonged modes of activation within both the peri-infarct zone and distant sites. *J. Neurosci.* 29, 1719–1734 (2009).
112. Chen, X., Leischner, U., Rochefort, N. L., Nelken, I. & Konnerth, A. Functional mapping of single spines in cortical neurons in vivo. *Nature* 475, 501–505 (2011).
- This live calcium imaging study in a mouse cortex provides a first view of spine ensemble function in situ.**
113. Jia, H., Rochefort, N. L., Chen, X. & Konnerth, A. In vivo two-photon imaging of sensory-evoked dendritic calcium signals in cortical neurons. *Nature Protoc.* 6, 28–35 (2011).
114. Miles, J. H. Autism spectrum disorders — a genetics review. *Genet. Med.* 13, 278–294 (2011).
115. Mitchell, K. J. The genetics of neurodevelopmental disease. *Curr. Opin. Neurobiol.* 21, 197–203 (2011).

4. Results

4.1

A microcircuit module to regulate plasticity and learning in the adult.

Flavio Donato and Pico Caroni

Unpublished work

4.1.1 Summary

Behavioral learning involves sensory perception of new information from the environment, the establishment of new associations related to goals, and corresponding long-lasting behavioral alterations that underlie the formation of a memory trace. The wiring pattern and physiological properties of cortical microcircuits confer to them the ability to carry out the computation needed at each step of the process of memory formation (Bourne and Harris, 2008, Hubener and Bonhoeffer, 2012); moreover, experience produces long-lasting alterations of both connectivity and physiology at identified synapses impinging on neurons recruited by the task (for a review, see introduction), which are thought to be the molecular correlate of learning and memory (Hubener and Bonhoeffer, 2012). Yet the extent to which cortical microcircuit might display different configuration which are suited to exploit the sequence of perception, computation and memory formation is an open question in neurobiology. Here, we take advantage of the hippocampal microcircuit to study how experience alters the network configuration to regulate plasticity and learning. We focus our analysis on the network of Parvalbumin expressing interneurons for their role in regulating plasticity during development: hence, we found that experience can modulate the PV network in opposite ways, with different impact on structural plasticity and further learning. Environmental enrichment induced a net increase in the density of inhibitory synapses onto PV neurons (disinhibition), which in turn produced a modulation of the level of PV expression intensity in single neurons enhancing the fraction of neurons in the network that express low levels of PV; the modulation of the PV network distribution was causally linked to an overall enhancement of structural plasticity and further learning, thereby defining a “Plastic State” for cortical microcircuits. In contrast, contextual fear conditioning induced a net increase in the density of excitatory synapses onto PV interneurons (feedforward inhibition), which in turn produced a modulation of the level of PV expression intensity in single neurons enhancing the fraction of neurons in the network that express high levels of PV; the modulation of the PV network distribution was causally linked to an overall decrease of structural plasticity and learning performances, thereby defining a “Crystallized State” for cortical microcircuits.

Surprisingly, complex “incremental” forms of learning exploited a sequence of states during training favoring the Plastic State during learning, to shift to the Crystallized State upon learning completion. The transition to the plastic state was induced via the recruitment of a dedicated microcircuit module which enhanced disinhibitory connectivity produced by VIP positive interneurons onto PV cells: the modulation of this pathway was necessary and

sufficient to modulate learning in the hippocampus upon learning of the Morris water maze, but the same module was recruited in motor cortex upon rotarod learning.

In conclusion, we show evidence that supports a mechanism by which changes in connectivity impinging onto PV neurons can modulate the configuration of the PV network to define states of enhanced or reduced cognitive performance and structural plasticity in cortical microcircuits. Moreover, we show that incremental forms of learning require the establishment of a first Plastic state based on the recruitment of a dedicated VIP-PV disinhibitory microcircuit module that might support exploration during learning; then, enhancement of FFI connectivity from a specific input source mediates the transition to the Crystallized state that might support exploitation upon learning completion.

4.1.2 Introduction

Behavioral learning involves sensory perception of new information from the environment, the establishment of new associations related to goals, and corresponding long-lasting behavioral alterations that underlie the formation of a memory trace. The wiring pattern and physiological properties of cortical microcircuits enable them to carry out the computation needed at each step of the process of memory formation (Bourne and Harris, 2008, Hubener and Bonhoeffer, 2012); moreover, experience produces long-lasting alterations of both connectivity and physiology at identified synapses impinging on neurons recruited by the task (for a review, see introduction), which are thought to be the molecular correlate of learning and memory (Hubener and Bonhoeffer, 2010). Yet the extent to which cortical microcircuits might display different configuration which are suited to exploit the sequence of perception, computation and memory formation is an open question in neurobiology.

The existence of different configurations upon learning phases might be related to their different requirements: machine learning algorithms pose that reinforcement learning consists of a tradeoff between the exploration of new combinations or strategies, which involve gathering information about the task or the environment, and the exploitation of previously acquired knowledge to solve the task (for further reading, see the problem of the Multi-Armed bandit in Game theory). Therefore, cortical microcircuits might go through a series of configurations which support the specific requirement of each phase, thereby optimizing the learning process: indeed, many reports pose that, at a structural microcircuit level, learning can be organized in distinguishable phases which implement synapse formation early during learning, to produce synapse elimination later on (Roberts et al., 2010, Hofer SB et al., 2008, Yang et al., 2009;). These reports therefore pose that structural plasticity might be tightly and differentially regulated during learning.

The potential for plasticity that cortical microcircuits experience is not equal during the life of the animals. The pioneer work of Hubel and Wiesel in the 60s, and the sequential contribution of many labs worldwide, has shown how plasticity is enhanced during “critical periods” of development when cortical microcircuits are able to autonomously overcome external perturbations of the proper development (i.e., the development of the binocular region in the cat visual cortex upon monocular deprivation). Recent works have shown that the temporal extent of this enhanced plasticity, which is signaled by the opening and closure of the critical period, is tightly regulated by the maturation of the inhibitory component of cortical microcircuits: hence, the maturation of perisomatic inhibition exerted by PV+

interneurons would define the critical period (Hensch, 2005; Sugiyama et al., 2008, Southwell et al., 2010). Interestingly, interventions in the adult that have been showed to reinstate a period of enhanced plasticity which molecularly might converge on the same pathways exploited during development (Pizzorusso et al., 2002, Fazzari et al., 2010), directly target the PV inhibitory component of cortical microcircuits. It has indeed been shown that enzymatic digestion of perineuronal nets via topical application of the enzyme Chondroitinase ABC are able to restore plasticity in the visual system (Pizzorusso et al., 2002); to which extent this form of plasticity is similar to the developmentally regulated critical periods remain to be determined. Nevertheless, experiments in other model organisms (for example the barn owl visual system) have clearly demonstrated that even adult microcircuit are capable of elevated plasticity without external manipulations, although reaching that state proved to be more difficult after critical period ending (deBello and Knudsen, 2004).

Maturation of PV interneurons is tightly coupled to the maturation of excitatory and inhibitory connectivity upon these interneurons, for which the opening of the critical period would underlie strong inhibitory drive upon their dendrites, while the end of the critical period would be accompanied by a net increase in the excitatory connectivity as well as the formation of thick and organized perineuronal nets of chondroitin-sulfate proteoglycan impinging on PV basket cells. In addition, the process of interneuron maturation during development might also underlie important features of learning: previous studies in zebra finches have posed that song learning (which in birds is mediated by the exposure of the young males to the singing of an adult tutor) coincides with the maturation of PV+ interneurons in the area which is critically involved in the process (HVC, REF). Therefore, the formation of PNNs around PV interneurons would signal the closure of a period of learning in which the bird is able to learn to sing by practicing the proper song it heard from the tutor via a trial-and-error process, to crystallize the proper repetition of syllables that constitute the mature song. Importantly, if birds are raised in isolation and never listen to the tutor, PV interneurons in HVC never develop the proper extent of perineuronal nets. Moreover, in an elegant study published last year, Ruediger S et al., have demonstrated that learning in the adult mice is accompanied by a similar change in the connectivity impinging onto PV interneurons both in the hippocampus and the cerebellar cortex: here, learning completion would produce an increase in the number of excitatory synapses impinging onto fast-spiking interneurons via the formation of filopodial synapses from mossy fiber terminals. The extent of filopodial growth was correlated to, and necessary for, memory precision upon learning (Ruediger S et al., 2011).

Here, we hypothesize that the parvalbumin network might undergo structural modification upon experience that underlies states of enhanced or reduced plasticity and learning in adult

microcircuits. Hence, we study the structural changes induced by environmental enrichment (which is known to induce an enhancement of cognitive performances and learning) and contextual fear conditioning (which induces an increase in excitatory connectivity upon parvalbumin interneurons), taking the hippocampal CA3 as a model microcircuit; then, we determine how incremental learning might exploit the PV network to implement exploration and exploitation in the hippocampus and cortex, and which elements of the cortical microcircuits are recruited to produce transitions among states.

4.1.3 Results:

Parvalbumin+ interneuron network state regulates plasticity and learning.

In order to investigate the existence of microcircuit configurations favoring plasticity or crystallization, we tested how experience-induced microcircuit rearrangements would influence structural plasticity and further learning. We took the CA3 area of the hippocampus as a model microcircuit, due to its critical involvement in incidental learning, and the defined configurations in which experience shapes connectivity on excitatory and inhibitory neurons in the area (Galimberti et al., 2006; Bednarek and Caroni, 2011; Ruediger et al., 2011): here, environmental enrichment (EE) is able to increase performances in various set of learning paradigms, and to enhance structural plasticity (Bednarek and Caroni, 2011); on the other hand, an hippocampus-dependent pavlovian-conditioning task (contextual fear conditioning, cFC) shapes the CA3 microcircuit with the increase of excitatory connectivity onto parvalbumin-expressing interneurons (feed-forward inhibition, FFI. Ruediger et al., 2011). Therefore, we analyzed how previous experience would impact on further incidental learning using the Novel Object Recognition (NOR) task as readout of CA3 microcircuit configuration. In this task, mice are allowed to interact with a novel and a familiar object, and their ability to discriminate between them is quantified as a function of time spent with each. At a microcircuit level, discrimination index is critically linked to active zones turnover in mossy fiber terminals (MFTs) (Bednarek and Caroni, 2011).

As previously reported (Bednarek and Caroni, 2011), EE enhanced discrimination index in NOR (Discrimination Index Control: 0.33, Enrichment: 0.52, $p < 0.01$. Fig 1A) and active-zone turnover at MFTs (Difference to controls: 6h $p < 0.01$; 12h: $p < 0.05$; 24h: $p < 0.001$. FIG 1B); in stark contrast, cFC produced a significant decrease in discrimination (DI: 0.15, $p < 0.05$. FIG 1A) accompanied by slower synapse turnover (Difference to controls: 12h $p < 0.05$; 24h $p < 0.001$ FIG 1B). To specifically rule out any stress-related effect on incidental learning due to the conditioning protocol, we performed a slightly modified task that resulted in fear learning without involvement of the hippocampus (FC in the dark, Ruediger et al., 2012). Mice conditioned in the dark showed no significant difference to controls in the NOR, strongly associating incidental learning performances to FFI increase upon parvalbumin expressing interneurons (Discrimination index: 0.36, non-significant. Fig 1A). Thus, to analyze how experience could affect the network of Parvalbumin (PV) expressing

interneurons in CA3, we looked at the intrinsic structural properties of these neurons upon enrichment and fear conditioning (see Materials and methods). EE induced a robust increase in the fractions of PV IN that exhibited low level of PV expression (“Low PV”, controls: 2%; enrichment: 35%. $P < 0.001$ Fig 1C and D), while cFC resulted in more high-expressing PV IN (“High PV”, controls: 19%, conditioning: 52%. $P < 0.001$. Fig 1C and D). Moreover, PV expression in single interneurons could be correlated to GAD-67 (an enzyme that critically determines the levels of GABA synthesis, CIT, Suppl fig 1. Pearson correlation: 0.92), and to firing frequency upon 300pA stimulation in acute slices (with higher firing frequency for higher PV content, Manxia Zhao Unpublished work). Taken together, these data indicate that experience regulates the state of the PV interneurons network along with the regulation of structural plasticity and further learning. To determine whether rearrangements in the PV IN network are sufficient to enhance NOR performance and AZ turnover, we infused mice topically in CA3 with Chondroitinase ABC and BDNF via chronically implanted cannulas. While the first is commonly used to shave perineuronal nets around PV+ interneurons and reopen plasticity in the adult (Pizzorusso et al., 2002), the second activates pathways involved in PV IN maturation during development (Huang et al., 1999) (a period when PV, GAD expression, and firing frequency are known to change in defined directions, He et al., 2010). Both treatments were sufficient to alter the state of PV IN network in the same way and to the same extent as enrichment and cFC, respectively (fig 1x), with ChABC increasing the fraction of Low PV (28% over total PV IN, $p < 0.01$. FIG 1E), and BDNF increasing the High PV (45% over total PV IN, $p < 0.05$. Fig 1E); moreover, both induced modulation of NOR performances (ChABC: enhanced discrimination, DI: 0.48, $p < 0.01$; BDNF: impaired discrimination, PI: 0.17, $p < 0.05$, Fig 1F) and synapse turnover (ChABC induced higher turnover: 6h $p < 0.001$; 12h $p < 0.05$; 24h $p < 0.01$. BDNF induced higher stability: 12h $p < 0.01$; 24h $p < 0.001$. Fig 1G).

These results demonstrate that the network of parvalbumin interneurons is plastic, experience regulates the state of the PV interneurons network to increase the fractions that express extreme levels of the protein parvalbumin, and the amount of Low or High PV is causally linked to the extent of structural plasticity and to performances in an incidental learning paradigm. Moreover, they suggest the existence in cortical microcircuits of a “plastic state” relying on Low PV and characterized by enhanced structural plasticity and learning, and a “crystallized state” relying on High PV and characterized by reduced structural plasticity and learning.

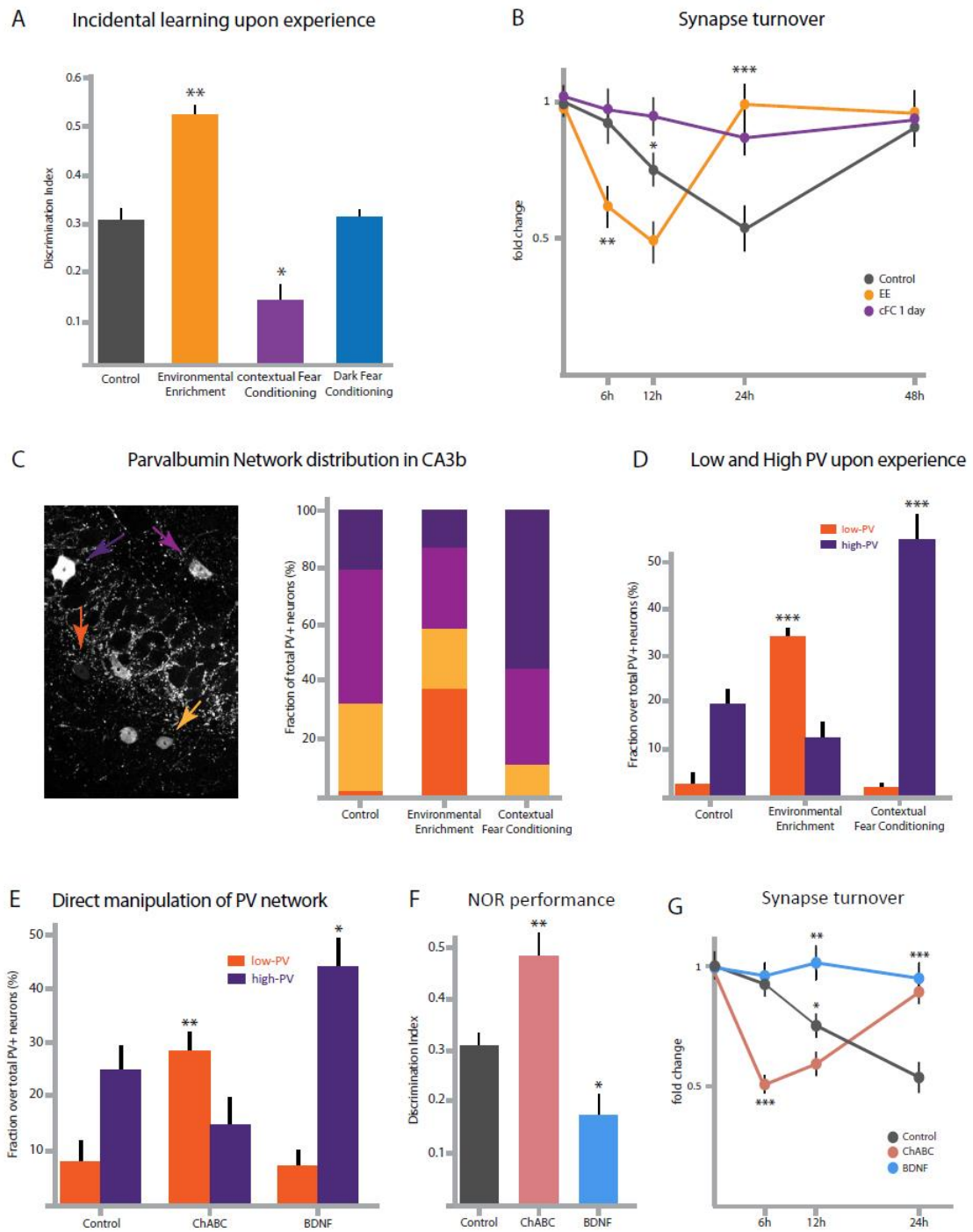


Figure 1: Parvalbumin network state regulates structural plasticity and learning

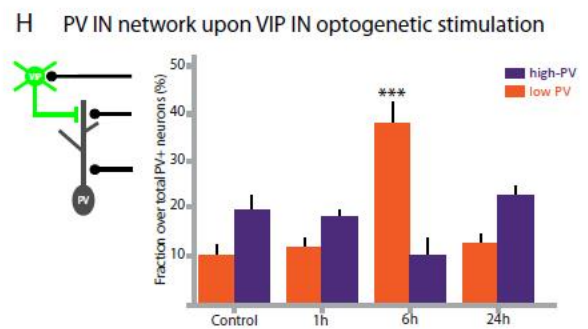
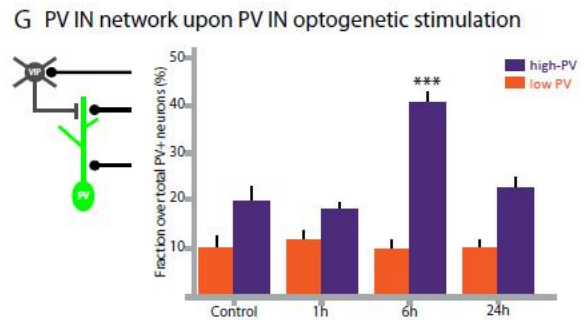
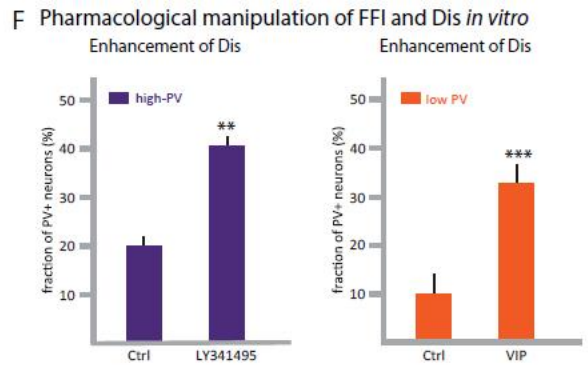
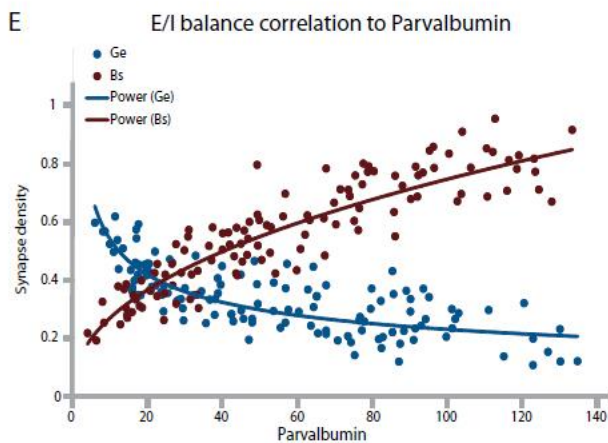
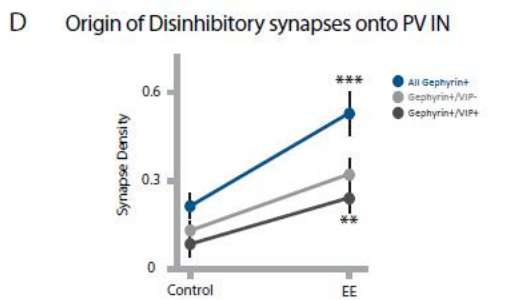
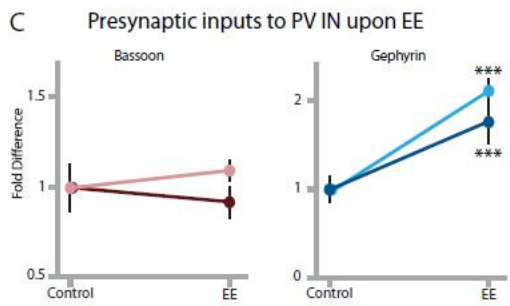
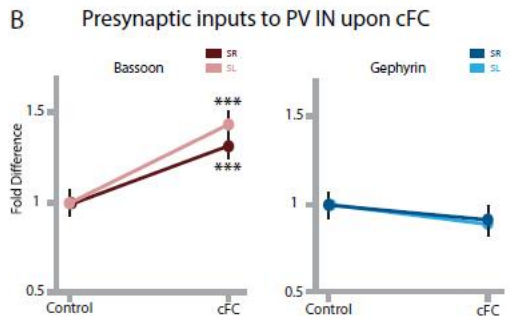
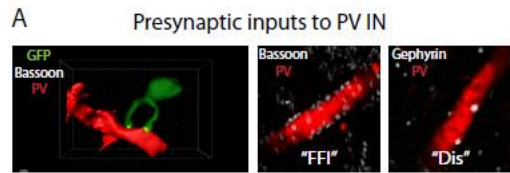
Experience impinges on CA3 microcircuits to modulate performance (A) and structural plasticity (B). Moreover, it modulates the composition of the network of PV interneurons to enhance the fractions that express extreme levels of the protein PV (C and D), to which other structural and functional properties of these interneurons correlate (suppl. Fig. 1). Moreover, topic interventions that reproduce the modulation of the network observed upon experience are sufficient to regulate structural plasticity and learning in similar ways (E, F, G), providing causality for experience-induced modifications.

Presynaptic connectivity upon PV interneurons modulates the expression of PV

What might be the mechanism by which experience acts upon the network of PV expressing interneurons to regulate structural plasticity and learning? During development, changes in PV IN properties are accompanied by changes in the excitatory or inhibitory drive upon these neurons. Moreover, learning completion is accompanied by an increase of FFI synapses upon PV IN dendrites. Therefore, we analyzed how experience could impact on presynaptic inputs to PV interneurons by looking at the density of excitatory (mediating feed forward inhibition, FFI) and inhibitory (mediating disinhibition, Dis) synapses onto their dendrites. For this purpose, we quantified the density of bassoon (excitatory synapse marker, Bs) and gephyrin (inhibitory synapse marker, Ge) immunodetected puncta upon the dendrites of genetically labeled, Parvalbumin expressing interneurons in hippocampus CA3b (PV-Cre/ rosa-CAG-STOP-tdTomato, Fig 2A). cFC produced an increase in excitatory synapse density on PV neurons both in stratum lucidum (input from mossy fiber terminals, consistent with previous reports. 1.44 fold difference to controls, $p < 0.001$, Fig 2B) and stratum radiatum (input from other CA3 pyramidal cells. 1.35 fold difference to controls, $p < 0.001$. Fig 2B), while inhibitory synapses were comparable to controls (in a balance that favors FFI over Disinhibition, Fig 2B. SL: 0.91 fold difference, SR: 0.89 fold difference. Not significant); on the contrary, EE produced minor changes in the density of excitatory synapses (SL: 0.89 fold to controls, SR: 1.1 fold to controls. Not significant. Fig 2C), but a significant increase in the density of inhibitory synapses of both strata (in a balance that favors Disinhibition over FFI, FIG. SL: 2.12 fold to controls, $p < 0.001$; SR: 1.94 fold to controls, $p < 0.001$. Fig 2C).

Figure 2: Presynaptic connectivity onto PV+ interneurons defines PV levels

Experience produces changes in presynaptic connectivity onto PV+ interneurons (A) that favor feedforward inhibition (B) or Disinhibition (C) upon cFC and EE, respectively. Both types of changes are input-aspecific (B, C and D). At the level of single cells, a balance between excitatory and inhibitory synapses density correlates to PV levels (E), thereby defining Hig PV interneurons as those having high density of excitatory, low inhibitory synapses; and Low PV interneurons as those exhibiting high density of inhibitory, low excitatory synapses (E). enhancement of FFI or Dis can be causally linked to the regulation of PV expression in the network via both pharmacology and optogenetic experiments (F, G and H)



Despite hippocampal excitatory inputs, which are largely stratum-specific, the origin and organization of disinhibitory synapses is far less clear: they can however be distinguished by

their nature in those that come from purely disinhibitory neurons (i.e., interneurons that selectively innervate other interneurons, Acsady et al., 1996 a and b, Somogy-Klausberger 2008), and those made by interneurons with no specificity for excitatory or inhibitory targets. Since PV Interneurons receive purely disinhibitory inputs only from VIP+ neurons (David C et al., 2007), we classified the inhibitory synapses present on PV IN in two classes: those that come from purely disinhibitory, VIP expressing interneurons (Ge+/VIP+), and those made by the other interneurons (Ge+/VIP-). Therefore, to test if both sources contributed equally to the increase of disinhibition, we quantified the prevalence of Ge+/VIP+ synapses in control and after environmental enrichment: while only a fraction of Ge puncta were VIP+ at baseline (42% VIP+ over total Ge positive. Fig 2D), both input contributed equally to the increase in inhibitory synapse density observed upon experience ($p < 0.001$, Fig 2D).

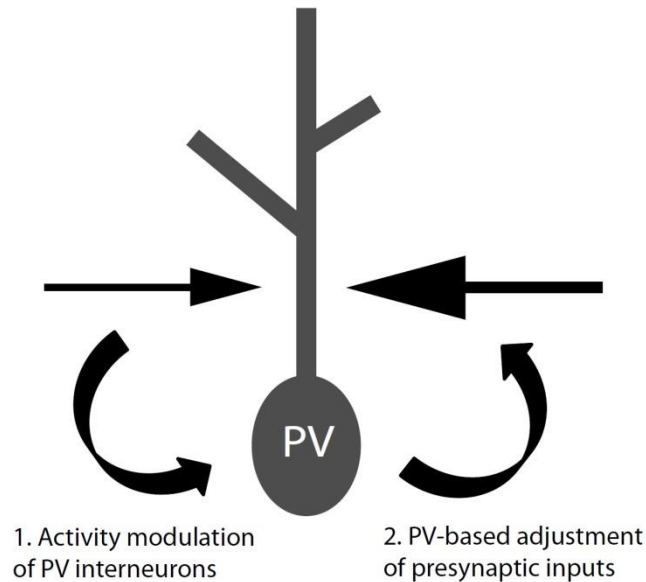
Prevalence of High PV in contextual fear conditioning is accompanied by the increase in FFI connectivity on PV IN at each input level. In contrast, increase in Low PV after environmental enrichment is accompanied by the increase in disinhibitory (Dis) connectivity arising from both VIP+ and VIP- interneurons. To determine whether a balance between FFI and Dis could modulate PV expression, we analyzed synapse density on each dendritic arbor as a function of PV intensity. When analyzing the data as a pool from different network states, excitatory and inhibitory synapse density correlated with PV expression following a robustly significant power law (Pearson correlation Bs-PV: 0.9, $p < 0.0001$; Pearson correlation Ge-PV: 0.73, $p < 0.001$. Fig 2E). Thus, higher levels of PV were associated to higher bassoon and lower gephyrin puncta density ("High PV", Fig 2E), and lower levels of PV to higher gephyrin and lower bassoon puncta density ("Low PV", Fig 2E). When considering the data distribution as a function of the network state (i.e. filtering based on experience), each condition produced a shift of the cloud of data along the ideal trend line defined by the power law, with no effect on the correlation between FFI, Dis and PV (Supplementary figure 2). This implied that, for each value of PV intensity, each neuron is defined in a logarithmic correlation space as a function of the balance between excitatory and inhibitory input that it receives, and that each variable can largely predict the others.

To verify that connectivity on PV IN regulates the state of the network, we enhanced FFI or Dis synaptic activity in organotypic slice cultures (that preserve all microcircuit elements, Supplementary figure 3) and analyze the effects on the PV network. Hence, pharmacological enhancement of FFI release from MFTs (LY341495, mGluR2 antagonist, 100 nM, Supplementary figure 3) increased the fraction of High PV (Saline: 20% over total PV+; LY341495: 41%. $P < 0.01$. Fig 2F), while enhancement of disinhibition via VIP neurons (VIP, 1nM, REF, Supplementary figure 3) produced increase of Low PV (saline: 12% ; VIP: 31%. $P < 0.001$. Fig 2F). Moreover, to further causally link recruitment of FFI or Dis to network

states, we used optogenetic to stimulate directly PV+ (enhanced FFI) and VIP+ (enhanced Dis) interneurons by targeted expression of a high sensitivity Channelrhodopsin construct ("Catch", Kleinlogel S et al., 2011) in defined interneurons subpopulations (Supplementary figure 4). Thus, direct photostimulation of PV neurons (PV-cre VIRUS) produced a transient increase of High PV at about 6 hours after stimulation (pooled controls: 19%. 6h after stimulation: 40%. $P < 0.001$, Fig 2G), to be back at baseline at 24h (24h: 21%, not significant. Fig 2G); besides, photostimulation of VIP neurons (which could contact directly PV dendrites, Supplementary figure 4) increased Low PV with similar temporal dynamics (Fig 2H), with a peak effect at 6h and return to baseline levels 24h after stimulation (pooled controls: 10%. 6h after stimulation: 38%. $P < 0.001$. 24h after stimulation: 12%, not significant. Fig 2H). These experiments causally link the prevalence of FFI or Dis to the state of the PV network.

Likewise, to investigate whether the state of an interneuron expressed by the level of PV could impact on its presynaptic inputs, we studied FFI and Dis after ChABC and BDNF treatment. Topical ChABC produced an overall increase in both VIP+ and VIP- puncta density (Total Ge positive synapses: SL: 1.7 fold to controls, SR: 1.66 fold to controls, $p < 0.001$. VIP+ and VIP- increase to controls: $p < 0.01$. Excitatory synapses: SL: 1.05 fold to controls, SR: 0.96 fold to controls, not significant. Supplementary figure 5) (fitting the increase in Low PV, Fig 1E), while BDNF increased Bs density (SR Bassoon puncta: 1.61 fold to controls, $p < 0.001$; SR Gephyrin puncta: 0.83 fold to controls, not significant. Supplementary figure 5)(fitting the increase in High Pv, Fig 1E).

Altogether, these data provide evidences for a bidirectional modulation of the PV network based on the prevalence of FFI or Dis, where an initial, activity based modulation of PV intensity induces the adjustment of presynaptic input to the interneuron itself (Schema 1). We then sought to determine if rearrangements in presynaptic connectivity upon PV IN produced a functional effect on the pyramidal cell network in CA3, since increase in FFI or Dis could affect the number of excitatory cells recruited upon experience. Therefore, we confirmed that changes in PV expressions at the soma were mirrored at the level of CA3 pyramidal cells baskets (Supplementary figure 6); moreover, enhanced disinhibition by Low PV after EE correlated with higher number of cFOS positive cells upon NOR, while enhanced FFI by High PV after fear conditioning decreased that fraction (control: 14% of cFOS positive cells over total NeuN positive; EE: 21%, $p < 0.01$; cFC: 6%, $p < 0.01$. Supplementary figure 6).



Schema 1: Bidirectional modulation of PV network

Data support a view where an initial, possibly activity-based modulation of activity onto PV cells (1) could produce a shift toward Low or High expression of PV. Then, presynaptic connectivity impinging on the neuron would be adjusted to support the newly achieved state of the cell (2).

Implementation of a plastic state during learning, and a crystallized state upon learning completion during incremental learning

In contrast to single-trial learning tasks like the fear conditioning, trial-and-error forms of learning proceed in an incremental way for which mice learn to master the task progressively along the course of several days; moreover, they likely progress through defined stages of learning in which information about the task is collected and consolidated to define strategies for task solution, and later exploited to reach a goal (Exploration and Exploitation, March J., 1991). One of such complex incremental learning paradigms is the Morris water maze (MWM), in which mice learn to navigate a maze toward a hidden platform based on the external reference cues present in the room (vorhees CV, Williams MT, 2006). Since the task is hippocampus-dependent (Morris et al., 1982), and learning produces an increase in FFI in CA3 that is comparable to the cFC and accountable for memory precision (Ruediger et al. 2011), we investigated the impact of learning the water maze on the PV IN network. To this end, we analyzed High and Low PV relative abundance at defined time points early

during learning (MWM day 2 and 4, Fig 3A) and upon learning completion (MWM Day10). Surprisingly, we observed two phases of structural rearrangements: during the learning process (Day2 and 4), Low PV increased compared to swim controls, while High PV remained unaffected (MWM 2d: 27% low PV. $P < 0.001$., Fig 3B); in stark contrast, learning completion produced an increase in High PV, with Low PV largely comparable to controls (MWM 10d: 42% High PV. $P < 0.001$., Fig 3B). This would suggest that, instead of a linear progression toward network states supporting enhanced or reduced plasticity and learning (EE and cFC respectively, Supplementary figure 7), a complex incremental learning task would deploy a bimodal progression through a first, “open” phase of plasticity early during learning, followed by a final, “crystallized” configuration upon learning completion. Supporting the hypothesis that maze learning progresses through two stages of plasticity regulation by PV IN, we observed enhanced NOR and synapse turnover respect swim controls upon prevalence of Low PV on day2 (Fig 3C and D. Synapse turnover difference to controls: 6h: $p < 0.001$; 24h: $p < 0.001$. Discrimination index difference to controls: 1.7 fold, $p < 0.01$), and reduced performances and synapse turnover upon prevalence of High PV on day 10 (Fig 3C and D. Synapse turnover difference to controls: 24h: $p < 0.01$. Discrimination index difference to controls: 0.6 fold, $p < 0.01$). These results confirm the existence of a plastic state supported by Low PV prevalence early during learning, and a crystalized state relying on High PV upon learning completion.

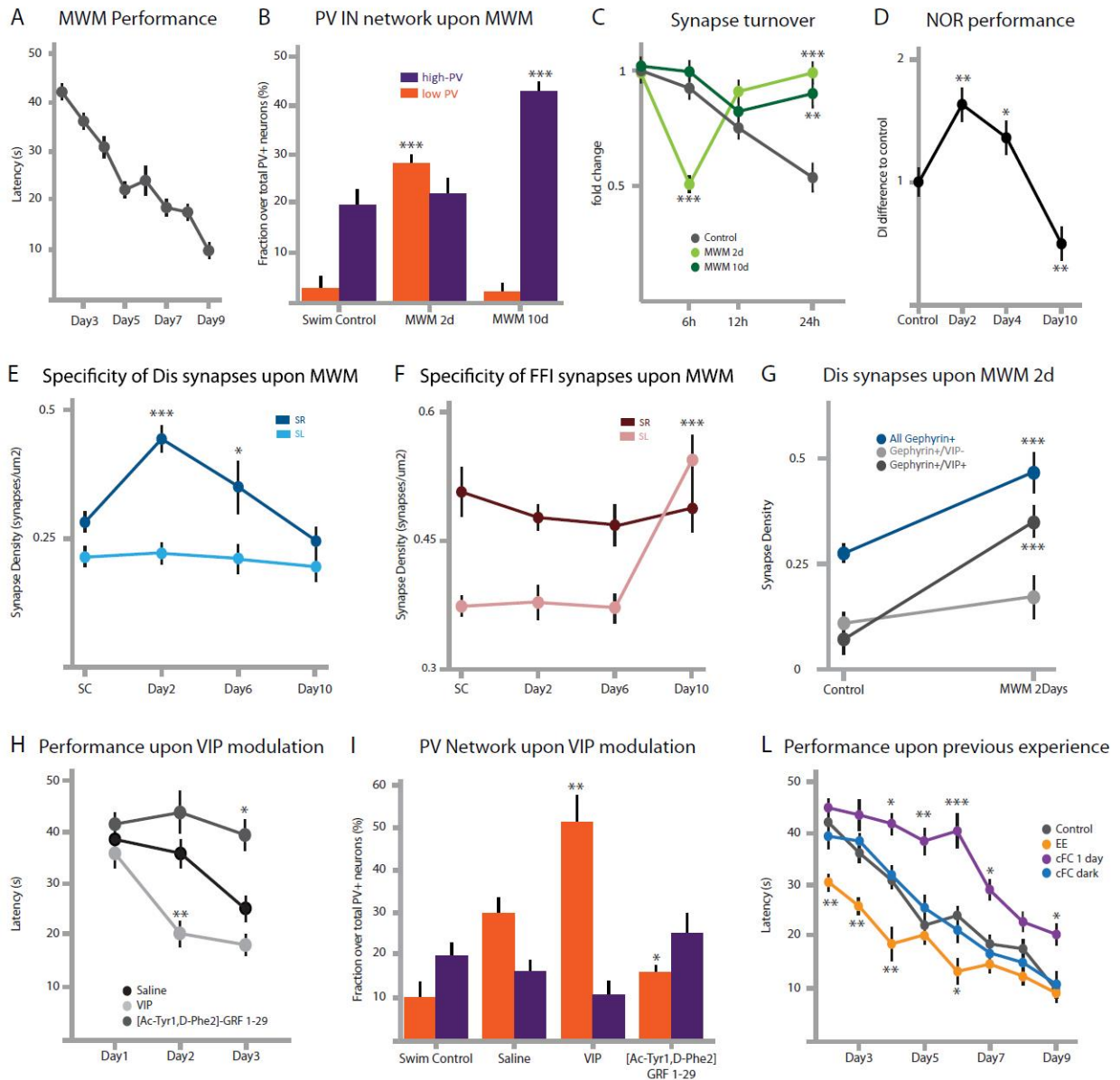


Figure 3: A microcircuit module to implement the Plastic state during learning, Crystallized state upon learning completion

Learning the morris water maze task (A) requires the implementation of a first, plastic state during learning, followed by a shift to the crystallized state upon learning completion (B, C and D). The connectivity underlying transitions to these states is input specific, for which only VIP+ inhibitory synapses in Stratum Radiatum produce enhancement of Low PV during the plastic state (E and G), and only excitatory synapses in stratum lucidum shift the network to the crystallized configuration (F). Moreover, targeted modulation of VIP transmission is sufficient to modulate learning at a behavioral (H) and structural level (I). This provides a mechanism to explain metaplasticity (L) as a result of different starting configurations exhibited upon previous experience.

To determine if the same mechanism modulating PV expression upon experience is responsible for the network-state transitions associated with the water maze, we quantified

prevalence of FFI or Dis on PV dendrites at different stages during learning. Whereas the overall mechanism was conserved (enhancement of disinhibition during learning, FFI upon learning completion, Fig 3E and F), we could observe a higher degree of specificity in synapse density increase. This implied that only increased Dis in SR would account for the “open” state during learning (Fig 3E and supplementary figure 8. MWM 2d gephyrin in SR: 1.6 fold to controls, $p < 0.001$), while only FFI in SL would induce the shift toward “crystallization” upon learning completion, with the complementary input sources largely unaffected at each time point (Fig 3F. MWM10d Bassoon in SL: 1.4 fold to controls, $p < 0.001$). Besides, and in contrast to environmental enrichment, the increase in disinhibition observed during learning was produced exclusively by the increase of VIP+ synapses on PV dendrites (Fig 3G VIP+/Ge+ synapse increase to control: $p < 0.001$; VIP-/Ge+ synapse increase to control: not significant), pointing toward a dedicated VIP-PV microcircuit module responsible for the enhancement of disinhibition that produces the “open” network configuration observed early during water maze (Supplementary figure 8) .

To investigate if targeted modulation of VIP+ disinhibition was sufficient to regulate maze learning, we treated mice with topical infusion (supplementary figure 9) of VIP receptor agonist (VIP, Tocris, Cunha-Reis D, et al., 2004, 1nM) and antagonist ([Ac-Tyr¹,D-Phe²]-GRF 1-29, Tocris, Cunha-Reis D, et al., 2004, 300 nM), and tested their performances in the early phase of learning. VIP-treated mice were faster in locating the platform on day 2 and 3 (Fig 3H, $p < 0.01$), exhibited a significant reference memory already on day 4 (Supplementary figure 10, Target quadrant occupancy: 41%, $p < 0.05$), and were characterized by an enhanced proportion of Low PV compared to controls (Fig 3I Low PV: 51% over total PV+ interneurons, $p < 0.01$): therefore, modulation of VIP+ disinhibition is sufficient to modulate learning. In contrast, [Ac-Tyr¹,D-Phe²]-GRF 1-29 completely prevented learning (Fig 3H, difference to control on day3: $p < 0.05$), did not affect reference memory formation (Supplementary figure 10, occupancy of target quadrant not significantly different to controls), and largely prevented the increase in Low PV neurons during the initial phases of the water maze (Fig 3I Low PV: 20% over total PV+ interneurons, $p < 0.05$), providing evidences that VIP mediated disinhibition is necessary for learning.

Both experiments prove that VIP-mediated disinhibition on PV IN is causally responsible for the network transition toward the “open” state, which is necessary for maze learning: this suggests that starting the water maze training in a disinhibited configuration might improve performances and reference memory acquisition to the same extent as VIP treatment, while the opposite would be true with FFI as the starting point. Hence, we studied how previous experience would influence further incremental learning by training mice that had previously experienced an enriched environment or learned the fear-conditioning task (being in the Low

or High PV state, respectively). Enriched mice showed enhanced performances on the first phase of learning (Fig 3L, orange curve: difference to control on day 2, 3 and 4: $p < 0.01$; difference to controls on day 6: $p < 0.05$), and significant reference memory on day 4 (Supplementary figure 11, target quadrant occupancy: 43% of time, $p < 0.02$); conditioned mice instead lagged behind controls in the learning curve for the whole training (Fig 3L, purple curve. Difference to controls on day 4, 7 and 9: $p < 0.05$; day 5: $p < 0.01$; day 6: $p < 0.001$), and showed impaired reference memory on day 10 (Supplementary figure 11. Difference to controls on target quadrant occupancy: $p < 0.001$. Left quadrant: $p < 0.05$). Mice conditioned in the dark showed no difference to controls in performance or reference memory (Fig 3L, blue curve and supplementary figure 11), again linking performance to experience-induced states of VIP-PV microcircuit.

A microcircuit module mediating the transition toward the plastic state during learning in cortical microcircuits

To test whether the VIP-PV module could be recruited to regulate learning beyond the hippocampus, we analyzed a form of motor learning that is incremental, hippocampus-independent, and produces long-lasting effects on specific cortical microcircuits. We therefore choose to study the regulation of Rotarod learning (RR) in primary motor cortex (M1), a task in which mice learn to coordinate their movement to run on an accelerated rod (Yang G et al., 2009). This has been shown to require at least 6 consecutive days of repeated training to reach stable, plateau performances (Fig 4A), and to produce long lasting alterations in connectivity in primary motor cortex (M1). In M1, rotarod learning produced an initial increase in the Low PV interneurons in the early phases (Fig 4 C. RR Day2: 30% Low PV over total PV+ IN, difference to control $p < 0.001$), followed by a shift toward High PV increase upon learning completion (Fig 4B and C. RR day7: 39% High PV over total PV+ IN, difference to controls $p < 0.0001$). The proportions of Low or High PV during rotarod learning or upon learning completion resembled the ones observed in the hippocampus during maze learning (Supplementary figure 12). Moreover, learning-induced transitions among PV IN network states were supported by the same mechanism based on FFI and Dis prevalence onto PV IN (Fig 4D., Gephyrin puncta upon RR 2d: $p < 0.001$ difference to controls; Bassoon puncta upon RR 7d: $p < 0.01$), with VIP+ interneurons being largely responsible for the increase in disinhibition (Fig 4E, Difference to control $p < 0.001$). As a control, neither changes in FFI, Dis or PV expression, nor changes in NOR performances could be detected in the hippocampus at any time during rotarod learning (Supplementary figure 13).

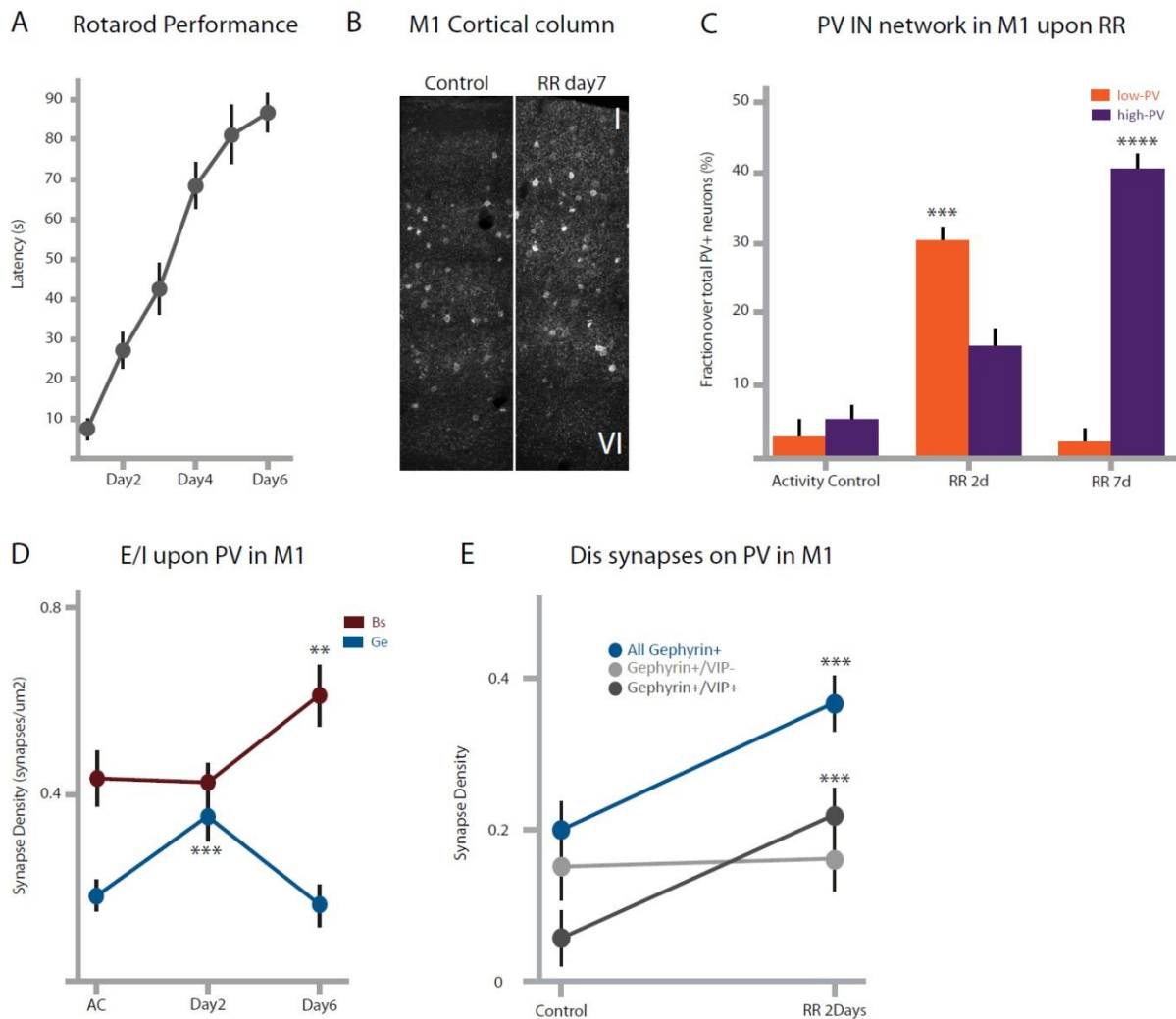
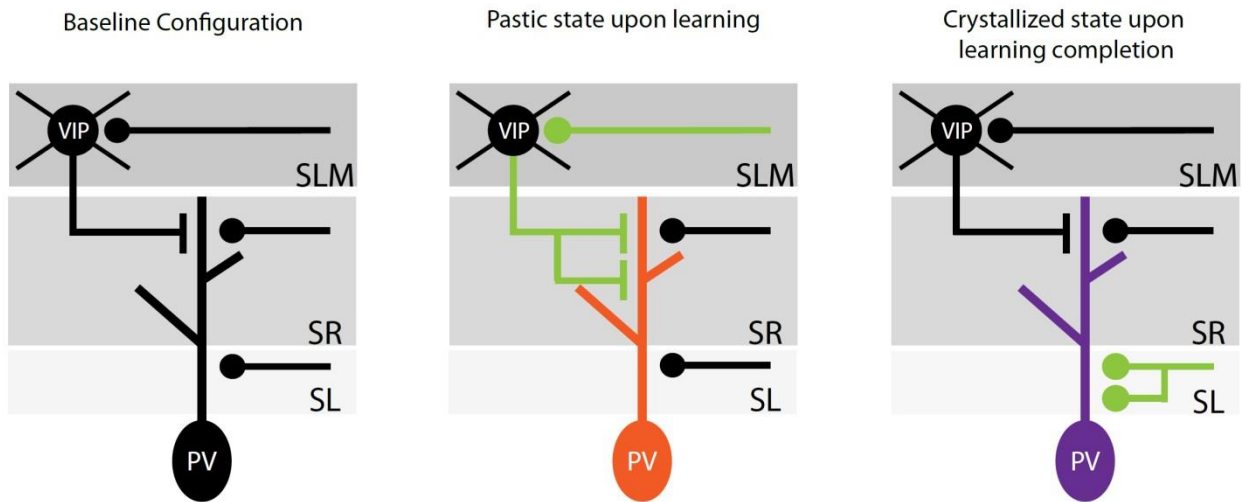


Figure 4: VIP-PV module implemented upon incremental learning in neocortex

In M1, incremental learning (A) requires the implementation of a plastic state followed by crystallization (B and C) to the same extent as hippocampal learning (suppl. Fig. 12). The mechanism underlying states transitions is conserved between hippocampus and cortex, where an enhancement of VIP+ inhibitory synapses mediates the plastic state, while excitatory synapse density produces a shift to the crystallized state (D and E).

Thus, incremental forms of learning proceed through a first, “open” configuration with the recruitment of a VIP-PV microcircuit module that supports prevalence of Low PV, and a network state enhancing learning and structural plasticity. Then, they shift to a FFI based, “crystallized” phase that supports prevalence of High PV and is characterized by reduced learning and plasticity, but is necessary for memory precision (Ruediger et al., 2011) (Schema 2). The recruitment of the disinhibitory VIP-PV module to regulate plasticity and learning can be extended to diverse cortical areas upon incremental learning, and produce effects that can be transferred to different learning paradigms relying on the same

microcircuits; nevertheless, it is strictly specific to those cortical microcircuit involved in the task.



Schema 2: Implementation of the Plastic state upon learning, Crystallized state upon learning

Our model poses that the shift between a baseline and a plastic configuration, necessary for learning, is carried out by a dedicated microcircuit module relying VIP interneurons to make disinhibitory synapses onto PV interneuron, thereby shifting the network configuration toward Low PV. The specificity of input highlighted in the schema is inferred from the hippocampal connectivity, but a similar principle might stand in cortex too, where VIP+ neurons, which are abundant in the superficial layers, receive massive connections from Thalamus.

Moreover, upon learning completion, an increase in FFI connectivity would mediate the transition toward the crystallized state via High PV prevalence, to support memory precision.

4.1.4 Discussion

To summarize, this study reveals that learning recruits a dedicated microcircuit module impinging on VIP+ and PV+ interneurons to regulate the amount of learning and structural plasticity of cortical microcircuits. Hence in hippocampal CA3, environmental enrichment and contextual fear conditioning were able to produce the enhancement or decrease in structural plasticity and learning, and induce a rewiring in the network of PV expressing interneurons to enhance the formation of inhibitory or excitatory synapses onto the dendrites of these interneurons, respectively. Change in connectivity would underlie the amount of expression of the protein Parvalbumin (which correlated with Gad-67 expression and firing frequency): accordingly, enrichment increased the fraction of interneurons which display Low levels of Parvalbumin, and were characterized by high density of inhibitory synapses and low density of excitatory synapses onto their dendrites; conversely, conditioning increased the fraction of interneurons that display High levels of Parvalbumin, and were characterized by low density of inhibitory synapses and high density of excitatory synapses. Changes in synapses density were causally linked to the modulation of PV expression and interneuron distribution in the network, which would in turn be causally responsible of regulating the amount of plasticity and learning in the microcircuit. Therefore, enrichment produced an increase in PV-mediated disinhibition that would underlie a “Plastic state” of enhanced learning, while conversely conditioning increased feed-forward inhibition via PV interneurons to produce a “Crystallized state” of reduced further learning.

Incremental, trial-and-error forms of learning are hypothesized to proceed through two distinguishable phases, in which information about the task is acquired (exploration), and later used to solve the task (exploitation). Similarly, we observed that a hippocampal dependent incremental learning paradigm like the Morris water maze would deploy a plastic state during learning, followed by a crystallized state upon learning completion. In stark contrast to enrichment and conditioning, the amount of structural plasticity mediating the network transitions toward the plastic or crystallized state was highly input specific: enhancement of disinhibition upon learning was mediated exclusively by VIP+ interneurons making synapses onto the portion of PV dendrites in stratum radiatum, while enhancement of FFI upon learning completion was carried out exclusively by filopodia sprouting by mossy fiber terminals in stratum lucidum. This uncovered a dedicated microcircuit module impinging on VIP-PV connectivity that is used upon incremental tasks to regulate plasticity and learning: accordingly, the transition to a plastic state was necessary for learning, and targeted modulation of VIP release was sufficient to modulate learning itself. In addition, the

recruitment of a VIP-PV module to regulate plasticity and learning was not specific to the hippocampus, but could be observed in other cortical areas upon specific recruitment during learning.

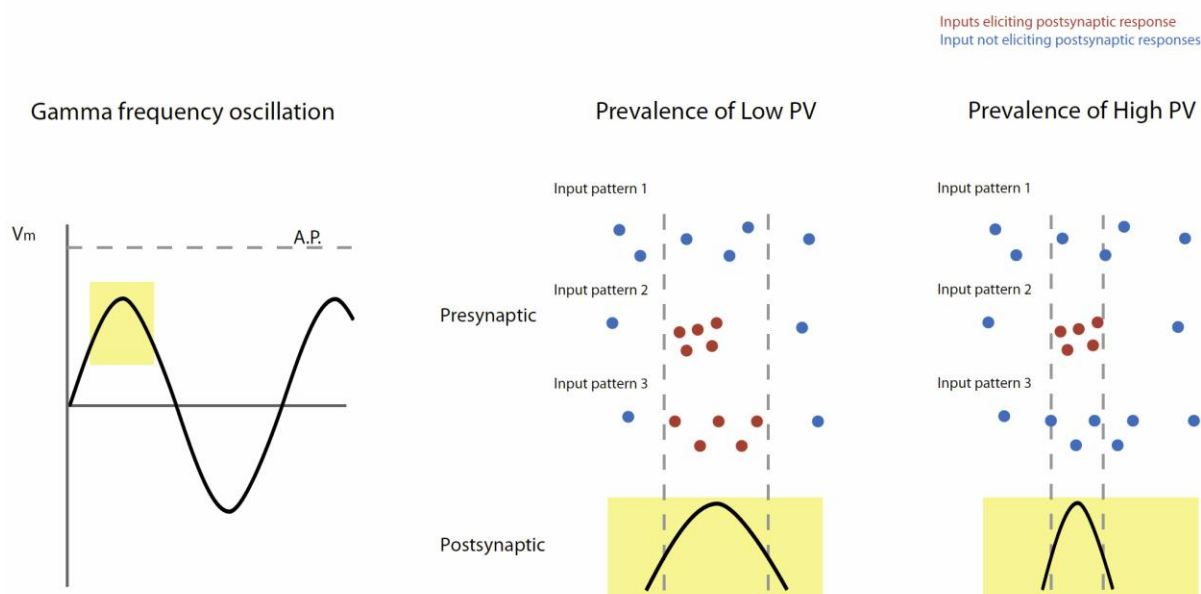
What might be the significance of having an interneuron network shifted toward High or Low PV? PV expression in single cells might just be an indicator of a whole peculiar state in the cell, with effect on physiology (frequency of spiking), connectivity (higher or lower density of excitatory or inhibitory synapses), or gene expression profile. This last aspect in particular would be fascinating to explore: dendritic connectivity might determine parvalbumin intensity (and vice versa), which in turn might signal calcium concentration intracellularly. Previous literature has shown how membrane depolarization and calcium influx in the cell are able to induce new transcription (West AE et al., 2001). Therefore, High and Low PV cells might be characterized by a set of differentially expressed transcripts and proteins which might underlie their functional significance; exploring how differential regulation might be brought about (i.e., via transcriptional, translational or epigenetic mechanisms) might help us to understand peculiar properties characterizing the plastic or crystallized state.

Nevertheless, the correlation between parvalbumin expression and GAD-67 as well as firing frequency strongly suggests that the state of PV network might have significant functional implications for cortical microcircuits computation. Therefore, prevalence of Low PV might underlie a decrease in the inhibition exerted on pyramidal cells that makes those cells more prone to be recruited upon external stimulation (Supplementary figure 6), while prevalence of High PV would increase inhibition and reduce the fraction of cells recruited upon further experience (Supplementary figure 6). In this scenario, the state of the PV network would control a threshold by which sensory experience can recruit pyramidal cells in cortical microcircuits. In complex, incremental forms of learning we would thereby assist to two independent phases: a first state in which pyramidal cells would be more excitable by sensory experience, followed by a configuration which would in turn make it harder for excitatory microcircuits to be recruited by non-salient stimuli. In a behavioral prospective, these two phases would coincide with what computer scientists call Exploration and Exploitation: in the first phase (exploration), a lower threshold for excitation (produced by the disinhibitory configuration of the PV network) would promote acquisition of sensory experience, facilitating those stimuli that, although weak, might correlate with a positive outcome in the task (thereby allowing the microcircuits to keep an “open mind” about the environment); once a successful association has been created, an increase in the threshold for the acquisition of new sensory information (exploitation), achieved by the FFI

configuration of the PV network, would filter all those stimuli that might function as “distractors”, and hence allow the microcircuit to increase its attention toward those input which have been successfully (via dopamine or serotonin?) correlated to positive outcome in the task (thereby allowing consolidation via the strengthening of previous associations or strategies).

What would be the mechanism by which the network of PV interneurons would modulate the threshold for excitation, thereby filtering sensory experience? One striking feature that distinguishes High and Low PV biologically is the density of excitatory or inhibitory synapses onto their dendrites. Previous work has shown that excitatory recruitment of PV+ interneurons produces the emergence of coherent membrane fluctuations in the population of pyramidal cells in cortical microcircuits, which gives rise to rhythms in the gamma band (30-80 Hz) (Penttonen et al. 1998, Gloveli et al. 2005 a and b, Hasenstaub et al. 2005, Mann et al. 2005, Quilichini et al. 2010, Buzsaki and Wang, 2012); moreover, excitation onto PV interneurons was found to enhance gamma, while inhibition onto these interneurons to suppress it (Sohal et al., 2009). Modeling a network with reduced amount of parvalbumin expression at the PV-to-PC synapse produced a decrease in both power and frequency of gamma oscillation (Volman et al., 2011). For brain rhythms, the frequency of the oscillation influences the length of the window for the dendritic integration (usually 10-30 ms, coincident to one gamma cycle) of inputs from multiple upstream sources (which present a certain temporal jitter, Harris et al., 2003). All things considered, the amount of excited or inhibited PV interneurons in the network might therefore modulate the length of the window for dendritic integration. Many inhibited PV interneurons (Low PV) might reduce the frequency of oscillation to lower levels: this would increase the duration of the window for dendritic integration in the excitatory network, thereby allowing weak inputs with no temporal organization (like those of the input pattern 2 in the schema 3) to elicit a response in a postsynaptic excitatory neuron. In stark contrast, many excited PV interneurons (High PV) might increase gamma oscillation to higher levels: this would shorten the duration of the window for dendritic integration in the excitatory network, thereby allowing only strong input with a clear temporal structure (that is, inputs arriving with a delay of few milliseconds like the ones of the input pattern 3 in the schema 3) to elicit a response in the postsynaptic excitatory neuron. Moreover, this mechanism might impact on the number of neurons recruited synchronously upon stimulation, with an High PV network organizing the activity of an ensemble of neurons so that their collective spiking would be seen from the postsynaptic “reader” neuron (in our example, CA1 upon CA3 network reorganization) as a single event (as reviewed by Buzsaki, 2010).

Model for differential filtration of input stimuli based on gamma power/PV network state



Schema 3: Proposed model for differential filtration of input stimuli based on PV network state

The model poses a possible mechanism by which the composition of the PV network, by modulating the frequency of the gamma rhythm, is able to regulate the filter to incoming input patterns based on strength and temporal coincidence.

The recruitment of the VIP-PV module upon the learning phase of the Morris water maze showed a high degree of specificity, for which the transition to the network configuration in which Low PV are prevalent was carried out entirely by the increase in VIP+ inhibitory synapses onto the stratum radiatum portion of PV dendrites in CA3. To achieve such a high level of specificity in structural plasticity, two different scenarios could be hypothesized: in the first, regulatory mechanisms in the postsynaptic PV interneuron would restrict the amount of structural plasticity only in a specific segment of the dendrite, but not in the neighboring fraction; moreover, another layer of regulation would be required to enhance solely synapses coming from VIP interneurons, probably relying on a highly specific code of adhesion molecules expression. The first hypothesis instead relies instead on the presynaptic partner to achieve the level of specificity exhibited during learning. In CA1, VIP+ disinhibitory interneurons have been divided in two classes according to their shape (Acsady et al., 1996): multipolar VIP neurons ramify their dendrites in both stratum radiatum and

stratum oriens, and contact postsynaptic partners in both strata as well; in contrast, some VIP+ neurons show a very polarized morphology for which they stratify their dendrites only in stratum lacunosum-moleculare, and contact postsynaptic partners only in stratum radiatum. The observation that such a type of neurons exist also in CA3 (Supplementary figure 8) allowed us to hypothesize that the recruitment of polarized VIP+ neurons upon learning could be entirely responsible for the specificity observed during learning (Supplementary figure 8). That would also imply that the two inputs to hippocampal area CA3 would dissociate their impact in separate parts of the learning process: the perforant path from Medial Entorhinal cortex would produce recruitment of VIP+ interneurons to induce disinhibition via PV interneurons during learning, thereby promoting the transition to the Plastic State (See Schema 2); on the contrary, the mossy fiber pathway from the dentate gyrus would be recruited to promote the enhancement of FFI upon learning completion and hence the transition to the crystallized state (See schema 2). Moreover, enhancing inhibition only onto the stratum radiatum of PV interneurons might selectively influence the efficiency by which excitatory inputs from CA3 pyramidal cells recruit those interneurons, due to the high degree of shunting inhibition that dendritic inhibition exerts. This would imply that the auto-association pathway, which usually exerts a strong FFI in the network for which stimulation of the Shaffer collaterals produce IPSC in CA3 pyramidal cells (Chevalleyre V, and Siegelbaum SA, 2010), would be facilitated during learning so to allow the formation of spatial representation in CA3, which might later be recalled with a high degree of specificity upon learning completion (when the strong FFI from MFTs filopodial synapses would suppress any unrelated neuronal ensemble). Therefore, disinhibition upon learning would be meant to facilitate the strengthening of those synapses among the ensemble of neurons that underlie the association learned, while FFI upon learning completion would arise from the consolidation of that ensemble to suppress unrelated representations.

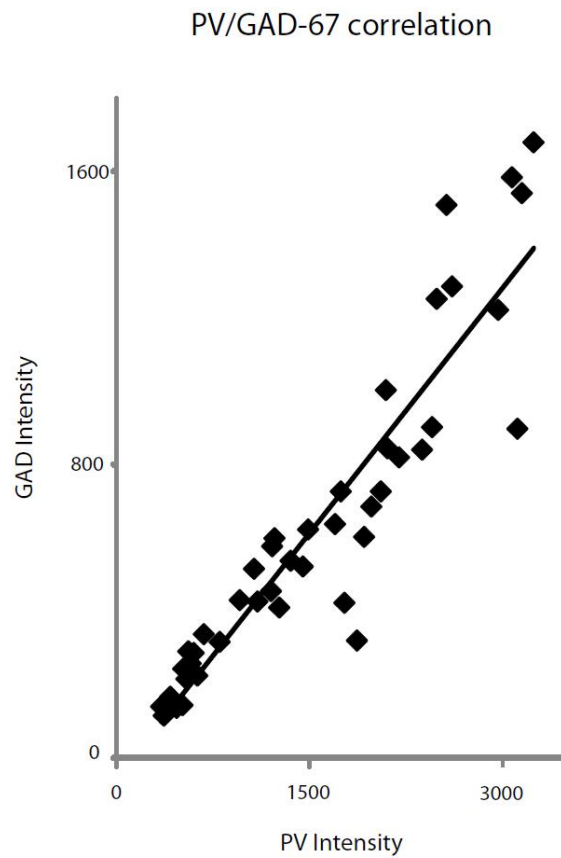
What mechanisms might trigger the recruitment of VIP+ disinhibitory interneurons upon learning to promote transition to the Plastic state? We have shown that the modulation of VIP signalling during learning is sufficient to modulate learning; therefore, understanding the principles underlying such recruitment might provide a useful entry point to produce cognitive enhancement or rescue deficits in pathological conditions. A limited excitatory activity driving VIP+ interneurons might not be sufficient to permanently shift the system toward the Plastic state (the effect of optogenetic stimulation of VIP+ interneurons onto the PV network are only transitory and not sustained at 24 hours). Therefore, we should hypothesize that a second signal might strengthen the extent of VIP interneurons recruitment to produce a stable transition toward plasticity. Hence, a fraction of VIP+ interneurons express ionotropic

receptors for both serotonin (5HT₃ Yang et al., 2009) and acetylcholine (Porter et al., 1999). It is tempting to speculate then that VIP+ interneurons might be activated by the coincidence of 2 signals: one carrying sensory information (Entorhinal cortex for the hippocampus, Thalamus for motor cortex), and the other signaling the salience of the sensory information to produce associations. Only coincidence in these two signals would then be sufficient to allow the stable transition toward the plastic state observed early during learning.

Nevertheless, this process should be highly specific for the brain areas recruited upon learning, which would be the only areas to transition to the plastic state (Supplementary figure 13). At least two scenarios could be envisioned to obtain this specificity. The first implies that neuromodulator axons originating in different nuclei would specifically innervate different cortical areas: if this were true, specificity would be achieved by selective recruitment of neuromodulatory nuclei upon learning. The second scenario instead poses that specificity is entirely ascribed to sensory experience, and neuromodulatory release would instead happen unspecifically in a variety of sensory areas. This would imply that learning might happen only in those regions where sensory stimulation coincide temporally with neuromodulatory stimulation, thereby impinging a plastic state in those systems that are sensory recruited upon learning. This latter hypothesis would imply a mesmerizing consequence: upon whatever type of incremental learning, we could induce ectopic transitions toward the plastic state in systems that are not selectively recruited by the learning itself by means of artificial stimulation (which would pair with the general neuromodulatory release induced by learning).

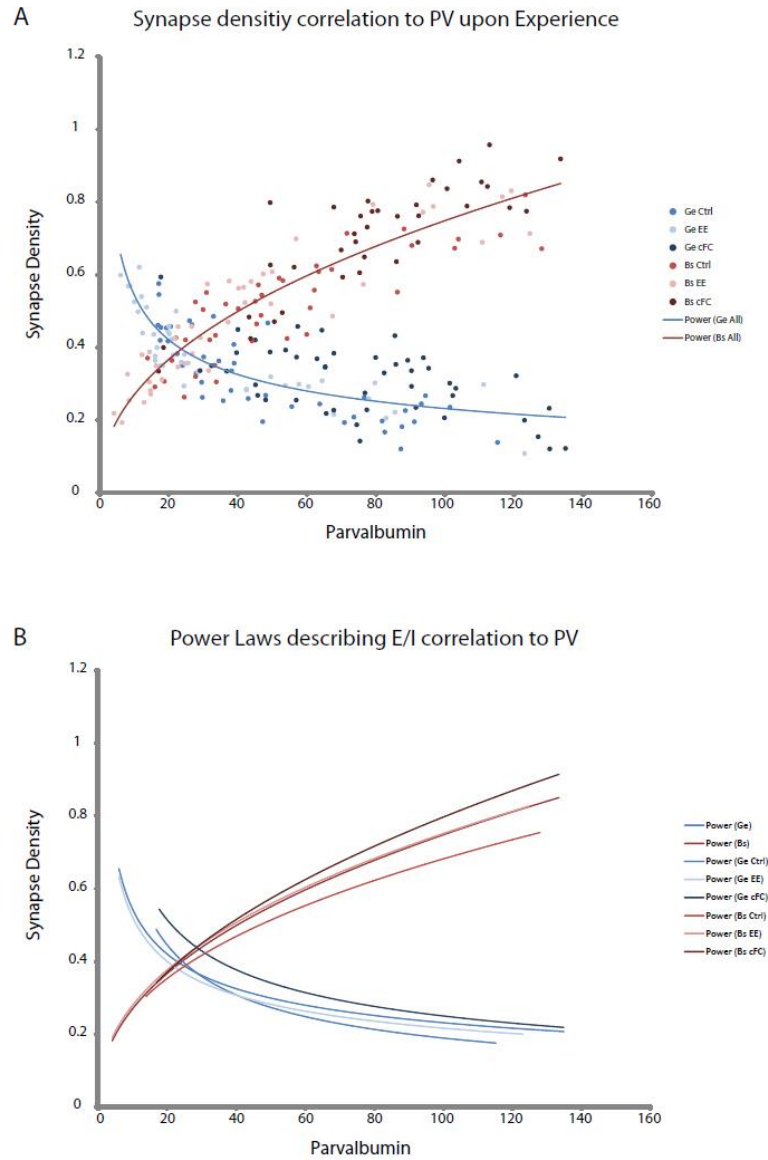
4.1 5 Supplementary material

Supplementary Figure 1: PV-GAD correlation



PV expression in single interneurons correlates with levels of GAD-67, which are critical to determine the amount of GABA synthesized and released in the synaptic cleft (Lau, CG 2012)

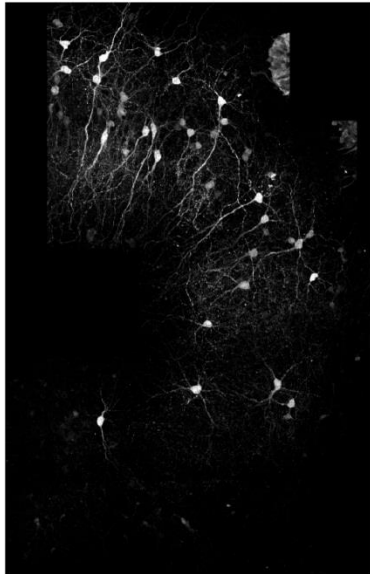
Supplementary figure 2: E/I balance correlation to PV



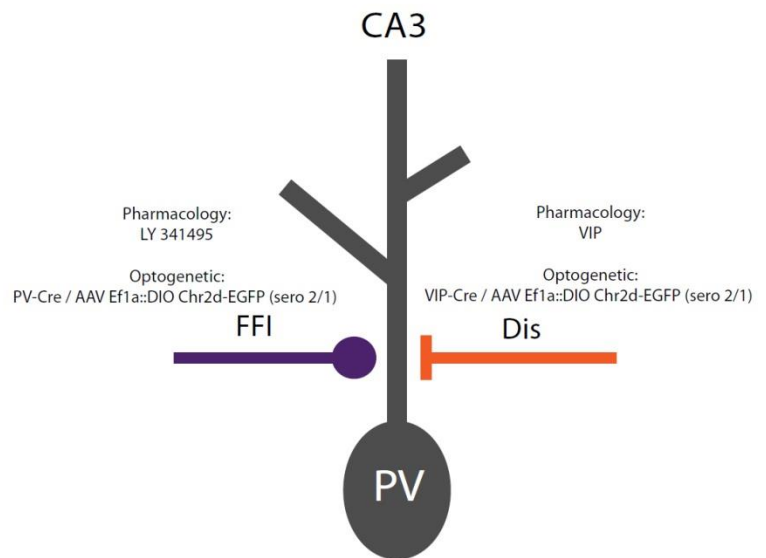
Power laws describing the correlation between excitatory or inhibitory synapse density and expression of PV in CA3 network upon different experiences.

Supplementary figure 3: FFI and Dis in slice cultures

A PV network in Hippocampal Slice culture, Div 30



B Enhancement of FFI or Dis in slice cultures



Targeted enhancement of feedforward inhibition or disinhibition via pharmacological modulation of synaptic activity (LY 241495 and VIP), or direct excitatory recruitment of PV+ and VIP+ interneurons via optogenetics.

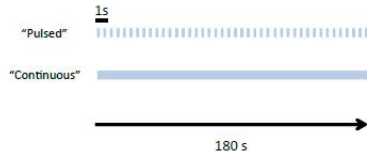
Supplementary figure 4: optogenetic *in vitro*

A Infection and stimulation

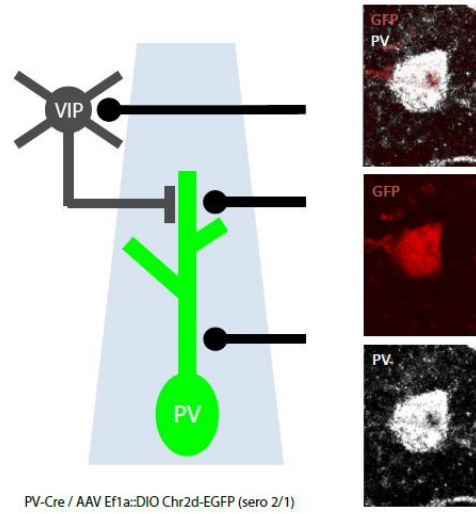
Infection:

Slice cultures performed on P7 pups;
infected using the droplet method on Div 12;
stimulation performed on Div 30.

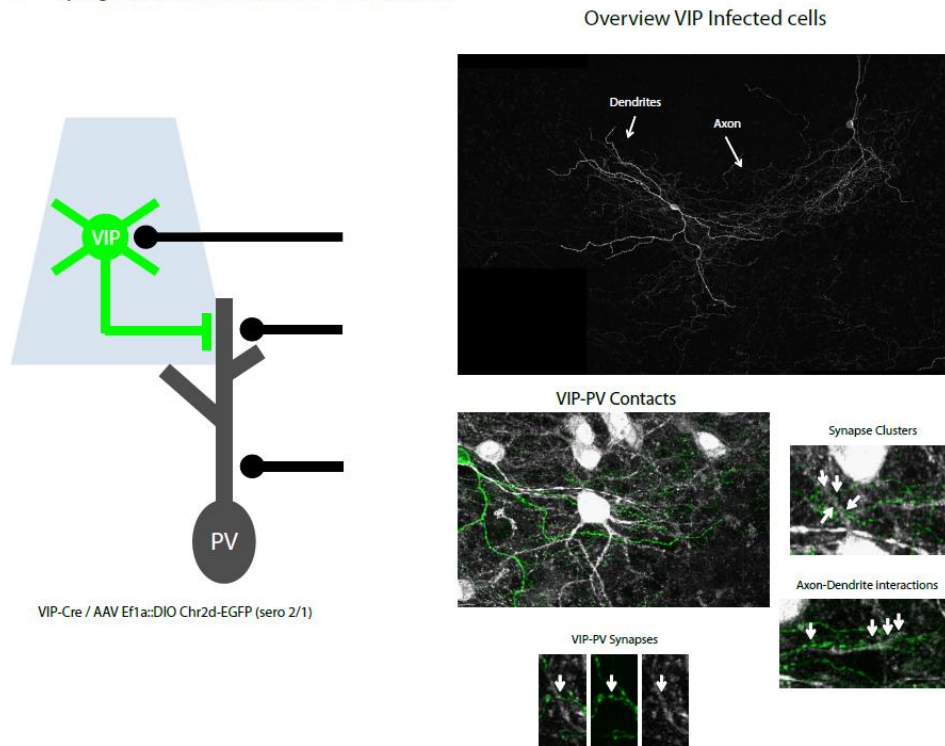
Stimulation:



B Optogenetic stimulation of PV Interneurons

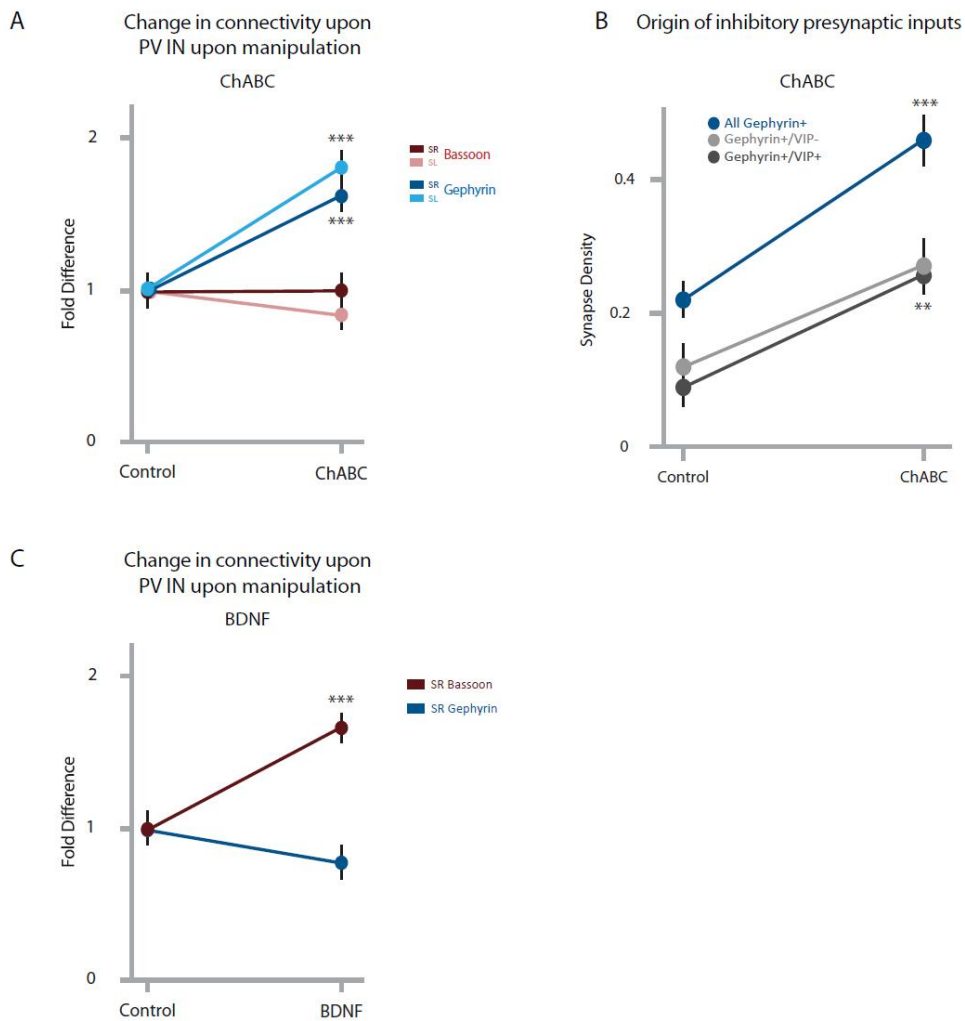


C Optogenetic stimulation of VIP Interneurons



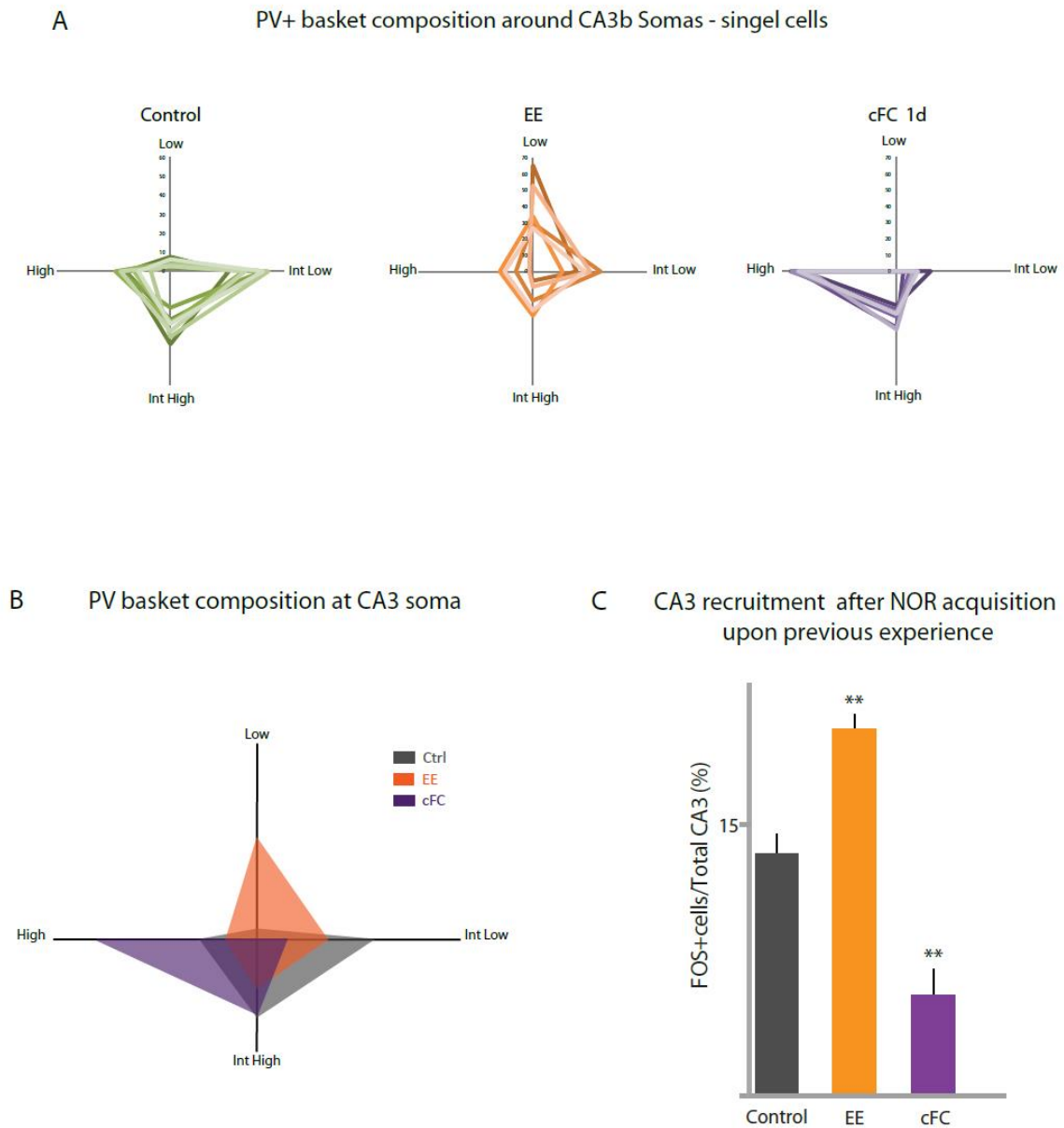
Optogenetic stimulation of VIP+ or PV+ interneurons *in vitro*. Panel C provides histological identification of VIP interneurons, and their synapses onto PV+ interneurons.

Supplementary figure 5: Synaptic rearrangements upon PV manipulation



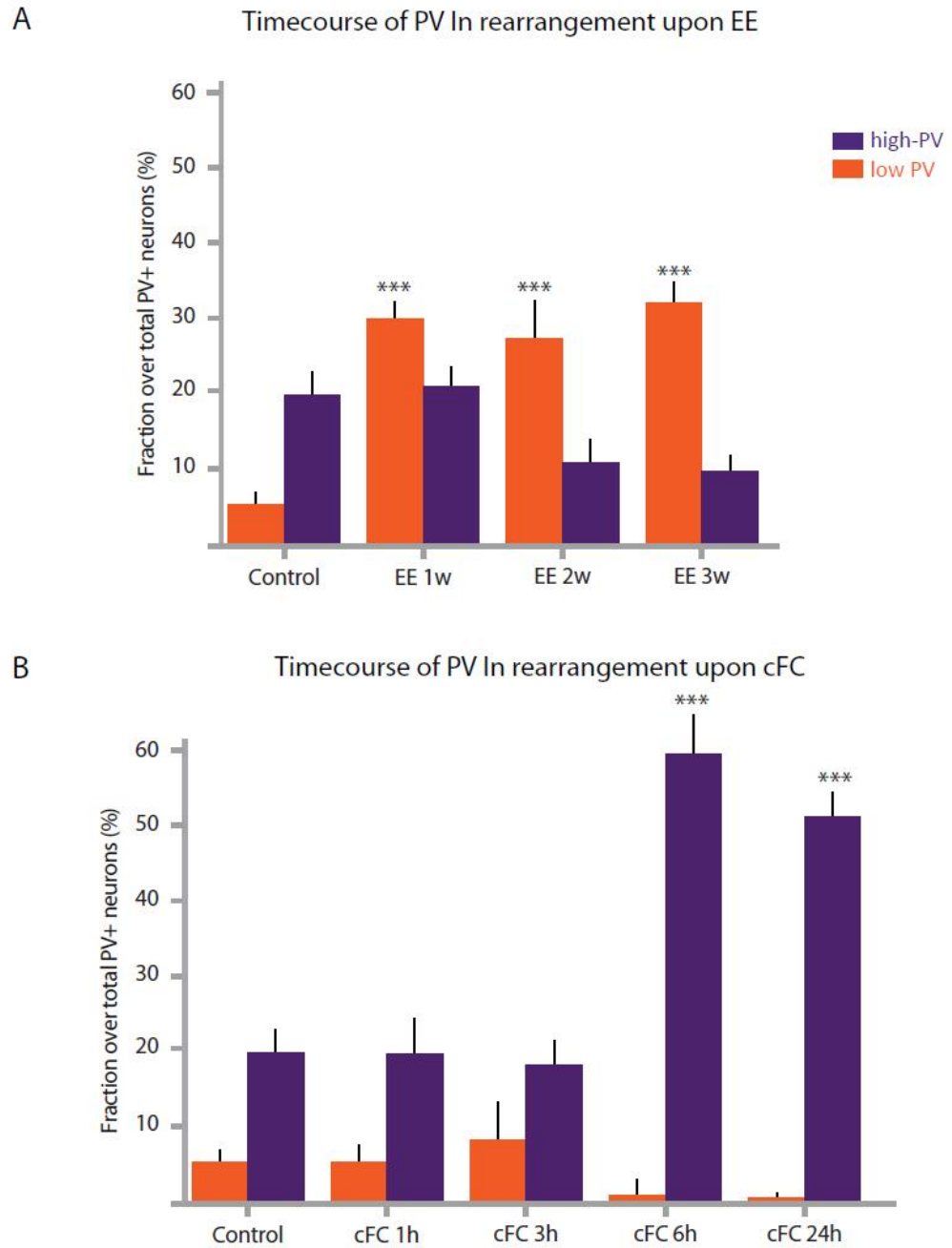
Direct manipulations targeting PV interneurons and modulating PV content are sufficient to induce structural plasticity onto their dendrites. Increase in Low PV via ChABC treatment (fig 1E) is sufficient to induce enhancement of inhibitory synapse density from both VIP+ and VIP- inputs (A and B); increase in High PV via BDNF (fig 1E), in contrast, increases excitatory synapse density onto PV dendrites.

Supplementary figure 6: Enhanced FFI and Dis in CA3 pyramidal cells upon experience



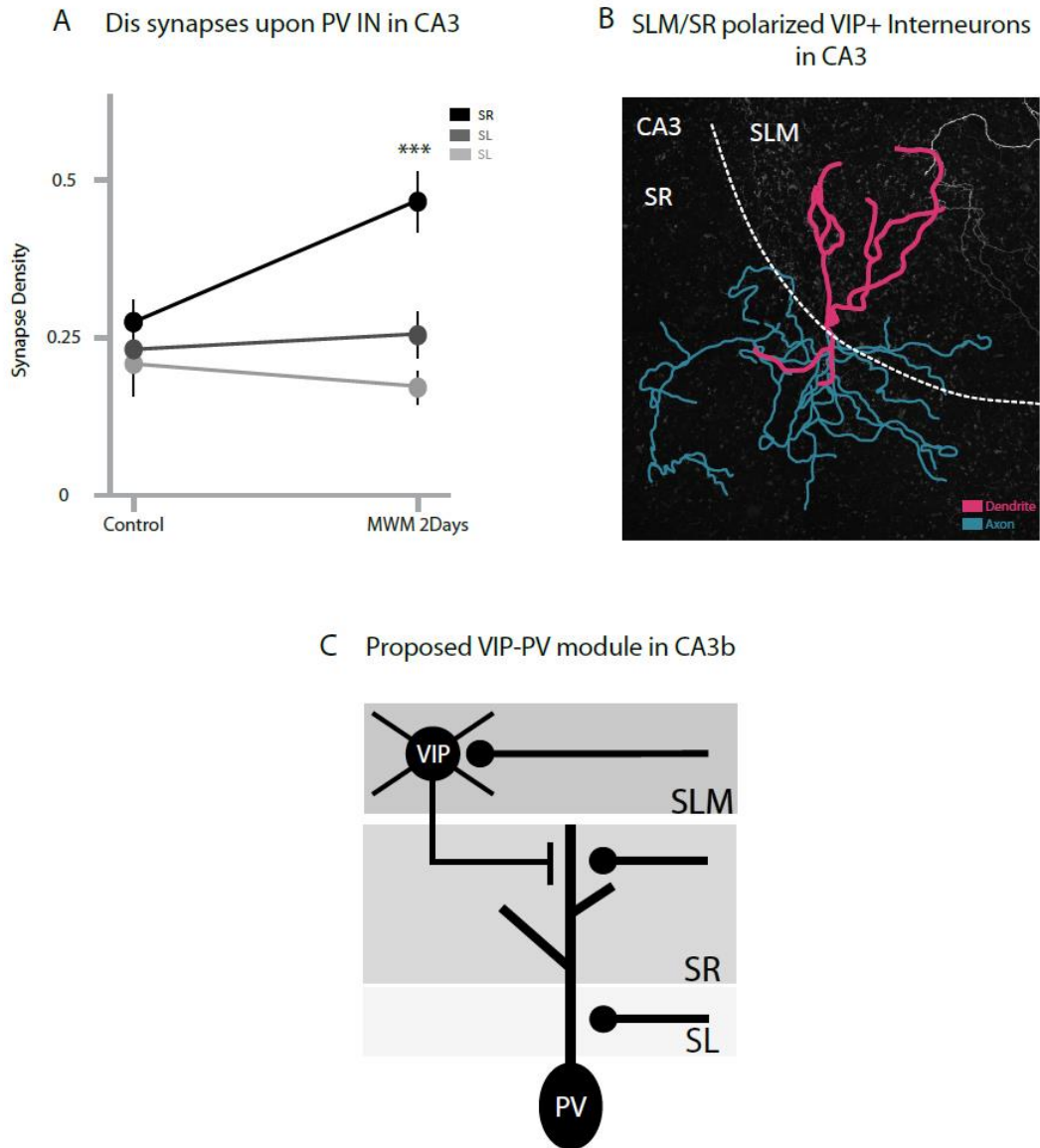
Enhanced Disinhibition and FFI upon experience is reflected in the probability of CA3 pyramidal cells recruitment upon further learning.

Supplementary figure 7: Timecourse of PV IN network rearrangement upon EE and cFC



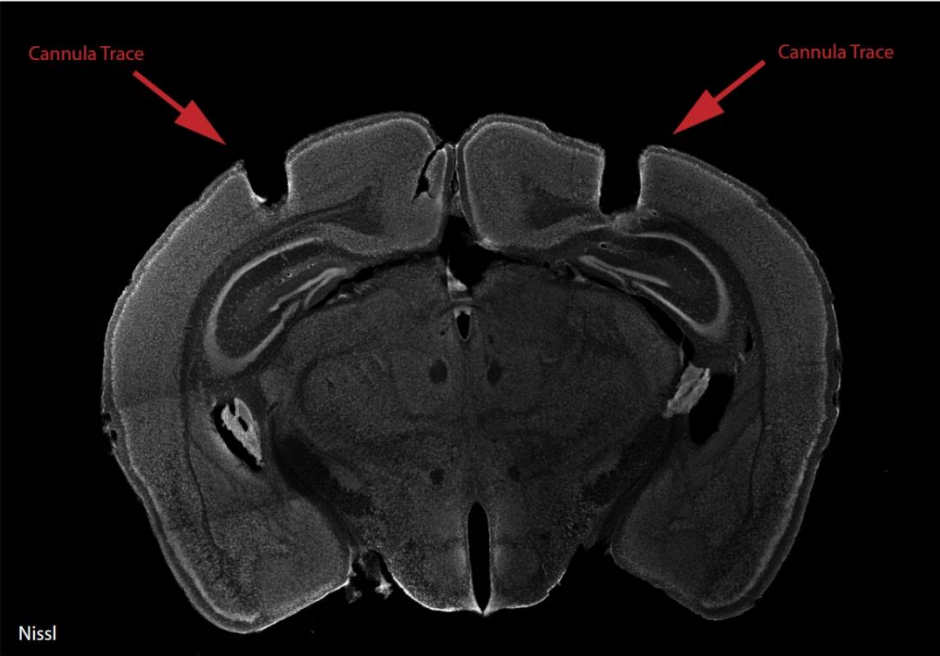
Linear progression in the PV network distribution toward the plastic or crystallized state upon enrichment and fear conditioning.

Supplementary figure 8 : Specificity in Disinhibitory connectivity upon MWM 2days



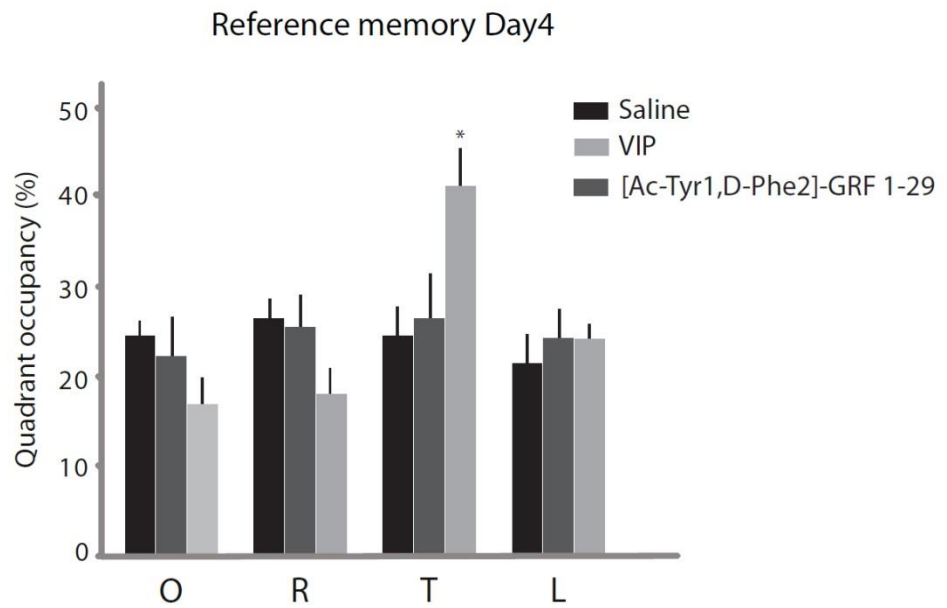
Specificity in the extent of structural plasticity upon MWM 2d (**A**) and the existence of polarized VIP+ neurons in CA3 exhibiting dendritic arborization in SLM and axonal ramifications in SR (**B**), suggest the existence of a microcircuit module that regulates learning in the first phase of the MWM (**C**).

Supplementary figure 9: Histology for chronic topic treatments



Coronal section of cannula-impalnted brains for VIP modulation upon learning.

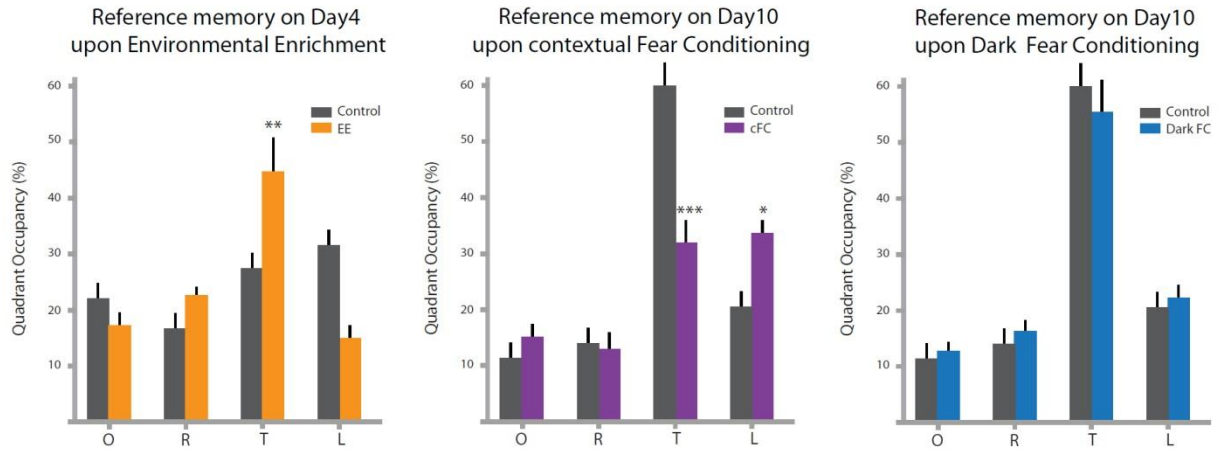
Supplementary figure 10: Reference Memory upon VIP modulation



Mice treated with VIP during the early phase of water maze learning exhibits a significant reference memory already on day 4, when saline or GRF treated mice show a permancece in the target wuadrant that is not different prom chance levels.

Supplementary figure 11: Reference Memory upon previous experience

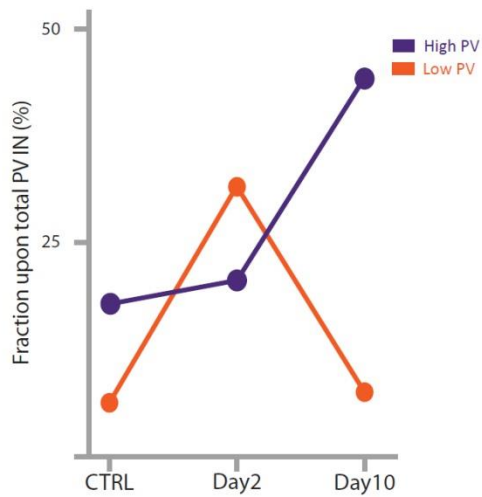
A Reference Memory upon previous experience



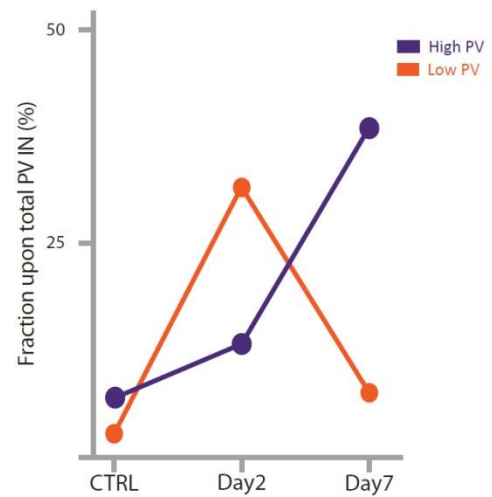
Enriched mice, which start the maze training in a plastic configuration of the CA3 network, show significant reference memory on day 4 (with controls performing slightly better than chance levels), with no difference to controls on day 10 (data not shown). In stark contrast, mice who learned the contextual fear conditioning immediately before training started were impaired in their performance on the whole timecourse of the experiment (figure 3L), and fail to form a proper reference memory on day 10. Conditioning in the dark did not produce any deviation to controls.

Supplementary figure 12:
Parallel rearrangements in PV IN network upon incremental learning
in Hippocampus and Motor Cortex M1

A PV Network in CA3 upon MWM

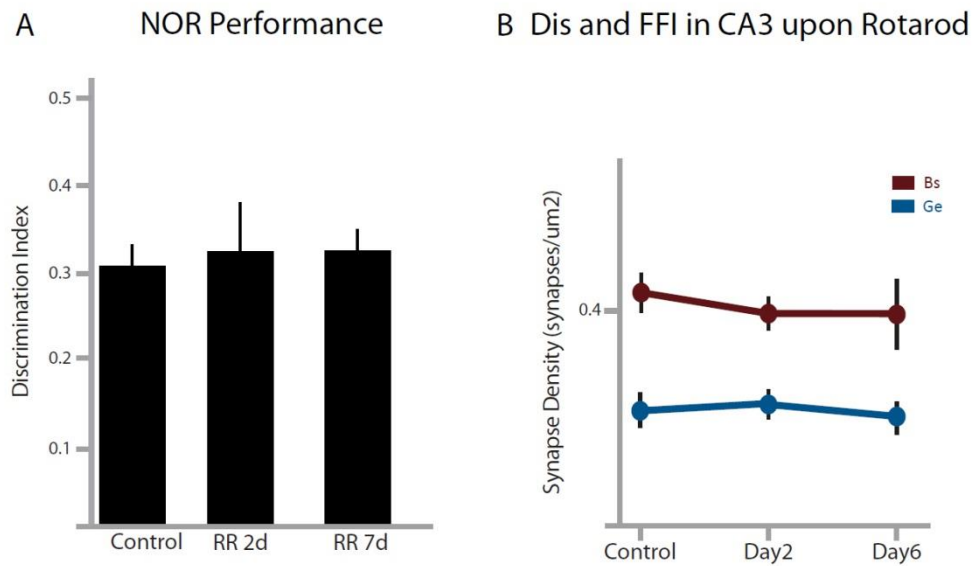


B PV Network in M1 upon RR



Comparable extent of PV network remodeling in the hippocampus and M1 upon incremental learning.

Supplementary figure 13: Specific PV network modulation in microcircuits recruited by learning



PV network rearrangement upon learning is specific for the microcircuits involved in the learning process. Indeed, upon rotarod learning (which is hippocampus-independent), neither rewiring upon PV neurons in the hippocampus, nor changes in NOR performances could be observed.

4.2

Goal-oriented searching mediated by ventral hippocampus early in trial-and-error learning

Sarah Ruediger*, Dominique Spirig*, Ivan Flavio Donato*
and Pico Caroni

*these authors contributed equally to the work

Published Article, Nature Neuroscience, 2012 Sept 23; 15 (11): 1563-71

4.2.1 Summary

Most behavioral learning in biology is trial and error, but how these learning processes are influenced by individual brain systems is poorly understood. Here we show that ventral-to-dorsal hippocampal subdivisions have specific and sequential functions in trial-and-error maze navigation, with ventral hippocampus (vH) mediating early task-specific goal-oriented searching. Although performance and strategy deployment progressed continuously at the population level, individual mice showed discrete learning phases, each characterized by particular search habits. Transitions in learning phases reflected feedforward inhibitory connectivity (FFI) growth occurring sequentially in ventral, then intermediate, then dorsal hippocampal subdivisions. FFI growth at vH occurred abruptly upon behavioral learning of goal-task relationships. vH lesions or the absence of vH FFI growth delayed early learning and disrupted performance consistency. Intermediate hippocampus lesions impaired intermediate place learning, whereas dorsal hippocampus lesions specifically disrupted late spatial learning. Trial-and-error navigational learning processes in naive mice thus involve a stereotype sequence of increasingly precise subtasks learned through distinct hippocampal subdivisions. Because of its unique connectivity, vH may relate specific goals to internal states in learning under healthy and pathological conditions.

4.2.2 Introduction

Trial-and-error forms of learning and memory involve the deployment of complex individual learning sequences that lead to sustained modifications of behavior and efficient mastery of complex tasks^{1,2}. Whether the learning sequences underlie principles reflected in the organization and recruitment of distinct brain systems has remained unclear. Trial-and-error learning has mainly been investigated in the context of striatal circuits, in which increasingly effective habits support optimization of learning processes, and it may be implemented by parallel loops of striatal subcircuits³⁻⁷. Accordingly, theoretical studies have predicted that complex trial-and-error tasks are best broken down into subtasks to be addressed independently by separate subsystems⁸. Further, studies of machine and animal learning have suggested that effective early search strategies should focus on local associations to goals, but whether and how such goal-oriented searching occurs has remained unclear^{1,8}.

The hippocampus provides an attractive system to investigate the notion that trial-and-error learning of biologically relevant tasks might involve the recruitment of functionally complementary subsystems. Thus, the hippocampus is of crucial importance in supporting trial-and-error navigation tasks that involve the rapid combination of episodes in space and time⁹⁻¹¹. Furthermore, although local circuits are comparable throughout the hippocampus, the vH, intermediate hippocampus (iH) and dorsal hippocampus (dH) subdivisions differ substantially in tuning, connectivity, gene expression and function¹²⁻¹⁹. Gene-expression studies have revealed the existence of discrete spatial boundaries between principal neurons in vH, iH and dH, suggesting that the subdivisions reflect discrete entities^{14,15,17}. On the basis of their connectivity in distinct brain networks^{15,20,21}, vH (anterior in humans) is thought to be more concerned with emotions and body states¹⁵, whereas dH (posterior in humans) has predominantly visuo-spatial and cognitive functions¹²⁻¹⁶. Although dH is important in spatial learning^{12,13,16}, the function of vH in learning has remained less clear¹⁵. This might be because most studies have focused on the endpoints of complex hippocampus-dependent tasks, which are often highly spatial and cognitive, and on average population performances instead of how individual animals learn a task.

Hippocampal learning can be associated with a robust local growth of new excitatory synapses by large mossy fiber terminals (LMTs) in CA3 onto fast-spiking GABAergic interneurons (FFI growth), which are crucial for memory precision²². The new synapses do not stabilize in mice lacking β -adducin²³, and local virus-mediated reintroduction of β -

adducin in granule cells restores structural plasticity and memory precision²². At the physiological level, FFI growth is required to recruit comparatively small ensembles of pyramidal neurons expressing the transcription factor c-Fos in CA3 upon learning, a function that seems to underlie the role of FFI growth in memory precision²². Here we exploited these structural traces of learning to map and probe the involvement of hippocampal subdivisions during navigational learning. We investigated longitudinally how individual naive laboratory mice learn to navigate a Morris water maze²⁴ and combined these detailed behavioral analyses with anatomical and local genetic-rescue studies to dissect the roles of the hippocampal subdivisions in this complex trial-and-error learning process.

4.2.3 Results

Individual mouse strategies reveal three learning phases

We first analyzed the average learning patterns of mice in the Morris water maze. In this task a platform is hidden at a fixed position in the water, and mice are released facing the wall at different positions in the circular maze. Performance is recorded as time to locate the platform (escape latency) during training trials (Fig. 1a), and spatial memory is assayed as persistence in searching the platform quadrant in the absence of the platform (reference memory)^{12,24}. In addition to these conventional readouts, and to augment the power of the analysis, we categorized the behavior of individual mice according to the incidence of distinct search strategies²⁵⁻²⁷ as a function of training trial (Fig. 1b and Online Methods). Consistent with previous reports²⁴⁻²⁶, this detailed behavioral analysis revealed that mice applied qualitatively different search strategies as they became more proficient at this spatial task: global (random swim) and then local search strategies (scanning and chaining) were predominant during early phases of learning, and spatial search strategies (directed search, focal search and direct swim) took over during late phases (Fig. 1c). Average latencies and strategies evolved continuously as a function of trial number (Fig. 1a,c).

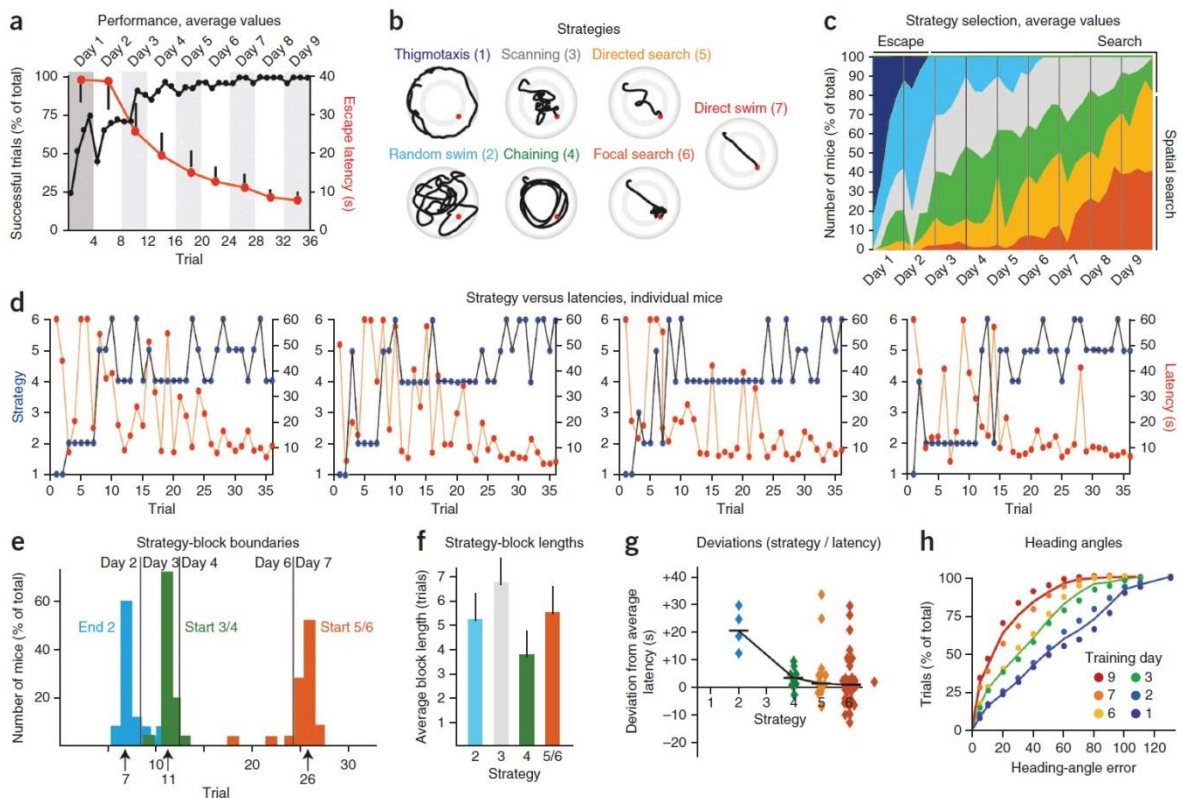


Figure 1: Sequential deployment of search-strategy habits during water maze learning.

(a–c) Behavioral analysis of water maze learning at the population level. Mean values for 30 mice. Performance (a) was evaluated as average escape latency and percentage of successful trials at each trial and training day. A schematic representation and color code for each strategy (b) and the average prevalence of each strategy by trial number (c) are shown. (d–h) Behavioral analysis of water maze learning in individual mice. (d) Strategy and latency versus trial number for four representative mice. (e) Distribution of strategy-block boundaries for 25 individual mice, with percentages of mice for which block 2 (blue) ended and blocks 3 or 4 (green) and 5 or 6 (orange) began, represented as a function of trial number. (f) Total block-length values for individual mice, averaged over 25 mice. (g) Extent to which the latencies of individual trials involving the exploration of alternative strategies differed from the mean latencies for that phase of the training process. The individual values represent the latency deviations for individual trials, ordered according to the strategy of the exploratory trials (25 mice; see Online Methods). (h) Prevalence of heading-angle error by training day. Cumulative plots; four trials per day, 25 mice. Each dot represents the relative incidence of angles ranging between two consecutive data points (for example, between 20° and 10°). The colored lines highlight learning phases and connect averages for indicated training day intervals. Error bars, s.e.m.

We then analyzed the learning curves of individual mice. In contrast to what could be detected at the population level, individual mice showed notable search habits, consisting of repeated use of the same search strategy in at least three consecutive trials (see Online Methods), interrupted by one or two trials involving alternative, and in most cases more ‘advanced,’ strategies (Fig. 1d). Individual latency curves oscillated substantially during the first half of the learning process (Fig. 1d). To provide average measures of these individual behaviors, we then determined whether features of the search habits were shared among cohorts of mice during learning. A detailed analysis of 28 individual learning curves revealed

that the majority of mice (21/28) ended a first block, involving strategy 2 (random swim) after trial 7 (just before the end of day 2), and initiated a second block, involving strategy 3 (scanning) or 4 (chaining) at trial 10–12 (during day 3), which was followed by a third series of blocks involving strategies 5 and 6 (directed search and focal search, respectively; denoted as 5/6) during trials 22–26 (between days 5 and 7) (Fig. 1e). The majority of mice (25/28) showed a strategy progression of 2-4-5/6 (13/25) or 2-3-5/6 (8/25), and a smaller fraction of mice (3/28) showed a 2-5/6 pattern (Fig. 1d, right, and Supplementary Fig. 1). Among different cohorts of mice, individual search habits seemed to begin and end at comparable stages during learning. Consistent with this notion, average total block lengths per mouse for each search habit were also comparable (strategy 2: 5.2 ± 1.2 trials; strategy 3: 6.7 ± 0.95 trials; strategy 4: 3.65 ± 0.85 trials; strategies 5/6: 5.46 ± 1.17 trials (s.e.m.); Fig. 1f and Online Methods). Furthermore, even when mice explored alternative strategies during a particular search habit, corresponding individual latencies matched average values for the particular learning phase across the mouse cohort (Fig. 1g). Finally, a population analysis of initial heading-angle errors as a function of training day (see Online Methods) provided additional independent evidence that progress during the maze learning process had some discontinuous features, with prominent improvements again occurring between days 2 and 3 and between days 6 and 7 (Fig. 1h). Taken together, these results suggested that the learning processes of individual naive mice might involve learning phases characterized by distinct search habits. In most mice, the learning phases corresponded to training days 1–2 (trials 1–8; first phase: blocks of strategy 2, >50% of trials with heading-angle errors >50°), days 3–6 (trials 9–24; second phase: blocks of strategies 3 and 4, >50% of trials with heading-angle errors <30°) and days 7–9 (trials 25–36; third phase: blocks of strategies 5/6, >50% of trials with heading-angle errors <10°).

FFI growth at hippocampal subdivisions during learning

To investigate the neural basis of the sequential phases of maze learning, we investigated hippocampal patterns of FFI growth at LMTs in CA3b (ref. 22). Cohorts of mice underwent repeated daily training periods of different total durations (four trials per day, as described above), and we determined values for number of filopodia per LMT (filopodia/LMT) on the day after the final training day. We detected distinct baselines and learning-related patterns of filopodia/LMT values in vH, iH and dH (mean baseline number of filopodia/LMT = 1.74 ± 0.1 (dH), 2.32 ± 0.1 (iH) and 3.11 ± 0.15 (vH); Fig. 2a,b and Supplementary Fig. 2; see Online Methods). In vH, filopodia/LMT values increased abruptly after day 2 (in 12/12 mice

analyzed) and reached plateau levels 1.8-fold higher than ventral baseline values by day 3 (Fig. 2b). No filopodial increases were detected at 1 h or 4 h after the last trial on day 2, suggesting that this FFI growth reflected an overnight memory consolidation process (data not shown). The marked increase in synapse numbers was accompanied by a corresponding increase of c-Fos recruitment upon training in CA3b pyramidal neurons from day 3 in vH (percentage of c-Fos+ vH neurons = 2.34 ± 1.2 (day 1) and 3.2 ± 1.6 (day 2), not significant (n.s.), and 13.4 ± 2.4 (day 3), $P < 0.001$; Fig. 2b). In iH, filopodial growth was first detectable on day 3 and increased gradually to reach plateau values (also ~1.8-fold higher than intermediate baseline levels) by day 5–6 (Fig. 2b). FFI growth in iH was specifically correlated to increasing c-Fos recruitment upon training in the same subdivision (percentage of c-Fos+ iH neurons = 2.68 ± 1.3 (day 3) and 16.95 ± 1.7 (day 6), $P < 0.01$; Fig. 2b). Finally, in dH, filopodia/LMT values did not increase significantly up to day 5 of the training protocol, and then they increased gradually to reach plateau values (also ~1.8-fold higher than dorsal baseline values) at day 8–9 (percentage of c-Fos+ dH neurons = 1.8 ± 1.2 (day 1) and 15.4 ± 2.2 (day 9), $P < 0.01$; Fig. 2b). As with vH and iH, FFI growth in dH was specifically correlated to increased c-Fos recruitment in that hippocampal subdivision (percentage of c-Fos+ dH neurons = 1.8 ± 1.2 (day 1) and 15.4 ± 2.2 (day 9), $P < 0.01$; Fig. 2b). Furthermore, FFI growth in dH was correlated with the quality of reference memory in individual mice, whereas FFI growth in vH and iH was not (Pearson correlation $r = 0.75$ (dH), $P < 0.001$ and 0.24 (iH) and 0.03 (vH), n.s.; Fig. 2c).

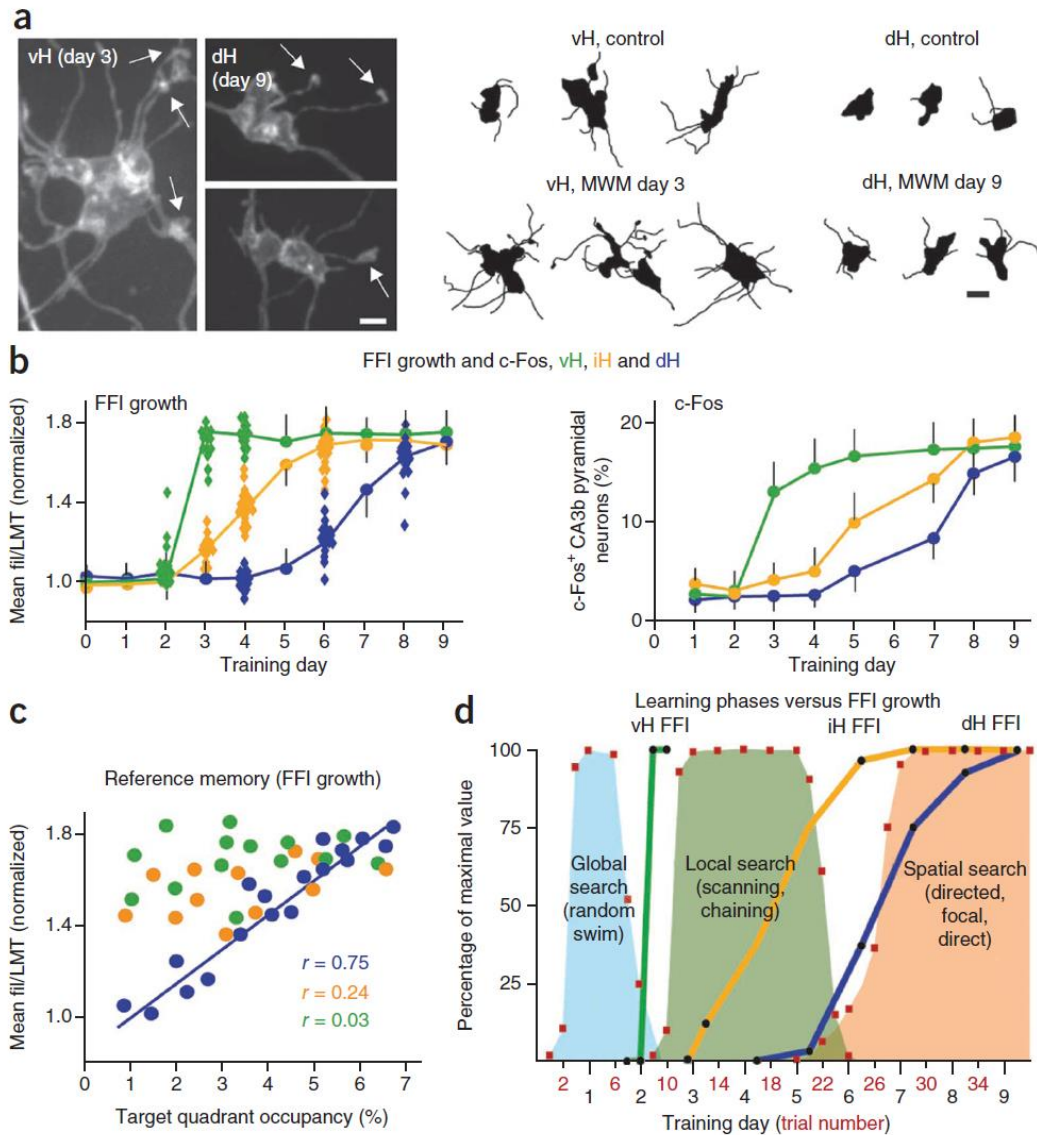


Figure 2: Sequential recruitment of hippocampal subdivisions during maze learning.

(a) Representative examples of GFP-positive LMTs (left, photographs; right, camera lucida drawings) in CA3b of vH and dH on days 3 and 9, respectively, of the maze training procedure (MWM). Arrows indicate varicosities (putative presynaptic terminals²²) at the tips of filopodia. Scale bars, 5 μ m. (b) FFI growth (left) and percentage of c-Fos⁺ CA3b pyramidal neurons (right) in vH, iH and dH during maze training. $n = 6$ – 10 mice. Individual dots at days 2, 3, 4, 6 and 8: filopodia/LMT values for individual mice shown for transition time points (left). (c) FFI growth at dH (but not iH or vH) is correlated to spatial learning (reference memory). Fil, filopodia. Target quadrant occupancy, percentage of test time spent in target quadrant (values are given as 1/10 of actual percentage). Dots represent values for individual mice, collected between day 5 and day 9 of the training procedure. (d) Schematic illustration of the relationship between the prevalence of search-strategy habits (blue, green and orange areas) and FFI growth at vH, iH and dH as a function of trial number (for search habits; red) and training day (for FFI growth; black) during maze learning. Individual values are averages from the data shown in b and Figure 1e. Error bars, s.e.m.

We compared how average search-strategy habit distributions (per trial number) and FFI growth at hippocampal subdivisions (per day) evolved during maze learning (Fig. 2d). In most mice, vH FFI growth (beginning at day 3) anticipated the onset of local search habits

such as scanning and chaining (at trial 10, >80% of mice) (Fig. 2d). Gradual FFI growth at iH (from day 3 to day 6) coincided with the deployment of local search habits and reached plateau values when most mice had switched to spatial search habits. Finally, gradual FFI growth in dH coincided with the consistent deployment of spatial search strategies. Together, these findings suggested that, in mice, trial-and-error learning to navigate a water maze involves a stereotyped sequence of learning phases. These results were consistent with a specific role for dH in fine-scale spatial-map learning late in maze navigation and suggested that vH and iH may have distinct and sequential roles during earlier phases of maze learning.

vH FFI growth and the learning of specific task-goal associations

We next sought to determine what aspects of trial-and-error tasks might be learned through vH. Because this hippocampal subdivision is connected to goal-related networks, and recent studies have provided evidence that it contains single units tuned to goal^{15,18,19}, we explored the possibility that vH might support the learning and implementation of specific associations between invariant features of the task and reward-related goal²⁸. To this end, we first investigated mice that underwent a novel-object recognition task in the absence or presence of a positive food reward. In the absence of reward (incidental learning), mice did not show alterations in novel-object discrimination in subsequent training sessions or alterations in filopodia/LMT values in vH or dH (Supplementary Fig. 3). By contrast, when a food reward was repeatedly associated with the familiar object, relative exploration time for the familiar object increased gradually beginning on day 3–4 (Supplementary Fig. 3). Furthermore, beginning on day 11–12, but not yet on day 10, mice showed a strong preference for the familiar object, even in the absence of food reward (reference memory). Notably, mean filopodia/LMT values increased selectively between days 10 and 12 in vH but not dH, and the vH increase was closely correlated with reward-controlled learning in individual mice (Supplementary Fig. 3; see Online Methods). These results provided evidence that conversion of an incidental goal-free task into a reward-based one is sufficient to induce FFI growth at vH upon behavioral learning (tested as reference memory). Because acquisition of a behavioral bias and FFI growth were closely correlated at the individual level in mice, the results further suggested that FFI growth occurred in vH within 1 d of bias learning in these experiments.

In further experiments aimed at determining whether FFI growth in vH depends on behavioral learning of hippocampal associations to reinforcers, we carried out fear-conditioning experiments (negative reward) under normal light conditions (contextual conditioning, hippocampus dependent) and in complete darkness (conditioning to explicit cues, not hippocampus dependent). We found that, whereas mice that underwent contextual fear-conditioning showed FFI growth in vH and dH, those that had been conditioned in the dark froze when re-exposed to the same odor or cage floor but did not show alterations in mean filopodia/LMT values or c-Fos recruitment in vH or dH (Supplementary Fig. 3; see Online Methods). These results were reminiscent of the perceptual requirements for hippocampal encoding²⁹ and suggested that FFI growth upon behavioral learning is induced in vH only if the behavioral protocol involves conditions producing hippocampal associations between context and reward. We then determined whether vH FFI growth during maze navigation might involve learning about a specific task-goal relationship²⁸. As we expected, when we subjected mice to the maze protocol in the absence of a platform (and, hence, in the absence of a reward-related goal), we did not observe an increase in vH filopodia/LMT values at any time (filopodia/LMT = 3.25 ± 0.2 (naive mice) and 3.29 ± 0.3 (after 2 d of free swim), n.s.; Fig. 3a). We further found that (i) omitting the platform on the first or second day of training suppressed FFI growth; (ii) 2 d of training, each involving four trials, were required for FFI growth; (iii) the second day of training did not have to immediately follow the first day to elicit FFI growth and (iv) introduction of a goal-free training day between the first and second day of goal-oriented learning inhibited ventral FFI growth after the second platform training day (Supplementary Fig. 4). Further supporting an association between vH FFI growth and reward-related goals, the extent of induction of vH FFI growth was indistinguishable whether the platform was hidden or visible (Fig. 3a). Notably, however, when the position of a visible platform was changed from a peripheral position on day 1 to positions closer to the center of the pool on day 2, no vH FFI growth was detected on day 3, suggesting that the structural plasticity might reflect learning about a specific association between the platform and its distance from the wall (Fig. 3b, right). In support of this interpretation, changing the position of the visible platform with respect to the external cues while keeping it within a comparable distance from the pool wall did not suppress vH FFI growth on day 3 (Fig. 3b, left). Taken together, these results suggested that, in maze learning, structural plasticity in vH on day 3 might involve establishing a consistent association on day 1 between the goal (the platform) and a specific aspect of the task (for example, the distance of the platform from the wall) and confirming that association on day 2 (Fig. 3c). To provide additional evidence that FFI growth at vH involves a classical reward mechanism, we interfered with signaling by the reward neuromodulator dopamine³⁰ and its D1/D5 receptor during water maze learning³¹. To this end, the D1/D5 antagonist SCH23390

was applied systemically 20 min before each training day, and control mice were treated with vehicle lacking the drug. The antagonist interfered with learning and strategy selection throughout the training procedure and completely blocked FFI growth in vH (Supplementary Fig. 4).

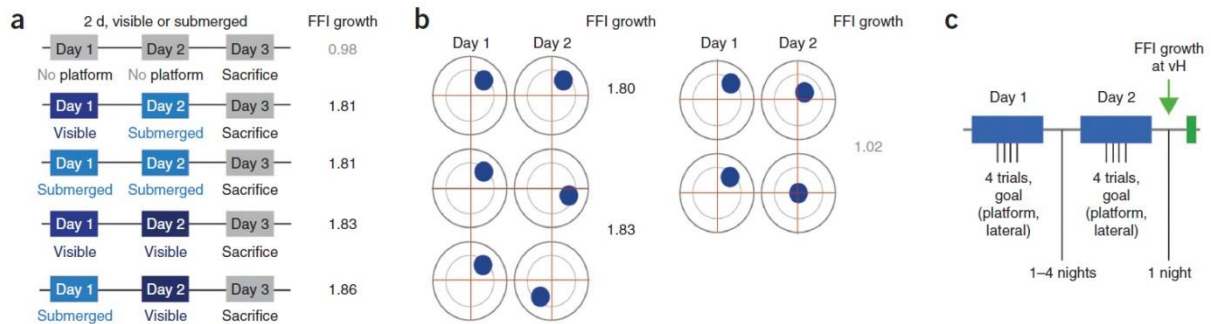


Figure3: Specific task-goal association reflected by vH FFI growth during maze learning.

(a) Analysis of experimental conditions (platform submerged, visible or absent) that produce FFI growth (fold increase) at vH. (b) Influence of platform position constancy on vH FFI growth. Moving a visible platform to a new position at a comparable distance from the wall on day 2 did not compromise FFI growth on day 3 (left), whereas moving the platform toward the center of the maze on day 2 suppressed FFI growth on day 3 (right). Mean values; $n = 5-8$ mice. (c) Schematic of requirements for FFI growth at vH.

Function of vH in water maze learning

Having defined task features that lead to FFI growth at vH early during maze training, we next addressed the function of this hippocampal subdivision during water maze learning. We reasoned that all hippocampal subdivisions might synergistically contribute to the learning process throughout training or that each subdivision might make its main, specific contribution at a distinct phase of the learning process.

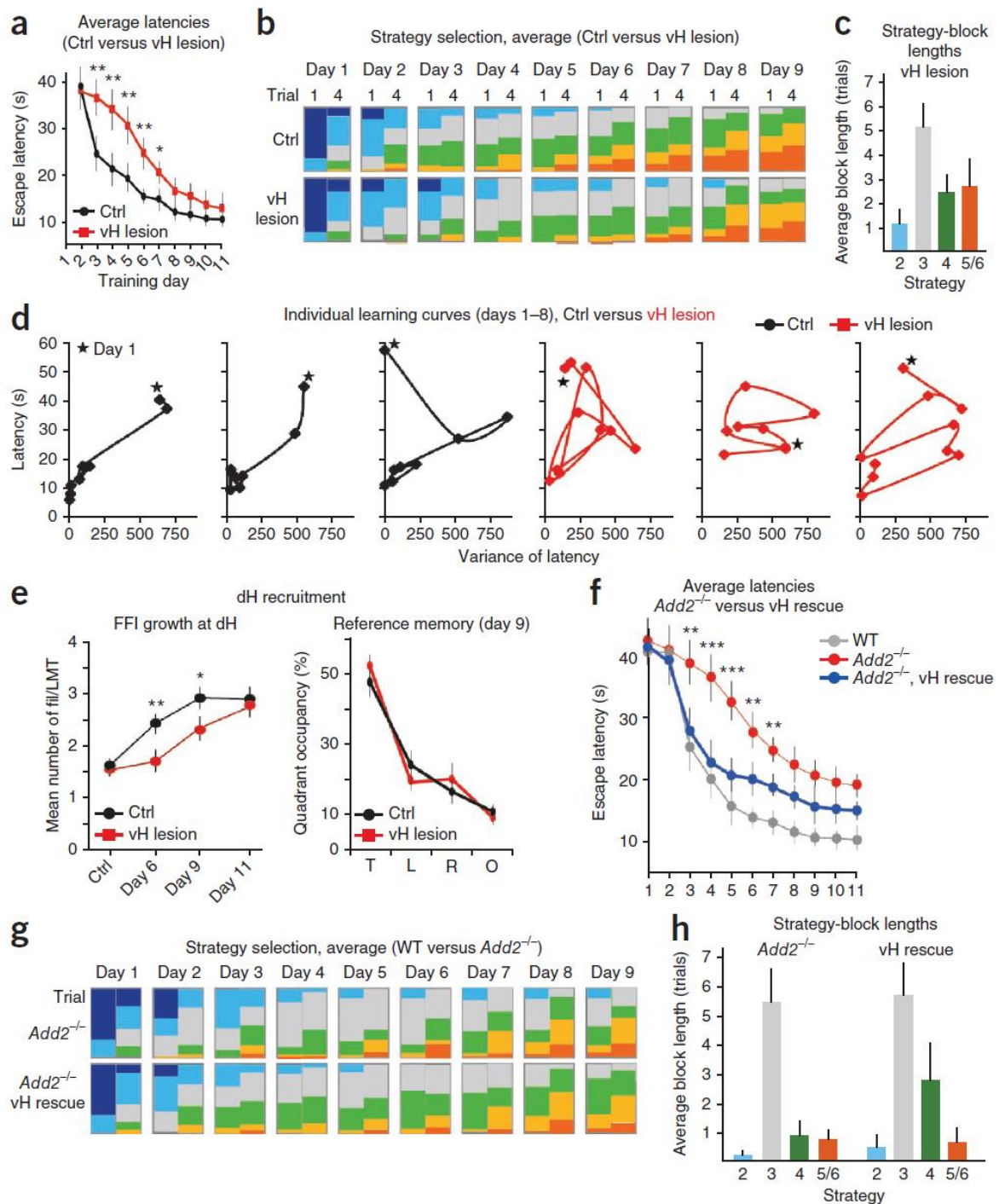
We first analyzed mice with excitotoxic bilateral lesions of vH. All mice included in the analysis had nearly complete lesions of vH CA3 (and CA1) and $<15\%$ losses at iH CA3 (Supplementary Fig. 5). Ventrally lesioned mice showed strongly compromised latency values at days 3–5 of training (day 3 escape latency = 23.2 ± 5.5 s (vehicle) versus 36.5 ± 4.1 s (vH lesion), $P < 0.01$) and improved later to reach values comparable to controls at days 10–11 (day 10 escape latency = 10.3 ± 2.2 s (vehicle) versus 12.2 ± 3.1 s (vH lesion), n.s.; Fig. 4a). Ventrally lesioned mice also showed disruption of the progression of local

search-strategy deployment during days 2–4 (use of strategy 4 on day 4 = $28 \pm 3.3\%$ of trials (vehicle) versus $15 \pm 6.5\%$ (vH lesion), $P < 0.01$), and a delayed onset of spatial search strategies, but use of those strategies during late phases of maze learning was comparable to that of control mice (use of strategy 5 and 6 on day 9 = $33 \pm 3.8\%$ of trials (vehicle) versus $29 \pm 5.1\%$ (vH lesion), n.s.; Fig. 4b). Strategy habits were less prominent in vH-lesioned mice; random swim was particularly affected by the lesions, whereas scanning habits were comparatively preserved (Supplementary Fig. 1 and Fig. 4c). Furthermore, vH lesions led to a loss of correlation between single-trial strategies, single-trial latencies and mean latencies (Supplementary Fig. 6). In what is probably reflective of this inconsistency in trial latencies, individual lesioned mice had notably unpredictable trajectories of daily variation in latency through most of the training procedure (Fig. 4d). In spite of these disruptions in performance consistency, ventrally lesioned mice showed delayed but ultimately normal reference memory¹⁶ and extents of FFI growth in dH (Fig. 4e). These results suggest that vH is important in learning during days 2–5, when global and local search strategies predominate, and in search and performance consistency throughout maze learning.

Figure 4: Role of vH in water maze learning.

(a,b) Population-level analysis of latencies (a) and strategies (b) in mice with excitotoxic lesions of vH (vH lesion) versus controls. To highlight progress within and between days, the strategy plot (b) reflects the mean strategy-recruitment values for the first and fourth trials of each day. Analysis in a,b as described in Figure 1c; $n = 15$ mice. (c) Strategy-block lengths for mice with vH lesions, as described in Figure 1f. (d) Enhanced variability of individual trials during maze learning in mice with vH lesion versus controls. Latency versus latency variance is plotted for three individual mice each. Stars indicate values for training day 1;

lines connect values from day 1 to day 8. (e) Delayed but undiminished dH FFI growth and reference memory in vH-lesioned mice. T, target; L, left; R, right; O, opposite. $n = 4$ (FFI growth) and 15 (reference memory). (f–h) Learning with FFI growth restricted to vH. Impaired maze learning in *Add2^{-/-}* mice and specific rescue of early learning phase upon reintroduction of β -adducin into granule cells of vH. Population- and individual-level analysis was done as described in a–c. $n = 12$ mice. WT, wild type; Ctrl, controls injected with vehicle only; fil, filopodia. Error bars, s.e.m.; * $P < 0.05$, ** $P < 0.01$, *** $P < 0.001$.



To further define the function of vH in maze learning, we devised experiments in which learning-related FFI growth was confined to vH. In mice lacking the actin cytoskeleton–cell cortex linker protein β -adducin (*Add2*^{-/-}), which are deficient in learning-related FFI growth and procedure (day 3 latency = 24.5 ± 1 s (wild type) versus 38.3 ± 3.4 s (*Add2*^{-/-}), $P < 0.01$; day 5 latency = 14.8 ± 3.2 s (wild type) versus 32.1 ± 2.6 s (*Add2*^{-/-}), $P < 0.001$; day 7 latency = 12.3 ± 2 s (wild type) versus 23.8 ± 2.3 s (*Add2*^{-/-}), $P < 0.001$; Fig. 4f,g). Furthermore, *Add2*^{-/-} mice showed very few learning-related habits throughout training (Fig.

4h). In Add2^{-/-} mice in which β -adducin had been reintroduced locally in vH (but not iH or dH) granule cells using a lentivirus expressing a β -adducin–green fluorescent fusion protein (GFP– β -adducin)²³, learning-related FFI growth was specifically rescued in vH (day 3 filopodia/LMT = 2.78 ± 0.3 (Add2^{-/-}) versus 5.96 ± 0.3 (vH rescue), $P < 0.0001$; Supplementary Fig. 7). Supporting the notion that behavioral learning involving vH is crucial specifically during early phases of maze learning, ventral rescue restored average latency and strategy curves to wild-type values beginning on day 3 and continuing until day 5 of training (day 5 latency = 14.8 ± 3.2 s (wild type) versus 20.1 ± 4 s (vH rescue), n.s.), whereas further improvements beyond that early phase were still inhibited (day 11 latency = 10.2 ± 1.1 s (wild type), 19.4 ± 1.9 s (Add2^{-/-}) and 16.1 ± 1.7 (vH rescue), $P < 0.05$; Fig. 4f,g). The analysis of individual mice revealed that the second learning phase (local search habits) was specifically rescued (average block length for strategy 4 = 3.65 ± 0.85 (wild type) and 1.1 ± 0.41 (Add2^{-/-}), $P < 0.01$, and 2.45 ± 1.1 (vH rescue), n.s.), whereas the first phase (average block length for strategy 2 = 5.2 ± 1.2 (wild type); 0.2 ± 0.1 (Add2^{-/-}), $P < 0.001$, and 0.51 ± 0.4 (vH rescue), $P < 0.01$) and the third phase (average block length for strategies 5/6 = 5.46 ± 1.2 (wild type), 0.84 ± 0.3 (Add2^{-/-}), $P < 0.001$, and 0.76 ± 0.4 (vH rescue), $P < 0.001$) were not (Supplementary Fig. 1 and Fig. 4h).

Function of iH in water maze learning

To investigate the function of iH in maze learning, we analyzed mice with complete bilateral excitotoxic lesions of iH (Supplementary Fig. 5). None of the mice showed neuronal losses extending >10% into the anterior-posterior extension of adjacent vH or dH (Supplementary Fig. 5). The learning curves of mice with iH lesions were specifically delayed between day 4 and day 7 of the learning process, and iH-lesioned mice reached latency values comparable to non-lesioned controls by day 11 (day 11 latency = 9.8 ± 2 s (vehicle) and 11.4 ± 2 (iH lesion), n.s.; Fig. 5a,b). iH-lesioned mice showed much smaller variations in latency across individual trials than vH-lesioned mice (Fig. 5c; compare to Fig. 4d). A strategy analysis revealed a very prolonged deployment of local search habits (scanning and chaining; average block length for strategy 4 = 6.12 ± 0.7 , $P < 0.05$) and delayed deployment of spatial search strategies (Fig. 5b,d). Consistent with this delay in spatial search strategies, spatial reference memory in iH-lesioned mice was greatly impaired at day 9 but comparable to control reference memory values at day 11 (day 9 target quadrant occupancy = $47.8 \pm 3\%$ (vehicle), $34.2 \pm 4\%$ (iH lesion), $P < 0.05$; day 11 quadrant occupancy = $48.1 \pm 5\%$, n.s. (iH lesion); Fig. 5e). Taken together, these results suggest that iH contributes during

intermediate phases of water maze learning³³, when local search habits are deployed and spatial search habits have not yet emerged. Consistent with previous reports¹⁶, the presence of an intact iH is not an absolute requirement for spatial learning.

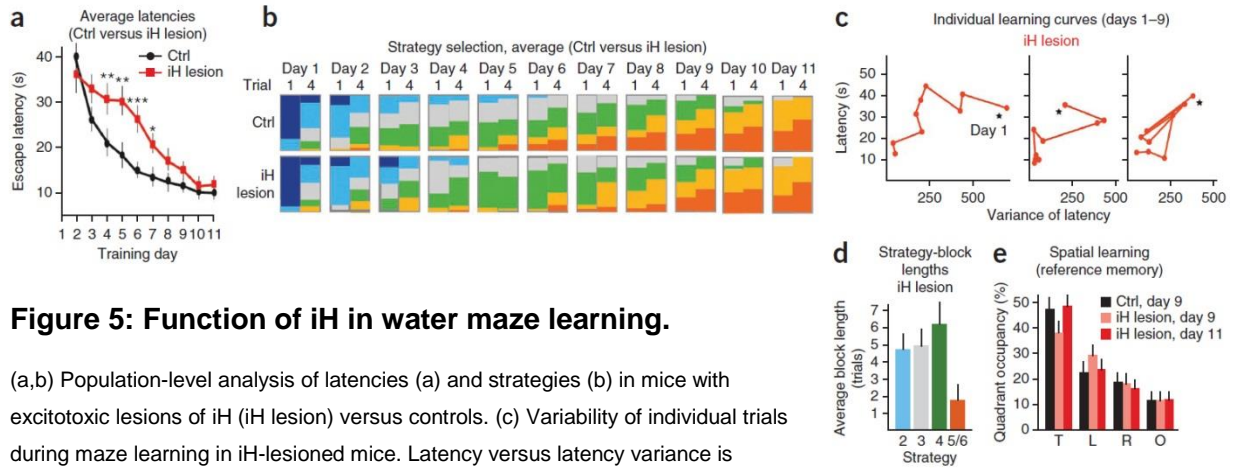


Figure 5: Function of iH in water maze learning.

(a,b) Population-level analysis of latencies (a) and strategies (b) in mice with excitotoxic lesions of iH (iH lesion) versus controls. (c) Variability of individual trials during maze learning in iH-lesioned mice. Latency versus latency variance is plotted for three individual mice (analysis as in Fig. 4d). (d) Strategy-block lengths, as described in Figure 1f. (e) Delayed but undiminished reference memory in iH-lesioned mice. $n = 8$ mice; analysis in a,b as described in Figure 4a,b; in c as in Figure 4d; in d as in Figure 4c; in e as in Figure 4e. Ctrl, controls injected with vehicle only. Error bars, s.e.m.; * $P < 0.05$, ** $P < 0.01$, *** $P < 0.001$.

Function of dH in water maze learning

Mice with bilateral excitotoxic dH lesions (Supplementary Fig. 5) were specifically impaired during the late phases (days 6–11) of maze learning (day 11 latency = 9.2 ± 2.3 s (control) and 16.5 ± 2.1 s (dH lesion), $P < 0.01$; Fig. 6a,b). dH-lesioned mice showed normal strategy deployments up to day 5 of training but failed to consistently deploy spatial search strategies during late phases of maze learning (average block length for strategy 5/6 = 0.9 ± 0.6 (dH lesion), $P < 0.001$; Fig. 6b,c). In addition, dH-lesioned mice did not show abnormally large variations in inter-trial latencies throughout maze learning (Fig. 6d; compare to Fig. 4d). Consistent with previous reports that dH is specifically required for spatial learning^{14,16}, mice with dH lesions did not establish a spatial reference memory (Fig. 6e). In control experiments, smaller, partial dH lesions with longitudinal extents comparable to those of the iH lesions (Supplementary Fig. 5; iH lesions: 800 ± 110 μm ; complete dH lesions: $1,250 \pm 120$ μm ; partial dH lesions: 600 ± 80 μm) produced late-phase learning latencies that were slightly better than those observed when complete dH lesions were present (Fig. 6a). Notably, however, the partial dH lesions also interfered with spatial searching (Fig. 6b) and

suppressed establishment of reference memory (Fig. 6e), further supporting the notion that dH is specifically required for spatial learning whereas iH is not.

β -adducin rescue specifically in dH of *Add2*^{-/-} mice markedly improved latencies at days 7–11 but did not influence latency values at days 3–5 of training (Fig. 6f). Consistent with a specific action of dH in spatial learning late during maze training, reintroduction of β -adducin in dH granule cells improved the progression of global spatial search strategies (Fig. 6g) and rescued the deployment of spatial search-strategy habits (average block length for strategies 5/6 = 0.84 ± 0.3 (*Add2*^{-/-}) and 3.95 ± 0.7 (dH rescue), $P < 0.001$; Fig. 6h), but it did not improve local strategy deployment (average block length for strategy 4 = 0.54 ± 0.1 , n.s.; Fig. 6g,h) or the correlation between single-trial and mean latencies (Supplementary Fig. 6). These results suggest that dH is required specifically to establish a spatial map of the task during late phases of water maze learning and that learning processes involving vH or dH may be recruited independently of each other during a hippocampal spatial task.

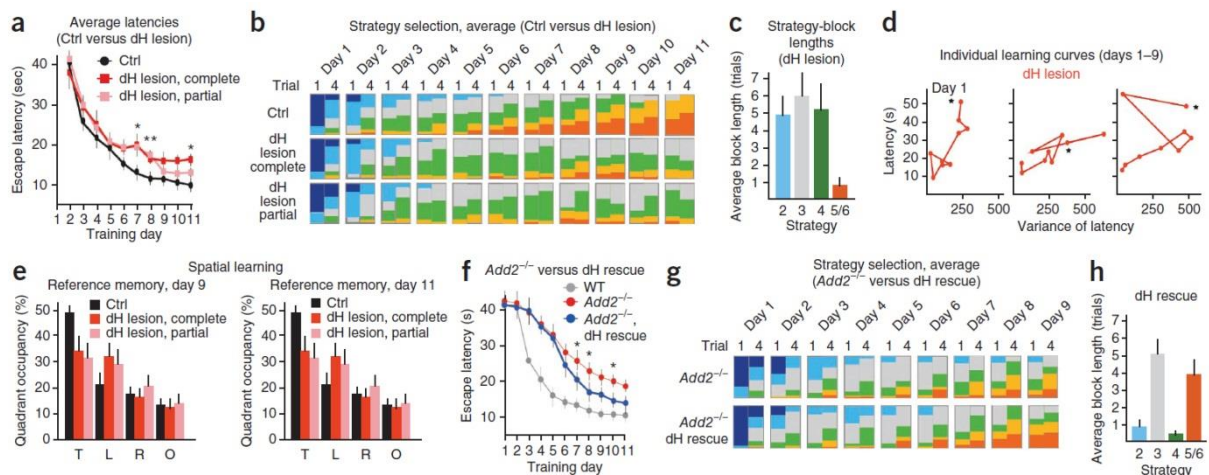


Figure 6: Function of dH in water maze learning.

(a,b) Population-level analysis of latencies (a) and strategies (b) in mice with complete or partial excitotoxic lesions of dH versus controls. (c) Strategy-block lengths in dH-lesioned mice, as described in Figure 1f. (d) Variability of individual trials during maze learning in dH-lesioned mice (complete lesions). Latency versus latency variance is plotted for three individual mice. (e) Absence of fine-scale spatial learning (reference memory) in dH-lesioned mice (complete and partial lesions). Analysis in a–h as described in Figure 4a–h. $n = 8$ mice each (a–e). (f–h) Learning with FFI growth restricted to dH. There is specific rescue of late learning phase in *Add2*^{-/-} mice upon reintroduction of β -adducin into granule cells of dH. Population and individual mouse analysis as described in a–c. $n = 12$ mice; Ctrl, control; WT, wild type. Error bars, s.e.m.; * $P < 0.05$, ** $P < 0.01$.

vH-dependent maze learning, independent of dH

To investigate whether maze learning involving vH can occur in the absence of a requirement for dH, we modified the water maze task so that it would not require fine-scale spatial learning. We reasoned that if the area of the hidden platform were larger, mice would no longer need to systematically apply spatial search strategies to effectively locate it. Indeed, when the standard platform area (A) was doubled from 78.5 cm² (corresponding to 10 cm in diameter) to 157 cm² (14 cm diameter, in a pool of diameter 140 cm), mice learned the task more rapidly (day 2 latency = 38.9 ± 4.6 s (A) and 23.8 ± 2.1 s (2A), $P < 0.001$; Fig. 7a). Mice also showed directed search and direct swim on the fourth trial throughout the training process (that is, they took ‘shortcuts’), but they did not show a consistent increase in the application of spatial search strategies during the second half of the training procedure (Fig. 7b,c). In what is probably a reflection of less challenging learning conditions and the successful application of ‘shortcuts’, the analysis of individual mice revealed a reduced deployment of habits (Supplementary Fig. 1 and Fig. 7c). Notably, although vH FFI growth was indistinguishable between the two platform areas (day 3 filopodia/LMT = 5.94 ± 0.7 (A) and 6.1 ± 0.8 (2A), n.s.), mice developed no reference memory of the platform quadrant (day 9 average target quadrant occupancy = 49.8 ± 4% (A) and 28.3 ± 2% (2A), $P < 0.01$) and did not learn to head directly for the platform between day 7 and day 9 of training. Further, mice did not show an increase in dH filopodia/LMT under 2A platform conditions (filopodia/LMT = 1.7 ± 0.1 (swim control), 2.88 ± 0.2 (A, day 9) and 1.74 ± 0.1 (2A, day 9), n.s.; Fig. 7d). iH filopodia/LMT also did not increase under 2A platform conditions (at day 9; data not shown). Consistent with the notion that dH is not required for mice to learn to navigate a maze with a 2A platform, learning curves and strategy progressions were indistinguishable between mice with complete dH lesions and controls under 2A conditions (day 2 latency = 22.5 ± 2.1 (control) and 20.8 ± 1.8 (dH lesions), n.s.; Fig. 7a,b).

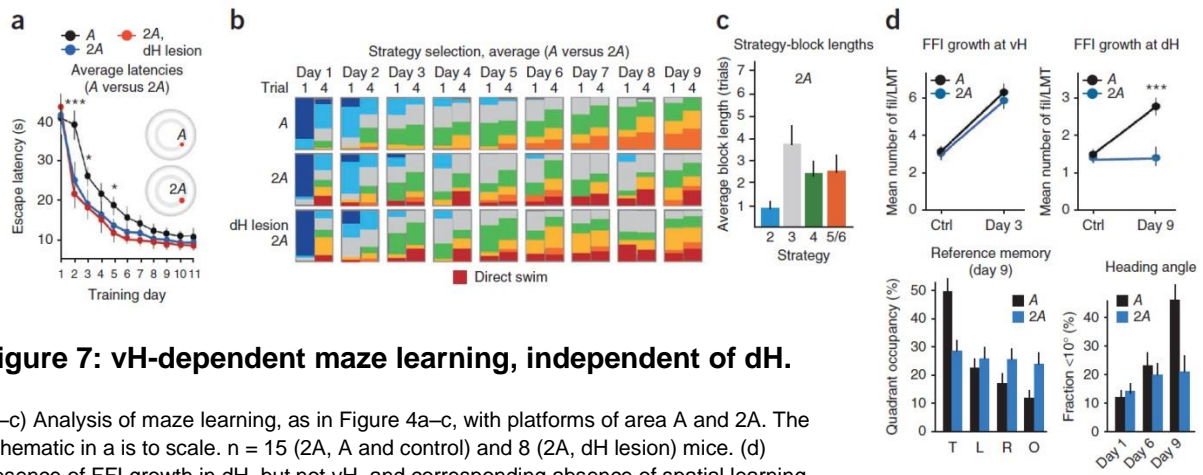


Figure 7: vH-dependent maze learning, independent of dH.

(a–c) Analysis of maze learning, as in Figure 4a–c, with platforms of area A and 2A. The schematic in a is to scale. $n = 15$ (2A, A and control) and 8 (2A, dH lesion) mice. (d) Absence of FFI growth in dH, but not vH, and corresponding absence of spatial learning (reference memory, heading angle) in mice navigating a maze with a 2A platform. Ctrl, swim control. $n = 15$ mice; fil, filopodia. Error bars, s.e.m.; * $P < 0.05$, *** $P < 0.001$.

ACKNOWLEDGEMENTS

We thank B. Sacchetti (University of Torino), C. Sandi (École Polytechnique Fédérale de Lausanne) and S. Arber (Friedrich Miescher Institut) for comments on the manuscript. The Friedrich Miescher Institut is part of the Novartis Research Foundation.

AUTHOR CONTRIBUTIONS

S.R. devised and carried out the analysis of hippocampal behavior, connectivity, vH lesions and β -adducin rescue; D.S. carried out the analysis of FFI growth and c-Fos immunoreactivity; F.D. devised and carried out behavioral and lesion studies relating vH, iH and dH FFI growth to subdivision function in learning. P.C. helped devise the experiments and wrote the manuscript. All authors discussed the results and commented the manuscript.

4.2.4 Discussion

Our detailed behavioral analysis of how individual mice learn to navigate a water maze—a biologically relevant task—combined with the analysis and local manipulation of its specific anatomical counterparts in the hippocampus, provides insights into the mechanisms of complex trial-and-error learning. We provide evidence that maze navigation involves a stereotyped sequence of subtasks that involve learning at distinct hippocampal subdivisions. The connectivity and functions of hippocampal subdivisions may thus influence how the individuals of a species address declarative trial-and-error tasks involving the hippocampus. Our results further reveal that vH is crucial early in goal-oriented learning and searching, and they thus assign a key function to vH (anterior hippocampus in humans) in complex behavioral learning. Our longitudinal analysis of water maze learning has revealed the presence of a structured learning process throughout the training procedure, as indicated by the sequential roles of vH, iH and dH during maze learning and the sequential deployment of increasingly sophisticated spatial search habits (Supplementary Fig. 8). The mechanisms linking successful subtask learning to FFI growth at hippocampal subdivisions remain to be determined and may differ among individual networks. For example, vH switches appear to occur abruptly, whereas incremental FFI growth at iH and dH during maze learning may be coupled to gradual error-function mechanisms^{3,30}. In a possibly related issue, the mechanisms underlying strategy selection and the establishment of search habits^{3,5} also remain to be determined. Because basal ganglia systems have prominent roles in the adjustment of learning and habits to performance through dopamine-mediated reward systems^{3,5,30}, it is tempting to speculate that the processes of strategy selection discovered in this study may involve cost-reward computations at striatal circuits. This possibility seems particularly plausible for learning involving vH, which has extensive connectivity with striatal circuitry^{15,21}.

Our study assigns a key function to vH in the early stages of complex trial-and-error learning. We provide evidence that FFI growth at vH reflects previous behavioral learning of consistent task-specific goal-context relationships and supports deployment of local search habits during further learning and that an intact vH is crucial in supporting performance consistency throughout maze learning. These results tie in well with previous reports that ‘simplified learning’, which consists of pre-training rats with a visible platform (a task involving learning in vH), accelerates subsequent maze learning and reduces its requirement for NMDA-mediated plasticity^{34,35}. Previous studies have not assigned functions to vH in

hippocampus-dependent spatial learning. That may be owing to a predominant focus on the endpoint of complex hippocampus-dependent learning, which usually involves cognitive and highly spatial aspects depending on dH, and to the fact that most studies have not focused on how learning is achieved longitudinally by individual animals³⁶. However, previous studies have provided evidence that vH lesions impair aversive learning and reduce anxiety^{15,37}, and these findings are consistent with the notion that vH has a crucial function in relating reinforcers to context in learning. The strong direct connectivity of vH with body state and emotional and reward systems¹⁵ might underlie its early function in goal-oriented learning and searching. Although it is possible that all hippocampal subdivisions participate in the learning process from its onset, vH might be more directly tuned to the detection and consolidation of consistent associations between goal and local task-specific features. According to this hypothesis, subsequent support of increasingly spatial and cognitive networks involving first iH and then dH might involve indirect connectivity of iH and dH with ventral reward-linked networks—for example, via thalamic nuclei and/or peri-postrhinal cortices¹⁵. Whether and how the specific connectivities of hippocampal subdivisions underlie their hierarchical recruitment during goal-oriented, trial-and-error learning remain to be determined, however. Our results provide evidence that vH acts in maze learning up to day 6, and they suggest a partially overlapping and later function for iH. The function of iH is poorly understood, but it can mediate rapid place learning³³ and has been suggested to integrate ventral and dorsal functions in hippocampus-dependent behavioral learning^{15,33}. One possibility consistent with our findings is that FFI growth at vH on day 3 is important to support place learning mediated by iH between days 3 and 6 (Supplementary Fig. 8).

The assignment to vH of a crucial function in early goal-oriented learning has implications for future research. Thus, efficient goal-oriented learning and searching and rapid mastering of intermediate goals are likely to be key determinants of success in realistic biological settings. Furthermore, the linkage of emotional processes to declarative learning through vH may affect behavioral learning in emotionally complex settings, including social interactions. Accordingly, it will be of interest to determine how vH influences the learning of emotionally complex tasks under healthy and pathologic conditions.

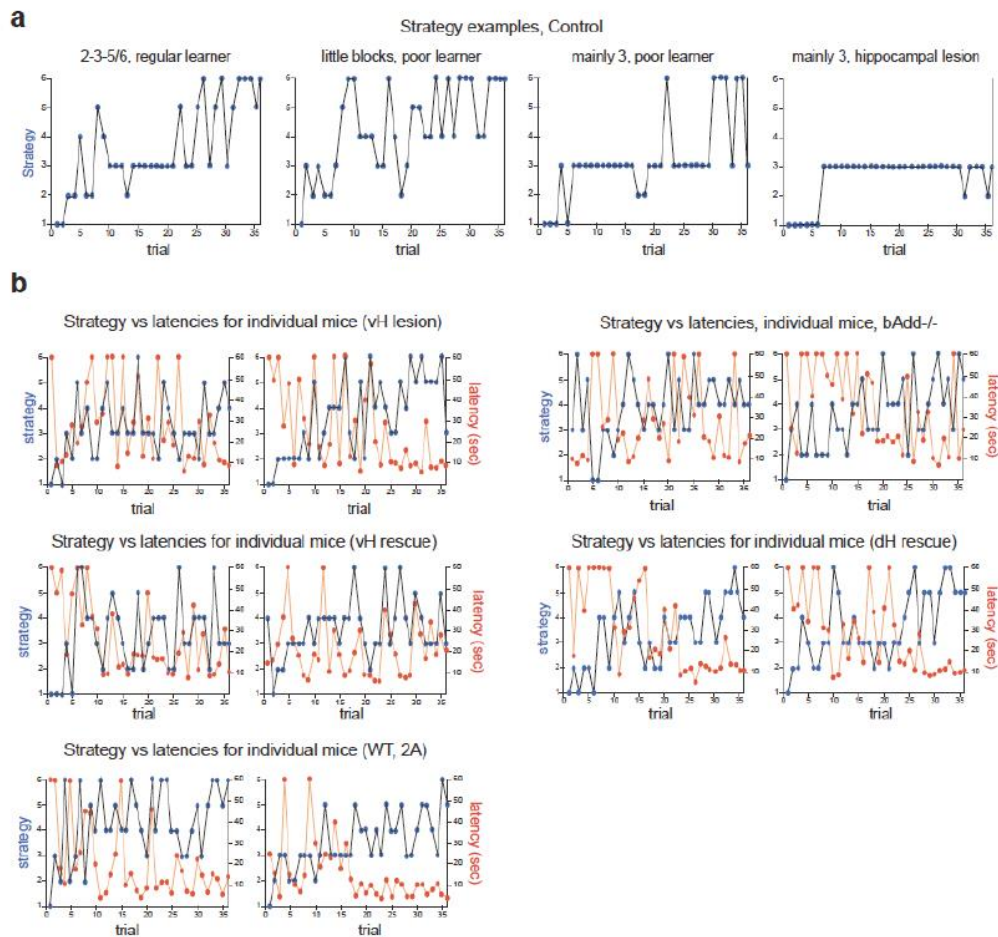
4.2.5 Supplementary Materials

Goal-oriented searching mediated by ventral hippocampus early in trial-and-error learning

Ruediger, S, Spirig, D., Donato, F., Caroni, P.

Suppl. Information

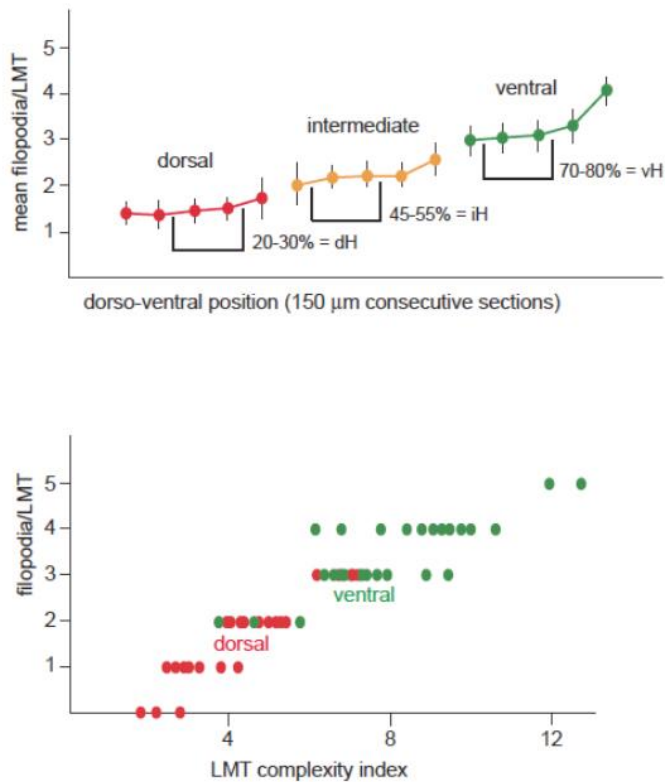
Supplementary Figure 1. Strategy/latency analysis of individual mice during maze learning. a, Additional examples of strategy deployment by individual mice under control conditions. The second (nearly no strategy blocks) and third (extensive strategy 3 blocks) mouse were among the 20% slowest learners, whereas the fourth mouse did not reach a latency of 25sec at trial 36, and exhibited an obvious reduction in hippocampal volume. **b,** Examples of strategy/latency plots for mice with vH lesions, β -Adducin mutant mice, mice with vH or dH β -Adducin rescue, and for mice learning a maze with a 2A platform.



Ruediger et al., Suppl. Fig. 1

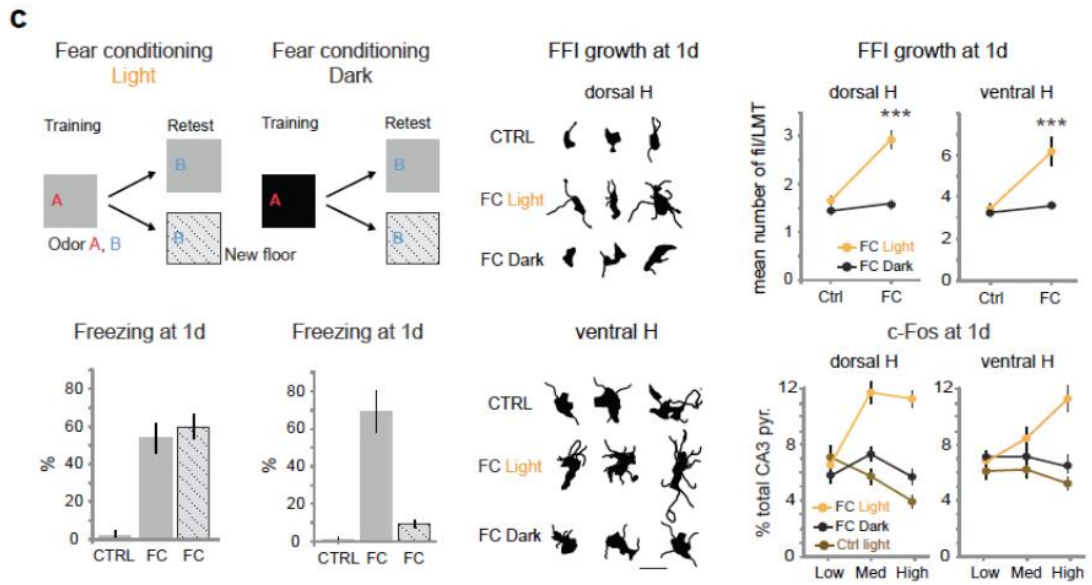
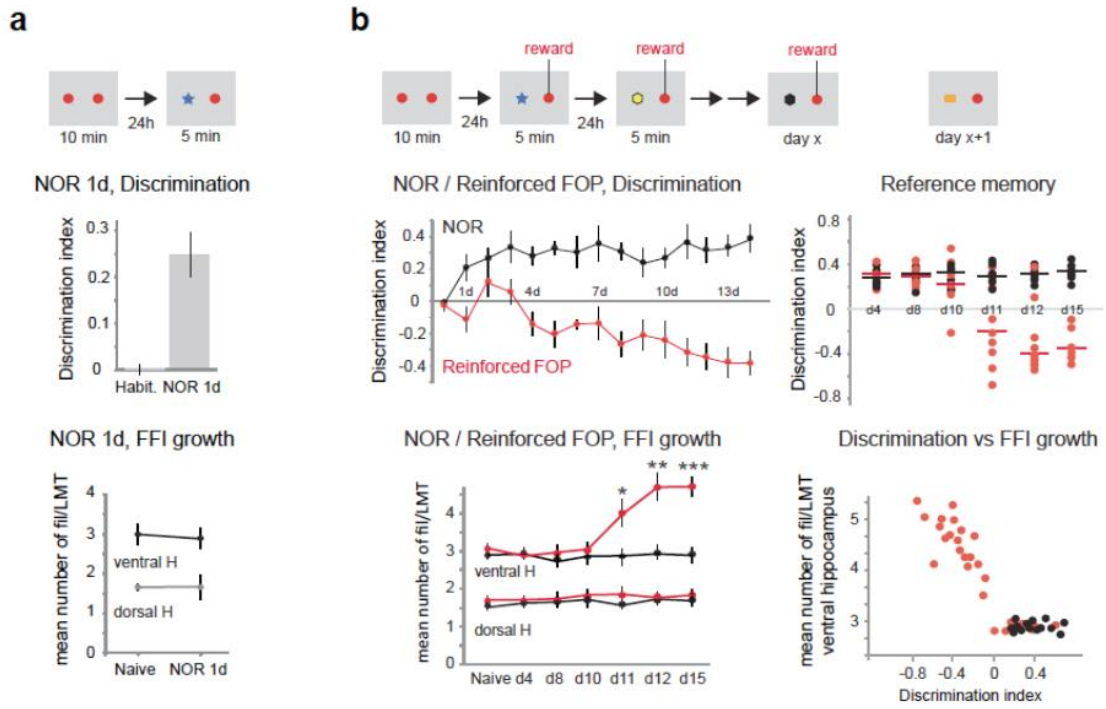
Supplementary Figure 2. Distinct filopodia/LMT baseline values correlated to LMT complexities

in dH, iH and vH. Upper graph: Mean filopodia/LMT values along the dorso-ventral axis in the hippocampus of mice housed under standard cage conditions. Isolated hippocampi were sectioned transversally, and the dorsal and ventral ends (ca. 250 μ m and 460 μ m respectively) were excluded from the analysis. The connected bars indicate the regions along the dorso-ventral axis of the hippocampus that were defined as dH (20-30% of total length), iH (45-55%) and vH (70-80%) in this study¹⁷. Note how mean filopodia/LMT values increase substantially along the dorso-ventral axis, but are comparable within hippocampal subdivisions. The ventral end of vH exhibited mean filopodia/LMT values that were substantially higher than those in the rest of vH. Lower graph: Positive correlation between filopodia/LMT values and LMT complexities for individual LMTs (Methods). This finding suggests that at the level of individual LMTs filopodial numbers (which are proportional to FFI synapses onto parvalbumin interneurons²²) are correlated to the numbers of feedforward excitatory synapses onto pyramidal neurons in CA3.



Ruediger et al., Suppl. Fig.2

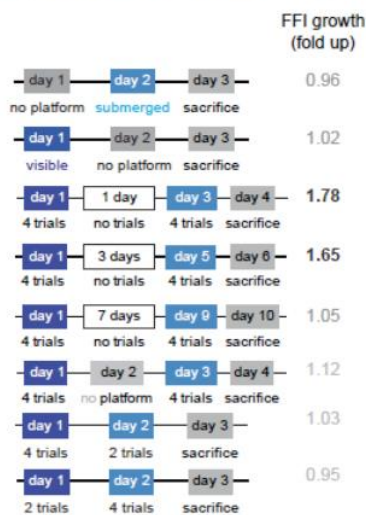
Supplementary Figure 3. vH FFI growth reflects behavioral learning of specific task-goal associations. **a**, Absence of FFI growth at vH and dH upon novel object recognition (NOR). Top: schematic of experimental protocol, involving habituation (10 min) on day 0, and discrimination test (5 min) on day 1. Familiar object in red. Mice explore identical objects equally (Habit.), but preferentially explore the novel object (NOR) on day 1. N=20. **b**, Converting an incidental NOR task into a reward-based one is sufficient to induce FFI growth specifically at vH upon learning. Top graphs: schematic of experimental protocols. Left, middle graph: training protocols with (red traces; Familiar Object Preference, FOP) and without (black traces; NOR) reward. Negative discrimination index values reflect longer exploration of familiar object. N=30. Left, lower graph: corresponding FFI growth values. N=3-7. Right: reference memory test (in the absence of reward) 1 day after last training day, as indicated; each dot represents an individual mouse, with (red) and without (black) reward. **c**, FFI growth in vH and dH upon contextual, but not upon explicit fear conditioning (FC). Left: schematic of FC protocols under light (contextual) and dark (explicit) conditions (top row), and corresponding freezing behavior 1d after learning (lower row). Center: representative camera lucidas of LMTs in CA3b of vH and dH. Bar: 10 μ m. Right: contextual, but not explicit FC induces FFI growth (upper graphs) and enhanced CA3b pyramidal neuron c-Fos recruitment (lower graphs) in vH and dH. FC values 1 day after learning. N=20.



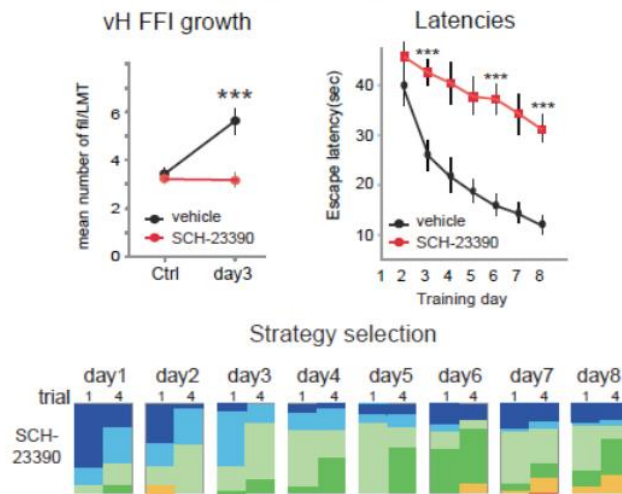
Ruediger et al. Suppl. Fig.3

Supplementary Figure 4. Specific task-goal association reflected by vH FFI growth during maze learning. Left: Analysis of experimental conditions that produce FFI growth at vH. No platform: four 60sec swim trials in the maze; no trials: mice kept in home cage. Mean values; N= 5-8 mice. Right: Requirement for signaling by reward neurotransmitter dopamine during maze learning. Impaired maze learning, absence of FFI growth at ventral hippocampus, and impaired strategy progression in mice treated with D1/D5 antagonist. N=10 each.

Requirements for ventral FFI growth

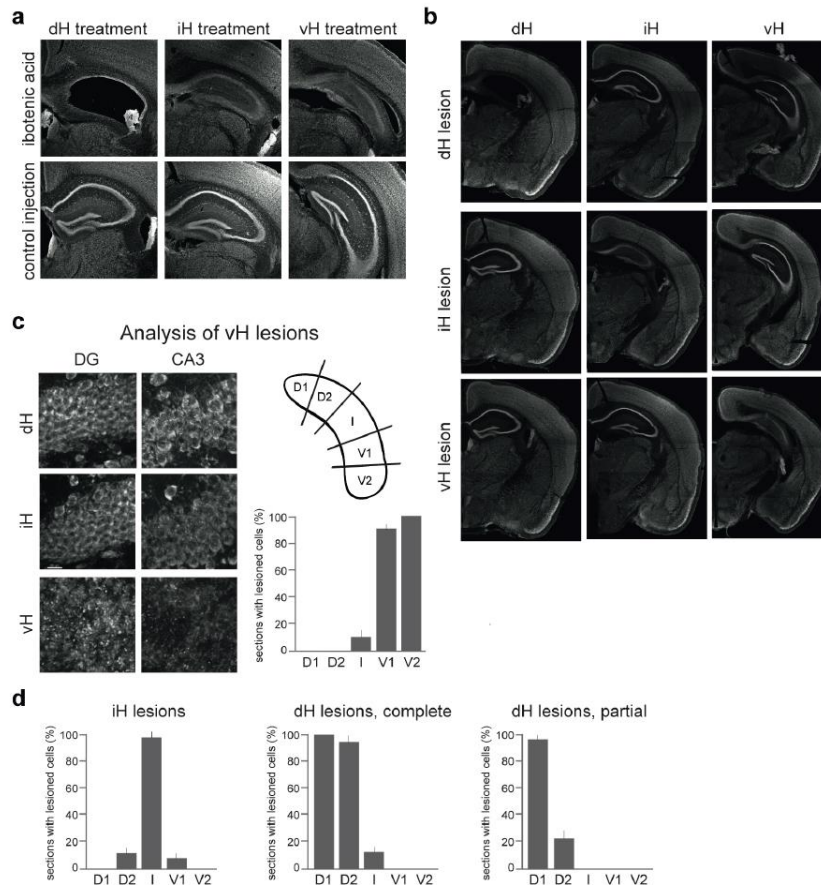


D1/D5 Antagonist



Ruediger et al., Suppl. Fig. 4

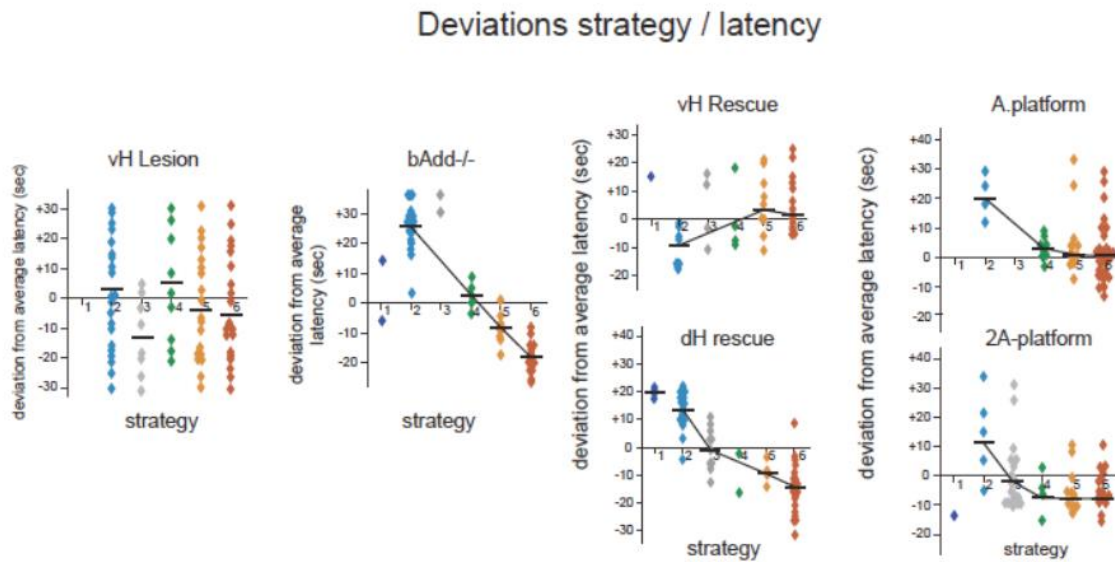
Supplementary Figure 5. Ibotenic acid lesions of hippocampal subdivisions. **a**, Representative examples of dH, iH and vH lesions, and of corresponding vehicle-treated hippocampi. Nissl staining. **b**, Examples of dH, iH and vH lesions. Representative low-magnitude views of Nissl stained sections from lesioned mice at dH, iH and vH levels. **c**, **d**, Representative analysis of hippocampal subdivision lesions. **c**, vH lesions. Left: Higher magnification views of Nissl stainings. Note near to complete absence of intact cells in dentate gyrus and CA3 of vH, and absence of detectable damage in iH and dH. Right: Analysis of excitotoxic damage spread along the hippocampus of ventrally lesioned mice. Schematic of hippocampal regions along dorso-ventral axis, and fraction of sections with at least 10% damaged cells in CA3. N=20 mice (five 50µm sections each per hippocampal region). **d**, Analysis of iH and dH (complete and partial (D1)) lesions, as described in **c**. N=10 (iH), 20 (dH, complete) and 10 (dH partial) mice.



Ruediger et al., Suppl. Fig.5

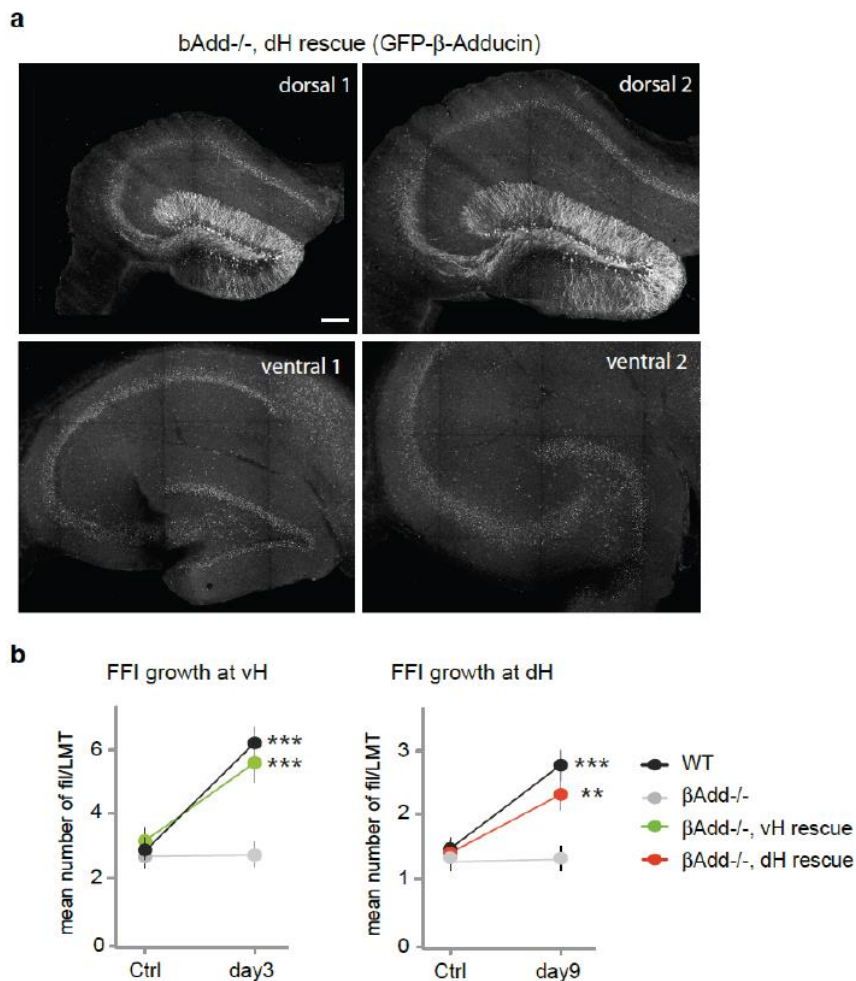
Supplementary Figure 6. Single trial latency deviations from the means for explorative strategies.

Extent to which the latencies of individual trials involving the exploration of alternative strategies differed from the mean latencies for that phase of the training process (see methods). Data analysis as described for **Fig. 1g**.






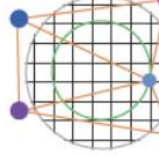
Ruediger et al., Suppl. Fig.6

Supplementary Figure 7. Local rescue of β -Adducin expression and FFI growth in vH or dH granule cells of β -Adducin^{-/-} mice. a, Lentivirus-mediated expression of GFP- β -Adducin specifically in dH granule cells of β -Adducin^{-/-} mouse. The panels show representative examples of GFP- β -Adducin signal in granule cells (note labeled dendrites in the dentate gyrus, and labeled mossy fibers in the hilus and along CA3) in dH, but not vH. Lentivirus-mediated rescue led to GFP- β -Adducin expression in 18-25% of the granule cells in dH. Bar: 100 μ m. b, Rescue of learning-related FFI growth upon GFP- β -Adducin expression in vH or dH. Data from water maze learning experiments. As previously reported²¹, lentivirus-mediated GFP- β -Adducin transduction rescued FFI growth specifically in those (GFP+) granule cells that exhibited virus-mediated expression. N=10 mice each.



Supplementary Figure 8. Sequence of subtasks involving ventral-to-dorsal hippocampal subdivisions in complex trial-and-error navigation learning. The schematic summarizes how an hippocampus-dependent trial-and-error learning process such as maze navigation is structured stereotypically into subtasks, which are implemented by individual hippocampal subdivisions (e.g. dH for spatial search). The subtasks build upon previously learned relationships (arrows), and lead to learning about increasingly defined features of the particular task. FFI growth upon learning focuses subsequent searches, supporting the deployment of strategy habits. Our results suggest that mice may: 1) learn on day 1 that there is a goal (platform), leading to a global search strategy; 2) learn on days 1-2 (vH) that the platform is consistently at a certain distance from the wall, supporting the deployment of local search strategies and local search habits; 3) learn on days 3-5/6 (iH) that the platform is consistently at the same position within the pool, supporting the deployment of spatial search strategies and spatial search habits; 4) learn on days 6-9 (dH) a fine scale spatial map of the task, leading to direct swim from any position in the maze.

Maze navigation learning structure: Subtask sequence involving ventral-intermediate-dorsal hippocampal subdivisions

Strategy	escape	global search	local search	spatial search
supporting learning		?	vH	vH
when	day 1	days 1-2	days 3-6	days 6-9
FFI growth		?	vH	iH
What learned	Invariant goal	Invariant goal-local context	Invariant place ?	Invariant spatial map
Cues used and learned				

Ruediger et al., Suppl. Fig. 8

4.2.6 Materials and methods

Reagents and anatomical procedures.

Add2^{-/-} mice³² were from Jackson Laboratories, Bar Harbor, Maine; the reporter line Thy1-mGFP(Lsi1) was as described³⁸. The GFP- β -adducin construct was cloned into a lentivirus vector, and dentate gyrus infections were done as described⁹. We analyzed structural traces of learning at GFP-positive LMTs of ventral and dorsal hippocampus (CA3b) using the 'sparse' transgenic reporter line Thy1-mGFP(Lsi1)²². In parallel, the main findings were confirmed in mice in which we labeled mossy fibers randomly using a lentivirus expressing membrane-targeted GFP (mGFP)²². On the basis of boundaries identified by previous gene-expression studies^{14, 17}, we defined subdivisions along the dorsoventral axis of the hippocampus as follows: dorsal, within 20–30% of total length; intermediate, within 45–55%; ventral, within 70–80%.

Behavioral procedures and their analysis.

Mice were kept in temperature-controlled rooms on a constant 12-h light-dark cycle, and all experiments were conducted at approximately the same time of the light cycle. Before the behavioral experiment, mice were housed individually for 3–4 d and provided with food and water ad libitum unless otherwise stated. All animal procedures were approved and performed in accordance with the Veterinary Department of the Canton Basel-Stadt.

All behavioral experiments were carried out with male mice that were 55–65 d old at the onset of the experiment and were performed according to standard procedures^{22, 23}.

The Morris water maze consisted of a circular (diameter: 140 cm) pool filled with opaque water at 24 °C. The circular escape platform (10 cm in diameter) was positioned at a fixed position 0.5 cm above (visible) or 0.5 cm below the water (hidden). Training involved four 60-s trials separated by 5-min intervals every day. For each trial, mice were placed at random starting locations in the pool facing the pool wall. At the end of each trial, mice were allowed to sit on the platform for 15 s; when trials were unsuccessful, mice were manually guided to the platform. Latencies and reference memories were determined as described. Heading

angles were determined using the starting position of the mouse, a line connecting that position to the platform and a second line connecting the start position to the position of the mouse after swimming 18 cm. We selected this distance to exclude variations due to initial rotations away from the pool wall.

We collected and analyzed data from training sessions and probe trials using Viewer2 Software (Biobserve, Bonn, Germany). The software Viewer III (Biobserve) was used to sample animal positions during Morris water maze trials. Search strategies were as defined in previous studies^{25, 27}. For quantitative identification of search strategies, we developed an algorithm in collaboration with Biobserve. We corrected all swimming trajectories to compensate for errors owing to incorrect object detection during the first 1.5 ± 1 s of tracking (for example, water movement caused by immersion of the mouse close to the border or experimenter's hand). We further corrected tracking to start subsequent to a 90° turn (away from the wall) around the center of a 5-cm radius defining the immersion point (center of gravity of the mouse body). Chaining annulus and direct-swimming corridor were adjusted accordingly, and prevailing strategies were then assigned automatically by the software's algorithm. Search strategies were defined as follows²⁷: thigmotaxis: $>35\%$ of swim time (60 s) within closer wall zone (5 cm from pool wall) and $>65\%$ of time within wider wall zone (10 cm from pool wall); random search: $>70\%$ surface coverage; scanning: $<70\%$ surface coverage and $>15\%$ surface coverage <0.7 s.d. distance to the pool center; chaining: $>65\%$ of time within annulus zone; directed search: $>80\%$ of time in goal corridor (rectangular goal corridor 20 cm wide, centered along direct connection between start and platform positions); focal search: <0.35 s.e.m. body angle, <0.25 s.d. mean distance to present goal; direct swim: 100% in goal corridor. When we used these definitions and the algorithm in combination with the adjustments described above, only $<3\%$ of the trials could not be assigned univocally to one strategy. Strategy blocks were defined as a sequence of at least three trials with the same strategy (or two trials for blocks of strategies 5 and 6). For block lengths, one-trial interruptions were tolerated but not counted (for example, a 2225223422 sequence was scored as a block length of 5 for strategy 2). Total block lengths were the sum of all blocks for one strategy and one mouse. For strategy/latency deviation values, mean latencies within days 1–2, days 3–6 and days 7–9 for a particular condition or genotype were subtracted from corresponding single-trial latencies when the strategies of those trials deviated from those of a sequence of at least two trials involving the same strategy by at least two strategy levels (for example, latency of the fourth trial in the sequence 222422). Statistical analyses were performed using Student's t-tests and one-way ANOVA; $P < 0.05$ in post hoc comparisons. Results are presented as mean \pm s.e.m.

For fear-conditioning experiments, the conditioning chamber was cleaned with 2% acetic acid before and after each session. Once placed inside the training chamber, mice were allowed to explore the apparatus for 2.5 min, and then they received a series of five footshocks (1 s and 0.8 mA each, inter-trial interval of 30 s). Control mice were subjected to the same procedure without receiving footshocks. We assessed contextual fear memory by returning mice to the training chamber 24 h after fear conditioning during a test period of 2.5 min. Freezing was defined as the complete absence of somatic mobility other than respiratory movements. Fear conditioning in the dark involved the same procedure but with all lights switched off. Recall 24 h after conditioning was in the following training context: in the presence of odor A (2% acetic acid) or B (0.25% benzaldehyde) and on a shock floor or plastic floor.

For novel-object recognition experiments, mice were first habituated to the testing arena for 10 min. On the next day, each animal was allowed to explore two identical objects placed in the arena for 10 min. Twenty-four hours later, mice explored the same arena for 5 min, with one of the familiar objects replaced by a novel object. Recognition memory was expressed by the discrimination index (D), which was defined as $D = (T(\text{novel}) - T(\text{familiar})) / (T(\text{novel}) + T(\text{familiar}))$.

For the reinforced-learning version of the object recognition task and its controls, we fed all mice sufficiently only after each training session to maintain their body weight at 85% of their initial weight. Wheat flakes (three to five flakes; 100–120 mg in total) were placed as a reward on top of the familiar object (a cube of ~4 cm in height with an inserted cylinder of an additional 3 cm in height; reward flakes were placed on top of the cube and the cylinder). To habituate mice to the reward, we placed two to three wheat flakes in the home cages after each habituation and training session. For all object recognition task protocols, we cleaned the testing arena with 70% ethanol after each mouse on each day.

Drug delivery and stereotactic surgery in vivo.

SCH23390 (Tocris Bioscience) was dissolved in saline 0.9% and injected i.p. at a doses of 0.05 mg/kg 20 min before water maze training at day 1 (habituation) and throughout the training. Coordinates for lentiviral injections into mouse dentate gyrus were (in mm from Bregma): 1.70 posterior, 1.10 lateral, 1.70 down (dorsal hippocampus); 3.16 posterior, -2.5

lateral, 2.10 down (ventral hippocampus). The lentivirus for β -adducin rescue was as described⁹. Add2^{-/-} mice were trained 5 weeks after injection of eGFP- β -adducin lentivirus. For hippocampal subdivision lesions, ibotenic acid (Ascent Scientific) was dissolved in PBS to a final concentration of 10 mg/ml, and injections of 50 nl were made at two or three sites. Injections coordinates were (in mm from Bregma): 3.08 posterior; 2.7 lateral; 3.2, 3.4 and 3.6 down (vH lesion); 2.3 posterior; 2.3 lateral: 1.3, 1.5 and 1.7 down (iH lesion); 1.58 posterior; 1.25 lateral; 1.3 and 1.6 down (dH lesion, complete). Upon injection, mice were given 7 d recovery before training.

Immunocytochemistry and histology.

Antibodies were as follows: rabbit antibody to GFP (Molecular Probes, Eugene, OR, USA), 1:1,000; rabbit antibody to c-Fos (Santa Cruz; sc-253), 1:10,000; mouse antibody to NeuN (Chemicon; MAB377), 1:200. Secondary antibodies were Alexa Fluor 568 (Molecular Probes; A10037 or 488 (Molecular Probes; A11008); 1:500.

Morris water maze, c-Fos expression.

Mice performed a single probe trial 24 h after the final training session and were returned to their home cage for 90 min before perfusion (transcardially with 4% PFA in PBS, pH 7.4). Brains were kept in fixation solution overnight at 4 °C. Hippocampi were dissected, embedded in 3% agarose gel and sliced transversally on a tissue chopper (McIlwain) to yield lamellar hippocampal sections of 100- μ m thickness. c-Fos immunocytochemistry was performed and analyzed as described²¹.

Imaging and image analysis.

For high-resolution imaging of LMTs in fixed tissue, we imaged lamellar sections on an upright spinning-disk microscope using an alpha Plan-Apochromat \times 100/1.45 oil-immersion objective (Zeiss) and Metamorph 7.7.2 acquisition software (Molecular Devices, Sunnyvale, CA, USA). Voxel size was 0.106 μ m \times 0.106 μ m \times 0.2 μ m. For c-Fos analysis, we processed all samples belonging to the same experimental set in parallel and acquired them with the

same settings on an LSM700 confocal microscope (Zeiss) using an EC Plan-Neofluar ×40/1.3 oil-immersion objective (Zeiss). We used transverse hippocampal sections at different dorsoventral levels (dorsal, intermediate and ventral hippocampus) for the analysis of LMT morphology and filopodial contents in CA3b. We analyzed 80–100 LMTs per animal and region; this involved three to four confocal stacks per section along CA3b and an average of three to four sections. We analyzed all objects that were completely included in the three-dimensional stack blind to experimental conditions. We analyzed high-resolution three-dimensional confocal stacks using Imaris 7.0.0 (Bitplane AG) software

4.2.7 Bibliography

1. Sutton, R.S. & Barto, A.G. Reinforcement Learning: An Introduction (MIT Press, 1998).
2. Dayan, P. & Balleine, B.W. Reward, motivation and reinforcement learning. *Neuron* 36, 285–298 (2002).
3. Graybiel, A.M. Habits, rituals, and the evaluative brain. *Annu. Rev. Neurosci.* 31, 359–387 (2008).
4. Barnes, T.D., Kubota, Y., Hu, D., Jin, D.Z. & Graybiel, A.M. Activity of striatal neurons reflects dynamic encoding and recoding of procedural memories. *Nature* 437, 1158–1161 (2005).
5. Desrochers, T.M., Jin, D.Z., Goodman, N.D. & Graybiel, A.M. Optimal habits can develop spontaneously through sensitivity to local cost. *Proc. Natl. Acad. Sci. USA* 107, 20512–20517 (2010).
6. Thorn, C.A., Atallah, H., Howe, M. & Graybiel, A.M. Differential dynamics of activity changes in dorsolateral and dorsomedial striatal loops during learning. *Neuron* 66, 781–795 (2010).
7. Amemori, K., Gibb, L.G. & Graybiel, A.M. Shifting responsibility: the importance of striatal modularity to reinforcement learning in uncertain environments. *Front. Hum. Neurosci.* 5, 47 (2011).
8. Botvinick, M.M., Niv, Y. & Barto, A.C. Hierarchically organized behavior and its neural foundations: a reinforcement-learning perspective. *Cognition* 113, 262–280 (2009).
9. O’Keefe, J. & Nadel, L. *The Hippocampus as a Cognitive Map* (Oxford Univ. Press, 1978).
10. Moser, E.I., Kropff, E. & Moser, M.B. Place cells, grid cells, and the brain’s spatial representation system. *Annu. Rev. Neurosci.* 31, 69–89 (2008).
11. Bird, C.M. & Burgess, N. The hippocampus and memory: insights from spatial processing. *Nat. Rev. Neurosci.* 9, 182–194 (2008).
12. Morris, R.G.M., Garrud, P., Rawlins, J.N.P. & O’Keefe, J. Place navigation impaired in rats with hippocampal lesions. *Nature* 297, 681–683 (1982).
13. Moser, M.B. & Moser, E.I. Functional differentiation in the hippocampus. *Hippocampus* 8, 608–619 (1998).
14. Dong, H.W., Swanson, L.W., Chen, L., Faselow, M.S. & Toga, A.W. Genomic-anatomic evidence for distinct functional domains in hippocampal field CA1. *Proc. Natl. Acad. Sci. USA* 106, 11794–11799 (2009).
15. Faselow, M.S. & Dong, H.-W. Are the dorsal and ventral hippocampus functionally distinct structures? *Neuron* 65, 7–19 (2010).
16. Moser, M.B., Moser, E.I., Forrest, E., Andersen, P. & Morris, R.G.M. Spatial learning with a minislab in the dorsal hippocampus. *Proc. Natl. Acad. Sci. USA* 92, 9697–9701 (1995).

17. Thompson, C.L. et al. Genomic anatomy of the hippocampus. *Neuron* 60, 1010–1021 (2008).
18. Viard, A., Doeller, C.F., Hartley, T., Bird, C.M. & Burgess, N. Anterior hippocampus and goal-directed spatial decision making. *J. Neurosci.* 31, 4613–4621 (2011).
19. Royer, S., Sirota, A., Patel, J. & Buzsaki, G. Distinct representations and theta dynamics in dorsal and ventral hippocampus. *J. Neurosci.* 30, 1777–1787 (2010).
20. Young, J.J. & Shapiro, M.L. Dynamic coding of goal-directed paths by orbital prefrontal cortex. *J. Neurosci.* 31, 5989–6000 (2011).
21. Pennartz, C.M., Ito, R., Verschure, P.F., Battaglia, F.P. & Robbins, T.W. The hippocampal-striatal axis in learning, prediction and goal-directed behavior. *Trends Neurosci.* 34, 548–559 (2011).
22. Ruediger, S. et al. Learning-related feedforward inhibitory connectivity growth required for memory precision. *Nature* 473, 514–518 (2011).
23. Bednarek, E. & Caroni, P. β -adducin is required for stable assembly of new synapses and improved memory upon environmental enrichment. *Neuron* 69, 1132–1146 (2011).
24. Morris, R. Development of a water-maze procedure for studying spatial learning in the rat. *J. Neurosci. Methods* 11, 47–60 (1984).
25. Wolfer, D.P. & Lipp, H.P. Dissecting the behaviour of transgenic mice: is it the mutation, the genetic background, or the environment? *Exp. Physiol.* 85, 627–634 (2000).
26. Janus, C. Search strategies used by APP transgenic mice during navigation in the Morris water maze. *Learn. Mem.* 11, 337–346 (2004).
27. Garthe, A., Behr, J. & Kempermann, G. Adult-generated hippocampal neurons allow the flexible use of spatially precise learning strategies. *PLoS ONE* 4, e5464 (2009).
28. Luo, A.H., Tahsili-Fahadan, P., Wise, R.A., Lupica, C.R. & Aston-Jones, G. Linking context with reward: a functional circuit from hippocampal CA3 to ventral tegmental area. *Science* 333, 353–357 (2011).
29. Wiltgen, B.J. et al. The hippocampus plays a selective role in the retrieval of detailed contextual memories. *Curr. Biol.* 20, 1336–1344 (2010).
30. Schultz, W., Dayan, P. & Montague, P.R. A neural substrate of prediction and reward. *Science* 275, 1593–1599 (1997).
31. Bethus, I., Tse, D. & Morris, R.G.M. Dopamine and memory: modulation of the persistence of memory for novel hippocampal NMDA receptor-dependent paired associates. *J. Neurosci.* 30, 1610–1618 (2010).
32. Rabenstein, R.L. et al. Impaired synaptic plasticity and learning in mice lacking β -adducin, an actin-regulating protein. *J. Neurosci.* 25, 2138–2145 (2005).

33. Bast, T., Wilson, I.A., Witter, M.P. & Morris, R.G.M. From rapid place learning to behavioral performance: a key role for intermediate hippocampus. *PLoS Biol.* 7, e1000089 (2009).
34. Bannerman, D.M., Good, M.A., Butcher, S.P., Ramsay, M. & Morris, R.G.M. Distinct components of spatial learning revealed by prior training and NMDA receptor blockade. *Nature* 378, 182–186 (1995).
35. Hoh, T., Beiko, J., Boon, S., Weiss, S. & Cain, D.P. Complex behavioral strategy and reversal learning in the water maze without NMDA receptor-dependent long-term potentiation. *J. Neurosci.* 19, RC2 (1999).
36. Gallistel, C.R., Fairhurst, S. & Balsam, P. The learning curve: implications of a quantitative analysis. *Proc. Natl. Acad. Sci. USA* 101, 13124–13131 (2004).
37. Kjelstrup, K.G. et al. Reduced fear expression after lesions of the ventral hippocampus. *Proc. Natl. Acad. Sci. USA* 99, 10825–10830 (2002).

4.3

Temporally matched subpopulations of selectively interconnected principal neurons in the Hippocampus.

Yuichi Deghichi*, Flavio Donato*, Ivan Galimberti* , Erik Cabuy and Pico Caroni

*these authors contributed equally to the work

Published Article, Nature Neuroscience 2011, April; 14(4): 495-504

4.3.1 Summary

The extent to which individual neurons are interconnected selectively within brain circuits is an unresolved problem in neuroscience. Neurons can be organized into preferentially interconnected microcircuits, but whether this reflects genetically defined subpopulations is unclear. We found that the principal neurons in the main subdivisions of the hippocampus consist of distinct subpopulations that are generated during distinct time windows and that interconnect selectively across subdivisions.

In two mouse lines in which transgene expression was driven by the neuron-specific Thy1 promoter, transgene expression allowed us to visualize distinct populations of principal neurons with unique and matched patterns of gene expression, shared distinct neurogenesis and synaptogenesis time windows, and selective connectivity at dentate gyrus-CA3 and CA3-CA1 synapses. Matched subpopulation marker genes and neuronal subtype markers mapped near clusters of olfactory receptor genes.

The nonoverlapping matched timings of synaptogenesis accounted for the selective connectivities of these neurons in CA3. Therefore, the hippocampus contains parallel connectivity channels assembled from distinct principal neuron subpopulations through matched schedules of synaptogenesis.

4.3.2 Introduction

Brain circuits show selective connectivities^{1–7} that might structure information processing, but the extent to which defined subpopulations of neurons are interconnected selectively and the underlying mechanisms of selective connectivity are unclear¹. The investigation of microcircuits poses unique technical challenges owing to the vast numbers of neurons and synapses in the central neuropil^{1,2,6}. However, transgenic mouse lines based on a modified mouse Thy1.2 promoter cassette produce stable transgene expression that is restricted to subgroups of neurons in the adult⁸. In ‘sparse’ Thy1 lines, high-level transgene expression in few neurons within several neuronal populations has been exploited to trace and image neuronal processes and their synaptic connections at high resolution^{9,10}. Notably, although the lines show clear variegation (that is, unpredictable variations in the numbers of transgene-expressing neurons among individuals of the same mouse line), the distribution of labeled cells in these Thy1 lines is not entirely random. For example, in three different sparse lines, transgene expression among retinal amacrine cells is restricted to very few defined subtypes¹¹. Sparse Thy1 lines may therefore provide suitable tools for investigating whether defined subpopulations of neurons establish selective synaptic connections.

The hippocampus is a cortical structure that has a central role in producing relational episodic representations from ongoing sensory information, to support learning and memory¹². How the intrinsic structure of hippocampal circuits shapes information processing is poorly understood. The main tri-neuronal feedforward circuit in the hippocampus, which relays information from granule cells in the dentate gyrus to pyramidal neurons in CA3 and then pyramidal neurons in CA1, provides an attractive system in which to investigate the idea that subpopulations of neurons are selectively interconnected¹². There is a wealth of anatomical and functional information about hippocampal circuits^{12–15}, and the principal neurons of the hippocampal subdivisions show prominent transgene expression in sparse Thy1 lines^{10,12}. In the hippocampus, anatomically distinct gene expression domains have been detected within the principal neuron populations^{13,14}, but no subpopulations or microcircuits of principal neurons have been described.

A modified expression cassette based on the mouse Thy1.2 promoter drives transgene expression in neurons, and independent transgenic lines can show expression in different subpopulations of neurons, or even in very few neurons (sparse Thy1 lines)^{10,12}. Here we used the two sparse Thy1 reporter lines (Lsi1 and Lsi2), which overexpress membrane-targeted GFP (mGFP) in few neurons^{10,16}, and whose granule cells show distinct structural

plasticity in the stratum lucidum¹⁷, to investigate the possible existence and connectivity of principal neuron subpopulations in the hippocampus. The two lines revealed two distinct subpopulations of principal neurons in each hippocampal subdivision. During hippocampal neurogenesis, the subpopulations were generated during distinct but partially overlapping early time windows. These temporal distinctions were even more pronounced during hippocampal circuit assembly, when Lsi1 neurons matured and established synapses ahead of Lsi2 neurons, and both preceded synaptogenesis by most principal neurons. The distinct schedules of synaptogenesis accounted for selective connectivity between Lsi1 (or Lsi2) dentate gyrus granule cells and Lsi1 (or Lsi2) pyramidal neurons in the stratum lucidum of CA3. Our results provide evidence that there are matched subpopulations of selectively interconnected principal neurons in the hippocampus, and suggest that temporal schemes of neuronal specification and synaptogenesis underlie the assembly of microcircuits in the hippocampus.

4.3.3 Results

Molecularly distinct principal neuron subpopulations

To investigate the possibility that mGFP-positive neurons in Lsi1 and Lsi2 reporter mice represent subpopulations of principal neurons in the hippocampus, we analyzed their transcriptomes in the adult and their appearance during hippocampal neurogenesis and development. We compared these properties of Lsi1 and Lsi2 neurons with those of a random population of principal neurons in dentate gyrus, CA3 and CA1 (Lmu1 mice; Supplementary Fig. 1).

We first analyzed patterns of gene expression in transgene-positive hippocampal granule cells from adult Lsi1 and Lsi2 mice. We collected 40–50 mGFP-positive cells individually from three defined hippocampal positions using laser-dissection microscopy, and then analyzed them as pools on Affymetrix chips¹⁸ (Fig. 1a). We repeated the procedure for three Lsi1 and three Lsi2 mice at 2, 4, 8 and 16 weeks of age (Fig. 1a). For comparison, we collected similar sets of granule cells from three Lmu1 Thy1 mice, which express mGFP broadly in the dentate gyrus¹⁰ (Fig. 1a). When compared to average values, Lsi1 and Lsi2 granule cells each contained 150–250 genes that were either upregulated or downregulated at least twofold at 16 weeks ($P < 0.05$; Fig. 1a,b and Supplementary Fig. 2). The ranges within which the fractions of transgene-expressing granule cells over total numbers of granule cells varied in individual transgenic mice were 3–20% (Lsi1) and 1–15% (Lsi2; $n = 50$ mice each), but gene enrichment values over average granule cells were closely comparable in granule cells from mice with different frequencies of transgene-positive neurons (Fig. 1b), suggesting that the fractions of Lsi1 and Lsi2 granule cells in dentate gyrus might be at least 20% and 15%, respectively, and that the subpopulations may be homogeneous.

Transgene-positive hippocampal CA3 and CA1 pyramidal neurons in Lsi1 and Lsi2 mice also showed unique gene expression patterns (Fig. 1c and Supplementary Fig. 3). As for granule cells, the subpopulation patterns of gene expression were independent of the frequencies of transgene-expressing cells in individual mice (Fig. 1c). To carry out a non-biased subpopulation test based on gene expression profiles, we took a group of 492 genes, consisting of 100 genes with the highest deviations from average values at 16 weeks in either Lsi1 or Lsi2 granule cells, CA3 pyramidal neurons or CA1 pyramidal neurons (total of

600 genes, minus 108 overlaps), and used the genes to analyze the combined gene profiling databases including four different postnatal ages (2, 4, 8 and 16 weeks), thereby generating hierarchical trees of cell-type relatedness (that is, determining which cell type, genotype or age samples were most related to each other). With the exception of the 2-week samples, in which developmental aspects were predominant, this unbiased in silico test for relatedness consistently separated Lsi1 and Lsi2 principal neurons from average populations, irrespective of age (Fig. 1d).

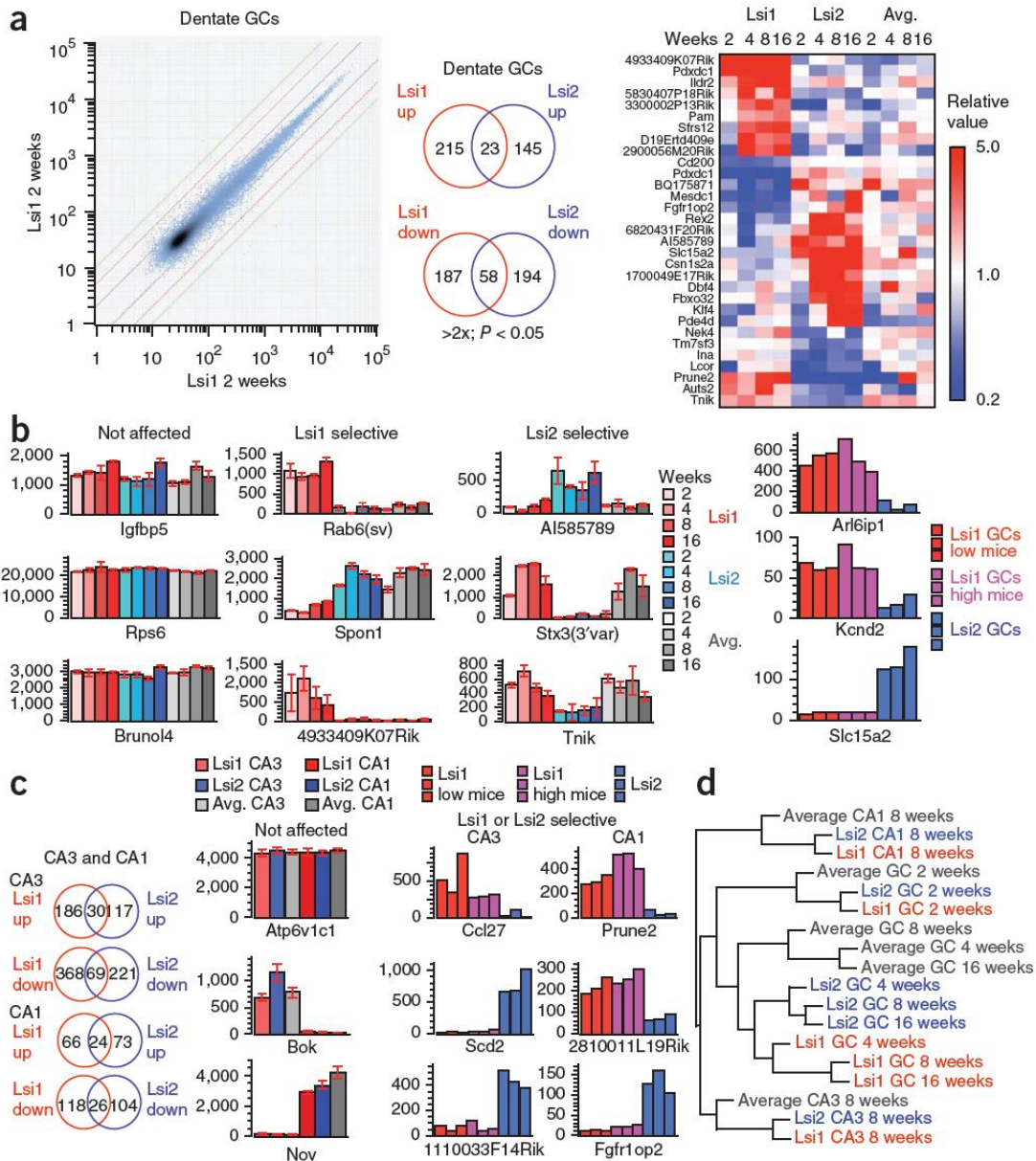


Figure 1: Distinct transcriptomes of Lsi1 and Lsi2 hippocampal principal neurons.

(a) Transcriptome analysis of Lsi1 and Lsi2 granule cells. Left, reproducibility of microarray analysis. Middle, numbers of genes up- or downregulated compared to average (16 weeks data). Right, heat map for 30 differentially regulated genes at 4 ages; note independent clustering in Lsi1 and Lsi2 granule cells (GCs). Error bars, s.e.m. (b) Differentially expressed genes in Lsi1 and Lsi2 granule cells. Left, columns are average values from three mice. Right, comparable gene expression profiles in granule cells from mice with many (15–20% of total) or few (2–5% of total) GFP-positive neurons; columns are values in one mouse each. (c) Transcriptomes of Lsi1 and Lsi2 pyramidal neurons. Details as in a and b. (d) In silico cell grouping. The unbiased hierarchical tree algorithm grouped cells according to subpopulations of granule cells, and pyramidal neurons in CA3 and CA1.

Early subpopulation emergence during neurogenesis

To determine whether Lsi1 and Lsi2 neurons reflect developmentally distinct subpopulations, we investigated their emergence during hippocampal development. In Lsi1 mice, we detected pairs and small groups of mGFP-positive radial glia in the hippocampal neuroepithelium at embryonic day 10.5 (E10.5), before precursor neurogenesis^{19–21} (Fig. 2a). Groups of mGFP-positive radial glia were arranged symmetrically along the left and right hippocampus primordia (Fig. 2a), in patterns that were comparable among different individuals (data not shown). In Lsi2 embryos, we also detected Nestin- and mGFP-positive radial glia at E10.5, although in smaller groups of cells (data not shown). We found increasing numbers of transgene-positive postmitotic neuroblasts along the hippocampal neuroepithelium in the two lines of transgenic mice from E11.5 on, suggesting that Lsi1 and Lsi2 granule cells, CA3 pyramidal neurons and CA1 pyramidal neurons²⁰ were already present at this early age (Fig. 2a and Supplementary Fig. 4). Systematic spatial mapping of labeled cells in several embryos at the same developmental time revealed that mGFP-positive cells were distributed according to specific, reproducible and distinct patterns in the two lines of transgenic mice (Fig. 2b). We also found comparable and distinct distributions of Lsi1 and Lsi2 neurons in the adult hippocampus (Supplementary Fig. 4). Time-lapse imaging of hippocampal explant cultures from Lsi1 embryos provided evidence that mGFP-positive postmitotic neuroblasts migrated and developed into granule cells (Supplementary Fig. 5). These results provide evidence that commitment to Lsi1 and Lsi2 subpopulation fates occurs early during hippocampal neurogenesis.

To investigate the possibility that Lsi1 neurons reflect early principal neuron subpopulations that might be generated according to specific patterns during hippocampal neurogenesis, we compared the spatial arrangements of mGFP-positive cells with those of cells that incorporated EdU (a BrdU analog that can be visualized under non-denaturing conditions²²). Between E11.5 and E12.5, spatial patterns of precursor neurogenesis (Tbr2+)²³ and of mGFP-positive Lsi neurons were closely comparable (Fig. 2c). Zones of early neurogenesis at E11.5 (refs. 20,21; EdU+) corresponded to reproducible discrete territories that were depleted of Nestin+ and Ki67+ neuronal precursors and enriched in mGFP+ neuroblasts 2 d later, suggesting that early hippocampal neurogenesis proceeded according to non-random spatial patterns (Fig. 2c). Neurons that were labeled with BrdU between E11.5 and E12.5 co-distributed with transgene-positive Lsi1 neurons in adult CA3, suggesting that Lsi1 neurons might represent the earliest principal neurons in the hippocampus (Supplementary Fig. 4).

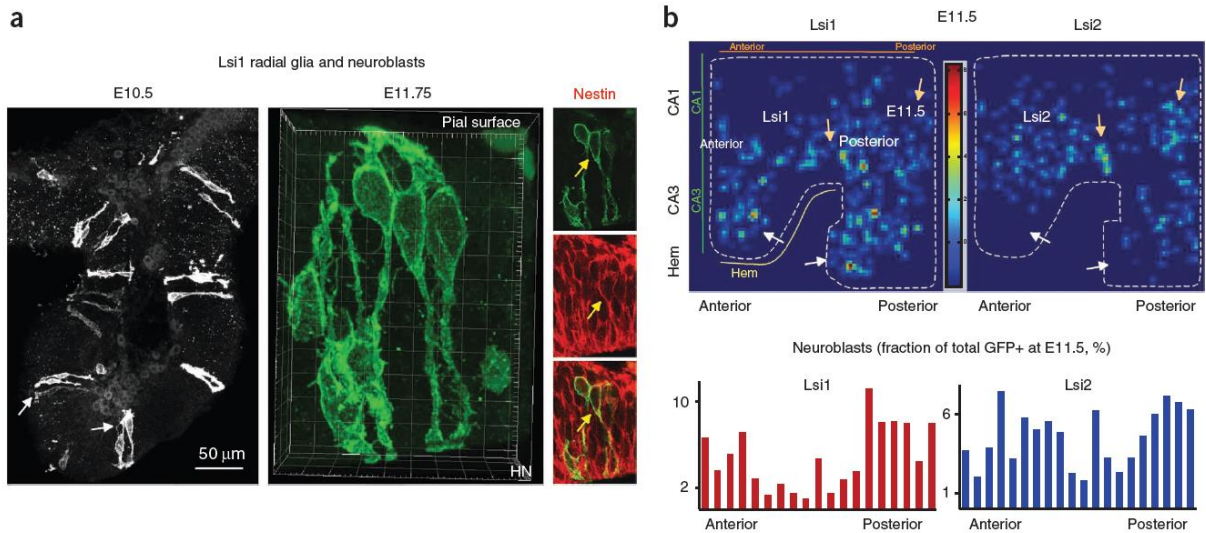
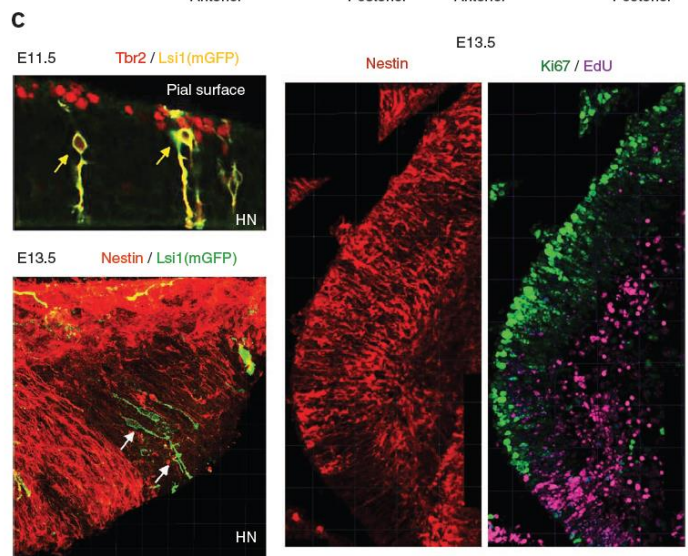


Figure 2: Detection of Lsi1 and Lsi2 precursors and neurons during hippocampal development.

(a) Transgene expression during hippocampal neurogenesis. Expression in radial glia cells (left) and neuroblast groups (right). Some of the GFP+ neuroblasts are Nestin+ (right, arrow). HN, hippocampal neuroepithelium. (b) Spatial distribution of GFP+ neuroblasts in hippocampal neuroepithelium of Lsi1 and Lsi2 embryos at E11.5. The heat map (top) visualizes specific differences between Lsi1 and Lsi2 embryos at the same developmental age (see also Supplementary Fig. 12); the quantitative analysis (bottom) represents average values for three embryos each. (c) Specification of Lsi1 neuroblasts during hippocampal neurogenesis. At E11.5, GFP+ neuroblasts (arrows) co-distribute with regions of proliferating precursors (Tbr2+; top, right). At E13.5, GFP+ neuroblasts (white arrows) accumulate in defined Ki67-depleted non-proliferating regions ($n = 6$) that had been labeled with EdU at E11.5 (arrow) and are now depleted of Nestin precursors (arrow). Scale bar, 50 μ m.



Distinct and matched neurogenesis time windows

To investigate the possibility that Lsi1 and Lsi2 principal neurons might be generated during defined and distinct temporal windows, we analyzed the temporal patterns of hippocampal neurogenesis in Lsi1 and Lsi2 mice. We injected transgenic mice with BrdU at defined times during embryonic development or soon after birth and analyzed hippocampal sections from

1-month-old mice for BrdU labeling and mGFP signals²⁴. We included in the analysis only cells that were strongly labeled with BrdU, which did not undergo further rounds of DNA replication and cell division subsequent to BrdU incorporation. Consistent with previous reports, the overall population of granule cells was generated during two broad rounds of neurogenesis, one peaking between E12 and E15 and the second peaking between P3 and P7 (refs. 19,25,26; Fig. 3a). Lsi1 granule cells showed narrower windows of neurogenesis, with peaks in the first 25% of each wave of granule cell neurogenesis (Fig. 3a). Lsi2 granule cells were produced about 2 d later than their Lsi1 counterparts but still within the first half of the embryonic and postnatal waves of neurogenesis (Fig. 3a). We found no Lsi1 or Lsi2 granule cells among adult-born granule cells (0/240 doublecortin-positive granule cells in 3 mice each at 4 months).

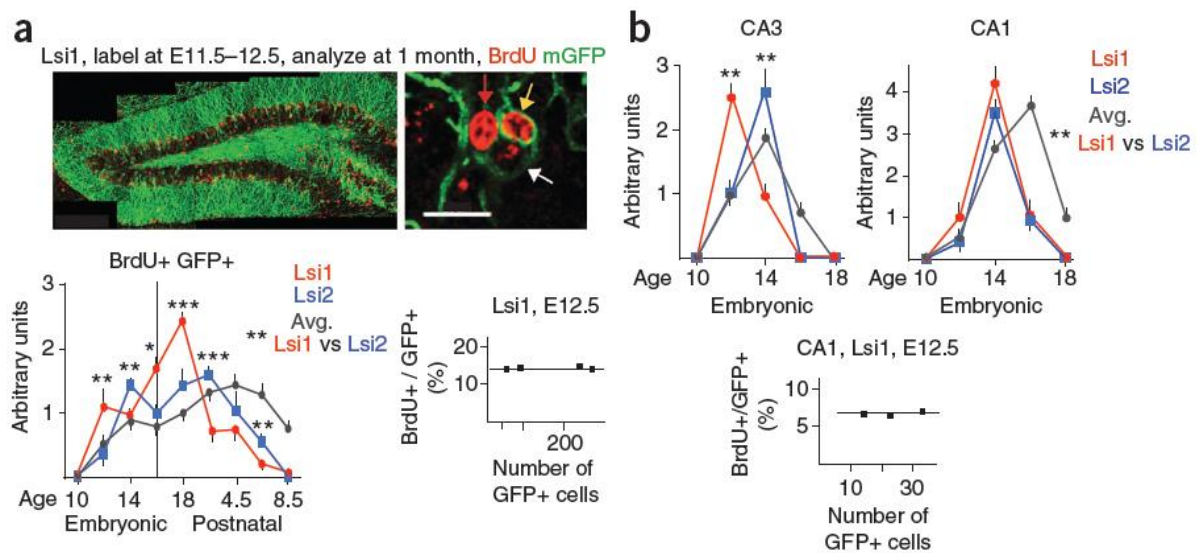


Figure 3: Temporal windows of Lsi1 and Lsi2 neurogenesis during hippocampal development.

(a) Lsi1 and Lsi2 granule cells are generated during early phases of neurogenesis. Top, BrdU labeling experiment; arrows, BrdU+ GFP+ granule cell (yellow), BrdU+ GFP- granule cell (red) and weakly BrdU+ granule cell (white). Bottom left, fractions of total GFP+ granule cells labeled with BrdU at different time intervals (avg., fractions of all granule cells labeled with BrdU). Averages from three mice each; values normalized to troughs between two neurogenesis peaks; vertical line, trough between early and late neurogenesis wave for average granule cells. Statistical analysis: comparisons between Lsi1 and Lsi2 values at individual ages; Mann Whitney test; **P < 0.001; ***P < 0.0001. Error bars, s.e.m. Bottom right, fractions of BrdU+ GFP+ neurons labeled at E12.5 are not affected by total numbers of GFP+ granule cells. (b) Neurogenesis of Lsi1 and Lsi2 hippocampal pyramidal neurons. Details as in a. Scale bar, 20 μ m.

Lsi1 CA3 and CA1 pyramidal neurons were also produced during the earliest phase of their corresponding neurogenesis processes (Fig. 3b). Lsi2 CA3 pyramidal neurons were produced during a defined early window of developmental time, slightly later than Lsi1 neurons, whereas production of CA1 Lsi2 and Lsi1 pyramidal neurons overlapped more

extensively (Fig. 3b). Consistent with the notion that the Lsi1 and Lsi2 subpopulations are generated during the first half of hippocampal neurogenesis, we found no Nestin and mGFP double-positive precursors in the hippocampal neuroepithelium in Lsi1 or Lsi2 embryos at E13.5, when Nestin-positive precursors were still abundant (data not shown). When we compared different individuals from the same mouse line, we found that the total number of Lsi1 or Lsi2 mGFP-positive granule cells (or pyramidal neurons) did not affect the fraction of transgene-positive cells that was produced during any neurogenesis interval (Fig. 3a,b), suggesting that variegation effects influenced only the probability of mGFP expression within defined subpopulations of granule cells. Therefore, Lsi1 and Lsi2 principal neurons are generated during partially overlapping but distinct early temporal windows of embryonic development, and the relative positions of these temporal windows are comparable for the dentate gyrus, CA3 and CA1.

Shared subpopulation gene expression patterns

To determine whether Lsi1 and Lsi2 principal neurons in the dentate gyrus, CA3 and CA1 share gene expression signatures, we compared the transcripts that were specifically regulated in Lsi1 and Lsi2 principal neurons in the main hippocampal subdivisions. A small group of unique transcripts was shared among granule cells in the dentate gyrus and among pyramidal neurons in CA3 and CA1 of the same line (Fig. 4a). These included a 3' UTR splicing variant of syntaxin 3 (STX3(3')), excluded from Lsi2 neurons, enriched in Lsi1 neurons), and a 3' UTR sequence of the gene for ribosomal protein S9 (RPS9(3')), excluded from Lsi1 neurons, enriched in Lsi2 neurons) (Fig. 4a). Double in situ hybridization of hippocampal sections confirmed these relationships at the level of individual neurons, suggesting that Lsi1 and Lsi2 subpopulations are homogeneous with respect to the expression of subsets of genes (Fig. 4b). In further support of the notion that the subpopulations show matched properties across hippocampal subdivisions, we found that shared genes were upregulated or downregulated to similar extents when compared with average expression in principal neurons in the dentate gyrus, CA3 and CA1 (Fig. 4c). For clarity, we will designate the entire subpopulation of potentially Lsi1- or Lsi2-positive hippocampal principal neurons as HP(Su1) and HP(Su2) neurons, respectively. HP(Su1) neurons are thus STX3(3')+S9(3')-, whereas HP(Su2) neurons are STX3(3')-S9(3')+.

To investigate what might underlie the visualization of hippocampal principal neuron subpopulations in sparse Thy1-mGFP transgenic mice, we identified the insertion sites of the

transgenes in these mice. Thy1-mGFP transgene copies had inserted at a single locus, near the centromere on chromosome 16 in Lsi1 mice, and near the centromere on chromosome 19 in Lsi2 mice (Supplementary Fig. 6). Those chromosomal insertion sites are close to olfactory receptor gene clusters²⁷ (less than 15 million base pairs (MB) from centromeric edge; Supplementary Fig. 6). A further sparse Thy1 line (Lsi3; ref. 17) also showed transgene insertion near an olfactory receptor gene cluster (on chromosome 10; data not shown). By contrast, the single transgene insertion site in Lmu1 mice was located on chromosome 2, neither near a centromere nor near an olfactory receptor gene cluster (Supplementary Fig. 6). A survey of published neuronal subtype marker genes revealed that these have a high probability of mapping near olfactory receptor gene cluster sites^{28,29} (about 50% probability to map within 1 MB of an olfactory receptor gene cluster; Fig. 4d and Supplementary Fig. 7). When we picked 400 genes randomly among those expressed in all granule cells, only 4.8% of the genes mapped within 1 MB of an olfactory receptor gene cluster (Fig. 4d). By contrast, when we considered only genes that were upregulated or downregulated in all HP(Su1) or HP(Su2) neurons (in the dentate gyrus, CA3 and CA1), 52% of them mapped within 1 MB of an olfactory receptor gene cluster (Fig. 4d). Genes that were specifically regulated in HP(Su1) or HP(Su2) principal neurons therefore shared with neuronal subtype marker genes a high probability of mapping near olfactory receptor gene clusters.

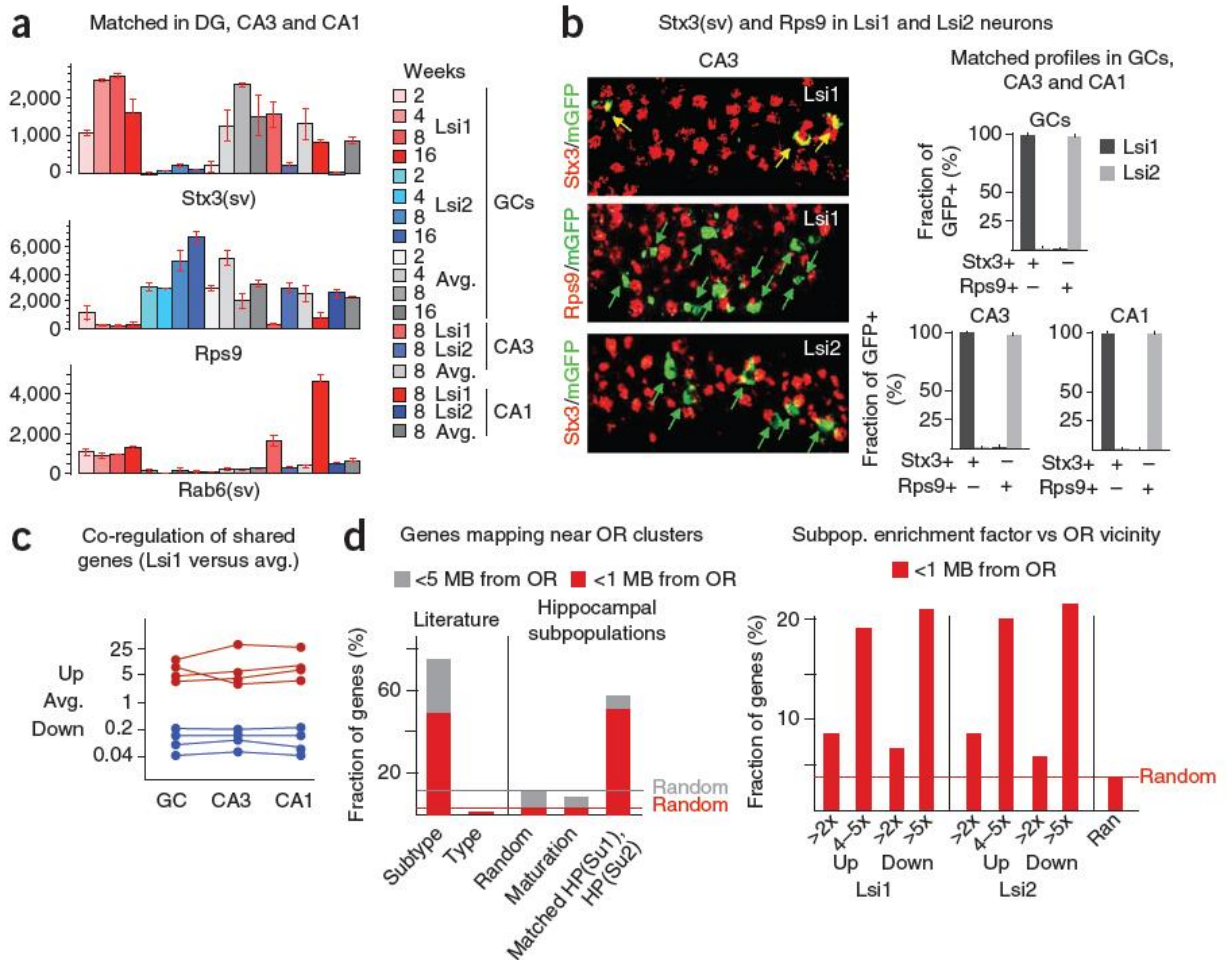


Figure 4: Transcripts shared among Lsi1 or Lsi2 subpopulations in dentate gyrus, CA3 and CA1.

(a) Examples of transcripts co-regulated in Lsi1 or Lsi2 principal neurons in dentate gyrus (DG), CA3 and CA1. Error bars, s.e.m. (b) Marker combinations identifying Lsi1 and Lsi2 principal neurons in the hippocampus. Combined GFP-in situ hybridization detection. Arrows, GFP+ marker+ (yellow) and GFP+ marker- (green). Quantitative analyses: data from eight sections each, covering all anterior-posterior levels of hippocampus; n = 3 mice each. (c) Genes that are up- or downregulated in all three types of Lsi1 hippocampal principal neurons are closely co-regulated in granule cells, and in pyramidal neurons in CA3 and CA1. Each line represents one gene and its deviation from average values. (d) High probability that subtype-specific genes map near olfactory receptor (OR) gene clusters. Left: relationship between subtype markers and olfactory receptor gene cluster vicinity. Random: 400 random genes in average granule cells; Maturation: genes enriched in Lsi1 (16 w) over Lsi1 (8 w) granule cells; HP(Su1), HP(Su2): genes selectively regulated in all Lsi1 or Lsi2 principal neurons. Right: optimization of OR vicinity for genes up- (4–5 fold) or downregulated (>5 fold) in Lsi1 or Lsi2 principal neurons.

Matched distinct temporal patterns of synaptogenesis

To investigate how the HP(Su1) and HP(Su2) subpopulations of principal neurons insert into hippocampal circuits, we analyzed the dendrites and axons of mGFP-expressing neurons

between postnatal days 5 and 10 (P5 and P10), during the early phases of adult hippocampal synaptogenesis³⁰. A comparison of Lsi1 and Lsi2 CA3 pyramidal neurons suggested that the development of Lsi1 neurons anticipated that of Lsi2 neurons by 2–4 d (Fig. 5a). Lsi1 and Lsi2 pyramidal neurons were each locally homogeneous with respect to maturation in CA3 or CA1, and showed no overlap in maturation or synaptogenesis between P5 and P10 (Fig. 5a). Consistent with these marked temporal differences in hippocampal circuit assembly, the developmental markers³¹ Doublecortin and Sema3C were downregulated in Lsi1 granule cells before Lsi2 granule cells, and both subpopulations matured before the average of all granule cells (Fig. 5b). Lsi1 mossy fibers established large mossy fiber terminals in stratum lucidum between P5 and P7, where these frequently contacted Lsi1 pyramidal neurons from P7 on (Fig. 5c). By contrast, we found no mossy fiber terminals along Lsi2 mossy fibers at P7; at P10, the terminals were rare and small, but they often contacted Lsi2 pyramidal neurons (Fig. 5c). In parallel to a delay in mossy fiber synaptogenesis, dendritic development in Lsi2 granule cells lagged by 3–4 d behind that in Lsi1 granule cells at all positions along the blades³⁰ (Fig. 5c). We found comparable distinct timings, rates and patterns of presynaptic maturation between Lsi1 and Lsi2 mossy fibers in organotypic slice cultures (Supplementary Fig. 8).

To provide independent evidence for the presence of hippocampal principal neuron subpopulations that differ in the timing of their synaptic maturation, we analyzed transgene-positive CA3 pyramidal neurons and mossy fibers in *Lmu1* mice, where mGFP is expressed in most granule cells and in about half of the pyramidal neurons (Supplementary Fig. 1). At P7, the analysis revealed the expected presence of subpopulations of mossy fibers and CA3 pyramidal neurons maturing in patterns comparable to those of HP(Su1) and HP(Su2) neurons, and that of additional transgene-positive neurons maturing after these early subpopulations of principal neurons (Fig. 5d). Together, these results provided evidence that HP(Su1) and HP(Su2) neurons insert into hippocampal circuits during distinct and matched temporal windows, suggesting that this might result in the formation of synapses preferentially among neurons of the same subpopulation.

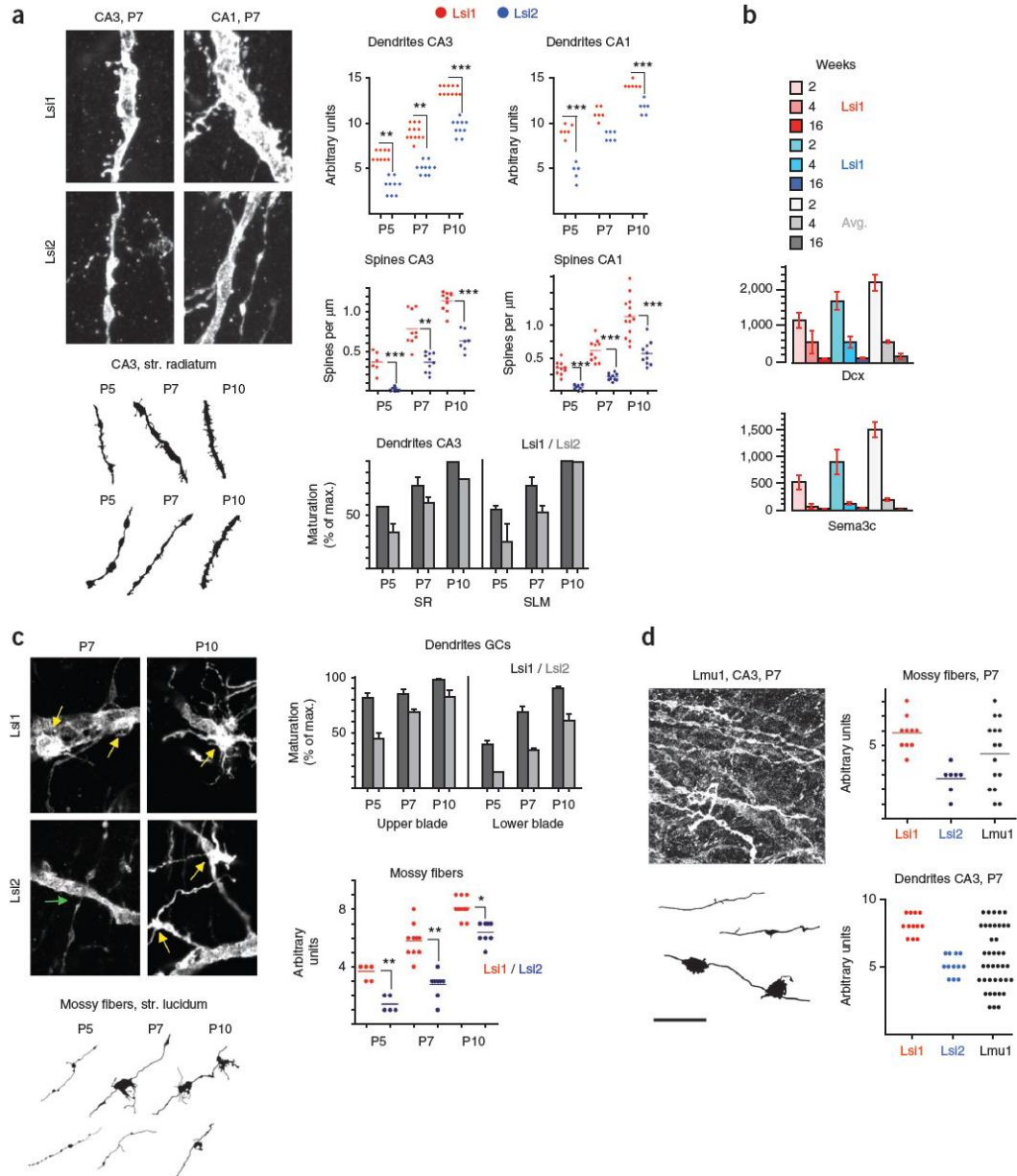


Figure 5: Distinct and matched synaptogenesis schedules by Lsi1 and Lsi2 subpopulations.

(a) Nonoverlapping dendritic maturation and synaptogenesis processes in Lsi1 and Lsi2 pyramidal neurons in CA3 and CA1. Left and center, representative panels and camera lucidas. Mann Whitney test; Error bars, s.e.m. (b) Immature granule cell transcript contents in Lsi1, Lsi2 and average granule cells. Dcx, doublecortin. (c) Nonoverlapping dendritic maturation and synaptogenesis processes by Lsi1 and Lsi2 granule cells. Arrows, presence (yellow) or absence (green) of specific contacts between mossy fibers and pyramidal neurons. Scatter plot, presynaptic maturation index values. (d) Synaptogenesis subgroups in Lmu1 pyramidal neurons and mossy fibers at P7. Panel and camera lucida: representative examples of labeled dendrites (panel, stratum radiatum) and mossy fibers (lucida). Scale bar, 10 μm . * $P < 0.05$, ** $P < 0.01$, *** $P < 0.001$.

Selective connectivity between DG and CA3

To determine whether matched HP(Su1) (or HP(Su2)) principal neurons within interconnected hippocampal subdivisions make synaptic contacts selectively with one another, we analyzed contacts between presynaptic mGFP-positive Lsi1 (or Lsi2) mossy fiber terminals and postsynaptic CA3 pyramidal neurons in adult mice. We considered as putative contact sites only events in which the distance between mossy fiber terminals (>3 μm diameter) and pyramidal neuron dendrites was smaller than 0.2 μm . For more than 70% of these putative synaptic contacts, we determined whether mGFP-Bassoon accumulation sites (presynaptic) were apposed to mGFP-Pi-GluR1 puncta (postsynaptic; Fig. 6a) and validated the majority of those putative functional synapses (48/50) by this procedure¹⁶. Owing to the low connectivity between granule cells and pyramidal neurons in dorsal hippocampus¹², the likelihood of finding such synaptic contacts by chance is extremely low. Nevertheless, a systematic analysis of 100 \times 100 \times 55- μm volumes yielded frequent contact sites between mGFP-positive cells (Fig. 6a). A statistical analysis based on binomial distributions (probability that contacts are chance events: $f(k; n; p) = (n!/k!(n-k)!) p^k(1-p)^{n-k}$, where k is the number of connections found, n is (number of mGFP+ mossy fibers) \times (average number of mGFP+ pyramidal neurons) and p is the probability for each contact), revealed that the likelihood that these frequencies were chance events was 10^{-5} or less for both dorsal and ventral hippocampus (Fig. 6a). We found comparable selective contacts between mGFP-positive granule cells and CA3 pyramidal neurons for Lsi2 neurons (Fig. 6a). Additional experiments using BrdU labeling to visualize the birthdates of CA3 pyramidal neurons provided evidence that early born HP(Su1) mossy fibers had established synaptic connections with early born but not late-born pyramidal neurons in CA3 (Supplementary Fig. 9).

To verify the presence of synaptic contacts among HP(Su1) neurons in stratum lucidum, we also analyzed contacts between mGFP-positive pyramidal neurons in CA3 and mGFP-positive mossy fibers by immuno-electron microscopy. The analysis confirmed the presence of synapses between immuno-labeled presynaptic mossy fiber terminals and postsynaptic thorny excrescences (Fig. 6b). In one set of experiments, 10 out of about 148 mossy fiber terminal profiles that contacted mGFP-positive pyramidal neuron dendrites in CA3b stratum lucidum (total of 30 mGFP-positive dendrites, from 3 mice) were mGFP-positive; given that about 2% of the granule cells were transgene-positive in these mice, this means that about 65% of the mossy fiber terminals that contacted Lsi1 pyramidal neurons in CA3 belonged to

Lsi1 granule cells. For technical reasons, not all mGFP-expressing profiles could be labeled unambiguously in these experiments; the 65% figure is an underestimate.

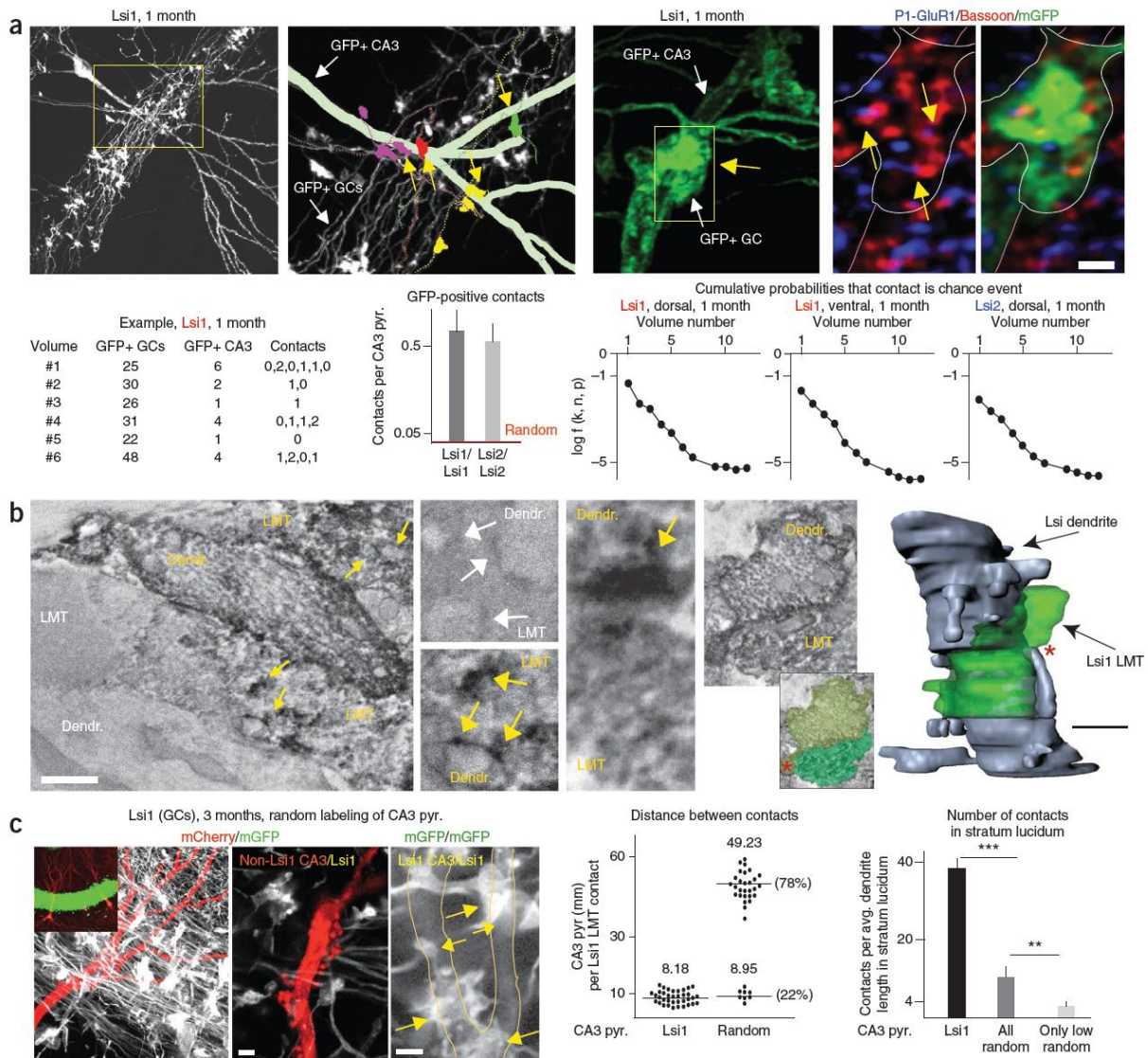
To provide independent evidence for selective connectivity between matched principal neuron subpopulations in stratum lucidum, we analyzed Lsi1 mice in which pyramidal neurons in CA3 were labeled randomly in adult animals using a rabies-mCherry virus (Fig. 6c). We found that 20–22% of the randomly labeled CA3 pyramidal neurons closely resembled Lsi1 neurons (average distance of Lsi1 mossy fiber contacts 8.95 versus 8.18 μm), whereas the remaining pyramidal neurons showed much less frequent contacts with Lsi1 mossy fiber terminals (average distance 49.23 μm ; Fig. 6c). About 92% of the 40–42 mossy fiber terminals on individual Lsi1 pyramidal neurons in CA3 were established by Lsi1 granule cells, whereas 8% were not (Fig. 6c). Although the lower estimate from immunoelectron microscopy (65%) probably reflected the presence of unlabeled axonal profiles in the electron microscopy samples, the two methods both strongly supported the notion that Lsi1-Lsi1 connectivity in stratum lucidum is much higher than chance.

To further investigate the notion that selective connectivity between Lsi1 or Lsi2 principal neurons in dentate gyrus and CA3 is based on selective recognition processes between subpopulations of cells, we analyzed the connectivity of Lsi1 and Lsi2 neurons in a Reelin $^{-/-}$ background, where cell identities are preserved but cell layer organization in the hippocampal dentate gyrus and CA3 are strongly disrupted³². The positions of granule cells and CA3 pyramidal neurons and the trajectories of mGFP-positive mossy fibers were abnormal in the absence of Reelin, but the disruption of hippocampal layer organization did not affect the frequencies with which Lsi1 or Lsi2 mossy fibers and CA3 pyramidal neurons established synaptic connections with each other (Supplementary Fig. 10).

Figure 6: Selective connectivity between matched granule cells and CA3 pyramidal neuron subpopulations.

(a) Light microscopic analysis of stratum lucidum mossy fiber synapses in Lsi1 mouse at 1 month. Left, overview, and higher magnification view with superimposed camera lucida; yellow arrows, verified contacts. Right, example of verified Lsi1 mossy fiber terminal-pyramidal neuron contact (yellow arrows). High-magnification panels, single confocal planes. Lower row, quantitative analysis of stratum lucidum synaptic contacts in Lsi1 and Lsi2 mice. Left, examples of synaptic contact analysis for six stratum lucidum volumes along CA3, including numbers of GFP+ mossy fibers, numbers of GFP+ pyramidal neurons, and numbers of contacts for each pyramidal neuron. Center, average numbers of Lsi1 (or Lsi2) mossy fiber terminals contacting Lsi1 (or Lsi2) CA3 pyramidal neurons. Normalized to 25 GFP-positive granule cells; 55 μm sections; $n = 60$ pyramidal neurons, from 3 mice each; random, expected values for random connectivity. Right, cumulative probability values that contacts are chance events for first 12 ($100 \times 100 \times 55 \mu\text{m}$) volumes in Lsi1 and Lsi2 mice (averages from 3 mice each). (b) Immunoelectron microscopic analysis of Lsi1-Lsi1 synaptic contacts in CA3 stratum lucidum. Immunolabeled (yellow) and non-labeled (white) dendrites (dendr.) and large mossy fiber terminals (LMT) at increasing magnification (left to right); yellow arrows, labeled thorny excrescence profiles inside labeled LMTs. Right, example, with three-dimensional reconstruction of labeled pre- and postsynaptic elements. (c) Connectivity between randomly labeled CA3 pyramidal neurons and Lsi1 granule cells. Left,

examples of mCherry-labeled pyramidal neurons (red) and Lsi1 granule cells and pyramidal neurons in stratum lucidum. Center, average distance between Lsi1 mossy fiber synaptic contacts on Lsi1 or mCherry-labeled pyramidal neurons; percentages, fractions of Lsi1-like and non-Lsi1-like pyramidal neurons. Right, average numbers of contacts by Lsi1 mossy fiber terminals with Lsi1 or randomly labeled CA3 pyramidal neurons. Only low random: putative Lsi1 CA3 pyramidal neurons with high densities of Lsi1 contacts removed from the dataset. Average dendrite length in stratum lucidum, 184 μm . $n = 60$ pyramidal neurons, from 3 mice each. Mann-Whitney test; ** $P < 0.01$, *** $P < 0.0001$. Error bars, s.e.m. Scale bars, 1 (a,b), 10 (c, left) and 2 (c, right) μm .



Selective connectivity between CA3 and CA1

To determine whether HP(Su1) neurons were also interconnected selectively between CA3 and CA1, we analyzed putative synaptic contacts between mGFP-positive Schaffer collaterals (the axons of CA3 pyramidal neurons) and mGFP-positive CA1 pyramidal neurons in stratum radiatum. We defined contact sites as distances of less than 0.2 μm (single confocal sections) and counted contacts as synaptic when they involved an axonal bouton (varicosity) of at least 1 μm diameter (Fig. 7a).

In control experiments, more than 95% of the boutons accumulated the synaptic vesicle marker synaptophysin, and more than 85% were adjacent to Pi-GluR1 puncta (not shown). The analysis revealed that 89% of the contacts between Lsi1 Schaffer collaterals and Lsi1 CA1 pyramidal neurons coincided with a bouton, whereas only 15% of the contacts between Lsi1 Schaffer collaterals and randomly labeled (rabies-mCherry virus) CA1 pyramidal neurons coincided with boutons (Fig. 7b). The difference between contacts with boutons among Lsi1-Lsi1 and Lsi1-random pairs was highly significant ($P < 0.0001$; Fig. 7b). By contrast, the distributions of all contact values (with and without bouton) were similar between Lsi1-Lsi1 and Lsi1-random pairs (Fig. 7b). Seven out of 62 randomly labeled CA1 pyramidal neurons exhibited synaptic contact values well within the Lsi1/Lsi1 range, consistent with the notion that these reflected labeling of Lsi1 pyramidal neurons (Fig. 7b).

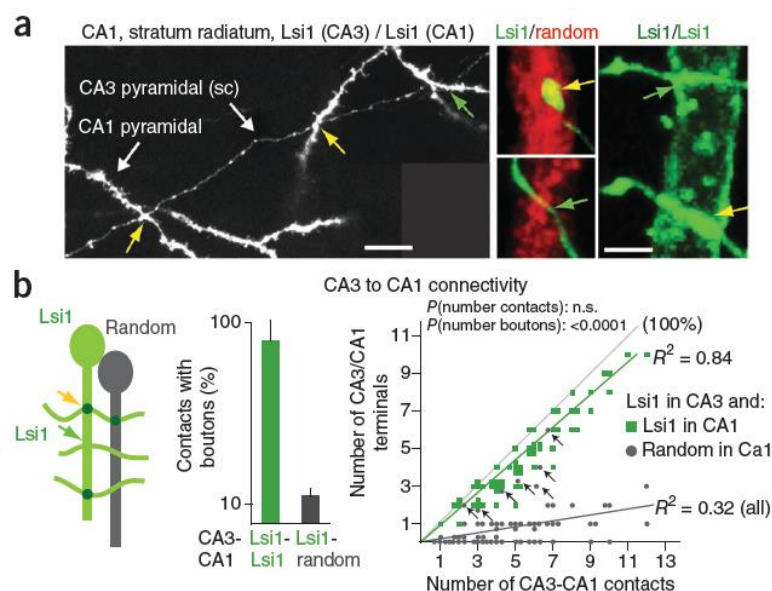


Figure 7: Selective connectivity between matched CA3 and CA1 pyramidal neuron subpopulations.

(a) Examples of labeled CA3 axons (Schaffer collaterals; sc) and CA1 pyramidal neurons in stratum radiatum. Left, Lsi1 Schaffer collateral contacting two Lsi1 CA1 pyramidal neurons. Right, examples of contacts with mCherry-labeled CA1 pyramidal neuron (left) and Lsi1 CA1 pyramidal neuron. Arrows, contacts with (yellow) or without (green) boutons. (b) Quantitative analysis of Lsi1 connectivity in CA1 stratum radiatum. Left, schematic of how Lsi1 or randomly labeled CA1 pyramidal neurons were analyzed in the same mice for contacts by Lsi1 Schaffer collaterals. Center, fraction of contacts with boutons for Lsi1-Lsi1 and for Lsi1-random CA3-CA1 pairs. $n = 90$ CA1 pyramidal neurons each, from 3 mice. Error bars, s.e.m. Right, contacts with boutons versus total numbers of contacts for individual Lsi1 and randomly labeled CA1 pyramidal neurons (individual green squares and red dots). Arrows, putative Lsi1 CA1 pyramidal neurons among randomly labeled sample. Gray line, values for 100% synaptic connectivity. CA3 Lsi1 axons contacted Lsi1 and randomly labeled pyramidal neurons with undistinguishable frequencies, but only Lsi1-Lsi1 pairs showed high frequencies of boutons. Scale bars, 25 μm (a, left), 2 μm (a, right).

Temporal matching determines selective connectivity

Finally, to determine whether it was synaptogenesis timing or subpopulation identity that influenced selective connectivity in stratum lucidum, we analyzed organotypic co-cultures of dentate gyrus and CA3 derived from mice of different genotypes and ages (Fig. 8a). These experiments allowed us to investigate how Lsi1 or Lsi2 subpopulations of granule cells established connections with matched or unmatched subpopulations of Lsi1 or Lsi2 CA3 pyramidal neurons.

We detected contacts between pyramidal neurons and mossy fibers with active zone markers and activated postsynaptic receptor markers in comparable numbers in Lsi1 (P2)-Lsi1 (P2), and Lsi2 (P3)-Lsi2 (P3) co-cultures of matched ages and subpopulations, and in Lsi1 (P2)-Lsi2 (P7) co-cultures of matched maturation state but distinct subpopulations; by contrast, we found no putative synaptic contacts when identity was matched but maturation was not (for example, Lsi1 (P2)-Lsi1 (P7); Fig. 8b). Although mossy fiber terminals were smaller when identities were not matched (Supplementary Fig. 9), these results provided evidence that selective connectivity in the principal neuron subpopulations mainly reflected temporally matched schedules of synaptogenesis.

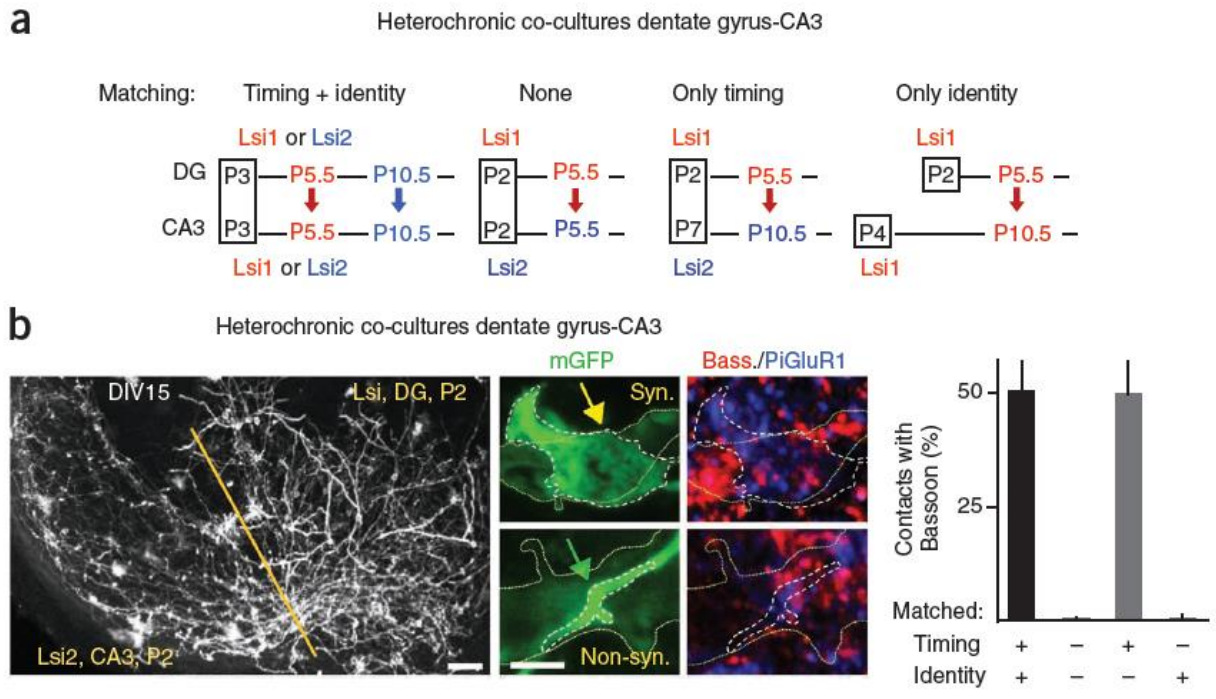


Figure 8: Influence of synaptogenesis timing and subpopulation identity on selective connectivity.

(a) Schematic representation of heterochronic co-culture experiments. Boxed: age of dentate gyrus (DG) and CA3 fragment at beginning of culture. Mossy fiber synaptogenesis timing is indicated in color (Lsi1: red; Lsi2: blue), and with an arrow pointing from DG to CA3. (b) Heterochronic co-culture experiments. The panels show a low-magnification view of an heterochronic co-culture (yellow line: DG/CA3 co-culture boundary), and high-magnification views of synaptic and non-synaptic contacts (single confocal planes). Bass: Bassoon. Quantitative analysis: fraction of synaptic (Bassoon+) versus total contacts on Lsi1 or Lsi2 pyramidal neurons in CA3 (see Methods). N = 60, from 3 independent cultures each. Error bars, s.e.m. Scale bars, 50 (b, left), 3 (b, right) μ m.

ACKNOWLEDGEMENTS

We thank S. Arber, A. Lüthi and B. Roska (Friedrich Miescher Institute; FMI) for comments on the manuscript, C. Genoud (FMI) for assistance with immuno-electron microscopy, M. Wiechert and A. Ponti (FMI) for data analysis assistance, and S. Arber for the rabies-mCherry virus. The FMI is part of the Novartis Research Foundation.

AUTHOR CONTRIBUTIONS

Y.D. conceived and carried out the gene expression and the adult subpopulation mapping analysis. F.D. conceived and carried out the neurogenesis and synaptogenesis analysis and parts of the electron microscopy and connectivity analysis. I.G. conceived and carried out most of the connectivity analysis. E.C. carried out and optimized the cell genomics experiments. P.C. helped devise the experiments and wrote the manuscript. All authors discussed the results and commented on the manuscript.

4.3.4 Discussion

We have provided evidence for the existence of matched principal neuron subpopulations in hippocampal dentate gyrus, CA3 and CA1 defined by their distinct neurogenesis time windows and distinct patterns of gene expression. We have also shown that the subpopulations have distinct schedules of synaptogenesis and selective connectivity at synapses between mossy fibers and pyramidal neurons in CA3 and between Schaffer collaterals and pyramidal neurons in CA1 (Supplementary Fig. 11). The subpopulations overlapped partially in time during neurogenesis, but there was homogeneity and no temporal overlap during synaptogenesis, supporting the notion that these neurons reflect separate subpopulations. A detailed analysis of the numbers of Lsi1 and Lsi2 principal neurons in the hippocampus provided further insights into how these subpopulations may be specified during development. Published figures of the total number of principal neurons in rat hippocampus, normalized to CA3, give values of 1 (CA3), 4.8 (granule cells) and 1.5 (CA1)¹², and corresponding values of total transgene-positive neurons were 1 (CA3), 4.4 ± 0.2 (granule cells) and 1.5 ± 0.1 (CA1) for Lsi1, and 1 (CA3), 4.6 ± 0.1 (granule cells) and 1.4 ± 0.1 (CA1) for Lsi2 ($n = 5$ mice each; absolute numbers within each mouse line varied by a factor of up to 2.7). The fractional prevalences of HP(Su1) (or HP(Su2)) neurons in the three main hippocampal subdivisions are therefore very similar, which suggests that the subpopulations are specified through a mechanism that allocates fixed proportions of neurons in the neurogenesis processes that lead to principal neurons in dentate gyrus, CA3 and CA1. Because the sizes of the hippocampal subdivisions are different and the distinct subpopulations were generated during partially overlapping time windows early in neural development, the allocation might manifest for each subpopulation as a probability function of time during neurogenesis. Such temporal specification schemes are reminiscent of the roles of temporal genes in neurogenesis^{33–35}.

Our finding that HP(Su1) and HP(Su2) neurons reflected two early subpopulations of hippocampal principal neurons is consistent with previous reports that neurons generated early during neurogenesis also mature and insert into circuits at faster rates^{36,37}. In vertebrates, timing schemes that relate specific neurogenesis windows and sub-windows to distinct neuronal identities have been described for retinal and cortical neurons, and for the interneurons that arise from the medial ganglionic eminence^{38–41}. Our results suggest that similar temporal schemes underlie the specification of subpopulations of principal neurons within each main hippocampal subdivision. However, whether and how temporal genes

contribute to the specification of subpopulations in the hippocampus remains to be determined. Likewise, it will be interesting to determine how the subpopulations relate to previously reported differential patterns of gene expression in the hippocampus⁴². That distinct temporal windows of neurogenesis are coupled to specific patterns of synaptogenesis has been shown for *Drosophila*^{36,37,43}.

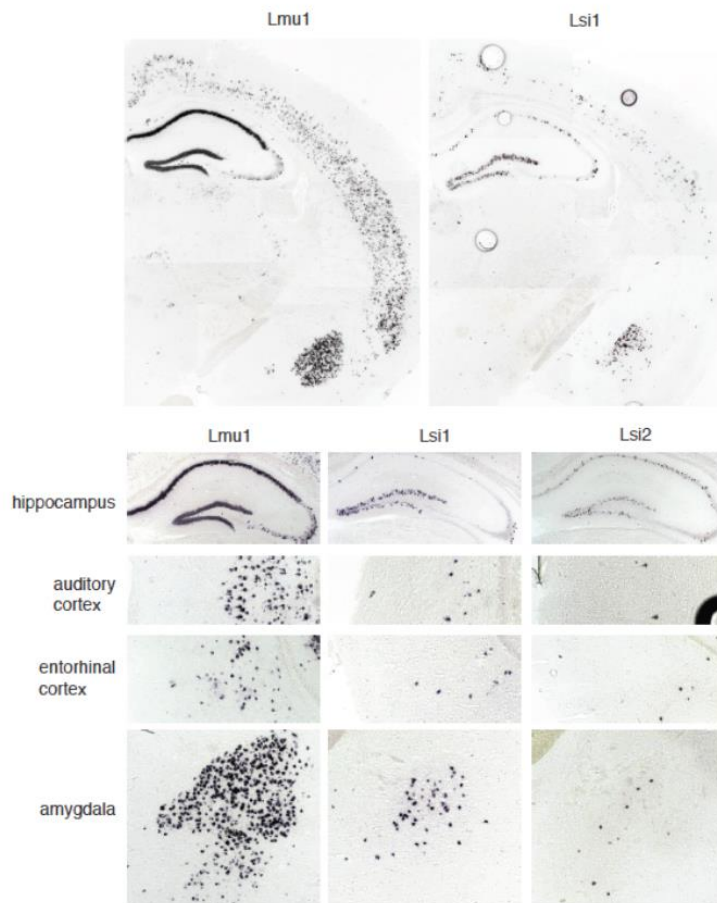
A recent study in zebrafish related sequential interneuron differentiation to distinct swimming functions⁴⁴, and one study related the timing of neurogenesis to differentiation in cerebellar granule cells⁴⁵. However, to our knowledge, there has been no evidence relating sequential neurogenesis or synaptogenesis to inter-areal connectivity in vertebrates. Our results provide evidence that temporal schemes underlie selective connectivity between matched principal neuron subpopulations belonging to the major hippocampal subdivisions in the mouse. It remains to be determined whether similar temporal schemes of neuronal specification and synaptic maturation underlie inter-areal connectivity in other neuronal circuits in vertebrates.

To what extent is hippocampal connectivity influenced by subpopulation specificities? Selective connectivity for the HP(Su1) subpopulation was about 92% in CA3 (i.e., 8% non-Lsi1 mossy fiber terminals onto Lsi1 CA3 pyramidal neurons) and 85–89% in CA1. Hippocampal representations might therefore form preferentially within subpopulations of principal neurons. Furthermore, as temporally coincident maturation determines synaptic specificity, overlaps between subpopulations might not be entirely random, and might be more frequent among subpopulations that mature in adjacent temporal windows. Our findings raise the issues of whether and how specificity may extend to new synapses established in the adult, most notably by the mossy fiber terminals of adult-born granule cells⁴⁶. When we matched the maturities of the Lsi1 and Lsi2 subpopulations through appropriate heterochronic co-cultures, synapses between the different subpopulations did form, but the presynaptic terminals were substantially smaller, suggesting that additional factors, possibly related to the molecular identities of the subpopulations, might also influence synapse specificity. Accordingly, it will be interesting to determine whether the mossy fibers of adult-born granule cells also show some selectivity with respect to their postsynaptic pyramidal neuron partners in CA3.

Our results have potential implications for information processing in the hippocampus, and raise the possibility that microcircuits of genetically predefined and selectively interconnected principal neurons might be recruited differentially during the establishment and retrieval of episodic representations. For example, differential recruitment of subpopulation networks may support the rapid remapping of related but distinct episodic representations in CA3 and

CA1 (ref. 47). Consistent with the notion that the subpopulations might show functional differences, Lsi1 and Lsi2 mossy fiber terminals show distinct and unique structural plasticity properties¹⁷. Future studies will therefore aim to determine whether and how the subpopulations and their microcircuits have specific roles in information processing.

4.3.5 Supplementary material



Deguchi Suppl. Fig. 1

Supplementary Fig. 1:

Distribution of transgene-positive cells in Lmu1, Lsi1 and Lsi2 mice.

In situ hybridization in 2 mo mice. Note how positive neurons are detected in the same structures but in different numbers in Lmu1, Lsi1 and Lsi2 mice.

Lsi1 vs. avrg. GC 16w >5X

	Lsi1/avrg.	Lsi1/avrg.
BC074974	21.9	B130021B11Rik 0.03
Trip11	16.5	Lpl 0.04
Ptprd	14.9	Skiv2l 0.04
Zc3hav1	14.0	Kcnj9 0.05
Rhobtb1	13.6	BE943757 0.06
Snx6	13.1	Smpd4 0.06
Zc3h8	11.9	Q330169B04Rik 0.06
Pdxdc1-sv1 (NM_053181.1)	11.6	BB024203 0.07
BB473548	11.5	BQ175871 0.08
Cnot6l	11.3	B6100453 0.08
Auts2	11.0	Rps0 0.08
Csn2	10.5	Stco4a1 0.08
Dgkd	10.2	Vt1a 0.08
Ssrp1	9.5	C1hd1 0.08
Rsrc1	8.5	Gpc6 0.09
A930018M24Rik	8.4	Stc39a8 0.09
5830407P18Rik	8.2	Bcat1 0.09
Bttb0	8.2	Kirrel3 0.09
Rd17	7.7	Mapk10 0.10
Lrp1b	7.2	DEEtd306e 0.10
Mapk10	7.1	Pcdh15 0.10
5830409G19Rik	6.7	Sox11 0.10
Gahrb3	6.6	Tsc22d1 0.11
Ev5	6.5	Lrch1 0.12
Lhx9	6.0	4732496O08Rik 0.12
B230334C09Rik	5.8	And5b 0.12
Schip1	5.7	Thumpd1 0.12
Ddk6	5.6	BB725777 0.13
Srp54a	5.5	Pou4f2 0.13
C730049O14Rik	5.5	Dnm3 0.13
Vav3	5.5	Serpina3n 0.14
BF472132	5.3	BQ266161 0.14
Lpin1	5.2	Wwtr1 0.14
Forn2	5.2	Agf1 0.15
D3Erd254e	5.2	5830426K05Rik 0.15
Trip12	5.1	Ptjg 0.16
Cops2	5.0	BG067986 0.17
		C130015C19 0.17
		Zfp396 0.17
		Zttb25 0.18
		Pdxdc1-sv2 0.18
		(NM_001039533) 0.18
		BB163080 0.19
		Agf2 0.19
		AV233159 0.20
		lfo2 0.20
		AW554842

Lsi2 vs. avrg. GC 16w >5X

	Lsi2/avrg.	Lsi2/avrg.
4930445G23Rik	19.1	Kirrel3 0.01
Rbm39	15.6	Prune2 0.04
Ptprd	11.6	Kcni9 0.04
9430085L16Rik	11.5	Skiv2l 0.04
Seid4	11.2	Gpc6 0.07
BB183349	10.1	Btrc 0.08
5830469G19Rik	9.8	BB354702 0.08
Ltp1	9.6	Stx3-sv1 0.08
BM213120	9.6	(NM_011502)
BB546207	9.2	Lnpop 0.09
C1hd1	9.2	C1hd1 0.10
Rpl17	8.5	Btbd11 0.10
Chm	8.5	Tmem29 0.10
B230114P17Rik	8.4	Fam70b 0.11
Fbxo32	8.3	Lpl 0.11
Mmm2	8.3	Eftud2 0.12
2610301B20Rik	8.1	Nsun6 0.12
Mef2c	7.8	Zfp398 0.12
BB180869	7.8	Zw10 0.12
5730510P18Rik	7.8	BB221678 0.12
Ttn	7.6	AK136698 0.13
Nav2	7.3	Mapk10 0.13
Sic15a2	7.2	BB750374 0.13
Rbm39	6.7	Ap3c2 0.13
BB251113	6.0	2410085M17Rik 0.13
Rhobtb1	6.0	Timm44 0.13
0030400A10Rik	5.9	C80889 0.14
C76246	5.8	Ncor1 0.14
Srd5a3	5.8	Map2k5 0.14
Bid1	5.7	Tax1bp1 0.14
Ccni	5.7	C77673 0.14
Ly86	5.5	Tmem41b 0.14
5330423111Rik	5.5	AH20166 0.15
Cd24a	5.1	5730470L24Rik 0.15
Ilf3	5.0	Gggs1 0.15
		Lphn2 0.16
		Rb1 0.16
		Eno1 0.16
		Kcnc2 0.16
		Pcdha4 0.17
		D5Erd798e 0.17
		Nfatc3 0.17
		Ankhd1 0.17
		BB461843 0.18
		2310008H04Rik 0.18
		Tgfbrc3 0.16
		BC043301 0.19
		Serpina3n 0.19
		Zfp148 0.19
		Igf2r 0.19
		BC021831.1 0.19
		Ilfo2 0.19
		Map3k5 0.20
		Fgfr1op2 0.20

Lsi1 vs. Lsi2 GC 16w >5X

	Lsi1/Lsi2	Lsi2/Lsi1
Prune2	97.8	Rps9 26.9
2900056M20Rik	31.6	BE943757 26.1
Snx6	17.2	Mesdcl1 20.5
BB473548	16.6	Fgfr1op2 15.0
Stx3-sv1 (NM_011502)	14.4	Lrch1 10.2
Zc3h8	13.9	C130015C19 10.0
Tgfbrc3	13.5	AU014072 9.9
2900017F05Rik	13.2	2910301B20Rik 9.8
Mkln1	12.0	BE075988 9.3
Tpd52l2	11.6	Thumpd1 9.3
Zw10	10.7	Arap3 8.7
Pdxdc1-sv1 (NM_053181.1)	10.4	Svil 8.6
Zfp597	9.9	Mmm2 8.5
Btrc	9.7	Cel6a2 8.5
Acap2	9.2	Csn152a 8.4
Asx3	9.1	BQ175871 8.4
5830407P18Rik	9.0	Ttn 7.8
5730470L24Rik	9.0	AH50353 7.4
Gggs1	8.8	Stc20a2 7.4
Auts2	8.2	Ccni 6.9
Kirrel3	7.9	D14Erd725e 6.7
6330526H18Rik	7.8	Stc15a2 6.5
Pds5a	7.8	Nr1 6.2
Spnb2	7.5	Zfp383 6.1
BB040234	7.2	Klf4 6.1
Ratb-sv1 (BC019118)	7.0	Pdgc 6.0
Auts2	6.9	C60279 5.8
Ankrip1	6.8	Pdxdc1-sv2 (NM_091039533) 5.8
E430022K19Rik	6.8	BE134355 5.8
BB221678	6.8	Hbs1l 5.5
Zbtb20	6.7	Ktd9 5.5
Tmem109	6.6	Fbxo32 5.5
BF472132	6.3	1810043G02Rik 5.4
Rbm39	6.2	Srd5a3 5.4
B230334C09Rik	6.2	Ube2w 5.1
Bttb9	6.1	Urm1 5.1
9430047L24Rik	6.0	Tclap4 5.0
Tro2b	5.8	
Srp54a	5.8	
E430026B21Rik	5.8	
Elovl7	5.7	
Rb1cc1	5.7	
Mapk6	5.6	
BB128657	5.4	
Fam70b	5.4	
Trip12	5.3	
D5Wsu178e	5.1	
3300002P13Rik	5.1	

Deguchi Suppl. Fig. 2

Supplementary Fig. 2:**Genes up- or downregulated in Lsi1 or Lsi2 granule cells.**

Values are medians from 3 mice (16 weeks). GC: granule cells.

Lsi1 vs. avrg. CA3 8w >5X

Lsi1/avrg.	Lsi1/avrg.
Pdx1(Ls1) (NM_053181.1)	27.2
Col8a1	25.6
Cdh	20.6
Vmn2b4	20.1
1500015016Rik	15.9
Slit3	14.0
Sox2	13.2
Stxbp6	13.1
BB232180	11.1
C030030A07Rik	10.8
Pitrd	10.7
0720403M19Rik	8.3
A330080G13Rik	7.7
Oit	7.2
Mal	7.0
AI953363	7.0
Gtcc1	6.7
Gpr137b	0.7
Wnt1	6.6
Pank1	6.4
D10Edt472e	6.2
Pchl1	6.1
Ccl27a	5.9
Fzd7	5.9
Con	5.5
Rab6-sv1 (BC010118)	5.4
Otd4	5.2
Rfx4	5.2
Sic10a1	5.1
3110052M02Rik	5.1
Slc15a2	0.03
Eno1	0.04
Epha5	0.05
Skiv2l	0.05
Sox2	0.05
Lor	0.06
Taf1b	0.06
Use1	0.07
Csnk1a	0.07
5031425E22Rik	0.08
AI447606	0.08
Hes1	0.09
Alpha3	0.10
BB186453	0.10
Hscb	0.10
Saca7	0.11
Sox1	0.11
EB284122	0.11
Linc3	0.11
EM195344	0.11
3110047P20Rik	0.11
Linc33	0.12
Cop4	0.12
Fam128b	0.12
Hba-a1	0.12
Thumpd1	0.12
543040L12Rik	0.13
Pfss35	0.13
Odap1l1	0.13
Gabrb3	0.13
Crx3	0.13
Zdhc24	0.13
Dync2h1	0.13
Nutpl	0.14
Mcm7	0.14
Entpd5	0.15
Fanc1	0.15
Cetn2	0.15
Enajc2	0.15
BB233300	0.16
Rbbp8	0.16
Gpr135	0.16

Lsi2 vs. avrg. CA3 8w >5X

Lsi2/avrg.	Lsi2/avrg.
Zkscan1	20.1
8430436O14Rik	20.0
Col8a1	17.9
Dnau7	9.6
6030405A18Rik	8.5
Slit8	8.0
Scn14	7.7
Zscan22	7.0
Pgpr1b	6.9
Ujlr8	6.9
BF472132	6.8
Mal	6.5
Fibp1l	6.5
Gsn	6.4
Sox2	6.2
Gir	5.9
Raf160	5.7
Ridr	5.4
Pitrd	5.4
Etbl2ip	5.4
Stard13	5.3
Gad2	5.1
Slk19	5.0
Skiv2l	0.03
BE948333	0.09
Csnk1e	0.10
Hba-a1	0.11
Zfp971	0.11
2900011L18Rik	0.11
Epha5	0.11
Ao2m1	0.11
A830021M18	0.12
Zfp277	0.12
Tnpo1	0.13
Pux1	0.14
Dicp2	0.14
Mif5	0.15
Gabrb3	0.15
Eno1	0.16
Akap13	0.16
5031425E22Rik	0.16
8430437O03Rik	0.16
5730661F06Rik	0.16
Mef1	0.17
Gsk3b	0.17
Ph21a	0.18
Sox2	0.18
B0063422	0.18
BB284122	0.18
Nfya	0.19
Ra50	0.19
Ankrd1	0.19
A10777281	0.19
Linc4	0.19
C77873	0.19
W13854	0.19
Sic15a1	0.19
Rhps1	0.20

Lsi1 vs. Lsi2 CA3 8w >5X

Lsi1/Lsi2	Lsi2/Lsi1
Ccl27a	44.4
Vmn2b4	23.4
Ccl27a	22.8
C030030A07Rik	19.6
Fdx1(Ls1) (NM_053181.1)	15.6
EM218851	13.0
Pank3	11.4
Fdtt1	11.3
Mid1	11.2
6720403M10Rik	10.5
Rbm39	9.3
D530037H12Rik	9.1
EM218897	8.9
Ccl27a	8.3
Gpr137b	7.7
Zfp92	7.5
BB20361	7.3
Otd4	6.8
EM250730	6.6
Sox3-sv1 (NM_011502)	6.6
Rab6-sv2 (AV334024)	6.4
Rfx4	6.3
Sicaa1	6.2
EO066123	6.1
E230325K18Rik	6.1
Ppat	6.1
Akap13	6.1
Rbm39	5.8
Rab6-sv1 (BC010118)	5.6
Hps1	5.6
A630091E24	5.5
Wnt1	5.4
AV227264	5.4
Slc15a2	61.1
Zic1	38.8
Sox2	34.7
Golga7b	12.2
Hch	11.0
Zfp703	11.0
Jam2	10.2
Thumpd1	9.9
Fes1	9.8
5730470L24Rik	9.3
Zscan22	8.9
Pitpc	8.8
Skiv2l	8.0
Zbtb20	7.7
Rps9	7.5
Nco1	7.4
Mfsd4	7.2
1110002H22Rik	7.1
Cram	7.0
Pgl2l	6.5
Ppp2r5c	6.5
EO066627	6.4
Mus61	6.3
Crx3	6.3
EM195344	6.2
Mal	6.1
Caprin2	6.1
Ec2113	6.0
5133401N00Rik	6.0
Ast1a	6.0
AJ450603	5.7
Frbp1l	5.6
BB395749	5.6
EE623356	5.4
Fdx1(Ls2) (NM_001036533)	5.2
Ptlib	5.2
Zdhc24	5.1
Ctln1	5.1
Ano4	5.0
Erd8	5.0
Mif5	5.0

Lsi1 vs. avrg. CA1 8w >5X

Lsi1/avrg.	Lsi1/avrg.
Sost	33.6
Pdx1(Ls1) (NM_053181.1)	24.5
BB428710	18.3
Ap2c1	15.3
Prune2	13.2
Papoa	9.7
Rab6-sv2 (AV334024)	7.4
Klf5	7.3
Rab6-sv1 (BC019118)	7.2
Trip11	7.1
0230104K21Rik	7.0
Pitrd	6.0
Epb4-14b	5.5
Ptgi1	0.03
Skiv2l	0.04
BB186453	0.05
Sox11	0.05
Kcnj9	0.05
Fgf10p2	0.08
BQ175071	0.10
Tra2a	0.10
Rbm39	0.12
Tct15	0.13
Thumpd1	0.13
Zfp309	0.14
Cdh	0.14
Otd2	0.15
C77873	0.15
Tcf5	0.15
AW491843	0.15
AV305314	0.15
A83004102Rik	0.18
BB926411	0.18
Ankrd44	0.19
Atrx	0.19
Pdx1(Ls2) (NM_001036533)	0.20

Lsi2 vs. avrg. CA1 8w >5X

Lsi2/avrg.	Lsi2/avrg.
Sost	31.2
Klf5	18.3
Ap2c1	18.1
BB428710	15.6
Trip11	11.5
Sox2	9.8
Epb4-14b	9.6
Papoa	9.0
Lcor	7.2
Slit8	7.2
Ndrp1	5.4
Skiv2l	0.03
Kcnj9	0.05
Sox3-sv1 (NM_011592)	0.05
BB180453	0.07
Chchd4	0.08
Zfp388	0.11
Tre2e	0.11
C77873	0.12
0430547G21Rik	0.19
BC021831.1	0.19
Lcor	0.19
Linc13c	0.19
Adams3	0.20
Fam107b	0.20

Lsi1 vs. Lsi2 CA1 8w >5X

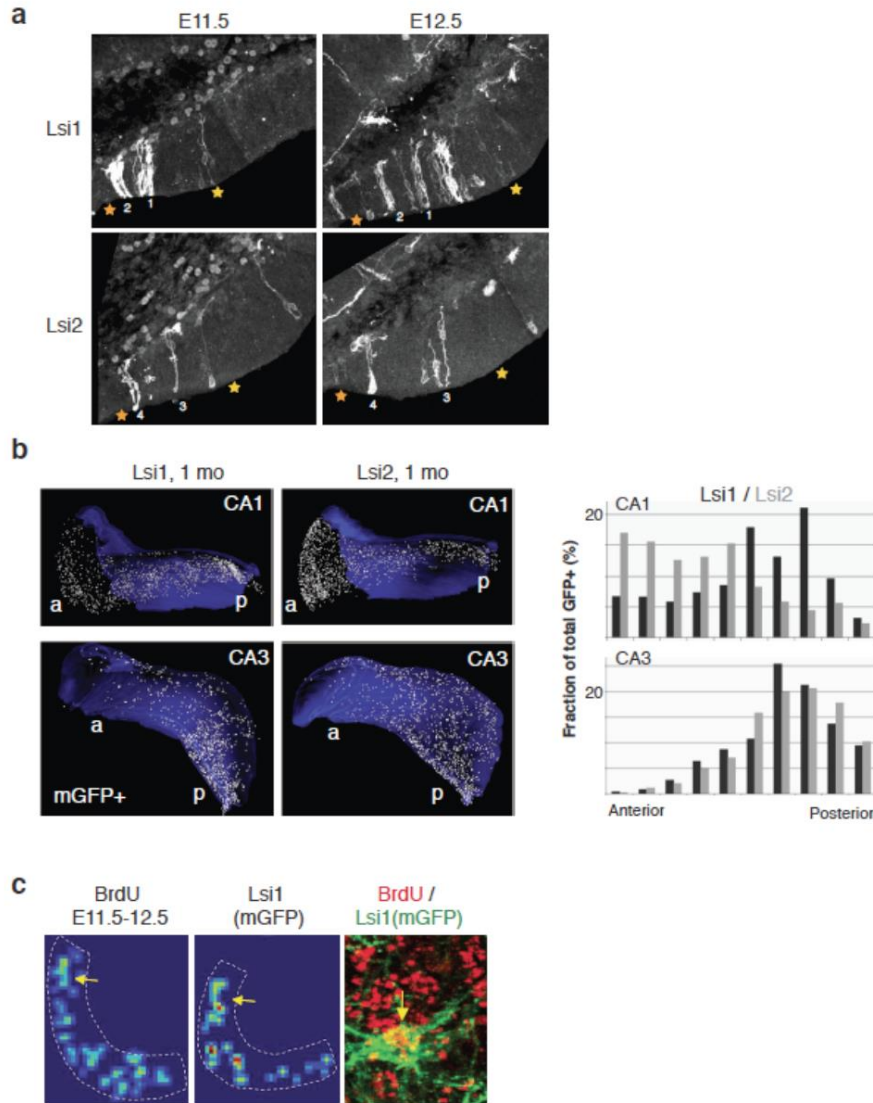
Lsi1/Lsi2	Lsi2/Lsi1
Pdx1(Ls1) (NM_053181.1)	29.5
Ptgi1	39.9
Sox2	14.8
Fgf10p2	10.7
BQ175871	9.8
Thumpd1	8.0
Sors1	6.0
Rab6-sv1 (BC019118)	8.6
Fam107b	8.4
Rab6-sv2 (AV334024)	7.5
A93064102Rik	5.6
Tct15	5.5
A93064102Rik	5.4
Sox11	5.2
Trip13	5.1
4930449A18Rik	5.1
Zbtb20	5.0

Deguchi Suppl. Fig. 3

Supplementary Fig. 3:

Genes up- or downregulated in Lsi1 or Lsi2 CA3 or CA1 pyramidal neurons.

Values are medians from 3 mice (8 weeks).

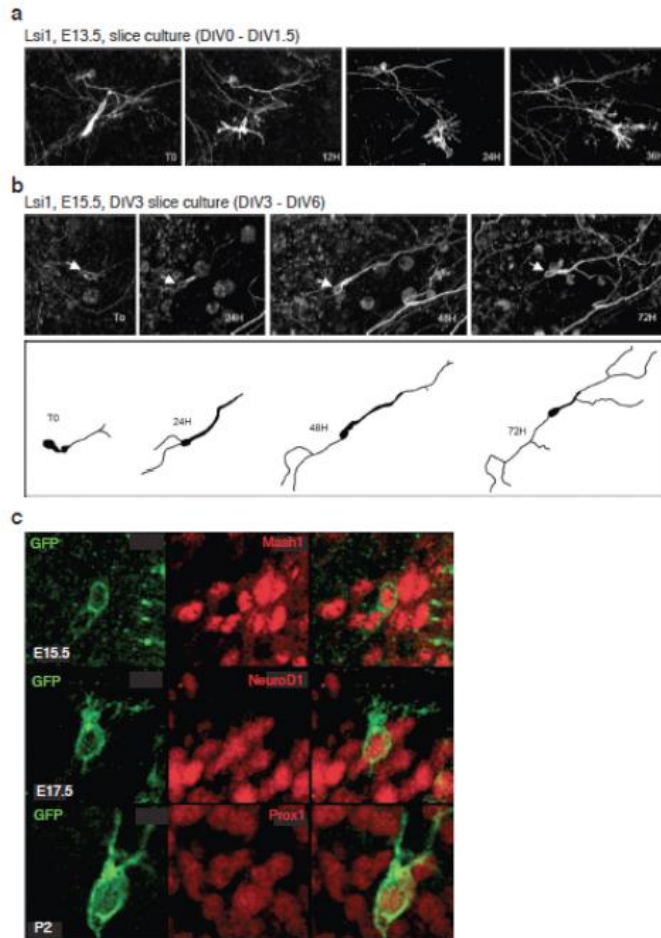


Deguchi Suppl. Fig. 4

Supplementary Fig. 4:

Distributions of Lsi1 and Lsi2 principal neurons in the hippocampus.

(a) Representative patterns of GFP+ neuroblast distributions in hippocampal neuroepithelium of Lsi1 and Lsi2 embryos at E11.5 and E12.5 (Hem to the left). Note comparable positions of neuroblast groups (numbers) at these two developmental stages. The stars indicate comparable positions along HN in the 4 embryos. (b) Distributions of Lsi1 and Lsi2 pyramidal neurons in the adult hippocampus. Left: representative 3D-maps of GFP+ pyramidal neurons (white dots) throughout CA1 and CA3. Consecutive 20 μ m coronal sections of the whole hippocampus were processed for in situ hybridization and images were aligned (AutoAligner, Bitplane). Positive cells were marked and the contour surface of the CA3 pyramidal cell layer was drawn manually using 3D/4D software (Imaris, Bitplane). Right: quantitative analysis of the distributions. Median values from 3 mice each; note resemblance to distributions in HN (Fig. 2b). (c) Comparable distributions of early (E11.5-12.5) BrdU-labeled and GFP+ Lsi1 pyramidal neurons (e.g. arrows). Heat map data from 1 mo mouse. Panel on the right: cluster of BrdU+/GFP+ pyramidal neurons in CA3 (arrow).



Deguchi Suppl. Fig. 5

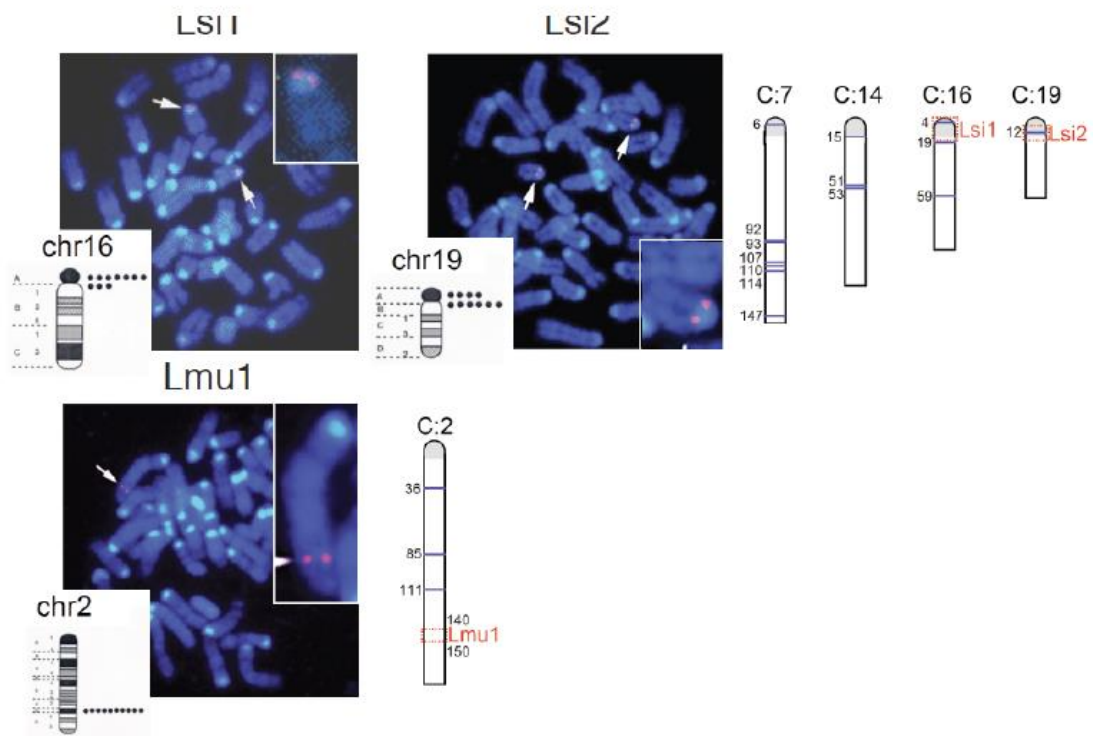
Supplementary Fig. 5:

Maturation of GFP-positive Lsi1 neuroblasts.

(a) Time lapse imaging of Lsi1 E13.5 slice culture. Embryonic explants were processed as described³⁴, and maintained in slice culture inserts (Millipore) for up to 10 days in 66% BME, 25% Hanks, 5% FBS, 1% N-2 and 0.66% d-glucose (35°C, 5% CO₂). Neuroepithelium on the right. Note mitotic division of Lsi1 neuroblast to generate GFP+ Lsi1 daughter cells.

(b) Time lapse imaging of DIV3 Lsi1 E15.5 slice culture. Embryonic explants were processed and imaged as described⁴⁸. The camera lucida highlights a neuroblast that develops dendritic and axonal primordia between DIV3 and DIV6.

(c) Maturation of mGFP-positive neuroblasts *in vivo*. Immunocytochemistry panels visualize mGFP+ cells co-expressing Mash1 (E15.5; early progenitors), NeuroD1 (E17.5; postmitotic neuroblasts) and Prox1 (P2; immature granule cells).



Deguchi Suppl. Fig. 6

Supplementary Fig. 6:

Visualization of transgene insertion sites by FISH.

Chromosomal spreads of spleen lymphocytes were processed by SeeDNA (Ontario, Canada). The positions of olfactory receptor clusters²⁷ are indicated by bars and numbers on the chromosome schematics on the right. The insertion sites for Lsi1 and Lsi2 mice are near centromeres, on two of the four mouse chromosomes with olfactory receptor clusters near centromeres (C7, C14, C16, C19).

Subtype genes)

retinal neuron subtype genes

	Mm	Hs
Grim6	0.1	2.4
Pknox	0.3	8.5
Rho	0.5	0.5
Fstl4-Spig1	0.6	>15
Slc6a9-Glyt1	0.8	>15
Scab2	0.9	1.1
Cj22-Cx36	1.8	>15
Th	2.2	2.1
Pde1b	5.0	0.6
Cjx1-Cx45	5.8	13.6
CalBP5	7.5*	>15
Aqp1	12.1**	>15
Chat	17.3	5.4

* 0.2 form vomeronasal 1 receptor
** 1.5 form vomeronasal 1 receptor

DRG subtype genes

	Mm	Hs
Tipv1	0.1	0.2
P2rx3-p2x3	0.3	0.5
Prg4	0.6	0.7
Ret- e-RET	1.6	2.2
Mrgprd	4.6	1.0
Calca-Cgrp	5.8	0.0
Ntrk1-TrkA	9.6	1.5

cerebellum subtype genes

	Mm	Hs
Nrgn	0.1	0.2
Sst	4.2	>15
Aldoc-Zetbin2	4.1	>15

cell type genes)

broad retinal cell type genes

	Mm	Hs
Dab1	14.0	>15
Cnga3	57.2	>15
Slc17a8-vGlut3	10.5	>15
Cja10-Cx-57	11.0	>15
Calb2	24.9	>15
Calb1	27.9	no OR
Opn4	15.1	>15

broad interneuron marker genes

	Mm	Hs
Pvalb	20.0	no OR
Chat	17.2	5.4
Gad2-GAD65	13.7	>15
Gad1-GAD67	14.8	>15

cerebellar Golgi cell type marker

	Mm	Hs
Gm2	66.7	>15

motor neuron marker

	Mm	Hs
Mnx1-HB9	no OR	12.5

Lsi1 co-regulated genes all DG+CA3+CA1) more than 3 fold

	Mm	Hs
Pdedc1-sv1 (NM_053181.1)	5.4	11.8
Rab6-sv1 (BC019118)	0.9	1.4
Fip17	0.8	>15
Rab6-sv2 (AV334024)	0.9	1.4
BB188453	0.2	-
Skiv2l	1.6	2.5
Pdedc1-sv2 (NM_001039533)	5.4	11.8
Thampd1	10.9	>15

Lsi2 co-regulated genes all DG+CA3+CA1) more than 3 fold

	Mm	Hs
Stx3-sv1 (NM_011502)	0.0	0.0
C77673	6.5	-

Lsi1 or Lsi2 co-regulated genes in 2 regions) more than 3 fold

	Mm	Hs
Zfp398	4.6	4.9
Fps9	0.7	>15*
Kcnj9	0.7	>15*
Spon1	4.9	6.2
Sost	6.7	14.4
Etfud2	5.8	13.3

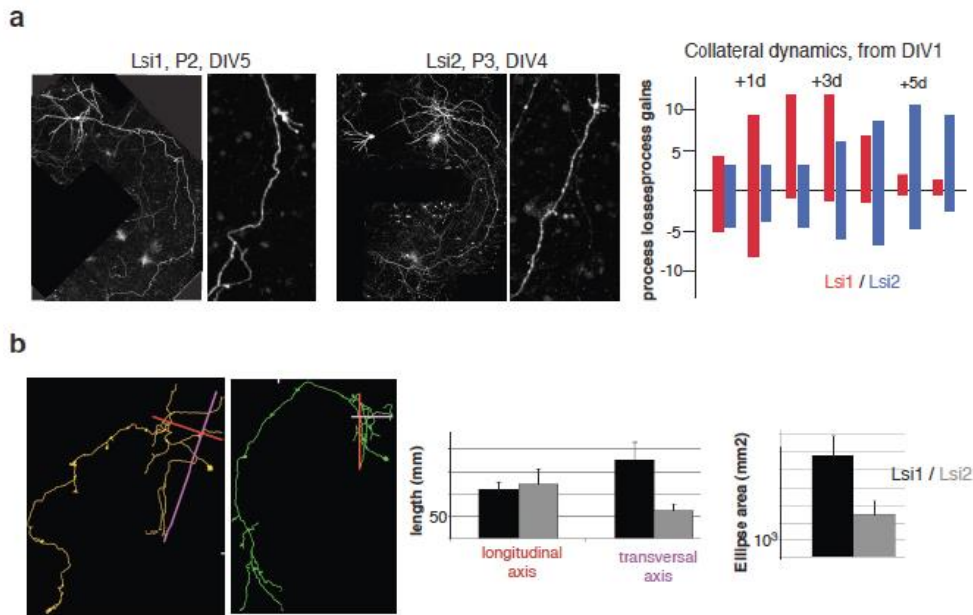
* There is an immunoglobulin gene less than 0.1 million bp.

Deguchi FigS7

Supplementary Fig. 7:

Subtype-specific genes and shared matched subpopulation genes have a high probability to map near olfactory receptor gene clusters.

The distance analysis was performed using *Mus musculus* (build 37.1) and *Homo sapiens* (build 36.3) genome data (NCBI). Subtype genes: comprehensive list of retinal neuron and DRG markers. Cell type markers: known general retinal and interneuron markers. Mm: mus musculus; Hs: homo sapiens; no olfactory receptor: there is no olfactory receptor gene on that chromosome.



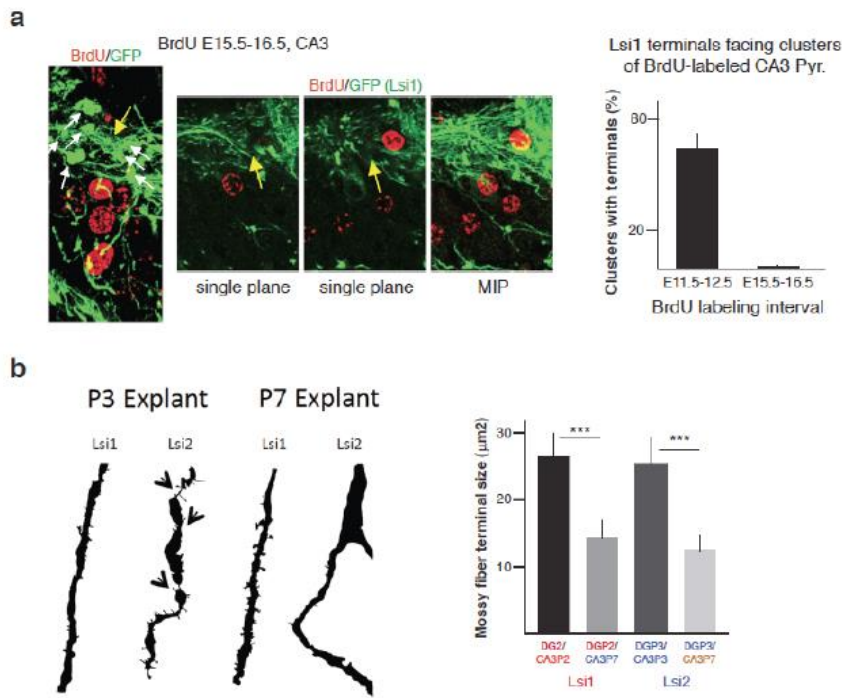
Deguchi Suppl. Fig. 8

Supplementary Fig. 8:

Distinct properties of Lsi1 and Lsi2 mossy fibers.

(a) Mossy fiber maturation *in vitro*. Panels: examples of comparable mossy fiber maturation stages in P2 + DIV5 Lsi1 and P3 + DIV4 Lsi2 slice cultures. The quantitative analysis is based on time lapse imaging of Lsi1-P2 and Lsi2-P3 cultures, from DIV1 on⁴⁸. Numbers of collaterals per mossy fiber that will have grown (process gains) or shrunk (process losses) one day later. Synaptogenesis coincides with a phase of increased collateral dynamics; it is maximal from days +1 to +3 in Lsi1 mossy fibers, and from days +3 to +6 in Lsi2 mossy fibers. Averages from 4 mossy fibers each.

(b) Distinct hilar collateral arborizations in Lsi1 and Lsi2 mossy fibers *in vivo*. Camera lucidas: illustration of longitudinal and transversal hilus collateral axes for a Lsi1 and a Lsi2 granule cells at 1 mo. Longitudinal axis: from cell body to beginning of CA3; transversal axis: longest extent of collateral extension perpendicular to longitudinal axis. Quantitative analysis: Lsi1 mossy fiber collaterals arborize through larger extent of hilus than their hilar counterparts. Ellipse areas were computed for individual mossy fibers, based on their longitudinal and transversal axes. N=20 each.



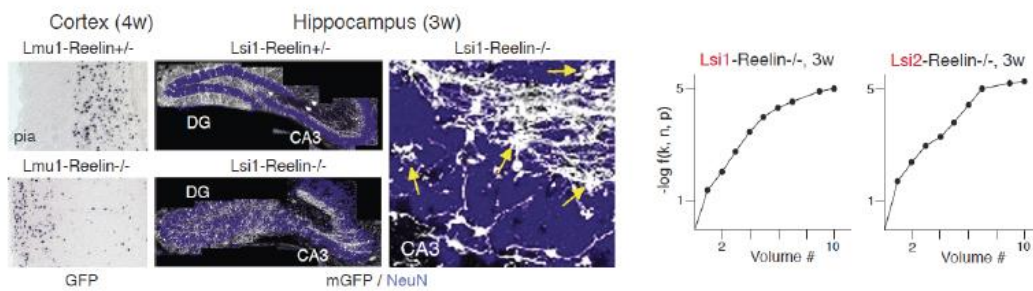
Deguchi Suppl. Fig. 9

Supplementary Fig. 9:

Influences of birth date and cell identity on stratum lucidum synaptogenesis.

(a) Lsi1 mossy fibers establish synapses facing clusters of early- but not late-born pyramidal neurons. Panels: examples from 1 mo Lsi1 mouse labeled with BrdU at E15.5-16.5 (late-born pyramidal neurons). Yellow arrows: Lsi1 mossy fiber stretch facing BrdU+ neurons, and devoid of mossy fiber terminals (white arrows). Quantitative analysis: 30 clusters each, from 3 mice.

(b) Influence of cell identity on stratum lucidum synaptogenesis. Left: Representative camera lucidas of CA3 dendrites at day in vitro 15 in dentate gyrus/CA3 co-cultures. Note comparable maturation gradients between Lsi1 and Lsi2 dendrites in vivo and in vitro. The arrows point to immature features of the Lsi2 dendrite in the P3 explant (abrupt transitions in dendritic diameter, and dendritic filopodia). Right: Sizes of mossy fiber terminals in heterochronic co-cultures. Note how terminals forming between Lsi1 (red) and Lsi2 (blue) subpopulations under conditions of matching maturation timing are smaller than those forming within Lsi1 or Lsi2 subpopulations. For synapses established by DGP3(Lsi2), postsynaptic partners in CA3P7 (orange) were not transgene-labeled, and contacts with CA3P7(Lsi1) dendrites were all non-synaptic. DG: dentate gyrus. N=30 terminals each, from 6 independent co-cultures. Mann Whitney test; ***: $p < 0.001$.

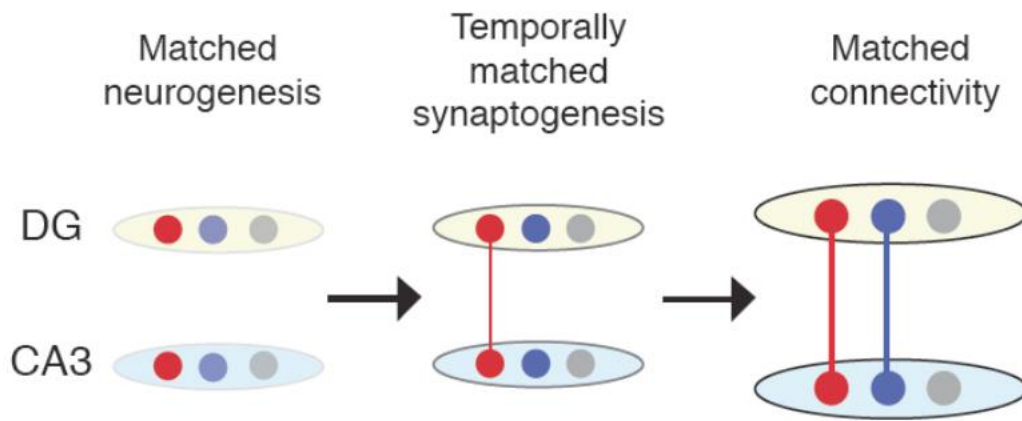


Deguchi Suppl. Fig. 10

Supplementary Fig. 10:

Selective connectivity between Lsi1 or Lsi2 subpopulations in the absence of Reelin.

Left: Disruption of cortical organization in *Reelin*^{-/-} mice: consistent with no alterations in cell identity, GFP⁺ Lmu1 neurons in layer 5 and 6 are displaced towards the pia in the absence of Reelin. Center: disruption of cell layering in the hippocampus, and clustering of Lsi1 mossy fiber terminals in CA3 (arrows) in the absence of Reelin. Right: selective stratum lucidum connectivity in Lsi⁻ and Lsi2-*Reelin*^{-/-} mice.

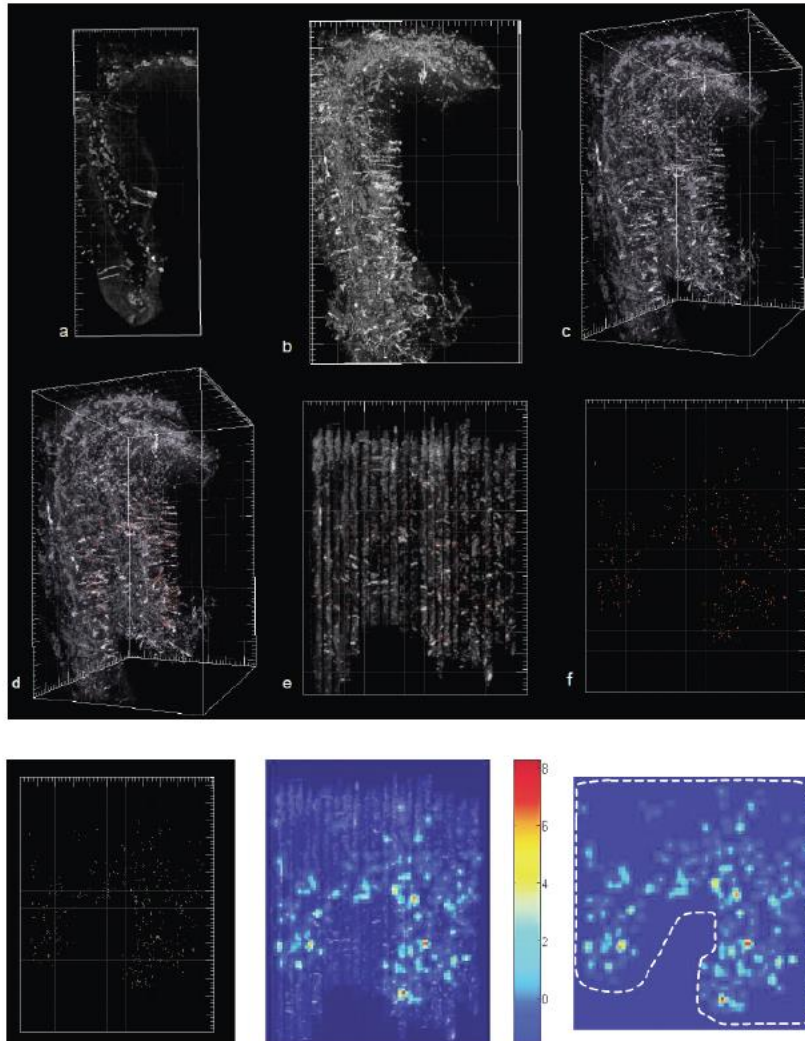


Deguchi et al., Suppl. Fig. 11

Supplementary Fig. 11:

Schematic of how matched schedules of synaptogenesis account for selective connectivity among principal neuron subpopulations.

Ovals: two major hippocampal subdivisions; circles: principal neuron subpopulations matched among the subdivisions; red and blue: HP(Su1) and HP(Su2).



Deguchi Suppl. Fig. 12

Supplementary Fig. 12:

Heat map procedure to analyze the distribution of transgene-positive cells in an E11.5 *Lsi1* embryo (Fig. 2b).

Upper panel: Workflow description for dataset acquisition. Confocal acquisition and 3D stitching (a; XuvTools); alignment at single plane level (b; Photoshop CS3); 3D reconstruction (c, Imaris); spot tracing (d); rotation and spot density analysis (Matlab).

Lower panels: Heat map generation based spot positioning procedure. A sliding window procedure (Matlab) based on local spot densities generates a heat map (center); background (revealing individual sections, center) is filtered, and HN outline is added (dotted line) to generate the final map on the right.

4.3.6 Material and methods

Mice and materials.

Thy1 reporter mice were as described¹⁰; Reelin^{-/-} mice were from Jackson Laboratories. All experiments were carried out in adherence to the guidelines of the veterinarian office of Kanton Basel Stadt. Antibodies: rabbit anti-GFP (Invitrogen), mouse anti-MASH1 (BD Pharmingen), mouse anti-Nestin and rabbit anti-Prox1 (Chemicon International), goat anti-NeuroD1 (Santa Cruz), rabbit anti-Tbr2/Eomes and rat anti-BrdU (Abcam). Rabies virus driving the expression of mCherry in postmitotic neurons was a gift from M. Tripodi and S. Arber (Friedrich Miescher Institut). Injections into CA3b of 5-month-old Lsi1 female mice were at bregma -2.18 (posterior), 2.7 (lateral), 1.75 (down). Mice were perfused 4 d after the injection, and mCherry was visualized with a specific antibody. The protocol for laser-dissection microscopy collection and microarray analysis of the few mGFP-labeled neurons was as described¹⁸. Average present call values were 40–48%.

In situ hybridization, immunocytochemistry and electron microscopy.

The double in situ hybridization protocol was as described⁴⁸; signals from DIG- or FITC-labeled probes were amplified and detected using TSA plus Cyanine 3 or TSA plus Cyanine 5 system (PerkinElmer). Immunocytochemistry was on PFA-fixed tissue (50- μ m floating sections); detection was with Alexa 488-, 568- and 647-conjugated antibodies (Molecular Probes). For analysis in the lamellar plane, hippocampi were dissected from perfused brains after overnight post-fixation, embedded in 3% agarose gel and sliced transversally with a tissue chopper (McIlwain, 100- μ m slices).

The detection of mGFP-positive axons and dendrites in Lsi1 mice by immuno-electron microscopy was as described⁴⁹. For the analysis, immunolabeled individual (Lsi1) CA3 pyramidal neuron dendrites in stratum lucidum were first identified and then scored for labeled and nonlabeled mossy fiber terminals in synaptic contact with their thorny excrescences. The prevalence of Lsi1-Lsi1 synapses was estimated on the basis of the frequency of labeled contacts, the fraction of mGFP-positive granule cells (light microscopy)

within the blocks used for electron microscopy, and the assumption that the total fraction of Lsi1 granule cells within that part of dorsal hippocampus was 21%.

The BrdU labeling method in vivo was carried out in 24-h intervals as described²⁴. We injected mice with BrdU at defined times during embryonic development or early postnatally and analyzed hippocampal sections from 1-month-old mice for BrdU labeling and mGFP signals. Only strongly BrdU-labeled cells that did not undergo further rounds of DNA replication and cell division subsequent to BrdU incorporation were included in the analysis. EdU detection was as described²² (Invitrogen Click-it EdU).

Heterochronic hippocampal co-cultures.

Hippocampi of appropriate ages were dissected and sliced as described⁵⁰. Sections (400 μm) were incubated in dissecting medium at 4 °C for 30 min. Dentate gyrus and CA3 were then dissected on an ice-cooled chamber and incubated for an additional 15 min at 4 °C. Dentate gyrus and CA3 from corresponding positions along the dorsoventral axis were recomposed on millipore filters and cultured for 15 d⁴⁸.

Data analysis.

For the analysis of Lsi1 and Lsi2 cells in transgenic embryos, consecutive sections of the whole archicortex primordium were acquired, and images belonging to the same coronal section were stitched in three dimensions using dedicated software. Stitched files (20 per embryo) were manually aligned and then imported into Imaris 6.3.1 for a complete three-dimensional reconstruction of the tissue. Neuroepithelium with prospective CA3 and CA1 cells was analyzed for every single cell (10- μm spot) included between the archicortex and neocortex (ventral border) or within the telencephalic vesicles between the two curves that separate the hippocampal neuroepithelium from the neocortical (dorsal) and amygdaloid (ventral) neuroepithelium (posterior). The three-dimensional dataset was then turned to project every spot onto the ventricular surface (projection plane). Spot densities were then determined, and values were normalized for mask numbers and color coded. This automatic process (Matlab) transformed discrete distributions into continuous ones (Supplementary Fig. 12).

Maturity scores were based on published immature and mature features³⁰, using three-dimensional Imaris software. Individual features were assigned a value between 0 (least mature) and 3 (most mature), and values were summed. Parameters for dendrites were: length, diameter, diameter change at branchpoint, swellings and spines; and for axons: swellings, collaterals, filopodia and volume of terminals. For spine densities, only protrusions shorter than 2 μm with an evident connection to the main shaft were included. Statistical differences were assessed by the Student's t-test.

To investigate transgene-positive mossy fiber-CA3 pyramidal neuron connectivities, we processed lamellar sections for immunocytochemistry (Bassoon and Pi-GluR1) and analyzed non-overlapping CA3 stratum lucidum volumes containing mGFP+ pyramidal neurons. Lengths were 100 μm (expect one terminal per 100–140 μm along CA3; ref. 12) and depths were 55 μm . The average number of pyramidal neurons within these volumes was 173 (dorsal third of hippocampus). For each mGFP+ pyramidal neuron within the volume we determined the number of putative synaptic contacts with mGFP+ mossy fibers. We then computed probability mass functions (binomial distributions) as follows: $\Pr(K = k) = f(k; n; p) = \frac{n!}{k!(n-k)!} p^k(1-p)^{n-k}$, where k is the number of connections found, n is (number of mGFP+ mossy fibers) \times (average number of mGFP+ pyramidal neurons) and P is the probability of each contact (1/173; independent and identically distributed).

We estimated the total number of synaptic contact sites in stratum lucidum using high-expressing Lsi1 mice in which 18–21% of the granule cells were mGFP+ (85–99% of total HP(Su1) granule cells). By combining average distances between mGFP+ terminals on pyramidal neurons in CA3 (8.18 μm) and the average lengths of pyramidal neuron dendrites in CA3 (184 μm) we reached average figures of 38 HP(Su1) terminals. Together with the non-HP(Su1) terminals, this yielded average totals of 41.2 terminals per pyramidal neuron, with 3.2 of them unmatched.

4.3.7 Bibliography

1. Brown, S.P. & Hestrin, S. Cell-type identity: a key to unlocking the function of neocortical circuits. *Curr. Opin. Neurobiol.* 19, 415–421 (2009).
2. Yoshimura, Y. & Callaway, E.M. Fine-scale specificity of cortical networks depends on inhibitory cell type and connectivity. *Nat. Neurosci.* 8, 1552–1559 (2005).
3. Song, S., Sjöström, P.J., Reigl, M., Nelson, S. & Chklovskii, D.B. Highly nonrandom features of synaptic connectivity in local cortical circuits. *PLoS Biol.* 3, e68 (2005).
4. Kampa, B.M., Letzkus, J.J. & Stuart, G.J. Cortical feed-forward networks for binding different streams of sensory information. *Nat. Neurosci.* 9, 1472–1473 (2006).
5. Brown, S.P. & Hestrin, S. Intracortical circuits of pyramidal neurons reflect their long-range axonal targets. *Nature* 457, 1133–1136 (2009).
6. Petreanu, L., Mao, T., Sternson, S.M. & Svoboda, K. The subcellular organization of neocortical excitatory connections. *Nature* 457, 1142–1145 (2009).
7. Yu, Y.C., Bultje, R.S., Wang, X. & Shi, S.H. Specific synapses develop preferentially among sister excitatory neurons in the neocortex. *Nature* 458, 501–504 (2009).
8. Caroni, P. Overexpression of growth-associated proteins in the neurons of adult transgenic mice. *J. Neurosci. Methods* 71, 3–9 (1997).
9. Feng, G. et al. Imaging neuronal subsets in transgenic mice expressing multiple spectral variants of GFP. *Neuron* 28, 41–51 (2000).
10. De Paola, V., Arber, S. & Caroni, P. AMPA receptors regulate dynamic equilibrium of presynaptic terminals in mature hippocampal networks. *Nat. Neurosci.* 6, 491–500 (2003).
11. Haverkamp, S. et al. The primordial, blue-cone color system of the mouse retina. *J. Neurosci.* 25, 5438–5445 (2005).
12. Amaral, D. & Lavenex, P. Hippocampal neuroanatomy. in *The Hippocampus Book* (eds. Andersen, P. et al.) 37–110 (Oxford Univ. Press, 2007).

13. Lein, E.S., Zhao, X. & Gage, F.H. Defining a molecular atlas of the hippocampus using DNA microarrays and high-throughput in situ hybridization. *J. Neurosci.* 24, 3879–3889 (2004).
14. Thompson, C.L. et al. Genomic anatomy of the hippocampus. *Neuron* 60, 1010–1021 (2008).
15. Kamme, F. et al. Single-cell microarray analysis in hippocampus CA1: demonstration and validation of cellular heterogeneity. *J. Neurosci.* 23, 3607–3615 (2003).
16. Gogolla, N., Galimberti, I., Deguchi, Y. & Caroni, P. Wnt signaling mediates experience-related regulation of synapse numbers and mossy fiber connectivities in the adult hippocampus. *Neuron* 62, 510–525 (2009).
17. Galimberti, I., Bednarek, E., Donato, F. & Caroni, P. EphA4 signaling in juveniles establishes topographic specificity of structural plasticity in the hippocampus. *Neuron* 65, 627–642 (2010).
18. Saxena, S., Cabuy, E. & Caroni, P. A role for motoneuron subtype-selective ER stress in disease manifestations of FALS mice. *Nat. Neurosci.* 12, 627–636 (2009).
19. Noctor, S.C., Flint, A.C., Weissman, T.A., Dammerman, R.S. & Kriegstein, A.R. Neurons derived from radial glia cells establish radial units in neocortex. *Nature* 409, 714–720 (2001).
20. Altman, J. & Bayer, S.A. Mosaic organization of the hippocampal neuroepithelium and the multiple germinal sources of dentate granule cells. *J. Comp. Neurol.* 301, 325–342 (1990).
21. Tole, S. & Grove, E.A. Detailed field pattern is intrinsic to the embryonic mouse hippocampus early in neurogenesis. *J. Neurosci.* 21, 1580–1589 (2001).
22. Chehrehasa, F., Meedeniya, A.C., Dwyer, P., Abrahamsen, G. & Mackay-Sim, A. EdU, a new thymidine analogue for labeling proliferating cells in the nervous system. *J. Neurosci. Methods* 177, 122–130 (2009).
23. Hodge, R.D. et al. Intermediate progenitors in adult hippocampal neurogenesis: Tbr2 expression and coordinate regulation of neuronal output. *J. Neurosci.* 28, 3707–3717 (2008).
24. Wojtowicz, J.M. & Kee, N. BrdU assay for neurogenesis in rodents. *Nat. Protoc.* 1, 1399–1405 (2006).

25. Li, G. et al. Hilar mossy cells share developmental influences with dentate granule neurons. *Dev. Neurosci.* 30, 255–261 (2008).
26. Altman, J. & Bayer, S.A. Migration and distribution of two populations of hippocampal granule cell precursors during the perinatal and postnatal periods. *J. Comp. Neurol.* 301, 365–381 (1990).
27. Godfrey, P.A., Malnic, B. & Buck, L.B. The mouse olfactory receptor gene family. *Proc. Natl. Acad. Sci. USA* 101, 2156–2161 (2004).
28. Dijk, F., Leeuwen, S.v. & Kamphuis, W. Differential effects of ischemia/reperfusion on amacrine cell subtype-specific transcript levels in the rat retina. *Brain Res.* 1026, 194–204 (2004).
29. Zylka, M.J., Rice, F.L. & Anderson, D.J. Topographically distinct epidermal nociceptive circuits revealed by axonal tracers targeted to *Mrgprd*. *Neuron* 45, 17–25 (2005).
30. Jones, S.P., Rahimi, O., O’Boyle, M.P., Diaz, D.L. & Claiborne, B.J. Maturation of granule cell dendrites after mossy fiber arrival in hippocampal field CA3. *Hippocampus* 13, 413–427 (2003).
31. Tremblay, M.E., Riad, M., Chierzi, S., Murai, K.K. & Pasquale, E. Developmental course of EphA4 cellular and subcellular localization in the postnatal rat hippocampus. *J. Comp. Neurol.* 512, 798–813 (2009).
32. Frotscher, M., Zhao, S. & Förster, E. Development of cell and fiber layers in the dentate gyrus. *Prog. Brain Res.* 163, 133–142 (2007).
33. Isshiki, T., Pearson, B., Holbrook, S. & Doe, C.Q. *Drosophila* neuroblasts sequentially express transcription factors which specify the temporal identity of their neuronal progeny. *Cell* 106, 511–521 (2001).
34. Noctor, S.C., Martínez-Cerdeño, V., Ivic, L. & Kriegstein, A.R. Cortical neurons arise in symmetric and asymmetric division zones and migrate through specific phases. *Nat. Neurosci.* 7, 136–144 (2004).
35. Baumgardt, M., Karlsson, D., Terriente, J., Diaz-Benjumea, F.J. & Thor, S. Neuronal subtype specification within a lineage by opposing temporal feed-forward loops. *Cell* 139, 969–982 (2009).
36. Petrovic, M. & Hummel, T. Temporal identity in axonal target layer recognition. *Nature* 456, 800–803 (2008).

37. Baek, M. & Mann, R.S. Lineage and birth date specify motor neuron targeting and dendritic architecture in adult *Drosophila*. *J. Neurosci.* 29, 6904–6916 (2009).
38. Elliott, J., Jolicoeur, C., Ramamurthy, V. & Cayouette, M. Ikaros confers early temporal competence to mouse retinal progenitor cell. *Neuron* 60, 26–39 (2008).
39. Gaspard, N. et al. An intrinsic mechanism of corticogenesis from embryonic stem cells. *Nature* 455, 351–357 (2008).
40. Miyoshi, G., Butt, S.J.B., Takebayashi, H. & Fishell, G. Physiologically distinct temporal cohorts of cortical interneurons arise from telencephalic Olig2-expressing precursors. *J. Neurosci.* 27, 7786–7798 (2007).
41. Gelman, D.M. & Marin, O. Generation of interneuron diversity in the mouse cerebral cortex. *Eur. J. Neurosci.* 31, 2136–2141 (2010).
42. Kamme, F. et al. Single-cell microarray analysis in hippocampus CA1: demonstration and validation of cellular heterogeneity. *J. Neurosci.* 23, 3607–3615 (2003).
43. Jefferis, G.S., Marin, E.C., Stocker, R.F. & Luo, L. Target neuron prespecification in the olfactory map of *Drosophila*. *Nature* 414, 204–208 (2001).
44. McLean, D.L. & Fetcho, J.R. Spinal interneurons differentiate sequentially from those driving the fastest swimming movements in larval zebrafish to those driving the slowest ones. *J. Neurosci.* 29, 13566–13577 (2009).
45. Espinosa, J.S. & Luo, L. Timing neurogenesis and differentiation: insights from quantitative clonal analyses of cerebellar granule cells. *J. Neurosci.* 28, 2301–2312 (2008).
46. Toni, N. et al. Neurons born in the adult dentate gyrus form functional synapses with target cells. *Nat. Neurosci.* 11, 901–907 (2008).
47. Colgin, L.L., Moser, E.I. & Moser, M.B. Understanding memory through hippocampal remapping. *Trends Neurosci.* 31, 469–477 (2008).
48. Pinaud, R. et al. Detection of two mRNA species at single-cell resolution by double-fluorescence in situ hybridization. *Nat. Protoc.* 3, 1370–1379 (2008).
49. Knott, G.W., Holtmaat, A., Trachtenberg, J.T., Svoboda, K. & Welker, E. A protocol for preparing GFP-labeled neurons previously imaged in vivo and in slice preparations for light and electron microscopic analysis. *Nat. Protoc.* 4, 1145–1156 (2009).

50. Gogolla, N., Galimberti, I., DePaola, V. & Caroni, P. Preparation of organotypic slice cultures for long term live imaging. *Nat. Protoc.* 1, 1223–1226 (2006).

4.4

A critical period for cognitive enhancement during hippocampal development

Flavio Donato and Pico Caroni

Unpublished work

4.4.1 Summary

Synaptic processing reflects the interplay between cortical excitation and cortical inhibition, and the importance of this balance is evident in those conditions when genetic mutations or an excessive or misplaced response to experience produce a long-lasting alteration that leads to pathologies. Moreover, this is also testified by the great deal of regulation impinging on the development of inhibitory microcircuits, which during development constitute the first source and target of synapses upon excitatory cells due to the transitory excitatory action of GABA.

In particular, the integration of microcircuits involving parvalbumin+ interneurons (PV+) seem to have a key role in regulating the occurrence of those periods of enhanced plasticity during development that are known as “critical periods”. PV maturation has long been studied in sensory areas, where it is clear that it requires sensory experience from the sensory organs that functions as a driving force for the process.

Here, we investigate how FFI microcircuits mature in the hippocampal area CA3, and which might be the driving force for PV maturation in a structure that lies further away from sensory experience. Hence, we provide evidence that release from mossy fiber terminals drive PV maturation in CA3, defining windows during development in which interneurons acquire defined properties that will characterize the network in the adult. Moreover, by pharmacological manipulations during these windows, we are able to produce long-lasting network alterations that underlie a permanent cognitive enhancement or disruption in treated mice.

4.4.2 Introduction

In cortical microcircuit, FFI microcircuits relaying PV interneurons to pyramidal cells are the last ones to integrate in the cortical architecture. Their maturation relies on sensory experience coming from sensory organs, which drive the maturation of PV interneurons via direct excitatory activity, release of growth factors (BDNF), formation of perineuronal nets (PNNs), and release of transcription factors (OTX2). These factors drive an extensive period of synaptogenesis onto and from PV IN, for which, in an area-specific time schedule, new excitatory and inhibitory synapses are formed onto these interneurons that likewise increase the extent of principal neurons innervation via basket formation on pyramidal cells. In different sensory cortices, the maturation of PV interneurons has been implicated in the opening and closure of windows of enhanced plasticity that are collectively known as “critical periods”.

At the level of single parvalbumin interneurons, maturation produces changes in structural (expression of increasing amounts of the protein parvalbumin, increasing size of dendritic and axonic arborizations, formation of perineuronal nets), as well as functional (frequency of firing increases as maturation progresses) features, thereby defining the properties that characterize the network in the adult. Strikingly, the properties on which maturation impinge during development are the same on which experience impinge in adult microcircuits to regulate structural plasticity and learning. Indeed, we demonstrated that learning can act on the PV network to modulate properties like PV expression, GAD-67 content, and firing frequency in a way that is strictly dependent on the balance between excitation and inhibition upon these neurons: experience define a “plastic state” based on the prevalence of disinhibition and Low PV interneurons during learning, as opposed to a “crystallized state” based on the prevalence of FFI and High PV interneurons upon learning completion. Moreover, interventions in the adult that are supposed to reopen plasticity to “critical periods” levels impinge on perineuronal nets around these interneurons. Nevertheless, the extent to which a proper developmental maturation of PV Interneurons could define their intrinsic properties and connectivity in the adult, and set the baseline level for the network state is still and open question.

In previous works, we showed how the maturation of cortical microcircuits can be divided in temporally defined windows which highlight the development of subpopulations of principal neurons (See previous part of the thesis). Nevertheless, if a sequential maturation highlights

intrinsic differences among subpopulations in the contribution that each one gives to the microcircuit development or is influenced by it, is not yet known.

Here, we investigate the maturation of feed forward inhibitory microcircuitry based on parvalbumin expressing interneurons in CA3, due to the defined microcircuit governing state transitions in the adult; the accessibility of the microcircuit for manipulation in slice culture;, and the defined role that CA3 microcircuit exploits during learning.

4.4.3 Results

Dynamics of FFI microcircuit maturation in hippocampal CA3

We studied the maturation of PV interneurons by following the expression of Parvalbumin along CA3 during postnatal development. In CA3, PV expression started with low intensity and a clear nuclear localization pattern around P7 (Fig 1A, P7); it acquired dendritic and synaptic localization along further development, with a marked spatial gradient showing higher density of expression in CA3a at earlier time points, followed by CA3b and c later on. Each subdivision was characterized by a continuous increase in PV positive interneurons during the whole process (Time course of PV development: average number of neurons per 300um² of CA3 area P7: 1.25; P10: 4.25; P12: 9.75; P14: 14; P16: 21. $P < 0.05$, One way ANOVA. Fig 1A).

To test whether excitatory activity would drive PV maturation in a manner that is closely comparable to other cortical areas, we repeatedly (one injection per day over three consecutive days, P8-P10) injected mice with diazepam (GABA_A agonist, 3 mg x Kg) to decrease excitatory activity in the developing brain. This treatment produced a decrease in the extent of parvalbumin expression both at the level of the soma intensity (Supplementary figure 1B), and in the extent of dendritic and synaptic site along the whole length of CA3, thereby suggesting a profound role of excitatory activity in driving PV maturation in the hippocampus.

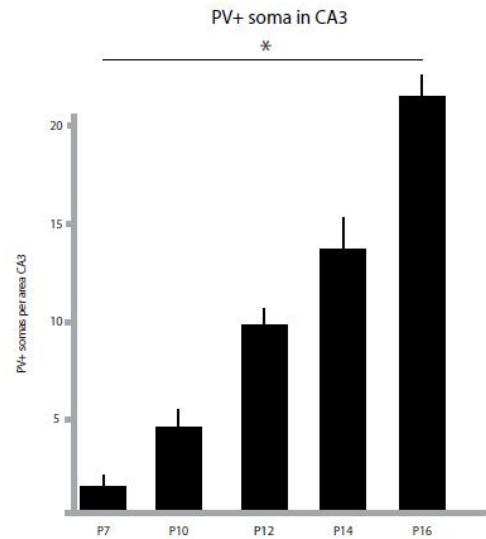
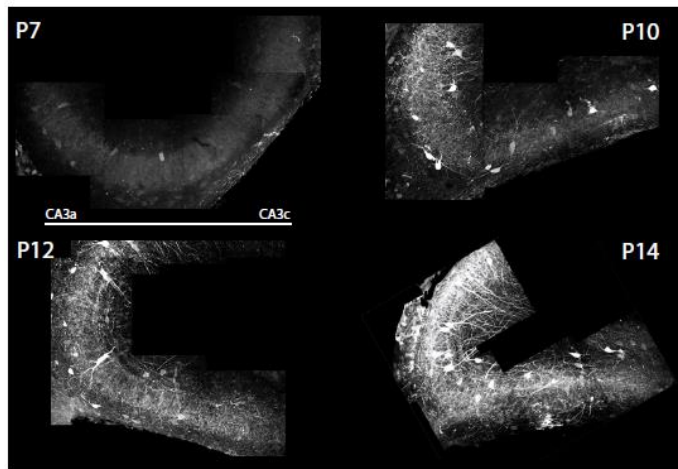
Figure 1: Maturation of the FFI microcircuit in Hippocampus CA3

Maturation of PV interneurons in the CA3 area of the hippocampus was characterized by maturation in the pattern of staining for PV (first somatic, then also dendritic and synaptic) (**A**, left), and the increase in the number of PV positive neurons with age (**A**, right).

Analysis of presynaptic inputs to PV IN focused on the number of filopodial synapses from MFT (**B**, left), in their quantitative (**B**, right) and spatial (**B**, centre) profile of formation.

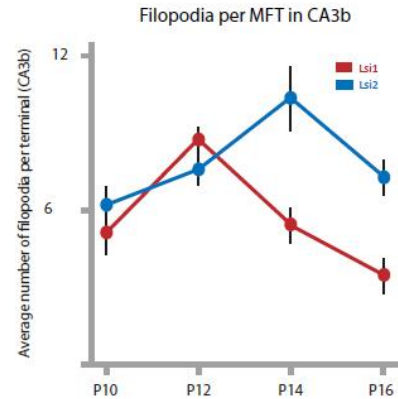
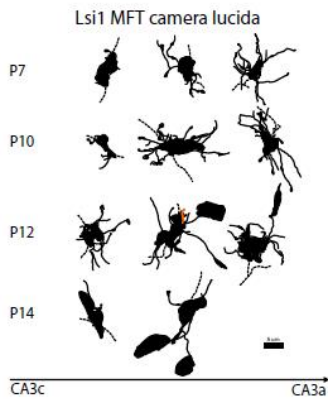
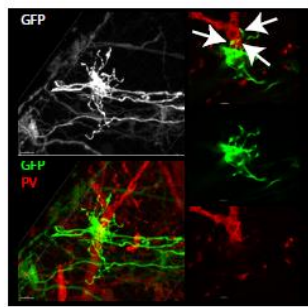
Analysis of perisomatic innervation upon CA3 pyramidal cells from PV (**C**, upper and centre) and CCK (**C**, lower and right) reveal a subpopulation-specific profile of development of PV+ synapses on Lsi1 and LSi2 pyramidal cells.

A Maturation of PV IN network in hippocampus CA3
 Overview PV immunoreactivity in CA3

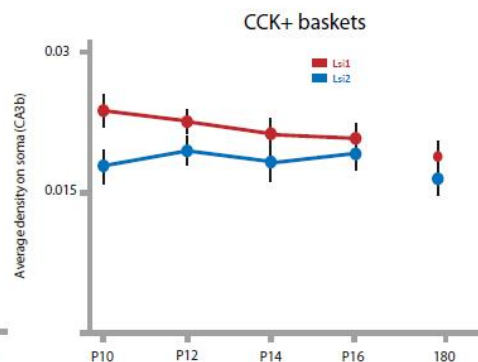
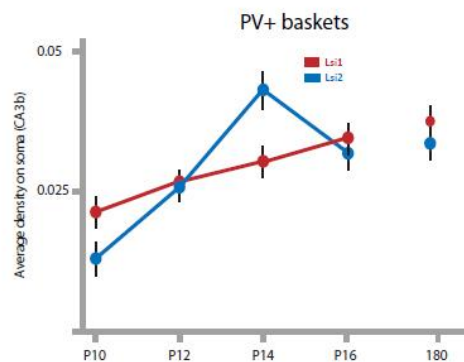
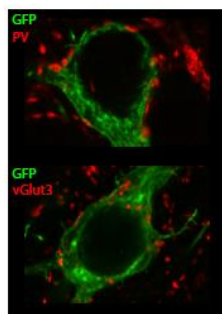


B Maturation of FFI synapses from MFTs in CA3

Filopodia contacts on PV interneurons



C Maturation of perisomatic inhibition around CA3 PC soma



We next sought to determine which input might provide the source of excitatory activity required for PV IN maturation. In sensory areas, sensory experience is the main driver of FFI maturation; the hippocampus however lies further away from direct sensory experience, and moreover PV maturation starts in a developmental window in which activity in the CA3

microcircuit seem to be autonomously generated (Crepel et al., 2007). Therefore, we studied the role of intrahippocampal connectivity in driving the maturation of PV interneurons. The CA3 microcircuit connects mossy fiber terminals (LMTs) from Granule cells to CA3 pyramidal cells via core and satellites LMT (feed forward excitation, FFE), and to Parvalbumin-expressing interneurons via filopodia (feed forward inhibition, FFI); moreover, CA3 pyramidal cells establish recurrent connectivity via ramification of the Schaffer collateral either onto pyramidal cells and PV expressing interneurons. Altogether, mossy fiber terminals and CA3 pyramidal cells constitute the main excitatory inputs on CA3 parvalbumin interneurons. Nevertheless, filopodia from mossy fiber terminals are sufficient to promote transition to the High PV state in the network upon learning completion (Donato and Caroni, in preparation). Therefore, we analyzed how connectivity from MFTs developed by analyzing the formation, characteristic and connectivity of LMTs filopodia.

First, we confirmed that, also in this stage, filopodia form functional contacts to PV Interneurons (Fig 1B, white arrows). Since establishment of FFE proceeds according to consecutive and non-overlapping window of synaptogenesis and maturation, for which Lsi1 granule cells restricts formation of mossy fiber terminals on Lsi1 CA3 Pyramidal cells between P5 and P7, while Lsi2 recapitulates the same event slightly later in time (P7 to P10), we decided to study independently the formation of filopodia in Lsi1 and Lsi2 MFTs. Thus, we observed an increase of the average number of filopodia per terminal in both Lsi1 and Lsi2 (Fig 1B), with a transitory peak phase and a rapid decline toward the levels that characterize each subpopulation in the adult. Moreover, the temporal order of synaptogenesis that sees Lsi1 maturing before Lsi2 was maintained in this process, with peak in the average filopodia per LMT content that were again few days apart (Fig 1B). Surprisingly, filopodia sprouting did not proceed homogeneously along the length of the mossy fiber, but followed a gradient of maturation for which CA3a was the first to mature, followed by CA3b and c at later time points (Fig 1B, camera lucidas).

Maturation of presynaptic connectivity onto parvalbumin expressing interneurons is accompanied by the formation of perisomatic basket of PV+ synapses around pyramidal cells. Since presynaptic connectivity matures in a subpopulation-specific manner, we studied if perisomatic inhibition would mature according to separate schedule on Lsi1 and Lsi2 CA3 PC. Therefore, to study the timecourse of basket formation in CA3, we quantified the number of PV+ puncta around the soma of Lsi1 or Lsi2 pyramidal cells. Surprisingly, the two subpopulations exhibited different profiles of basket formation. Lsi1 was characterized by a linear increase in puncta density during development to reach the adult levels by P16, with no apparent gradient in maturation between CA3a, b or c (Fig 1C, red line). In stark contrast, Lsi2 basket formation showed a bell shaped curve in puncta density exhibiting a defined peak during development, which then decreased to reach the level in mature circuits (Fig

1C, blu line). Moreover, basket development around Lsi2 CA3 showed a marked topographic maturation ranging from CA3a to c over the course of maturation (data not shown).

To test if this specific difference in baskets formation was a general feature of the overall maturation of inhibition on these two subpopulation, or if it had to be attributed specifically to the maturation of the PV IN network, we analyzed the development of the other component of the perisomatic inhibition, which is represented by CCK basket cells. These neurons are non-fast spiking, have a different developmental origin than PV expressing INs, and their maturation proceeds with a different time course respect the other class of basket cells. Therefore, we quantified the formation of CCK baskets around CA3 pyramidal cells by analyzing the density of vGlut3 (marker for CCK synapses, Fig 1C) puncta around PC somas. To our surprise, vGlut3 puncta density didn't exhibit any peak in density during development and proceed in the same way between Lsi1 and 2, indicating that subpopulations-based differences in the maturation of perisomatic inhibition are specific for the PV expressing component (Fig 1C).

Filopodia sprouting from MFTs drives PV maturation during development

Therefore, filopodia sprouting from mossy fiber terminals and parvalbumin IN maturation proceed with a similar spatio-temporal pattern in CA3, and anticipate perisomatic inhibitory synaptogenesis upon CA3 PC. Moreover, the Lsi1 filopodia peak seemed to anticipate the increase in parvalbumin, with a similar mechanism observed during learning upon transition toward the Chrystallized state (see part one of results). We therefore sought to determine if filopodia sprouting might be the driving force underlying PV maturation during development. To determine whether filopodia sprouting and release could be responsible for Parvalbumin interneuron maturation, we studied early MFT maturation in hippocampal slice cultures, a model system that is more accessible for manipulation of activity. First, we confirmed that filopodia sprouting and PV maturation *in vitro* would resemble the counterpart *in vivo*: both spatiotemporal sprouting from MFT, PV IN maturation, and its dependence on activity were preserved in slices (Supplementary figure 1A and B). Then, we investigated whether the presence of PV IN would be necessary for filopodia sprouting by analyzing slice cultures produced at P2: at this age, PV IN have not yet terminated their migration toward CA3 from their source in the medial ganglionic eminence (Supplementary figure 1C and D); thereby hippocampal slices result depleted of PV IN during and after maturation. Here, we found that even in the absence of PV IN, sprouting of filopodia would proceed with the same temporal progression as *in vivo* or in P7 slices, suggesting that filopodia formation during development is a cell autonomous process in which PV interneurons are dispensable. Deprived of their

natural counterpart, filopodia in P2 slices engage synaptic contacts with CA3 pyramidal cells, thereby increasing the number of satellite (Supplementary figure 1C, grey arrows) and shifting the microcircuit toward prevalence of FFE.

At last, to assess a critical role on the dependence of PV maturation of MFTs filopodia, we conducted an experiment in which we took advantage of the temporal difference between maturation of P2 and P7 slices. In P7 slice, PV maturation starts upon filopodia sprouting on Div6; on the other hand, filopodia sprouting is a cell autonomous process that in P2 slice starts around Div10 and does not require presence or maturation of PV IN to occur. Therefore, we produced heterochronic slice cultures in which the Dentate Gyrus of a P2 pup was co-cultured with the CA3 of an older, P7 animal. These cultures are viable and present no gross differences with control slices in the correct maturation of mossy fibers, formation of MFT and maturation of PV IN (Deguchi*, Donato*, Galimberti*, Cabuy and Caroni, 2011 and figure 2A). We reasoned that, if the MFT would be driving interneurons maturation, then PV expression profile should follow the DG P2 timeline of filopodia sprouting; on the contrary, if it were independent from filopodia sprouting, it should be insensitive to the mismatch in maturation of the two regions, and follow the P7 timeline. As a result of co-culturing, PV interneurons in the P7 CA3 showed a marked delay in maturation when compared to time-matched cultures (Fig 2A), favoring a driving role for filopodia sprouting in driving the process.

To further test the effect of MFT activity on PV maturation, we pharmacologically enhanced or reduced synaptic release from mossy fiber terminal and studied the effect on PV expression. Therefore, we treated slices with mGluR2 agonist (DCG-IV, 1 μ m, Tocris, Ewell LA and Jones MV., 2010) or antagonist (LY341495, 0.1 μ m, Rocris, Ewell LA and Jones MV., 2010), due to the known role of mGluR2 in regulating MFT transmission. Hence, DCG-IV treated slices showed a decrease in PV expression in CA3, while LY 341495 treated slices showed a marked increase of immunoreactivity to PV antibody (Fig 2B). Thus, we conclude that modulation of MFT release during development is sufficient to regulate PV IN maturation in CA3.

A PV IN maturation in CA3 upon temporal mismatch between DG and CA3

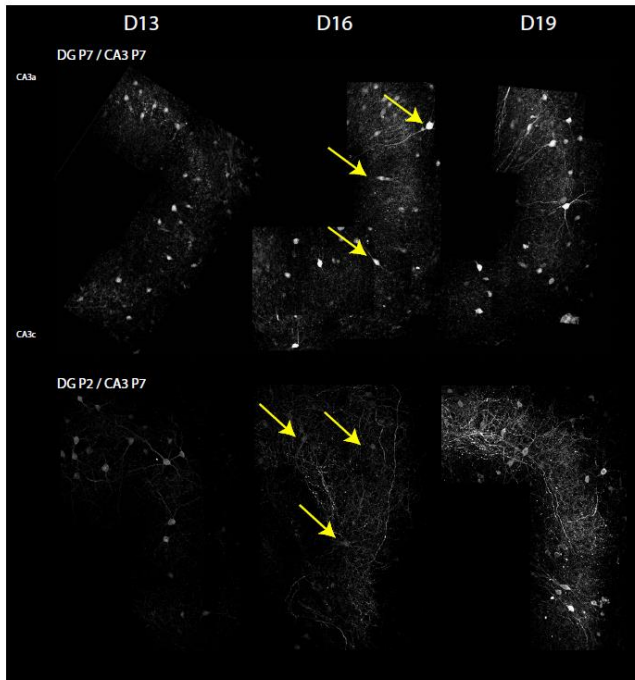
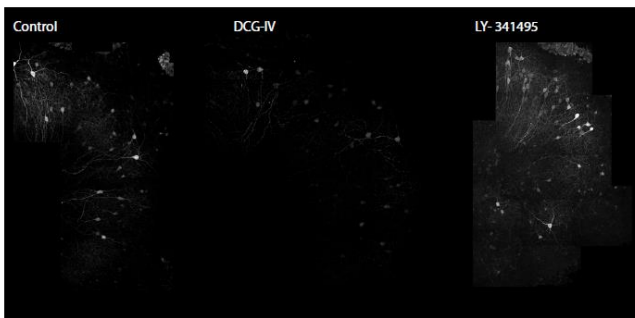


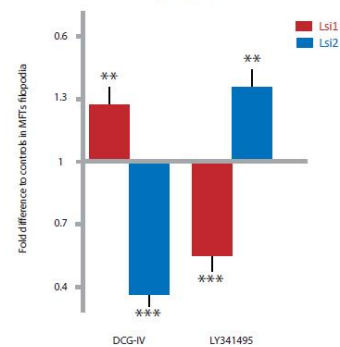
Figure 2: MFTs release drive PV maturation *in vitro*

Eterochronic experiments reveal that PV maturation follows the temporal profile of MFT filopodia sprouting (A). Moreover, pharmacological manipulation of MFT release is sufficient to regulate the extent of PV network maturation in CA3 (B). Subpopulation-specific response to pharmacological manipulations can be observed between Lsi1 and Lsi2 MFTs (C)

B PV IN network upon modulation of MFTs release



C Subpopulation-specific response to MFT release modulation during development *in vitro*



Differential contributions from MFT subpopulations to PV maturation in CA3

The previous experiments indicate the mossy fiber terminal as a driver synapse for PV IN maturation in CA3. The mechanism by which this would be achieved relies on a phase of filopodia sprouting that is reduced in later phases of development. Importantly, Lsi2 peak in filopodia is delayed respect that of Lsi1 of 2-4 days, consistent with delayed neurogenesis and synaptogenesis of this population. Moreover, maturation of PV IN is not a continuous process in which all interneurons proceed through the same process at once, but rather that subgroups of interneurons might insert in the microcircuit at different times (Fig1). These evidence might imply that the contribution of the two subpopulations to PV IN network maturation might be distinct. Therefore, to test whether MFTs from different subpopulations would react in the same way upon pharmacology during development, we quantified how Lsi1 and Lsi2 responded to modulation of MFT release upon DCG-IV and LY *in vitro*.

Surprisingly, subpopulations responded to the modulation of MFT release in opposite ways: Lsi1 increased the average number of filopodia per terminal upon DCG-IV (1.28 fold to controls, $p < 0.01$. Fig 2C), while concomitantly decreasing the average number of filopodia upon LY (0.56 fold to controls, $p < 0.001$. Fig 2C) ; in stark contrast, DCG-IV treatment decreased the number filopodia in Lsi2 MFTs (0.4 fold to controls, $p < 0.001$. Fig 2C), while LY increase this number (1.31 fold to controls, $p < 0.01$. Fig 2C). These data suggest that principal neurons subpopulation have a different potential in interacting with PV interneurons during development: Lsi1 would act as a pure driver onto PV maturation by counterbalancing external manipulations, while Lsi2 would respond homeostatically to modulation of MFT release to restore the proper balance of excitation and inhibition in the microcircuit.

Three lines of evidences (delayed profile of filopodia sprouting, different profile of perisomatic PV innervation on CA3, differential response to modulation of MFTs release *in vitro*) suggest that during development Lsi1 and Lsi2 neurons might contribute differently to microcircuits maturation. Therefore, we next sought to determine if interfering with the network at different time during maturation (possibly in an Lsi1 or Lsi2 time window) would affect PV interneurons to the same extent. To this end, we defined different time windows based on the time course of filopodia sprouting from MFT subpopulations, as a measure of recruitment of subsets of PV interneurons into the CA3 microcircuit.

Previous reports highlighted a period of enhanced plasticity during granule cells development which is correlated to the high expression of the NMDA receptor subunit NR2B (Ge, S et al., 2008). This particular subunit display a characteristic profile of expression for which its amount starts to be downregulated during maturation in favor of the expression of NR2A, which characterize mature cells NMDA complexes. Although its expression is present in all the classes of excitatory cells in the hippocampus, it is downregulated according to specific timelines: CA3 and CA1 downregulate NR2B immediately after birth, while Granule cells continue to express it during the first postnatal weeks. Hence, we hypothesized that NR2B antagonists would be a likely candidate to modulate selectively activity during sensitive periods during development, with a possible preferential effect on granule cells; moreover, since the profile of Lsi1 and Lsi2 subpopulations development proceed with a temporal delay, there could be time window in which treatment with NR2B antagonist should be able to influence Lsi1 or Lsi2 selectively. Therefore, we treated mice with ifenprodil (20 mg x Kg of weight), a potent and selective NR2B agonist, in two different time windows during development *in vivo* that would cover the extent of pronounced parvalbumin maturation in CA3. The time windows coincided with the ascending phase of the peak of filopodia for each subpopulation, and extend from P8 to P10 (Lsi1 ascending phase) and from P11 to P13 (Lsi2 ascending phase). Treatment with ifenprodil in both time window

produced an overall decrease in the expression of parvalbumin, but the extent of the effect on the PV network was different for each window: Ifenprodil treatment early during development (P8-P10) produced a decrease in PV expression in over 80 % of the interneurons (Fig 3A, $p < 0.0001$ one way ANOVA), while ifenprodil treatment late during development (P11-P13) produced a decrease in PV expression in about 50% of the interneurons, while 20% of them (Fig 3A, black arrow) increased PV levels ($p < 0.0001$ one way ANOVA) to values which were far exceeding the maximal expression levels observed in time-matched controls (but typical of adult “High PV” cells, see section 1 of results). Therefore, modulation of NR2B dependent NMDA transmission modulate the extent of PV Interneuron integration into CA3 microcircuit, in a partially opposite way depending on the time window of the treatment.

Next, we sought to determine if the opposite profile of modulation observed upon ifenprodil treatment during early and late windows of development could be ascribed to differences in excitatory cells recruitment. Indeed, treatment during the early window produced an effect in MFT filopodia number only in Lsi1 but not Lsi2 (1.47 fold to controls in Lsi1, $p < 0.001$, Fig 3B), while treatment in the late window elicited a response only in Lsi2 MFTs, but not Lsi1 (0.65 fold to controls, $p < 0.001$ Fig 3B). Taken together, these results confirm that modulation of excitatory activity by ifenprodil has a preferential effect on granule cells, slows down the maturation of the Parvalbumin interneuron network, and identify time windows for specific modulation of Lsi1 or Lsi2 subpopulations.

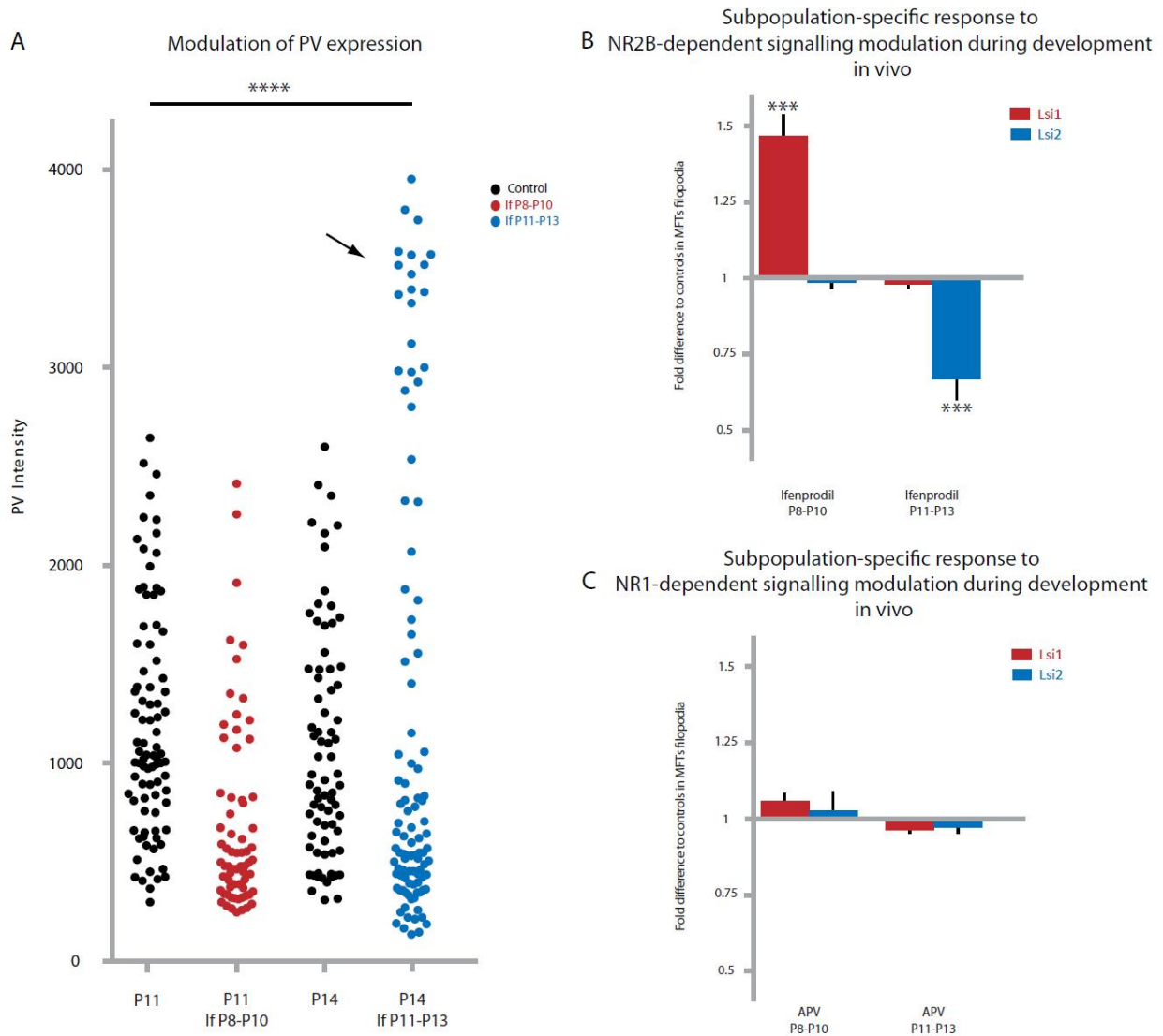


Figure 3: pharmacological modulation of PV maturation *in vivo*

NR2B signaling modulation via Ifenprodil treatment *in vivo* produce different effects on PV network maturation depending on the time of injection. Early treatment (P8-P10), targeting selectively Lsi1 terminals (**B**), decrease PV expression in the large majority of interneurons (**A**), while late treatment (P11-P13), targeting selectively Lsi2 MFTs (**B**), produce an increase of PV expression in about 20% of the neurons to levels comparable to adult High PV (**A**, arrows). No effects on MFT could be observed upon NR1 manipulation (**C**).

To verify whether the specific antagonism of NR2B would be responsible of the modulation of filopodia number at MFT observed upon ifenprodil treatment, or it would be rather an unspecific effect of activity modulation in hippocampal microcircuit activity, we treated mice with a NR1 antagonist in Lsi1 and Lsi2 specific windows. NR1 is the other main subunit of the NMDA receptor during development and in the adult, and is not associated to any

developmental regulation in the hippocampus. Treatments in both time windows did not affect significantly the average number of filopodia per terminal of either Lsi1 or Lsi2 (Fig 3C). We therefore concluded that specific modulation of NR2B-mediated activity is responsible for the alterations in MFT morphology and PV IN maturation during development.

Taken together, these results suggest that mossy fibers terminals from principal neurons subpopulations during development participate differently in driving the maturation of the parvalbumin network in vivo. Both subpopulations would explore an intrinsic sprouting and consequent reduction of FFI synapses from their mossy fiber terminals, but with different dynamics based on Parvalbumin interneurons: Lsi1 would exploit a proper driver function with a counter-homeostatic modulation of filopodia number from MFTs in relation to PV maturation; in stark contrast, Lsi2 would adjust its filopodia number in closer correlation to interneuron development to maintain a proper balance between excitatory and inhibitory microcircuits.

Developmental interference modulates the balance between subpopulations in the adult and shifts baseline conditions toward Plastic or Crystallized state.

Modulation of excitatory or inhibitory transmission during the maturation of parvalbumin expressing interneurons has been linked to long-lasting deficits that extend well into adulthood. (Belforte, JE et al., 2010). We then sought to determine if any long-lasting consequence might arise from the targeted modulation of the driving force inducing FFI integration into CA3 microcircuits. Therefore, we analyze the baseline state of the network of parvalbumin interneurons in adult mice that were previously treated with ifenprodil during development. Hence, early treatment (If P8-P10) produced a shift in the neuron distribution toward enhancement of Low PV (25% over total PV+ interneurons, $p < 0.001$ to controls Fig 4A, left panel), while late treatment (If P11-P13) modulated the network in the opposite direction toward enhancement of High PV (46% over total PV+ interneurons, $p < 0.001$ to controls Fig 4A, right panel). Strikingly, Ifenprodil-induced states were reminiscent of network configuration archived as a result of experience in the adult (Donato et al, in preparation, Fig 4A), which are sufficient to modulate structural plasticity and further learning. Therefore, we sought to study if developmental interventions impinging on NR2B signalling could produce shifts in the baseline configuration of the CA3 network toward the Plastic or Crystallized states.

To this extent, we analyzed the baseline structural properties of Lsi1 and Lsi2 mossy fiber terminals in adult mice treated with ifenprodil during development. NR2B antagonism in an

Lsi1 specific window produced a net increase in the number of satellites as compared to control condition, without any change in the average number of filopodia (2.75 fold to controls, $p < 0.001$, Fig 4C Left panel). No change could on the contrary be observed in Lsi2 MFTs, consistent with the specificity of the treatment for Lsi1 granule cells (Fig 4C, left panel). In stark contrast, NR2B antagonism in the Lsi2 specific window produced a decrease in the number of satellites in Lsi2 mossy fiber terminals (0.45 fold to controls, $p < 0.01$ Fig 4C, right panel), with unaltered number of filopodia. Moreover, no change could be observed in Lsi1 MFTs, consistent with the specificity of the treatment for Lsi2 granule cells (Fig 4C, right panel). Therefore, ifenprodil treatments during specific developmental time window alter the baseline configurations of subpopulation specific microcircuits with the enhancement of the FFE (Lsi1 upon early treatment) or FFI (Lsi2 upon late treatment) component.

Moreover, Lsi1 MFTs showed enhance active zone turnover on baseline condition as a consequent of early ifenprodil treatment, a feature physiologically associated with the “Plastic State” (6 and 24h: $p < 0.001$ difference to controls Fig 4B); in stark contrast, late ifenprodil treatment reduced active zone turnover from Lsi2 mossy fiber terminal, a feature that is associated with “Crystallized state” upon learning (24h: $p < 0.001$ difference to controls Fig 4B).

Moreover, we analyzed how the CA3 pyramidal cell network would be affected by developmental manipulations. Mice treated early in development exhibited a higher fraction of pyramidal cells expressing cFOS at baseline when compared to controls ($p < 0.001$, Fig 4D), consistent with an enhanced disinhibition due to Low PV state during enrichment (Donato and Caroni, in preparation); in contrast, mice treated late during development exhibited a lower fraction of pyramidal cells expressing cFOS at baseline ($p < 0.05$, Fig 4D), consistent with increase FFI.

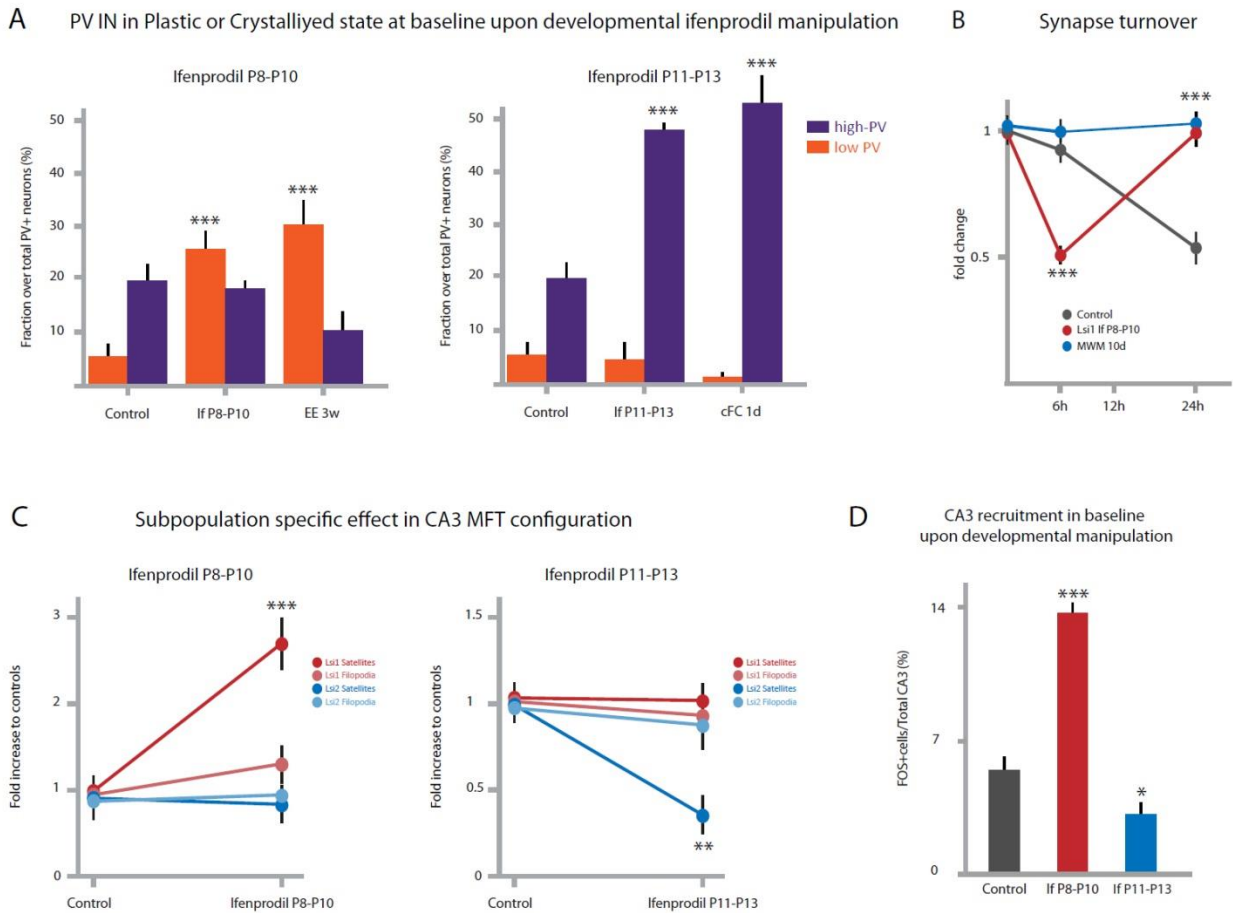


Figure 4: permanent modification of baseline CA3 network configuration upon developmental NR2B interference

The effects of the treatment with ifenprodil during development extend further into adulthood. This produces a shift in the baseline configuration of the CA3 network for which early treated mice present enhanced Low PV (A), structural plasticity (B), satellite contents (C) and cFOS + cells among CA3 pyramidal neurons (D); in stark contrast, mice treated later during development present enhanced High PV (A), and reduced structural plasticity (B), satellite contents (C), and cFOS+ cells among CA3 pyramidal neurons (D)

Taken together, these results indicate that ifenprodil treatment in the Lsi1 specific time window produced an increase in the speed of active zone turnover, a shift in the network of PV expressing interneurons toward Low PV, and structural alterations in the MFT of Lsi1 granule cells enhancing FFE upon FFI: all these features have been previously associated to the changes induced by 3 weeks of environmental enrichment in the CA3 microcircuit, characterizing a new state of enhanced structural plasticity and learning in the network (“Plastic state”). In stark contrast, ifenprodil treatment in the Lsi2 specific time window produced a decrease in the speed of active zone turnover, a shift in the network of PV expressing interneurons toward High PV, and structural alteration in the MFT of Lsi2 granule cells enhancing FFI upon FFE: all these features have been previously associated to the

changes induced by learning completion in the CA3 microcircuit, characterizing a new state of reduced structural plasticity and learning in the network (“Crystallized state”).

A critical period for cognitive enhancement during hippocampal development.

In previous work, we provided evidence that the CA3 network state is associated with enhanced or reduced performances in a further learning paradigm. Therefore, we tested if ifenprodil treatment during development, which is sufficient to confer features associated to the plastic or crystallized state to the CA3 microcircuit at baseline, is sufficient to modulate learning performances in adult mice. To this end, we tested mice that were treated with ifenprodil in the Lsi1 or Lsi2 specific windows in different learning paradigms, and scored their performances.

When tested for their ability to perform NOR, mice treated early with ifenprodil showed enhanced performances in correlation to their plastic state in CA3, to the same extent as mice that had been enriched (Discrimination ratio upon ifenprodil P8-P10: 0.53, $p < 0.001$. Fig 5A). In comparison, mice treated late showed a severe impairment in discrimination, as correlated to their intrinsic crystallized state in CA3 microcircuit (Discrimination ratio upon ifenprodil P11-P13: 0.17, $p < 0.05$. Fig 5A). As a control, we analyzed the impact of treating with ifenprodil in a developmental time window when both subpopulations are reducing their filopodia after the postnatal peak: when ifenprodil treatment was delivered to the mice during a P14-P16 window, no modulation of PV distribution in adult microcircuits could be observed (Fig 5B). Moreover, when mice were treated with ifenprodil for the whole interval of filopodia sporuting by Lsi1 or Lsi2 during development (P8 to P13), they exhibited a combination of both configurations at a structural level (increased High and Low PV IN, Fig 5B). While performance for the first control (ifenprodil P14-P16) exhibited no significant difference to saline treated controls (Fig 5A), the second instead performed the task with a significant impairment of performances (As if mice were treated in the P11-P13 window. Discrimination ratio upon ifenprodil P8-P13: 0.07, $p < 0.05$ Fig 5A).

We then tested mice for their ability to learn the Morris water maze. Consistent with the performances upon NOR, and the structural features of CA3 configuration, mice treated early showed enhanced learning during the initial phase of the training and a significant reference memory already on day 4, consistent with results of enriched mice (Fig 5C); late treatment in contrast produced impaired performances during maze learning (Fig 5C).

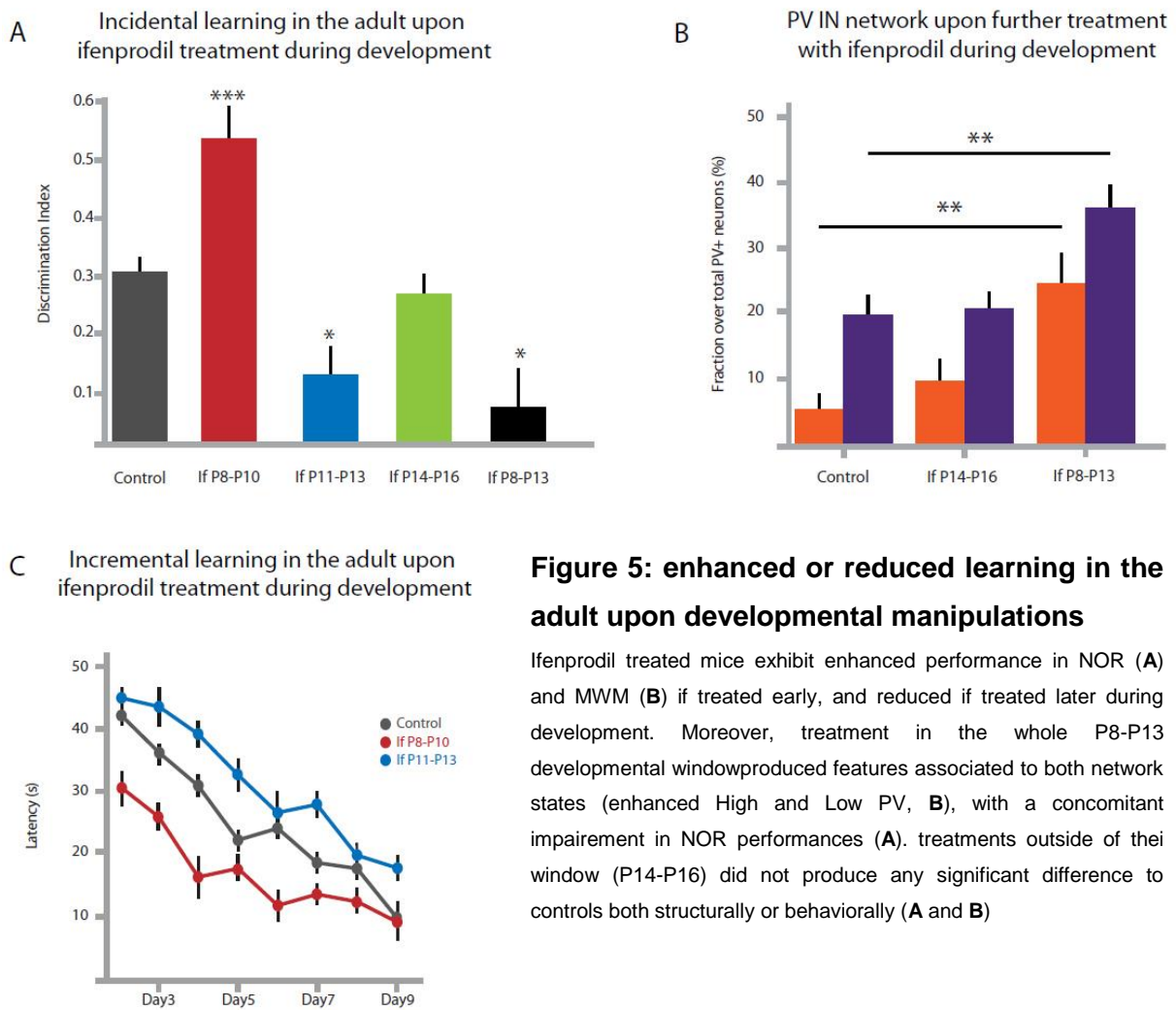


Figure 5: enhanced or reduced learning in the adult upon developmental manipulations

Ifenprodil treated mice exhibit enhanced performance in NOR (**A**) and MWM (**B**) if treated early, and reduced if treated later during development. Moreover, treatment in the whole P8-P13 developmental window produced features associated to both network states (enhanced High and Low PV, **B**), with a concomitant impairment in NOR performances (**A**). Treatments outside of their window (P14-P16) did not produce any significant difference to controls both structurally or behaviorally (**A** and **B**).

Taken together, these results demonstrate that ifenprodil-induced plastic and crystallized states structurally and functionally resemble those achieved physiologically as a result of experience. Moreover, they point toward the existence of a critical period during CA3 development in which manipulation of NR2B activity produces cognitive enhancement in the adult.

To investigate if early ifenprodil treatment would closely mimic enrichment and hence produce stable enhancement of plasticity, we tested if both states would rely on the same pathways to achieve enhanced performances. Therefore, we tested the effect of ifenprodil treatment in the Lsi1 specific window on mice that are deficient for the protein β -Adducin, which are unable to stabilize newly formed synapses in the adult (Bednarek and Caroni, 2011; Pielage et al., 2011), and, as a consequence, the enhancement of structural plasticity produced by environmental enrichment produces a net loss of active zones in mossy fiber terminals (Bednarek and Caroni 2011), and a decrease in NOR performances. We reasoned that, if ifenprodil treatment during Lsi1 window would act on the same mechanisms to induce

enhanced plasticity and learning, we should observe a worsening of the discrimination index upon NOR in these mice. Moreover, if enrichment and early ifenprodil treatment would impinge on the same pathways, the enrichment protocol should have no further effect in ifenprodil-treated mice. Indeed, when tested for NOR, β -Add KO mice treated with ifenprodil in the Lsi1 specific window performed poorly in discrimination as compared to control (Discrimination index: 0.06, $p < 0.01$ Fig 6A), to levels comparable to enriched β -AddKO mice (Fig 6A). Moreover, mice treated with ifenprodil early during development were insensitive to the enrichment protocol (Fig 6B): they did not present any shift in the configuration of the parvalbumin interneuron network (data not shown), nor show any further improvement of NOR performances. Moreover, enrichment could not rescue the deficit in performance induced by late ifenprodil treatment during development (Fig 6B).

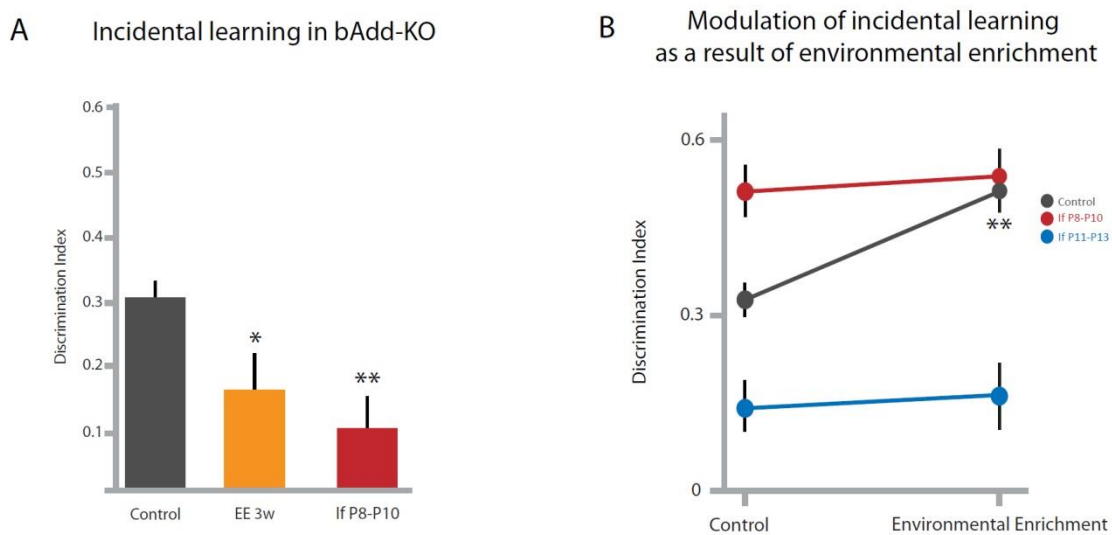


Figure 6: ifenprodil-induced plasticity resembles enrichment

Ifenprodil P8-P10 produces changes that resemble enrichment in adult mice, and share with enrichment the same dependence on synapse stabilization (A, AddKO are impaired in the stabilization of new synapses, and hence Enrichment produces a decrease in NOR performances). Moreover, no further enhancement of performance can be achieved on ifenprodil P8-P10 with adult enrichment, meaning that the whole plastic potential has been exploited with the developmental intervention (B). Nevertheless, developmental manipulation greatly reduce the potential for adult plasticity (B): this implies that a further enrichment is not sufficient to overcome NOR impairment induced by late ifenprodil treatment during development (B)

In order to investigate if the ifenprodil induced plastic state would indeed become the new stable baseline configuration, we produced perturbations to the microcircuit to analyze the extent of relapse to baseline. To this extent, we subjected mice treated with ifenprodil in Lsi1 specific window to the fear conditioning, and analyzed PV distribution at defined time points after learning. When analyzed at 1 day after the conditioning, ifenprodil treated mice in the Lsi1 specific window showed a shift in PV distribution toward higher levels of expression that was consistent with the effect of conditioning learning on the system (High PV difference to

controls: $p < 0.01$. Low PV difference to controls: $p < 0.01$. Fig 7A). We then analyze to which configuration the system would revert back when the transitory changes induced by learning would wear off. Indeed, ifenprodil treated mice would go back to their ifenprodil-induced configuration, suggesting that the enriched like configuration is indeed the new baseline condition for these mice (Fig 7B).

At last, we analyzed the stability of the plastic state acquired by ifenprodil treatment during Lsi1 window over time. To this extent, we analyzed how NOR performance enhancement would decay with ageing. Enriched-like mice obtained with early ifenprodil treatment were still performing better than controls when tested at 6, 12 and 16 months, suggesting a permanent enhancement of cognitive performances that does not decay with ageing (Difference to controls: 2 months: $p < 0.001$; 6 months: $p < 0.01$; 12 months: $p < 0.001$; 16 months: $p < 0.001$. Fig 7C). Moreover, ifenprodil treated mice did not show any decay in enhanced performances at any age analyzed, despite the fact that ageing is accompanied by decline in performances in NOR (Fig 7C). The impact of such discovery will be discussed in the following part.

Taken together, these results confirm that mice treated with ifenprodil in the early time window show a stable enhancement of cognitive performances as a result of treatment. Moreover, they hint toward the possibility that the PV network possess a sort of long term memory of its state, since both ageing or perturbation in microcircuit configuration do not shift the network from its plastic state.

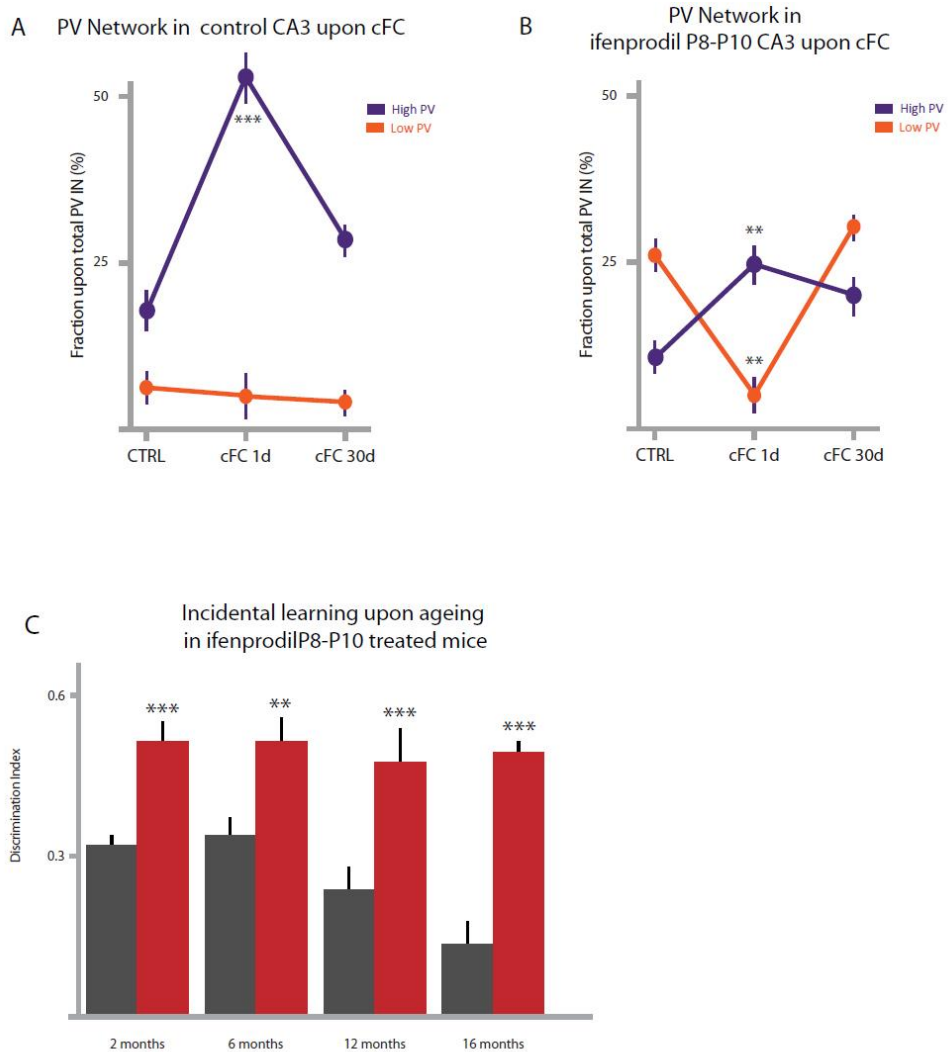


Figure 7: permanent shifting to plastic state for ifenprodil P8-P10 treated mice

Ifenprodil treatment produce a stable shift of the baseline CA3 network configuration toward a plastic state (A and B), which produce a protective effect against ageing in the adult (C, and see following part of results).

4.4.4 Discussion and future directions

Microcircuit development is a complex and prolonged phenomenon that is based in a fine regulated interplay between excitation and inhibition. The prevalence of each one over the other produces pathological conditions that extend well into adulthood (Turrigiano, 2011). Moreover, due to the extreme variety of subpopulations of inhibitory neurons, the maturation of each might be a separated phenomenon recruiting different driving forces and principles.

The development of perisomatic inhibition exerted by PV+ basket cells has received a lot of attentions due to some peculiar properties: its sensory-driven maturation seem to regulate the opening and closure of periods of enhanced plasticity during cortical development known as “critical periods” (For review, see Hensch 2005); moreover, modulation of PV maturation seem to be at the basis of important psychiatric pathologies, like Schizophrenia (Belforte et al., 2010). In addition, the PV network is implicated in the regulation of learning upon experience, by means of defining states of enhanced or reduced plasticity in the adult (Donato et al., in preparation).

Therefore, we studied how PV maturation would proceed in a region which is far away from sensory experience, and in which development proceeds according to a defined schedule of principal neurons subpopulations maturation (Deguchi*, Donato*, Galimberti*, Cabuy and Caroni, 2011). Hence, we elucidated a mechanism by which a transitory sprout of filopodial synapses from Mossy fiber terminal would drive the maturation of PV interneurons in the CA3 area in the hippocampus in an activity-dependent manner. Moreover, we were able to show that principal neurons subpopulations go through the same process of filopodia sprouting and reduction with a slight delay in time (probably set by defined neuronegenesis time windows in granule cells), and respond to MFT release modulation in an opposite way: Lsi1 tries to contrast the perturbation of PV maturation in the network (“driver response”), while Lsi2 adapts to MFT release (“homeostatic response”).

Based on these premises, we hypothesized that perturbation of the maturation *in vivo* would result in opposite outcomes, maybe based on subpopulations properties. Therefore, we could target selectively Lsi1 or Lsi2 mossy fiber terminals via ifenprodil treatment during defined time windows along development, and observe the response in the PV network: while both largely reduced PV expression in the PV network in CA3 (as expected for reduction of granule cells activation), early treatment involved a larger fraction of PV

interneurons which all reduced their level of PV expression, while later treatment produced increase in PV expression in around 20% of interneurons, and reduction of it in another 50%.

Then, we analyzed if this developmental intervention might produce any long-lasting alteration in the CA3 network in the adult. Hence, ifenprodil treated mice exhibited a permanently altered configuration of the CA3 network in the adult: early ifenprodil treatment produced a shift of the PV network toward prevalence of Low PV, enhancement of Feed forward excitation and cFOS expression at baseline, and active zone turnover in mossy fiber terminals; in contrast, late ifenprodil treatment produced a shift of the PV network toward prevalence of Low PV, reduced feedforward excitation and cFOS expression at baseline, and reduced active zone turnover in mossy fiber terminals.

Since these features were previously associated to regulation of learning in the adult (Donato et al., in preparation), we tested if early or late ifenprodil treatment during development was able to produce alterations in cognitive performances. We therefore tested early or late ifenprodil treated mice in NOR and MWM, and consistently found an enhancement of cognitive performance in both tasks for early treated mice, and an impairment for late treatment. Moreover, treatment outside of this large window produced no effect on PV network or cognitive performances. Therefore, we provide evidence that hint to the existence of a sensitive period for cognitive enhancement during hippocampal development in CA3.

These preliminary data offer different elements for discussion and further study. First of all, they provide a possible mechanism by which PV interneuron maturation might happen in cortical areas which lie further away from sensory experience: it would be interesting to determine if a mechanism based on the cascade maturation of principal neurons subpopulations might take place even in other brain areas, like the prefrontal cortices (although, unlike prefrontal, hippocampus matures before the sensory microcircuits underlying the sensory modality that will have a major role in its recruitment in the adult, which is the visual pathway). Moreover, which signal might orchestrates the cascade of excitatory cells subpopulations maturation? Preliminary data would suggest that the earliest born subpopulation (Lsi1 in the hippocampus) would respond to a graded molecular signal present in CA3 that induce filopodia sprouting (involving to a certain extent EphA4 signaling); Lsi1 would then modulate the maturation of the later subpopulation (Lsi2) which would in turn be driven solely by Lsi1 activity (Flavio Donato, data not shown). Additional experiments are definitely needed to confirm this mechanism.

Another interesting concept arises from the fact that both the maturation of principal neurons subpopulations and the effect of the ifenprodil treatment at different ages might force us to

rethink how development proceeds. Indeed, it appears clear that, even when considering the same process (i.e. MFT-to-CA3 synaptogenesis, or CA PV interneuron maturation), more than a uniform process, we might look at a series of events which are carried on by specific players and involve (to a certain extent) specific pathways. Development therefore might be constituted by the sequence of determined “windows of opportunities”, in which defined manipulations might have opposite consequences which enhance or reduce brain functions (with the extreme scenario of pathology), while the same manipulation outside of these windows might not elicit any consequence at all (for example, P8-P10 Vs P11-P13 Vs P14-P16 ifenprodil treatment and cognitive performances in the adult).

Via the temporal parcellation of the PV development process, we have defined time windows in which modulation of NR2B activity might produce long-lasting consequences, ultimately leading to permanent cognitive enhancement and impairment. What might be the mechanism by which the same manipulation might exert opposite effects in two adjacent time windows? This will likely be one interesting concept that I am going to explore in the near future. And yet, it is tempting to speculate that the basis for these opposite effects might lie in the peculiar response of Lsi1 to activity manipulation during development. In this scenario, a decrease in Lsi1 activity (induced by ifenprodil between P8 and P10) might freeze the PV interneurons that rely on Lsi1 activity for maturation to an immature, “plastic” state for the rest of their life; in contrast, decreased maturation of PV network induced by a P11-P13 treatment might elicit a counterbalancing response in Lsi1, which would exert enhanced excitation onto a fraction of PV interneurons that might then be frozen into a FFI, “crystallized” state for the long term. Moreover, have the interneurons which express excessive levels of PV upon the P11-P14 ifenprodil treatment undergone a premature development, and therefore missed their proper window of maturation? Recent literature (Clemens JP et al, 2012) shows how accelerated maturation of excitatory cells produces long-lasting cognitive deficits that are characteristic of Autism Spectrum Disorder. It will be interesting to test if this is the case also for Parvalbumin interneurons. A fascinating hypothesis in this prospect would suggest that, upon Ifenprodil P8-P10, a fraction of interneurons would fail to conclude their maturation properly, and therefore be stuck forever in a “critical period” configuration that confers enhanced plasticity and learning to the whole CA3 network; in contrast, premature maturation of a fraction of interneurons upon ifenprodil P11-P13 could crystallize these neurons in FFI configuration that decreases plasticity and learning in the CA3 microcircuits.

Both these hypotheses pose that a brief NR2B antagonism during development produce long lasting consequences in the adult, as my experiments seem to suggest. Moreover, they suggest that at least a fraction of PV interneurons establish some of their basic properties

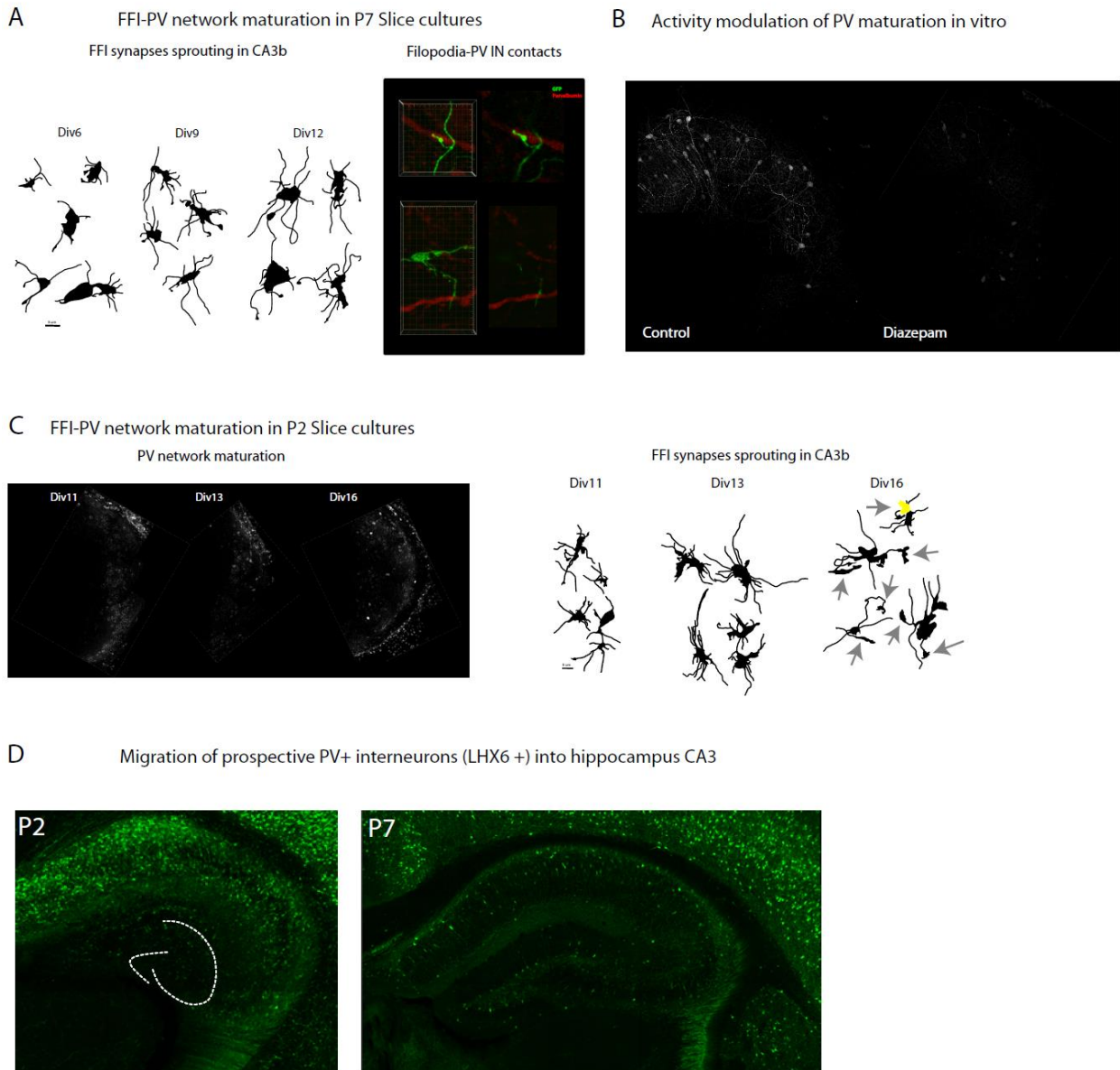
(like PV expression) during a sensitive windows during development which defines their “identity” (a definition that includes structural and functional properties, which seem to correlate to PV expression), and that can be modified by pharmacological manipulation during these critical periods. Indeed, ifenprodil-induced configurations are not lost when the system receives a strong perturbation in the adult, as it is the case of learning induced by a conditioning protocol: when the network effects of learning wear off in P8-P10 ifenprodil treated mice, the CA3 network relapses in the “plastic-like” state induced by developmental manipulation, and not to the regular baseline. This implies that the network is able to maintain a memory of its ifenprodil-induced state that goes beyond what is induced by experience. The molecular identity of this “memory” is likely to be extremely interesting in itself. If this memory is actually stored in the connectivity pattern on PV IN (i.e., if ifenprodil induces a permanent enhancement of disinhibitory connectivity over FFI in the adult), or if it lies in individual interneurons via modification of its genetic profile (maybe even at the level of the epigenetic landscape of the genome), is something that we will determine in the future.

Taken together the behavioral experiments performed in adult mice that were treated with ifenprodil during development, one of the probably most unexpected features that can be detected is the reduced magnitude experience-induced plasticity in CA3 upon treatment. Hence, mice that are constitutively in the crystallized state lose the beneficial effect that a protracted housing in an enriched environment can exert both at the microcircuit (data not shown) and behavioral level; moreover, mice that are constitutively in the plastic state seem to be completely insensitive to the decline in cognitive performance produced by ageing. While a partial explanation to this last phenomenon will be laid down in the next and last part of this thesis, further experiments will be needed to investigate it further, as it likely will have a major impact in our understanding of how microcircuits respond to ageing (and how to prevent cognitive decline).

Taken together, we provide evidenced for a subpopulations-based mechanism for PV maturation in the hippocampus; we identify windows of opportunity in which we can modulate this phenomenon in opposite ways; we define treatments that are able to permanently modify the baseline configuration of the CA3 microcircuit and cognitive performances in CA3 dependent tasks; we define sensitive windows for cognitive enhancement during hippocampal development, which are able to rescue cognitive impairment caused by physiological phenomena (i.e. ageing, see the next section).

4.4.5 Supplementary material

Supplementary figure 1: Maturation of FFI in hippocampal slice cultures



Hippocampal slice cultures produced from P7 pups preserve the element of the microcircuit involved in PV maturation in CA3: filopodial sprouting is preserved and directed to CA3 PV+IN, whose maturation is activity dependent (**A** and **B**). Nevertheless, slice produced at P2 are devoided of PV IN (**C**), probably because their proper migration has not terminated yet (**D**). Nevertheless, filopodial sprouting happens in a cell autonomous manner, although excessive filopodia end up contacting CA3 pyramidal cells when PV In are missing (**C** right, grey arrows)

4.5

A network mechanism underlying age-related cognitive decline in the hippocampus

Flavio Donato and Pico Caroni

Unpublished work

4.5.1 Summary

In the adult cortex, experience produces substantial structural modifications in microcircuit connectivity that underlies learning at the level of newly formed synapses. Moreover, cortical microcircuits can display different configurations supporting enhancement or reduction of further plasticity and learning based on the state of the network of interneurons expressing the calcium binding protein parvalbumin. Hence, enhanced learning is supported by prevalence of interneurons that express low levels of PV, while reduced performances are associated to prevalence of High-expressing PV interneurons. Nevertheless, the extent to which physiological processes enhancing or reducing plasticity and learning can impinge on the same network of PV interneurons is still an open question.

Previous reports have described a significant reduction of cognitive performances in different hippocampal-dependent learning paradigms upon ageing. In particular, ageing has been related to a decline in performances in incidental learning tasks, like the novel object recognition.

Here, we test if a microcircuit mechanism based on the state of the parvalbumin interneuron network might be involved in the age-related decline of episodic memory. By correlating performances of single mice to the state of their CA3 microcircuit, we highlight a strong correlation between the integrity of the PV network and NOR performances. Moreover, we start to investigate which principle might underlie the age related neuronal loss that we observe with ageing, and provide at least two possible treatments by which neuronal loss and cognitive impairment can be slowed down upon modulation of the PV network.

4.5.2 Introduction

It has long been known that ageing is associated with a marked decline of cognitive function that relies upon the medial temporal lobe and prefrontal cortex, such as learning, memory and executive functions (for a review, see Burke and Barnes, 2006). These dysfunctions can be associated to different molecular pathways that range from functional plasticity to cell-cell interactions, from intrinsic biophysical properties to gene expression. However, it is still unknown if any structural rearrangement happening at a microcircuit level could be held accountable for any aspect of age-related cognitive decline.

One of the brain areas mostly affected by ageing is the hippocampus. For example, ageing can affect place cell function: aged rats can show a certain degree of impairment in the stability of hippocampal maps, for which if allowed to explore an environment to which they had already been exposed to, they can fail to retrieve the proper hippocampal map established during the first exposure (Barnes et al., 1997). Moreover, hippocampal circuitry shows a high degree of age-associated changes both in its structural plasticity and functionality in the CA3 area. Here, ageing is accompanied by a continuous growth that mainly involves the largest subpopulation of mossy fiber terminal, which expand along the longitudinal axis of CA3 pyramidal cells (thereby expanding the dendritic territory that each mossy fiber terminal covers along a single pyramidal cell) (Galimberti et al., 2006). Moreover, ageing is accompanied by a slow but steady decline in NOR performances, in which mice have to discriminate between a novel and a familiar object, which likely underlie a deficit in episodic memory formation.

Previous work in the lab has demonstrated that NOR discrimination is critically dependent on the integrity of the mossy fiber-to-CA3 synapses; moreover, in the first part of these thesis I have demonstrated how the state of the PV network can regulate the performance in this task by underlying enhanced or reduced cognition, Therefore, I will investigate if any modification that occurs in the PV network in CA3 during ageing might underlie these cognitive deficits, and possibly modulate the extent of cognitive impairment with targeted manipulations of the interneuron network.

4.5.3 Results

Age-related decline of incidental learning performances correlates with rearrangements in parvalbumin interneuron network.

Previous reports have described a significant reduction of cognitive performances in different hippocampal-dependent learning paradigms upon ageing. In particular, ageing has been related to a decline in performance in incidental learning tasks, like the novel object recognition. This task analyzes the function of the hippocampus in underlying episodic memory, by testing for the ability to discriminate between a familiar and a novel object. Many molecular aspects correlated with ageing have been involved in producing this decline; here, we test if a microcircuit mechanism based on the state of the parvalbumin interneuron network might be involved in the age-related decline of episodic memory.

In agreement with previous reports, we could observe a significant decrease in NOR performance upon ageing in mice that were up to 24 months old. This decline would become evident after the first year of age, and progress linearly toward disrupted discrimination (12 months difference to 2 months: $p < 0.05$; 16 months difference to 2 months: $p < 0.01$; 24 months difference to 2 months: $p < 0.001$. Fig 1A).

In order to study whether ageing would affect the properties of the PV IN network, and if any of these properties would correlate to cognitive decline, we analyzed the state of the PV network at different stages during ageing. In CA3, ageing correlated with the decrease of the overall number of parvalbumin immunoreactive interneurons per area CA3 (Normalization to 6 months: 2 months: 0.8 fold, $p < 0.01$; 12 months: 0.61 fold, $p < 0.001$; 24 months: 0.26 fold, $p < 0.001$ Figure 1B and C). Moreover, the number of PV interneurons was strongly correlated with NOR performances per single animal (Pearson correlation: 0.83. Fig 1D).

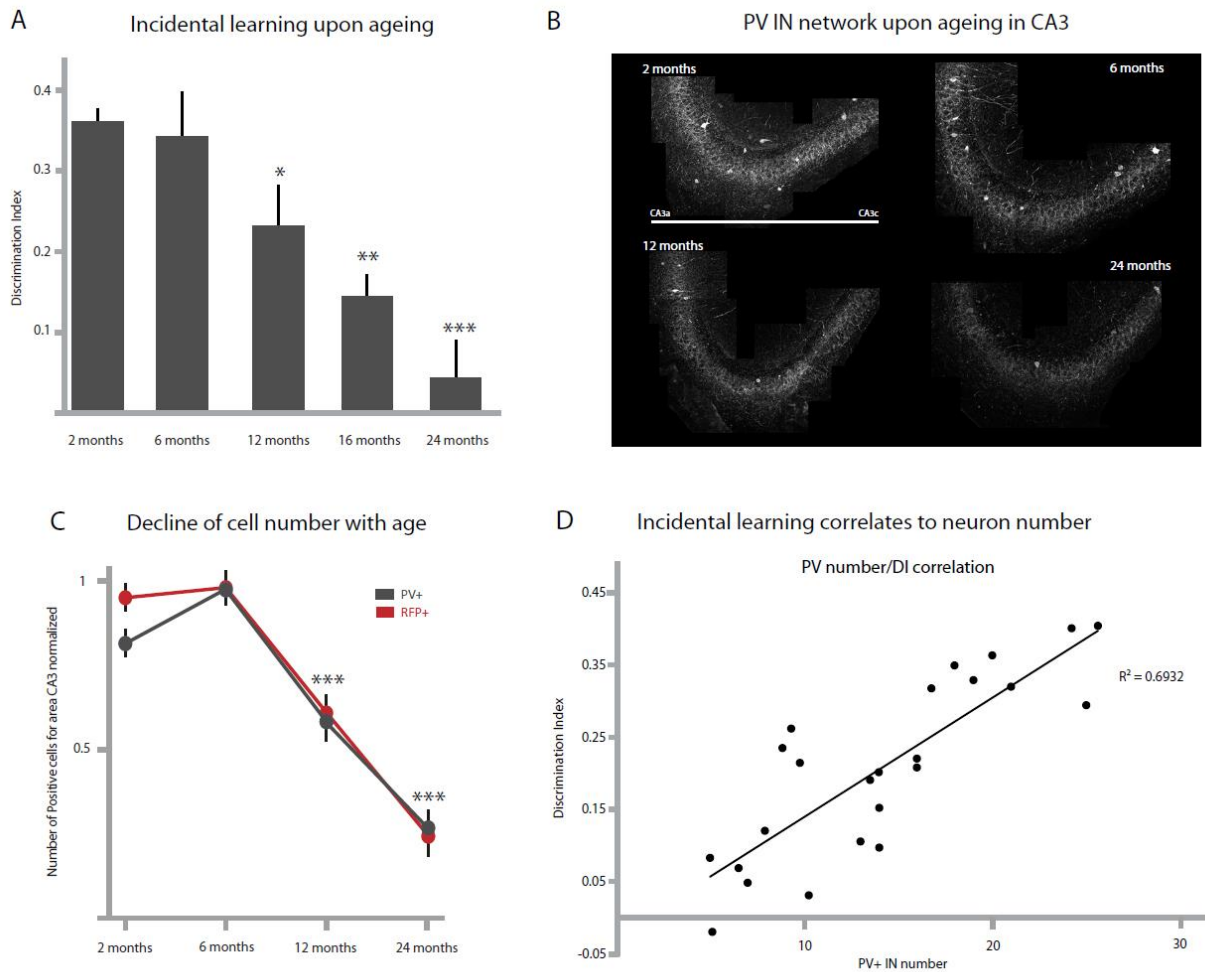


Figure 1: Cognitive decline upon ageing correlates to PV IN loss in CA3

Ageing is accompanied by a marked decline in cognitive performance in incidental learning tasks like the NOR (A), which goes hand in hand with a marked decrease in the number of PV+ interneurons in CA3 (B and C), whose microcircuit state regulates performances (Donato et al., in preparation). Indeed, NOR performance correlates with the absolute number of PV+ interneurons in CA3 for individual mice (D)

To study the nature of the decrease in PV immunoreactive neurons upon ageing, we tested if it could be attributed to the decrease in expression under the limit of detection of the protein parvalbumin, or to neuronal loss. To differentiate between the two scenarios, we studied the temporal evolution of the TOMATO+ neurons network in PV-cre/Rosa26-CAG-Lox-STOP-Lox tdtomato mice. In this mouse line, the PV promoter drives cre expression with the same pattern of the endogenous protein, and therefore produces recombination upon the tdtomato locus in PV+ neurons. Nevertheless, since the tdtomato construct is under the control of a different promoter its expression becomes independent of PV after recombination (although is restricted to PV+ neurons). If age related decline in the number of

immunoreactive PV interneurons would be due to decrease expression of PV, then the overall number of TOMATO+ neurons in these mice should be stable with ageing. Nevertheless, if the decline should be attributed to neuronal loss, then the amount of TOMATO+ neurons should decline as well. When quantifying the number of TOMATO+ neurons per CA3 area, we could observe an age-related decline in the number of immunoreactive neurons that could closely resemble the one observed for PV immunoreactivity, thereby suggesting a significant neuronal loss of Parvalbumin interneurons upon ageing (Normalization to 6 months: 2 months: 0.93 fold, not significant; 12 months: 0.63 fold, $p < 0.001$; 24 months: 0.23 fold, $p < 0.001$ Fig 1C). Moreover, the discrepancy between the two timecourse in the early life of the animal (2 to 6 months) would suggest the presence of potential PV+ interneurons, which are undetectable with PV immunostaining (probably due to the low level of expression of the protein), and that might underlie prolonged development of this component of CA3 microcircuit.

Taken together, these data provide evidence that the number of parvalbumin interneurons decreases upon ageing, and this process strongly correlates with performances in incidental learning for single mice.

Vulnerability to Age-related neuronal loss correlating to PV expression

The previous data indicate a strong link between the number of PV+ interneurons and the performance in the NOR task upon ageing. Besides the effect on the number of interneuron, ageing was also accompanied by a modulation in the proportions of High or Low PV cells (progressive increase in Low PV: 2m: 2%; 6m: 7%, 12m 19.5%; 24m: 30.2%. $p < 0.01$, one way ANOVA, Fig 2A): this would suggest that neuron loss have to happen preferentially in some classes of PV interneurons, which in proportion should decrease their prevalence in the overall distribution. Therefore, we quantified how age-related neuronal loss would impact each class of PV expression by normalizing the overall number of neurons to the levels observed at 6 months (peak of PV immunoreactivity), and calculating the prevalence of each class over the normalized ensemble. Confirming the hypothesis of a preferential targeting, the decrease in the overall number of interneurons was directly correlated with the magnitude of expression of the protein parvalbumin, with High PV being the most affected class (5 fold decrease in prevalence, $p < 0.01$, One way ANOVA. Fig 2B, C and D). The increased vulnerability toward age-related neuronal loss determined by PV levels was even more evident when comparing the integrity of the PV network at 6 Vs 24 months (Fig 2C and

D): in this time interval more that 50% of neurons are lost in the CA3 network (Fig 2C), with a loss that is targeting preferentially classes with higher expression of PV (Fig 2D).

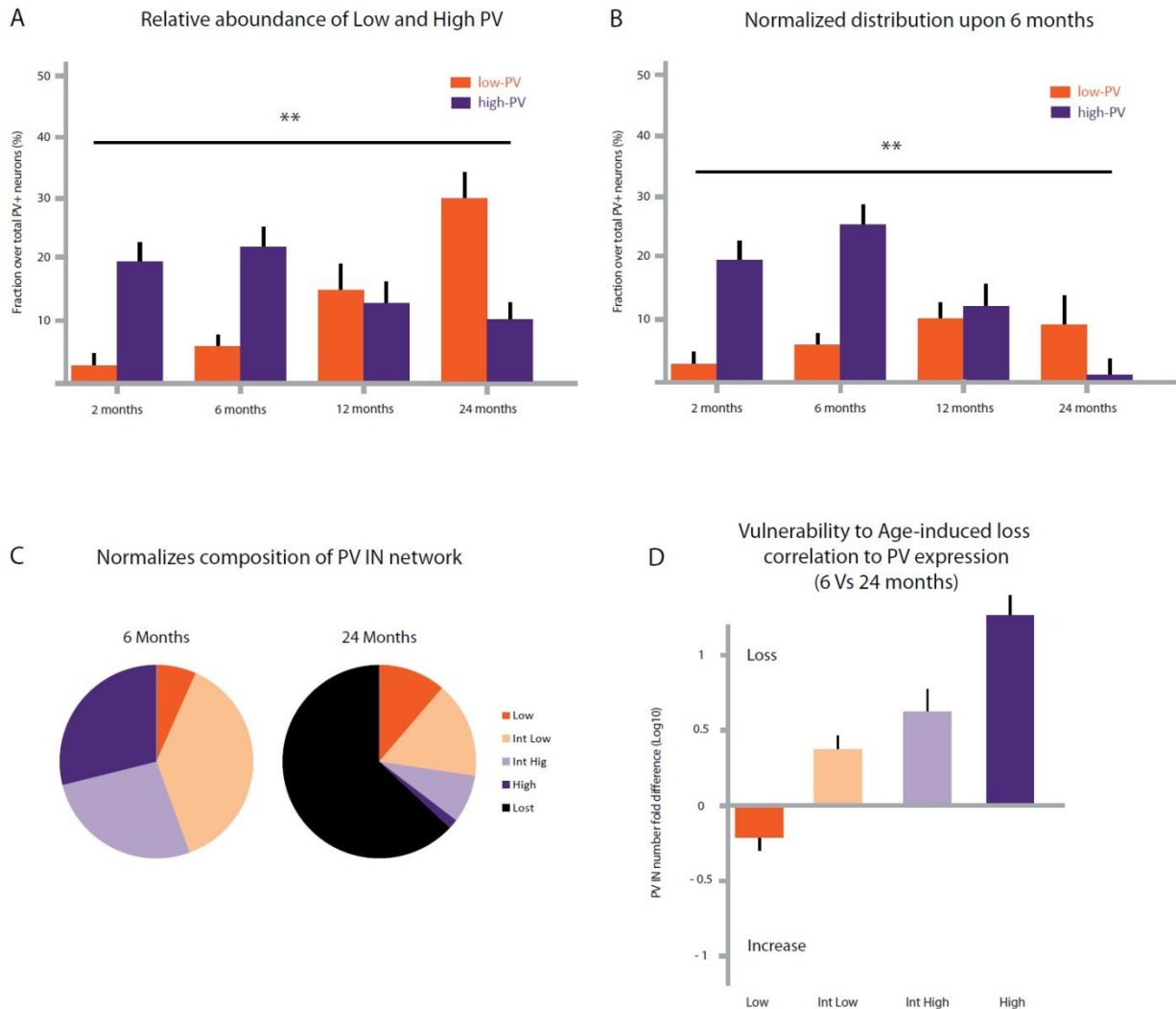


Figure 2: Increased vulnerability to age-related cell loss for higher expressing PV interneurons

Age related neuronal loss does not impact to the same extent in all PV In classes, but rather produces a shift in the network toward prevalence of Low PV (A). This is produced by the prevalent loss of neurons that express higher levels of Parvalbumin (B), as can be inferred by a direct comparison between the number of neurons for each class between 6 months and 24 months (whose absolute extent has been normalized to 6 the overall number on PV neurons at 6 months) (C). here we can see that neuronal loss is logarithmically related to PV expression (D)

Modulation of neuronal loss is able to modulate age-related cognitive decline.

Therefore, we hypothesized that interventions that might decrease the expression of PV could be protective against age-related cell loss, and conversely increasing PV expression might worsen this phenomenon.

In previous studies, we showed that experience is able to modulate the composition of the PV network enhancing the fractions that express extreme levels of the protein. Hence, environmental enrichment is able to enhance Low PV neurons while contextual fear conditioning learning increase the High PV class. Therefore, we used these protocols to modulate PV expression and test if remote experience might promote survival among PV interneurons at later stages: to this end, adult mice (10 months) were trained in either the environmental enrichment or the contextual fear conditioning, and the effect on the PV network was assessed long after experience (16 months) (Fig 3A).

First, we confirmed that environmental enrichment and fear conditioning would have the same impact on PV network at every age during the life of the animal, thereby allowing us to perform a targeted modulation of the PV network composition (Supplementary figure 1). Therefore, we subjected mice of different ages to the two paradigms, and studied the effect on PV network and NOR performances. Environmental enrichment was able to modulate PV network toward enhancement of Low Pv fractions both at 12 and 16 months of ages (Supplementary figure 1B and C); moreover, enriched mice performed better than age-matched controls at both ages, indicating that the overall pathways underlying the effect of environmental enrichment at 2 months of age are conserved upon ageing (Supplementary figure 1 A, B and C). Besides, conditioned mice presented an enhancement of the fraction of High PV interneurons upon learning at each time point during ageing; nevertheless, this shift would not correlate with decreased performance in the NOR test, which were comparable to age-matched controls and probably due to a saturation effect present for low performances (Supplementary figure 1A, B and C).

Thereby we tested if a prolonged permanence in the “plastic state” could prevent age-related cognitive decline by modulating PV network. To stably decrease the fraction of neurons expressing high levels of parvalbumin, we subjected 10 months old animals to 3 weeks of environmental enrichment, and analyzed PV network composition and behavioral performances after 6 months from the end of the enrichment (when enrichment-related effects have most likely wore off. Gogolla et al., 2008. Fig 3A). This showed us that remote enrichment experience produced deep rearrangements in the PV network: the number of

immunoreactive neurons were significantly higher than age matched controls, and comparable to the levels of a 12 months old animal ($p < 0.01$. Fig 3B); likewise, performances in NOR were comparable to the extent of 2 months old animals, with a significant increase in respect to both age matched controls and enrichment upon age matched controls ($p < 0.01$. Fig 3C). Moreover, we normalized the PV network to 6 months level in neuronal number, and compared each class of PV expression to age matched controls: this analysis confirmed that a remote enrichment experience was sufficient to modulate age-related PV loss by preserving High PV interneurons ($p < 0.01$: One way ANOVA. Fig 3D), and this was sufficient to rescue incidental learning performances.

Likewise, we tested if a prolonged permanence in the “crystallized state” might accelerate cognitive decline for its higher prevalence of High PV. To obtain a prolonged crystallized state, we performed three times the contextual fear conditioning protocol (with 2 months intervals between sessions) in 10 months old mice (fig 3A). When analyzed at 16 months, these subjects showed a significant decrease in the number of parvalbumin immunoreactive neurons in age matched controls ($p < 0.05$. Fig 3B Fig 3B), to levels comparable to 24 months old animals; likewise, performances in NOR were robustly impaired to level comparable to 20 months old mice ($p < 0.05$ Fig 3C). Note that this prolonged crystallized state was the only paradigm that was able to worsen performance in NOR, as 16 months old controls whom learned the fear conditioning at this age would not show any impairment. Likewise, a comparative normalized analysis revealed that the most extensive effect on neuronal loss was exerted on High PV neurons, consistently with the hypothesis that the prolonged crystallized state would critically expose this fraction to age related effects ($p < 0.01$: One way ANOVA. Fig 3D).

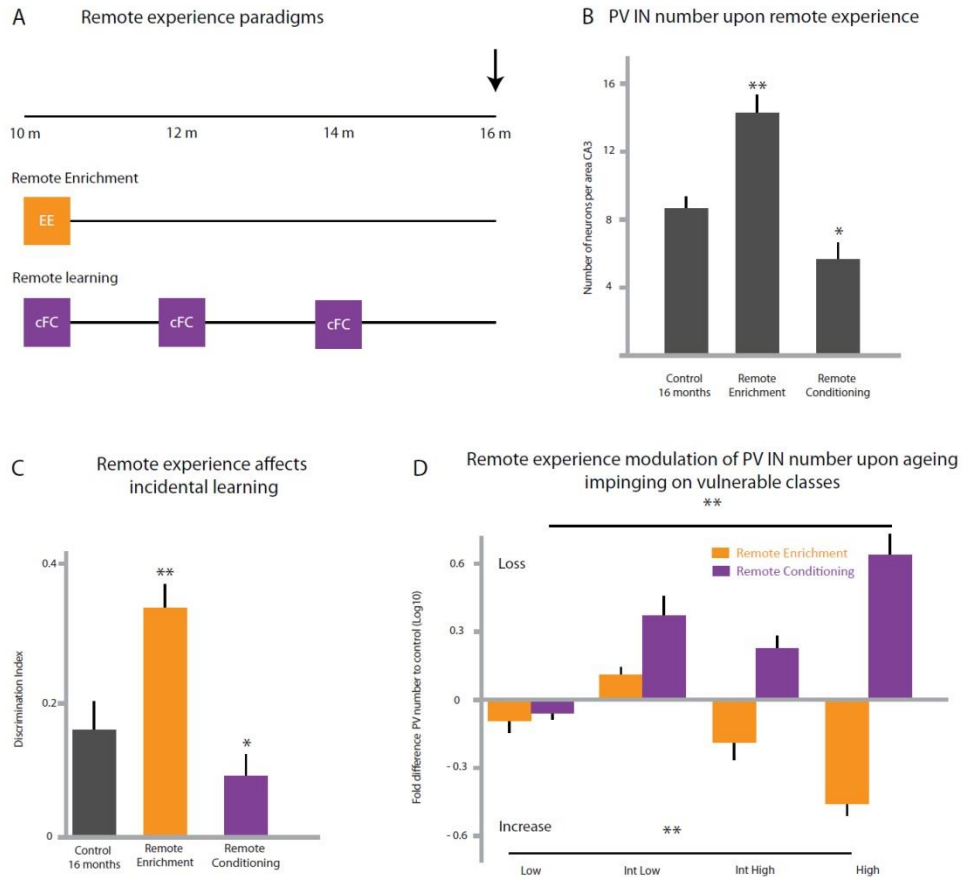


Figure 3: remote experience modulates ageing via PV IN network

Remote experiences (A), which highlight a long-term permanence in the Plastic or Crystallized state, modulates the extent of ageing on the CA3 network both at a structural (B) and behavioral (C) level. In particular, remote EE reduces the fraction of IN that are lost with ageing, with a greater effect for High expressing PV (B and D); in stark contrast, remote conditioning increases the fraction of IN that are lost with ageing, with a greater effect on High PV interneurons (B and D).

To further strengthen this observation, which allows us to modify the cognitive decline upon ageing, we followed how ageing would impinge on CA3 networks whose baseline has been permanently shifted toward High (ifenprodil P11-P13) or Low (ifenprodil P8-P10) PV network configuration (see previous parts of the thesis). Therefore, we monitored how developmentally treated mice would perform in the NOR task at 1 year of age, and analyzed how the microcircuit would evolve. Hypothetically, mice which have been frozen in a High PV configuration should be more sensitive to ageing, since the vulnerable interneurons would represent the majority of the network; in contrast, mice that have been frozen in the Low PV configuration should be protected, as it has been shown for remote enrichment. Mice treated with Ifenprodil P8-P10 showed indeed no decay in performances at 12 months (8p<0.001, Fig 4A), with a significant enhancement respect controls that was underlied by no significant

reduction of PV interneurons ($p < 0.001$., Fig 5B); in contrast, mice treated with ifenprodil P11-P13 showed a significant reduction in performances at 12 months ($p < 0.05$., Fig 4B), accompanied by a reduction of PV+ interneurons (to levels comparable to 18 months. $P < 0.05$. Fig 4B).

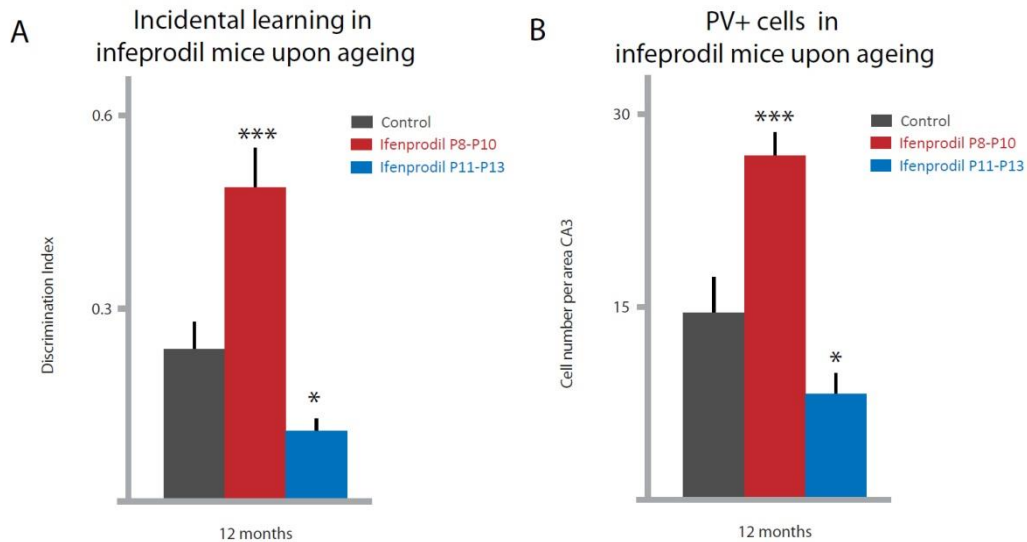


Figure 4: Ageing upon permanently-altered CA3 network configuration

Developmental ifenprodil treatments modulate ageing-related behavioral and neuronal changes due to the enhancement or reduction of PV expression in baseline levels (A and B)

Moreover, mice treated with ifenprodil P8-P10 showed no decrease in NOR performances or PV number up to 16 months of age (NOR difference to controls: 2 months: $p < 0.001$; 6 months: $p < 0.01$; 12 months: $p < 0.001$; 16 months: $p < 0.001$. Number of PV difference to controls: 12; months $p < 0.001$; 16 months: $p < 0.0001$ Fig 5A and B). This result would suggest that not only this developmental treatment is sufficient to induce cognitive enhancement in the adult, but that it might abolish ageing in the CA3 microcircuit structure and performances.

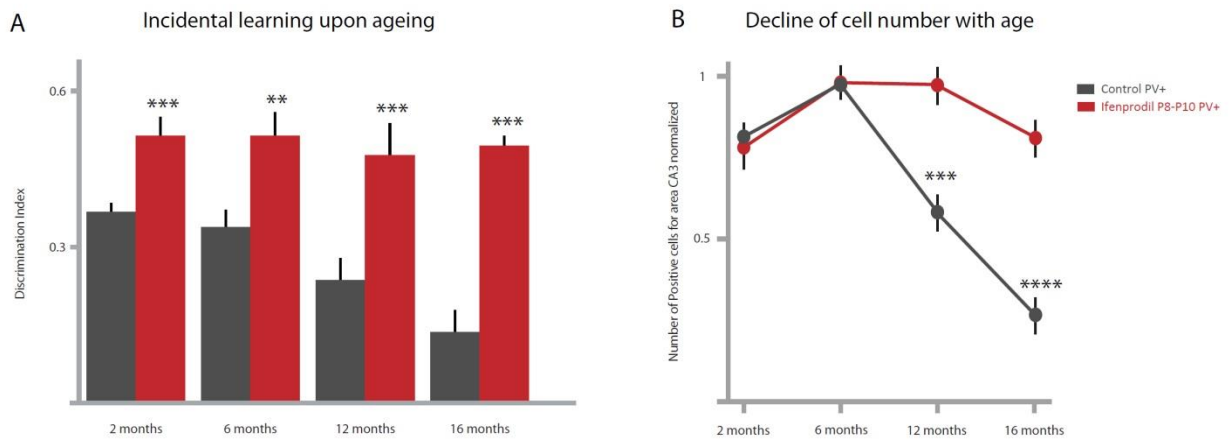


Figure 5: Ageing is suppressed in ifenprodil P8-P10 treated mice

The constitutive shift toward the plastic configuration mediated by ifenprodil P8-P10 is able to prevent completely age-related cognitive impairment (A) and PV IN loss (B). Moreover, performance are maintained at levels that characterize enhanced performances in young adults (A)

4.5.4 Discussion and future directions

By analyzing the maturation of the network of PV interneurons in hippocampal area CA3, we have shown that the age-related decline in cognitive performances for an incidental learning paradigm (which underlies defect in the production of episodic memory) can be largely correlated to the gradual loss of parvalbumin+ interneurons in the microcircuit which is critically involved in the task. As a matter of fact, performance in the NOR of mice of different age were proportional to the absolute number of PV+ interneuron per area CA3, which highlights the possibility that the integrity of the CA3 network might be essential for proper performance. Moreover, ageing impacted not only the absolute number, but also the proportion of PV interneurons belonging on each class of PV expression that we have previously described. This strongly suggested that age-related neuronal loss did not affect each class to the same extent, but interneurons might exhibit selective vulnerability based on intrinsic properties. We indeed showed that the proportion of cell loss was strongly correlating with PV expression, with High PV being more sensitive to ageing than Low PV interneurons (which were hardly affected by it). Therefore, we hypothesize that a prolonged modulation of PV expression might be able to impact on neuronal loss and hence on NOR performances upon ageing. Hence, prolonged “Low PV” state (achieved via remote environmental enrichment or via developmental pharmacological treatment) showed to be protective against age related cognitive decline and PV loss, while a prolonged “High PV” state accelerated ageing at a behavioral and network level. Therefore we propose new strategies to mitigate the cognitive decline in episodic memory that is usually occurring with ageing, by promoting survival of PV+ interneurons in CA3 via targeted modulation of PV expression (and probably of the properties correlated to it).

The selective vulnerability of High PV interneurons to ageing is confirmed also by those experiments that, by producing a prolonged plastic state with the prevalence of Low PV, rescue to a certain extent the loss of interneuron. A normalized analysis in fact reveals how High PV interneurons are those that most benefit from the effect of remote experience, or developmental pharmacological manipulation. Then why are those interneurons more vulnerable in the first place? In our previous work about network states, we have shown how PV expression would correlate with a series of properties ranging from GAD-67 expression to firing frequency. It is reasonable to hypothesize then that those interneurons are indeed the most active of their kind, also because they are the ones that bear the higher density of excitatory connections on their dendrites. Therefore the burden of activity that is impinging

on these neurons for a prolonged time, both for their intrinsic higher spiking phenotype and their higher metabolic demand, might be the cause of their selective vulnerability to ageing. Indeed, it has been described by many labs, including ours, that a higher cellular stress might be at the basis of selective susceptibility for neurodegeneration of specific cell types upon pathological conditions (Saxena, Cabuy and Caroni, 2009). We wonder to what extent higher expression of PV might signal an enhanced vulnerability to ageing based on the same principles.

One striking feature showed by this study was the tight correlation between behavioral performances and the number of interneurons lost/maintained at each age, and how specific the loss seemed to be for neurons expressing higher levels of PV. Would behavioral performances decline to the same extent if all PV interneurons would show the same vulnerability to neuronal loss? The question boils down to understand if the impact of high PV interneurons in a cortical network is higher than the average PV interneuron. In graph theory, networks are defined as a series of nodes which are connected by links; the degree of connectivity of each node (that is, the number of links it possesses, k) define the network model (Albert-Lazlo Barabasi, 2002 and 20010). “Small world” networks are defined by power laws distributions of the number of nodes with k links, which highlight the presence of few nodes with a very high number of links, or “hubs”, whose impact in the network is higher than the remaining nodes: they reduce the number of passages to reach a specific node from every other node in the network. In this scenario, a random elimination of nodes in the network should not cause damage to its function due to the intrinsic resilience of the network itself (Albert-Lazlo Barabasi, 2002). However, a target elimination of hubs in the network has a greater impact due to their higher connectivity: an extreme scenario foresees the complete shutdown of the network when a critical number of hubs is eliminated. To better understand this, I will provide an example with a well known network, the Internet: a hacker attack which randomly takes down web pages will likely have no impact on the user experience and network function, since the most of the pages will be websites that receive a very few number of visits (which numerically represent the largest fraction of internet websites); on the contrary, a targeted attack aimed at the internet hubs (search engines like Google or Yahoo, or social networks like Facebook or Twitter) will increase the path to any of the other internet web pages, decreasing efficiency. In biology, one of the most studied hubs existing in the cell is the protein p53, whose function is related to a multitude of signaling pathways, and whose deviations from physiological functions are a crucial step in the tumorigenic progression of a cell (again underlying how the loss of hubs in a network has a greater impact than the loss of low-connected nodes). In the CA3 PV network, High PV are indeed interneurons that receive a higher degree of connectivity from excitatory cells, and therefore

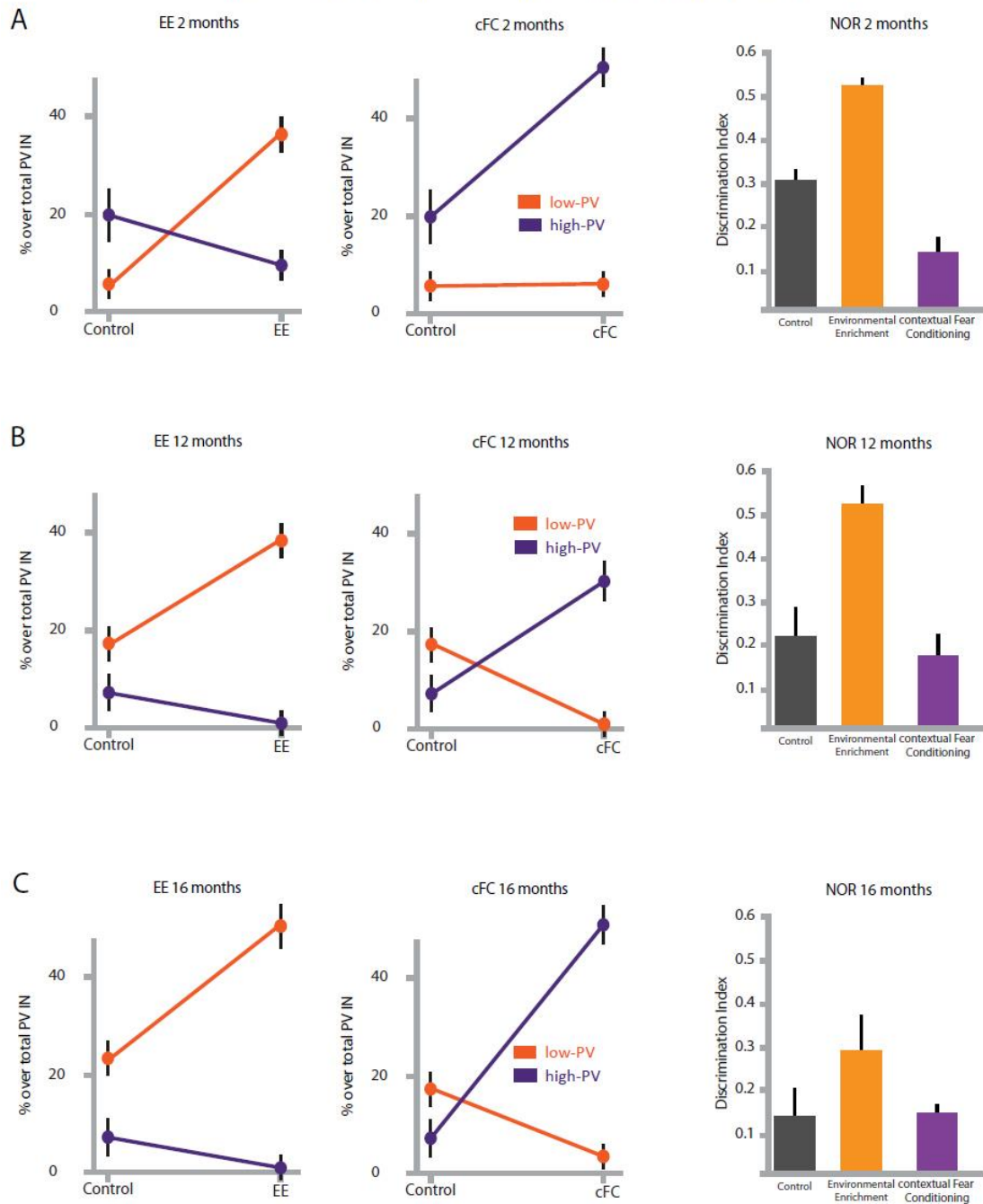
might possess features that make them Hub-like (in a similar fashion than other interneuron classes during development, Bonifazi et al., 2009); moreover, their higher firing frequency and GAD-67 content (which is related to the amount of GABA synthesized and release in the synaptic cleft) might increase their “fitness” in the network by means of higher inhibition exerted. If we should confirm the presence of Hub-features for High PV interneurons, we might understand why losing that component with ageing has such a great effect on hippocampal computation: they would represent the interneurons that are recruited more frequently to exert FFI on pyramidal cells, and that exert inhibition with the highest efficiency: eliminating this resource would destroy the temporal precision of pyramidal cells spiking (in the same line, ageing decreases the power of gamma oscillations in cortical microcircuits) .

Perhaps the most striking evidence presented in this work refers to the possibility that ageing, considered as a cognitive decline process, can be slowed down or accelerated by remote experience. In an extreme scenario, upon a condition for which the CA3 microcircuit is crystallized in a plastic configuration (ifenprodil treatment during development, see previous part of the thesis) the CA3 microcircuit shows no sign of either network (no loss of PV neurons) or behavioral (no impairment of juvenile performances in NOR) ageing. If the age-related loss of PV interneurons in CA3 should be confirmed at the level of human subjects, the knowledge of such a powerful way to interfere with the ageing process will likely be of relevant impact for therapeutic applications.

Along with this open question, other future experiments will focus on causally linking PV loss to impaired performances, by targeted elimination in young individuals; then, I will investigate if PV loss can be ascribed only to the CA3 area, or extended to other networks in the brain (with particular attention to computational areas like frontal cortices and Layer 2/3 in the cortex); finally, I will focus on possible network mechanisms aimed at decreasing vulnerability to neuronal loss by modulating the PV network composition (for example, prolonged activation of VIP+ neurons or inhibition of PV+ neurons themselves).

4.5.5 Supplementary material

Structural correlates of experience and further learning upon ageing



Experience-induced modulation of PV network and NOR performances are age independent, and follow the same dynamics at 2 (A), 12 (B) or 16 (C) months.

5. General Discussion and Outlook

Microcircuit states regulating structural plasticity and learning in the adult

The results presented in this thesis provide evidences that cortical microcircuits can display at least three “states”, which can be defined by connectivity, structural as well functional features of excitatory and inhibitory neurons, and modulate the extent of structural plasticity as well learning in the microcircuit. Moreover, the network of Parvalbumin expressing interneurons has a key role in defining these states, and structural rearrangement of the wiring diagram impinging on single interneurons can modulate the composition of the network to perform transitions among them. Hence, a state that enhances disinhibition connectivity on PV interneurons leaving FFI unaltered produces a higher fraction of Low PV interneurons, a higher degree of structural plasticity in excitatory microcircuits, and enhanced performances in further learning paradigms (“Plastic State”). In stark contrast, enhancement of FFI connectivity upon PV interneurons characterizes a state of higher fraction of High PV interneurons, low degree of structural plasticity in excitatory microcircuits, and reduced performances in further paradigms (Crystallized State”).

Surprisingly, incremental forms of learning are able to implement a sequential transition between states that might favor exploration during learning, and exploitation upon learning completion. In fact, incremental learning is characterized by the recruitment of a dedicated VIP-PV microcircuit module for which VIP+ interneurons, by means of an enhanced inhibitory drive on parvalbumin interneurons, mediate the transition toward the Plastic state (to revert back to baseline by the end of learning). In stark contrast, learning completion is marked by an increase in FFI connectivity from specific excitatory inputs impinging on PV interneurons, which mediates the transition toward the Crystallized state. The experiments presented in the first part of the thesis clearly show that the recruitment of the VIP-PV module to establish the plastic state is necessary for learning, and targeted modulation of disinhibitory release is sufficient to modulate performances.

Taken together, these experiments provide the first evidence that support the existence of discrete states in microcircuit configuration regulating plasticity and learning in the adult; moreover, they show how experience acts on cortical neurons to achieve transitions among states. Therefore, a further effort to understand the interplay between excitatory and inhibitory microcircuits upon experience, and elucidating the role of each neuronal subpopulation in performing those transitions, is fundamental in understanding how the brain learns about the environment.

Implementing transitions between states

Transitions between states exploit specific dynamics targeting directly excitatory or inhibitory microcircuits as a function of experience. In particular, excitatory microcircuits are driving the transition toward a reduced plasticity state upon learning completion (“Crystallized state”), while they respond to the Low PV configuration (“Plastic State”) upon environmental enrichment. Nevertheless, the extent to which the same subpopulation of randomly selected neurons could mediate both transition is unknown. Moreover, modeling a network in which both transitions would be performed by the same players would imply that the microcircuit would be allowed to implement only one configuration at the time, with no memory of previous states (“Common substrate model”); alternatively, a network in which subpopulations of neurons would be recruited specifically upon one transition, but selectively excluded by the other, would allow the microcircuit to exploit multiple configurations at the same time, and to retain a memory of previous states (“Specialized substrate model”). Indeed, when a mouse in the plastic state is subjected to a learning process (and hence to the transition to a crystallized state), it does so (both in the absolute extent of the transition as well as in the baseline it reverts back after learning) as if the Plastic would be the default state of the network (thereby exhibiting a lasting “memory” of previous states upon further experience) (Flavio Donato, data not shown). Moreover, preliminary results obtained in our lab support the hypothesis that genetically and developmentally defined subpopulations of principal neurons in the hippocampus, which we have shown to connect selectively across hippocampal subdivision by a mechanism that uses matched neurogenesis and synaptogenesis between synaptic partners belonging to the same subpopulations (See part three of the results), are differentially involved in mediating or responding to state transition (Dominique Spirig, unpublished results, and Flavio Donato, unpublished supplementary data). Specifically, Lsi1 mossy fiber terminals in the hippocampus would be recruited upon learning completion to mediate the increase in FFI connectivity necessary for transitions to the crystallized state. Moreover, they would be characterized by an intrinsically more stable synaptic turnover at MFT and would be able to induce FFI synapse sprouting upon learning even with a structurally compromised PV network. In stark contrast, Lsi2 mossy fiber terminals would not support FFI growth upon learning completion, but would be able to respond via increase in feed-forward Excitation upon CA3 pyramidal cells as a consequence of a prolonged plastic state. This might be a consequence of their intrinsic enhanced structural plasticity, which might explain their ability to respond with an increase of FFE also to enzymatic manipulations of the PV network toward the plastic state (in contrast to the Lsi1, which is unresponsive) (Flavio Donato, data not shown).

Modulating PV network to manipulate cognitive performances

Understanding the principles underlying each network state, and governing the transitions between them, is fundamental not only for understanding what learning is, and how experience is coded at the level of single microcircuits, but also to obtain important entry points in the attempt to influence cognitive performances in health and disease. In the last part of the thesis, preliminary results show two interesting phenomena pointing toward this direction. The first is that the integrity of the PV network is necessary for proper cognitive abilities: I have indeed showed how ageing affects the number of PV interneurons in the network producing a high degree of neuronal loss which target preferentially interneurons with higher expression of parvalbumin. Strategies aimed at producing a long-lasting shift toward low PV in adult animals are indeed successful in rescuing (at least partially) the age related impairment both at the network (with enhanced survival of PV interneurons for comparable ages) and behavioral level (mice perform to levels comparable to younger counterparts). The second aspect regards the possibility that basic properties of cortical network (like the distribution of PV interneurons classified by intensity) might be acquired during sensitive periods during development. In the fourth part of my thesis I have indeed shown that pharmacological manipulation during specific windows along the maturation of the PV interneuron network (that molecularly correspond to the period when Lsi1 and Lsi2 drive the integration of PV interneurons in the CA3 microcircuit), has a long lasting effect that extend well into adulthood: mice treated early during development (Lsi1-specific time window) display a baseline CA3 network configuration in the adult that is similar to the Plastic state achieved upon enrichment, with enhanced fraction of Low PV interneurons, enhanced active zone turnover, and enhanced performance in both incidental and incremental learning tasks. In stark contrast, mice treated late during development (Lsi2-specific time window) display a baseline CA3 network configuration similar to the Crystallized state achieved upon learning completion, with enhanced fraction of high PV interneurons, reduced active zone turnover, and reduce performance in both incidental and incremental learning.

What do Low and High PV INs do?

A powerful concept arising from the experiments presented in this thesis is that a modulation of the network composition that favors classes of interneurons with defined structural (and likely functional) properties, is sufficient to regulate computation and behavioral performance of the animal. To my knowledge, this is the first time that such a principle is hypothesized as a regulating component of learning. And yet, a profound question arises as to how the abundance of High or Low PV might impact on the whole CA3 network. A partial hypothesis that tries to answer to this question is provided during the discussion of the first part of the thesis. Moreover, a likely interesting subject to be developed further is how network distribution influence perisomatic inhibition per se. It is tempting to speculate that, since High PV should be responsible of higher power of Gamma in excitatory networks, their firing should be finely timely regulated so to synchronize discharge on pyramidal cells (which, as I have shown in the the part 4.1 supplementary figure 6, receive synapses from a large fraction of PV cells in the network, so to reproduce the distribution in intensity that is seen at the soma even at the level of single baskets). This would also partially explain the major effect that a loss of High PV has on the CA3 network (with ageing, see 4.5), which might be accompanied by decrease in power of gamma oscillation (See Barbas lab). On the contrary, low PV would likely exhibit asynchronous release impinging lower temporal precision on the PC discharge. Nevertheless, it would be unrealistic to hypothesize that low PV would only produce a loss of function (in this case, synchronicity). More likely they are able to modulate the network computation in another way, for which an increase in Low keeping the High constant would be sufficient to produce an effect on the CA3 network properties (as it is the case after 1 week of enrichment). How would Low PV impact on the network? Do they change non-linearly the properties of High PV or impinge on the tonic inhibition exerted in CA3? This will likely be a future direction to pursue, since their property to enhance cognitive performances makes them attractive also from a therapeutic point of view.

Outlook

Therefore, the work exploited during my thesis can shed new light on the question posed in the preface (“If we could know all the connections and wiring patterns of the brain of an individual, could we understand how he/she thinks, feels, and gives rise to behavior?”). Studying emotions belongs to a different realm of research that has not been touched by this thesis (for an entertaining analysis, look at Ledoux J., 1998 and 2003). Nevertheless,

focusing on the cognitive aspects of brain functions, my work has shown that, by knowing how microcircuits assemble; how experience shapes connectivity and recruits dedicated microcircuit modules; which neuronal substrates are targeted by experience and learning paradigms; and how the network evolves upon ageing, we can predict the potential to which the system is going to perform in defined learning paradigms (specifically, episodic and spatial navigation tasks critically relying on the hippocampus). Moreover, we can interfere *in vivo* in behaving animals to modify their cognitive potential, inducing an enhancement of cognitive performances that, in some cases, can last bona fide for the whole life of the animal.

Many unanswered questions arise from the evidence presented in this thesis. Understanding how the modulation of the PV network, with the prevalence of Low or High PV interneurons, might impact on the recruitment and activity of the pyramidal cells will almost certainly be crucial to understand how the states we described support learning. This will likely impact also on our understanding of the mechanisms that implement transitions among network configurations, and which pathways or cells subpopulations might be recruited upon them. Such a knowledge might open the way not only to new efforts in understanding how the brain learns about the environment, but also to trying to manipulate cortical microcircuits to achieve beneficial effects in physiological and pathological conditions. We have shown how these types of approaches will likely have an impact on the modulation of age-related cognitive decline, and their involvement in pathological conditions like schizophrenia or the autism spectrum disorders remains to be determined.

6. Materials and Methods

Mice and reagents.

Add2-/- mice were from Jackson Laboratories, Bar Harbor, Maine; the reporter line Thy1-mGFP(Lsi1) was as described. We analyzed structural traces of learning at GFP-positive LMTs of ventral and dorsal hippocampus (CA3b) using the 'sparse' transgenic reporter line Thy1-mGFP(Lsi1) and Thy1-mGFP(Lsi2). Lhx6-GFP mice were from Gensat at Rockefeller University, New York mouse strain: STOCK Tg(Lhx6-EGFP)BP221Gsat/Mmmh. PV neurons labelling was achieved via breeding of a PV-cre line with Rosa-CAG-STOP-tdTomato (both as a kind gift from Silvia Arber, Basel). Optogenetic experiments were performed on slice cultures from PV-cre and VIP-cre mice (kind gift from Anthony Dajer, Geneva). Channelrhodopsin-expressing AAV viruses was kindly provided from Santiago Romapani and Botond Roska as a mixture of serotypes 1 and 2 (AAV Ef1a::DIO Chr2d-EGFP (sero 2/1)).

Mice were kept in temperature-controlled rooms on a constant 12-h light-dark cycle, and all experiments were conducted at approximately the same time of the light cycle. Before the behavioral experiment, mice were housed individually for 3–4 d and provided with food and water ad libitum unless otherwise stated. All animal procedures were approved and performed in accordance with the Veterinary Department of the Canton Basel-Stadt.

All behavioral experiments were carried out with male mice that were 55–65 d old at the onset of the experiment and were performed according to standard procedures.

Fixations was carried on as transcardiac perfusion with 4% PFA as previously described (See 3.2.6). fixed tissue were stored at +4 degrees for one night in PFA, then ad libitum in PBS.

Stainings and histological analysis.

Staining procedures were carried on as previously described (3.2.6). Antibodies were as followed: Goat anti-PV (Swant biotechnologies, Bellinzona) 1:5000; mouse anti GAD-67 (chemicon) 1:500; rabbit anti cFOS (Santa Cruz biotechnology) 1:10000; guinea-pig anti vGlut3 (kind gift from Silvia Arber): 1:1000; Rabbit anti RFP (Rockland) 1:1000; rabbit anti GFP (Invitrogen) 1:1000; mouse anti Bassoon (RY) 1:200; mouse anti Gephyrin (RS) 1:500, Secondary detection was carried out with animal-specific secondary antibodies conjugated to Alexa fluorophores (488, 568 and 647, Molecular Probes, Invitrogen).

Dorsal hippocampus was located at -2.15 from bregma, and that position was maintained for any histological analysis. M1 was located at 1.58 from bregma.

Synapse density onto RFP positive dendrites and PV and vGlut3 density on pyramidal cells soma was quantified as the number of puncta detected on the dendritic surface. Dendritic surface was visualized using Imaris software (bitplane) with the construction of isosurfaces around individual dendritic segments (surface smoothness: 0.2 μm ; quality level: 5). Automatic spot detection algorithms were implemented for synapse detection (expected radius: 0.5 μm ; quality: 2000). VIP colocalization to Gephyrin was quantified via commercial software (Imaris, Bitplane).

MFTs structure was quantified as previously described (Galimberti et al, 2006). cFOS analysis was conducted as previously described (3.2.6).

Number of PV or RFP positive neurons was normalized toward CA3 areas.

PV interneurons somas were isolated and PV intensity was quantified automatically via commercially available softwares (Imaris, bitplane). Therefore, absolute intensities were plotted as a distribution of single neurons in arbitrary units of intensity (Graphpad, prism) and categories were defined based on statistical distributions upon controls. Hence, Low PV presented the lowest 5 percentile of the whole distribution (0-800 arbitrary units of intensity). Categories were then defined based on Low PV: 800-1600: intermediate Low; 1600-2400 intermediate High; > 2400: High).

For high-resolution imaging of LMTs in fixed tissue, we imaged lamellar sections on an upright spinning-disk microscope using an alpha Plan-Apochromat $\times 100/1.45$ oil-immersion objective (Zeiss) and Metamorph 7.7.2 acquisition software (Molecular Devices, Sunnyvale, CA, USA). Voxel size was 0.106 $\mu\text{m} \times 0.106 \mu\text{m} \times 0.2 \mu\text{m}$. For other staining analysis, we processed all samples belonging to the same experimental set in parallel and acquired them with the same settings on an LSM710 confocal microscope (Zeiss) using an EC Plan-Neofluar $\times 40/1.3$ oil-immersion or $\times 63/1.4$ oil immersion objective (Zeiss). We used transverse hippocampal sections or cortical coronal sections for imaging, and later analyzed high-resolution three-dimensional confocal stacks using Imaris 7.0.0 (Bitplane AG) software.

Pharmacology experiments.

Topic chronic treatments

Topic treatment was performed via implantation of cannula guides in the target region, and repeated cannula injections over consecutive days. Mice underwent surgeries as previously

described (Galimberti, Bednarek, Donato and Caroni, 2010). Guides (33G, Bilaney Consultants) were topically implanted so that the cannula would be penetrating at the center of the hippocampus proper (coordinates: see following), and fixed in position via glue and dental cement. Mice were allowed to recover for 1 week prior to the first treatment. The amount of solution injected did not exceed 200 nL.

Drugs topically applied were: BDNF (0.1µg x mL, peprotech), ChABC (0.08 units per injection, Sigma); VIP (1 nM, Tocris) and [Ac-Tyr¹,D-Phe²]-GRF 1-29 (300 nM, Tocris).

Coordinates:

BDNF and ChABC: Bregma: -1.58; Lateral 1.55; Deep 1.4

VIP and [Ac-Tyr¹,D-Phe²]-GRF 1-29: Bregma: -2.7; Lateral: 2.3; Deep 2.0

Acute pharmacological treatments:

Mice were anesthetized and injected as previously described (Galimberti, Bednarek, Donato and Caroni, 2010). ChABC and BDNF were injected in 6 different position in the brain, 3 per hippocampus, bilateral injections. The volume injected never exceeded 200 nL.

Coordinates:

Dorsal Hippocampus: Bregma: -1.58; Lateral 1.65; Deep 1.5

Intermediate Hippocampus: Bregma: -2.06; Lateral 2.3; Deep 1.7

Ventral Hippocampus: Bregma: -2.7; Lateral 3.25; Deep 2.25

In vivo IP and subcutaneous injections:

Adult mice and pups were injected IP upon brief anesthesia induction via isofluorane. Intraperitoneal injection route was chosen for Diazepam (3 mg x Kg, Roche Scientific), ifenprodil hermitrate (20 mg x Kg, Tocris) and APV (1 µM).

Subcutaneous injection of Anisomycin (50 mg x Gk, Applichem) was performed as previously described (Bednarek and Caroni, 2011).

In vitro pharmacology:

The designed drug was added to the culturing medium maintained at 37° C. Drugs were: VIP (1 nM, Tocris), [Ac-Tyr¹,D-Phe²]-GRF 1-29 (300 nM, Tocris), DCG-IV (1 µM, Tocris); LY 341495 (100 nM, Tocris), Diazepam (1 mM)

Behavioral Experiments:

Morris water maze, contextual fear conditioning, dark fear conditioning, rotarod and Environmental enrichment were performed as previously described (4.2.6, Ruediger et al., 2011; Bednarek and Caroni 2011).

Metaplasticity experiments were performed as follows:

NOR upon experience: mice were tested via NOR after having been for 3 weeks in enrichment. For testing conditioned mice, fear conditioning (contextual or dark) was performed on mice on the same day as the acquisition of the NOR, after at least 1.5 hours from exploration.

MWM upon experience: mice were trained at the MWM starting either after 3 weeks of environmental enrichment, or the day after contextual fear conditioning acquisition.

MWM upon chronic pharmacology: VIP, [Ac-Tyr¹,D-Phe²]-GRF 1-29 or saline solutions were applied topically for 2 consecutive days prior to MWM day1, and applied 75 minutes before training on each day on day 1, 2 and 3. Reference memory was assessed on day 4, with no prior pharmacological application.

Slice cultures and optogenetic experiments.

Slice cultures were obtained from P2 or P7 pups as previously described (4.3.6). Heterochronic slice cultures were processed as previously described (4.3.6). For histological analysis, slice cultures were briefly fixed with 4% PFA warmed to 37° C for 15 minutes at room temperature, and then subjected for 3 hours to a blocking solution of PBS, 0.3% triton plus 3% BSA before staining.

Optogenetics experiments were performed onto slice cultures obtained from P7 pups. AAV mediated infection of selected slices was performed on DIV 12 by applying a droplet (1uL) of viral solution on the top of the slice. Light stimulation was performed on DIV 30-35 using an Olympus microscope (Gogolla et al., 2006). Two regimens of optical stimulation have been tested (180 seconds of continuous light, or 180 repetitions of 500 ms light followed by 500 ms darkness), with similar results.

Statistical analysis.

All statistical analyses were performed using GraphPad Prism 6 (GraphPad Softwares, La Jolla, CA, USA). Unless otherwise stated, statistical groups were compared using unpaired, nonparametric student t Test (Mann-Whitney test). Average values in the text are expressed as means \pm S.E.M.

7. Abbreviations

5HT	Serotonin
AAV	Adeno-Associated Virus
Ach	Acetylcholine
Add	Adducin
BDNF	Brain Derived Neurotrophic Factor
BSA	Bovine Serum Albumin
CA	Cornu Ammonis
CB	Calbindin
CCK	Cholocistokinin
cFC	Contextual Fear Conditioning
CR	Calretinin
DG	Dentate gyrus
dH	Dorsal Hippocampus
Dis	Disinhibition
DIV	Day in vitro
EC	Entorhinal Cortex
EE	Environmental Enrichment
FBI	Feedback Inhibition
FFE	Feedforward Excitation
FFI	FeedForward Inhibition
GABA	γ -Amino Butirric Acid
GC	Granule Cell
iH	Intermediate Hippocampus
IN	Interneuron
LEC	Lateral Entorhinal Cortex
LMT	Large Mossy Fiber Terminal
M1	Primary Motor Cortex
MEC	Medial Entorhinal Cortex
MWM	Morris Water Maze
MF	Mossy Fiber
NMDA	N-Methyl-D-Aspartate
NOR	Novel Object Recognition
NPY	Neuro Peptide Y
P	postnatal Day
PC	Pyramidal Cell
PFA	Paraphormaldehyde

PFC	Prefrontal Cortex
PNN	PeriNeuronal Net
PP	Perforant Path
PV	Parvalbumin
RR	Rotarod
SL	Stratum Lucidum
SLM	Stratum Lacunosum-Moleculare
SO	Stratum Oriens
SOM	Somatostatin
SR	Stratum Radiatum
TA	Terminal Arborisation
vH	Ventral Hippocampus
VIP	Vasoactive Intestinal Peptide

8. Bibliography

1. Acsady, L., Arabadzisz, D. & Freund, T. F. Correlated morphological and neurochemical features identify different subsets of vasoactive intestinal polypeptide-immunoreactive interneurons in rat hippocampus. *Neuroscience* **73**, 299-315 (1996).
2. Freund, T. F. & Katona, I. Perisomatic inhibition. *Neuron* **56**, 33-42 (2007).
3. Acsady, L., Arabadzisz, D., Katona, I. & Freund, T. F. Topographic distribution of dorsal and median raphe neurons with hippocampal, septal and dual projection. *Acta Biol Hung* **47**, 9-19 (1996).
4. Acsady, L., Gorcs, T. J. & Freund, T. F. Different populations of vasoactive intestinal polypeptide-immunoreactive interneurons are specialized to control pyramidal cells or interneurons in the hippocampus. *Neuroscience* **73**, 317-334 (1996).
5. Acsady, L., Kamondi, A., Sik, A., Freund, T. & Buzsaki, G. GABAergic cells are the major postsynaptic targets of mossy fibers in the rat hippocampus. *J Neurosci* **18**, 3386-3403 (1998).
6. Altman, J. & Bayer, S. A. Migration and distribution of two populations of hippocampal granule cell precursors during the perinatal and postnatal periods. *J Comp Neurol* **301**, 365-381 (1990).
7. Altman, J. & Bayer, S. A. Prolonged sojourn of developing pyramidal cells in the intermediate zone of the hippocampus and their settling in the stratum pyramidale. *J Comp Neurol* **301**, 343-364 (1990).
8. Altman, J. & Bayer, S. A. Mosaic organization of the hippocampal neuroepithelium and the multiple germinal sources of dentate granule cells. *J Comp Neurol* **301**, 325-342 (1990).
9. Amaral, D. G. & Dent, J. A. Development of the mossy fibers of the dentate gyrus: I. A light and electron microscopic study of the mossy fibers and their expansions. *J Comp Neurol* **195**, 51-86 (1981).
10. Anderson, J. S., Carandini, M. & Ferster, D. Orientation tuning of input conductance, excitation, and inhibition in cat primary visual cortex. *J Neurophysiol* **84**, 909-926 (2000).
11. Ascoli, G. A. et al. Petilla terminology: nomenclature of features of GABAergic interneurons of the cerebral cortex. *Nat Rev Neurosci* **9**, 557-568 (2008).
12. Atallah, B. V. & Scanziani, M. Instantaneous modulation of gamma oscillation frequency by balancing excitation with inhibition. *Neuron* **62**, 566-577 (2009).
13. Balmer, T. S., Carels, V. M., Frisch, J. L. & Nick, T. A. Modulation of perineuronal nets and parvalbumin with developmental song learning. *J Neurosci* **29**, 12878-12885 (2009).
14. Bannerman, D. M. et al. Double dissociation of function within the hippocampus: spatial memory and hyponeophagia. *Behav Neurosci* **116**, 884-901 (2002).
15. Barabasi, A.-L. *Linked* (Perseus, 2002).

16. Barabasi, A.-L. *Bursts: The Hidden Pattern Behind Everything We Do 1st (first) edition* (2010).
17. Barnes, C. A., Suster, M. S., Shen, J. & McNaughton, B. L. Multistability of cognitive maps in the hippocampus of old rats. *Nature* **388**, 272-275 (1997).
18. Bartos, M., Vida, I. & Jonas, P. Synaptic mechanisms of synchronized gamma oscillations in inhibitory interneuron networks. *Nat Rev Neurosci* **8**, 45-56 (2007).
19. Bednarek, E. & Caroni, P. beta-Adducin is required for stable assembly of new synapses and improved memory upon environmental enrichment. *Neuron* **69**, 1132-1146 (2011).
20. Belforte, J. E. et al. Postnatal NMDA receptor ablation in corticolimbic interneurons confers schizophrenia-like phenotypes. *Nat Neurosci* **13**, 76-83 (2010).
21. Bilkey, D. K. & Schwartzkroin, P. A. Variation in electrophysiology and morphology of hippocampal CA3 pyramidal cells. *Brain Res* **514**, 77-83 (1990).
22. BLACKSTAD, T. W. Commissural connections of the hippocampal region in the rat, with special reference to their mode of termination. *J Comp Neurol* **105**, 417-537 (1956).
23. BLACKSTAD, T. W. On the termination of some afferents to the hippocampus and fascia dentata; an experimental study in the rat. *Acta Anat (Basel)* **35**, 202-214 (1958).
24. Bonifazi, P. et al. GABAergic hub neurons orchestrate synchrony in developing hippocampal networks. *Science* **326**, 1419-1424 (2009).
25. Bourne, J. N. & Harris, K. M. Balancing structure and function at hippocampal dendritic spines. *Annu Rev Neurosci* **31**, 47-67 (2008).
26. Burke, S. N. & Barnes, C. A. Neural plasticity in the ageing brain. *Nat Rev Neurosci* **7**, 30-40 (2006).
27. Buzsaki, G. The hippocampo-neocortical dialogue. *Cereb Cortex* **6**, 81-92 (1996).
28. Buzsaki, G. Neural syntax: cell assemblies, synapsembles, and readers. *Neuron* **68**, 362-385 (2010).
29. Buzsaki, G. & Chrobak, J. J. Temporal structure in spatially organized neuronal ensembles: a role for interneuronal networks. *Curr Opin Neurobiol* **5**, 504-510 (1995).
30. Buzsaki, G. & Wang, X. J. Mechanisms of gamma oscillations. *Annu Rev Neurosci* **35**, 203-225 (2012).
31. Buzsaki, G. Rhythms of the Brain. 464 (2006).
32. Cardin, J. A. et al. Driving fast-spiking cells induces gamma rhythm and controls sensory responses. *Nature* **459**, 663-667 (2009).
33. Caroni, P., Donato, F. & Muller, D. Structural plasticity upon learning: regulation and functions. *Nat Rev Neurosci* **13**, 478-490 (2012).

34. Chevaleyre, V. & Siegelbaum, S. A. Strong CA2 pyramidal neuron synapses define a powerful disynaptic cortico-hippocampal loop. *Neuron* **66**, 560-572 (2010).
35. Clement, J. P. et al. Pathogenic SYNGAP1 Mutations Impair Cognitive Development by Disrupting Maturation of Dendritic Spine Synapses. *Cell* **151**, 709-723 (2012).
36. Cobb, S. R., Buhl, E. H., Halasy, K., Paulsen, O. & Somogyi, P. Synchronization of neuronal activity in hippocampus by individual GABAergic interneurons. *Nature* **378**, 75-78 (1995).
37. Connors, B. W. & Gutnick, M. J. Intrinsic firing patterns of diverse neocortical neurons. *Trends Neurosci* **13**, 99-104 (1990).
38. Contreras, D. Electrophysiological classes of neocortical neurons. *Neural Netw* **17**, 633-646 (2004).
39. Cossart, R., Bernard, C. & Ben-Ari, Y. Multiple facets of GABAergic neurons and synapses: multiple fates of GABA signalling in epilepsies. *Trends Neurosci* **28**, 108-115 (2005).
40. Crepel, V. et al. A parturition-associated nonsynaptic coherent activity pattern in the developing hippocampus. *Neuron* **54**, 105-120 (2007).
41. Cunha-Reis, D., Sebastiao, A. M., Wirkner, K., Illes, P. & Ribeiro, J. A. VIP enhances both pre- and postsynaptic GABAergic transmission to hippocampal interneurons leading to increased excitatory synaptic transmission to CA1 pyramidal cells. *Br J Pharmacol* **143**, 733-744 (2004).
42. Czerniawski, J., Ree, F., Chia, C. & Otto, T. Dorsal versus ventral hippocampal contributions to trace and contextual conditioning: differential effects of regionally selective NMDA receptor antagonism on acquisition and expression. *Hippocampus* **22**, 1528-1539 (2012).
43. Danglot, L., Triller, A. & Marty, S. The development of hippocampal interneurons in rodents. *Hippocampus* **16**, 1032-1060 (2006).
44. David, C., Schleicher, A., Zuschratter, W. & Staiger, J. F. The innervation of parvalbumin-containing interneurons by VIP-immunopositive interneurons in the primary somatosensory cortex of the adult rat. *Eur J Neurosci* **25**, 2329-2340 (2007).
45. De Paola, V., Arber, S. & Caroni, P. AMPA receptors regulate dynamic equilibrium of presynaptic terminals in mature hippocampal networks. *Nat Neurosci* **6**, 491-500 (2003).
46. De Paola, V. et al. Cell type-specific structural plasticity of axonal branches and boutons in the adult neocortex. *Neuron* **49**, 861-875 (2006).
47. De Pasquale, R. & Sherman, S. M. Synaptic properties of corticocortical connections between the primary and secondary visual cortical areas in the mouse. *J Neurosci* **31**, 16494-16506 (2011).
48. DeBello, W. M. & Knudsen, E. I. Multiple sites of adaptive plasticity in the owl's auditory

- localization pathway. *J Neurosci* **24**, 6853-6861 (2004).
49. Deguchi, Y., Donato, F., Galimberti, I., Cabuy, E. & Caroni, P. Temporally matched subpopulations of selectively interconnected principal neurons in the hippocampus. *Nat Neurosci* **14**, 495-504 (2011).
 50. Dudek, F. E. & Sutula, T. P. Epileptogenesis in the dentate gyrus: a critical perspective. *Prog Brain Res* **163**, 755-773 (2007).
 51. Eichenbaum, H. The hippocampus and mechanisms of declarative memory. *Behav Brain Res* **103**, 123-133 (1999).
 52. Ewell, L. A. & Jones, M. V. Frequency-tuned distribution of inhibition in the dentate gyrus. *J Neurosci* **30**, 12597-12607 (2010).
 53. Fagiolini, M. et al. Specific GABAA circuits for visual cortical plasticity. *Science* **303**, 1681-1683 (2004).
 54. Fagiolini, M. & Hensch, T. K. Inhibitory threshold for critical-period activation in primary visual cortex. *Nature* **404**, 183-186 (2000).
 55. Fanselow, M. S. Contextual fear, gestalt memories, and the hippocampus. *Behav Brain Res* **110**, 73-81 (2000).
 56. Fazzari, P. et al. Control of cortical GABA circuitry development by Nrg1 and ErbB4 signalling. *Nature* **464**, 1376-1380 (2010).
 57. Fishell, G. Perspectives on the developmental origins of cortical interneuron diversity. *Novartis Found Symp* **288**, 21-35; discussion 35-44, 96-8 (2007).
 58. Fogel, A. I. et al. SynCAMs organize synapses through heterophilic adhesion. *J Neurosci* **27**, 12516-12530 (2007).
 59. Forster, E., Zhao, S. & Frotscher, M. Laminating the hippocampus. *Nat Rev Neurosci* **7**, 259-267 (2006).
 60. Freund, T. F. Interneuron Diversity series: Rhythm and mood in perisomatic inhibition. *Trends Neurosci* **26**, 489-495 (2003).
 61. Freund, T. F. & Buzsaki, G. Interneurons of the hippocampus. *Hippocampus* **6**, 347-470 (1996).
 62. Freund, T. F. & Gulyas, A. I. Inhibitory control of GABAergic interneurons in the hippocampus. *Can J Physiol Pharmacol* **75**, 479-487 (1997).
 63. Gaarskjaer, F. B. The organization and development of the hippocampal mossy fiber system. *Brain Res* **396**, 335-357 (1986).
 64. Galimberti, I., Bednarek, E., Donato, F. & Caroni, P. EphA4 signaling in juveniles establishes topographic specificity of structural plasticity in the hippocampus. *Neuron* **65**, 627-642 (2010).
 65. Galimberti, I. et al. Long-term rearrangements of hippocampal mossy fiber terminal

- connectivity in the adult regulated by experience. *Neuron* **50**, 749-763 (2006).
66. Ge, S., Yang, C. H., Hsu, K. S., Ming, G. L. & Song, H. A critical period for enhanced synaptic plasticity in newly generated neurons of the adult brain. *Neuron* **54**, 559-566 (2007).
 67. Glickfeld, L. L. & Scanziani, M. Distinct timing in the activity of cannabinoid-sensitive and cannabinoid-insensitive basket cells. *Nat Neurosci* **9**, 807-815 (2006).
 68. Gloveli, T. et al. Orthogonal arrangement of rhythm-generating microcircuits in the hippocampus. *Proc Natl Acad Sci U S A* **102**, 13295-13300 (2005).
 69. Gloveli, T. et al. Differential involvement of oriens/pyramidal interneurons in hippocampal network oscillations in vitro. *J Physiol* **562**, 131-147 (2005).
 70. Gogolla, N., Caroni, P., Luthi, A. & Herry, C. Perineuronal nets protect fear memories from erasure. *Science* **325**, 1258-1261 (2009).
 71. Gogolla, N., Galimberti, I. & Caroni, P. Structural plasticity of axon terminals in the adult. *Curr Opin Neurobiol* **17**, 516-524 (2007).
 72. Gogolla, N., Galimberti, I., Deguchi, Y. & Caroni, P. Wnt signaling mediates experience-related regulation of synapse numbers and mossy fiber connectivities in the adult hippocampus. *Neuron* **62**, 510-525 (2009).
 73. Gogolla, N., Galimberti, I., DePaola, V. & Caroni, P. Staining protocol for organotypic hippocampal slice cultures. *Nat Protoc* **1**, 2452-2456 (2006).
 74. Gogolla, N., Galimberti, I., DePaola, V. & Caroni, P. Long-term live imaging of neuronal circuits in organotypic hippocampal slice cultures. *Nat Protoc* **1**, 1223-1226 (2006).
 75. Gogolla, N., Galimberti, I., DePaola, V. & Caroni, P. Preparation of organotypic hippocampal slice cultures for long-term live imaging. *Nat Protoc* **1**, 1165-1171 (2006).
 76. Greene, A. J., Spellman, B. A., Dusek, J. A., Eichenbaum, H. B. & Levy, W. B. Relational learning with and without awareness: transitive inference using nonverbal stimuli in humans. *Mem Cognit* **29**, 893-902 (2001).
 77. Grove, E. A., Tole, S., Limon, J., Yip, L. & Ragsdale, C. W. The hem of the embryonic cerebral cortex is defined by the expression of multiple Wnt genes and is compromised in Gli3-deficient mice. *Development* **125**, 2315-2325 (1998).
 78. Hafting, T., Fyhn, M., Molden, S., Moser, M. B. & Moser, E. I. Microstructure of a spatial map in the entorhinal cortex. *Nature* **436**, 801-806 (2005).
 79. Hajos, N. et al. Cannabinoids inhibit hippocampal GABAergic transmission and network oscillations. *Eur J Neurosci* **12**, 3239-3249 (2000).
 80. HAMLYN, L. H. The fine structure of the mossy fibre endings in the hippocampus of the rabbit. *J Anat* **96**, 112-120 (1962).
 81. Hampson, R. E., Simeral, J. D. & Deadwyler, S. A. Distribution of spatial and nonspatial information in dorsal hippocampus. *Nature* **402**, 610-614 (1999).

82. Hanover, J. L., Huang, Z. J., Tonegawa, S. & Stryker, M. P. Brain-derived neurotrophic factor overexpression induces precocious critical period in mouse visual cortex. *J Neurosci* **19**, RC40 (1999).
83. Harris, K. D., Csicsvari, J., Hirase, H., Dragoi, G. & Buzsaki, G. Organization of cell assemblies in the hippocampus. *Nature* **424**, 552-556 (2003).
84. Hasenstaub, A. et al. Inhibitory postsynaptic potentials carry synchronized frequency information in active cortical networks. *Neuron* **47**, 423-435 (2005).
85. He, S., Ma, J., Liu, N. & Yu, X. Early enriched environment promotes neonatal GABAergic neurotransmission and accelerates synapse maturation. *J Neurosci* **30**, 7910-7916 (2010).
86. Hensch, T. K. Critical period plasticity in local cortical circuits. *Nat Rev Neurosci* **6**, 877-888 (2005).
87. Hensch, T. K. et al. Local GABA circuit control of experience-dependent plasticity in developing visual cortex. *Science* **282**, 1504-1508 (1998).
88. Henze, D. A., Urban, N. N. & Barrionuevo, G. The multifarious hippocampal mossy fiber pathway: a review. *Neuroscience* **98**, 407-427 (2000).
89. Henze, D. A., Wittner, L. & Buzsaki, G. Single granule cells reliably discharge targets in the hippocampal CA3 network in vivo. *Nat Neurosci* **5**, 790-795 (2002).
90. Hofer, S. B., Mrsic-Flogel, T. D., Bonhoeffer, T. & Hubener, M. Experience leaves a lasting structural trace in cortical circuits. *Nature* **457**, 313-317 (2009).
91. Holtmaat, A. & Svoboda, K. Experience-dependent structural synaptic plasticity in the mammalian brain. *Nat Rev Neurosci* **10**, 647-658 (2009).
92. Huang, Z. J. et al. BDNF regulates the maturation of inhibition and the critical period of plasticity in mouse visual cortex. *Cell* **98**, 739-755 (1999).
93. HUBEL, D. H. & WIESEL, T. N. Shape and arrangement of columns in cat's striate cortex. *J Physiol* **165**, 559-568 (1963).
94. HUBEL, D. H. & WIESEL, T. N. RECEPTIVE FIELDS OF CELLS IN STRIATE CORTEX OF VERY YOUNG, VISUALLY INEXPERIENCED KITTENS. *J Neurophysiol* **26**, 994-1002 (1963).
95. Hubener, M. & Bonhoeffer, T. Searching for engrams. *Neuron* **67**, 363-371 (2010).
96. Isaacson, J. S. & Scanziani, M. How inhibition shapes cortical activity. *Neuron* **72**, 231-243 (2011).
97. J.LeDoux. *J.LeDoux's Synaptic Self[Paperback]*(2003) (Penguin (Non-Classics), 2003).
98. Kandel, E., Schwartz, J. & Jessell, T. *Principles of Neural Science* (McGraw-Hill Medical, 2000).

99. Karayannis, T., De Marco Garcia, N. V. & Fishell, G. J. Functional adaptation of cortical interneurons to attenuated activity is subtype-specific. *Front Neural Circuits* **6**, 66 (2012).
100. Katzner, S., Busse, L. & Carandini, M. GABAA inhibition controls response gain in visual cortex. *J Neurosci* **31**, 5931-5941 (2011).
101. Kempermann, G., Kuhn, H. G. & Gage, F. H. More hippocampal neurons in adult mice living in an enriched environment. *Nature* **386**, 493-495 (1997).
102. Kjelstrup, K. G. et al. Reduced fear expression after lesions of the ventral hippocampus. *Proc Natl Acad Sci U S A* **99**, 10825-10830 (2002).
103. Klausberger, T. & Somogyi, P. Neuronal diversity and temporal dynamics: the unity of hippocampal circuit operations. *Science* **321**, 53-57 (2008).
104. Kleinlogel, S. et al. Ultra light-sensitive and fast neuronal activation with the Ca²⁺-permeable channelrhodopsin CatCh. *Nat Neurosci* **14**, 513-518 (2011).
105. Kosaka, T., Katsumaru, H., Hama, K., Wu, J. Y. & Heizmann, C. W. GABAergic neurons containing the Ca²⁺-binding protein parvalbumin in the rat hippocampus and dentate gyrus. *Brain Res* **419**, 119-130 (1987).
106. Kullmann, D. M. Interneuron networks in the hippocampus. *Curr Opin Neurobiol* **21**, 709-716 (2011).
107. Lawrence, J. J., Grinspan, Z. M. & McBain, C. J. Quantal transmission at mossy fibre targets in the CA3 region of the rat hippocampus. *J Physiol* **554**, 175-193 (2004).
108. Lawrence, J. J. & McBain, C. J. Interneuron diversity series: containing the detonation--feedforward inhibition in the CA3 hippocampus. *Trends Neurosci* **26**, 631-640 (2003).
109. Leao, R. N. et al. OLM interneurons differentially modulate CA3 and entorhinal inputs to hippocampal CA1 neurons. *Nat Neurosci* **15**, 1524-1530 (2012).
110. LeDoux, J. *The Emotional Brain: The Mysterious Underpinnings of Emotional Life* (Simon & Schuster, 1998).
111. LeDoux, J. *Synaptic Self: How Our Brains Become Who We Are* (Penguin Books, 2003).
112. Lee, I., Griffin, A. L., Zilli, E. A., Eichenbaum, H. & Hasselmo, M. E. Gradual translocation of spatial correlates of neuronal firing in the hippocampus toward prospective reward locations. *Neuron* **51**, 639-650 (2006).
113. Lee, I. & Kesner, R. P. Differential contributions of dorsal hippocampal subregions to memory acquisition and retrieval in contextual fear-conditioning. *Hippocampus* **14**, 301-310 (2004).
114. Lee, I. & Kesner, R. P. Encoding versus retrieval of spatial memory: double dissociation between the dentate gyrus and the perforant path inputs into CA3 in the dorsal hippocampus. *Hippocampus* **14**, 66-76 (2004).

115. Li, G. & Pleasure, S. J. Morphogenesis of the dentate gyrus: what we are learning from mouse mutants. *Dev Neurosci* **27**, 93-99 (2005).
116. Li, G. & Pleasure, S. J. Genetic regulation of dentate gyrus morphogenesis. *Prog Brain Res* **163**, 143-152 (2007).
117. Liu, B. H. et al. Broad inhibition sharpens orientation selectivity by expanding input dynamic range in mouse simple cells. *Neuron* **71**, 542-554 (2011).
118. Maccaferri, G., Toth, K. & McBain, C. J. Target-specific expression of presynaptic mossy fiber plasticity. *Science* **279**, 1368-1370 (1998).
119. Magloczky, Z. & Freund, T. F. Impaired and repaired inhibitory circuits in the epileptic human hippocampus. *Trends Neurosci* **28**, 334-340 (2005).
120. Mangale, V. S. et al. Lhx2 selector activity specifies cortical identity and suppresses hippocampal organizer fate. *Science* **319**, 304-309 (2008).
121. JG, M. Exploration and exploitation in organizational learning. *organization science* **2**, 71-87 (1991).
122. Marin, O., Anderson, S. A. & Rubenstein, J. L. Origin and molecular specification of striatal interneurons. *J Neurosci* **20**, 6063-6076 (2000).
123. Maya Vetencourt, J. F. et al. The antidepressant fluoxetine restores plasticity in the adult visual cortex. *Science* **320**, 385-388 (2008).
124. McNaughton, B. L., Battaglia, F. P., Jensen, O., Moser, E. I. & Moser, M. B. Path integration and the neural basis of the 'cognitive map'. *Nat Rev Neurosci* **7**, 663-678 (2006).
125. Megias, M., Emri, Z., Freund, T. F. & Gulyas, A. I. Total number and distribution of inhibitory and excitatory synapses on hippocampal CA1 pyramidal cells. *Neuroscience* **102**, 527-540 (2001).
126. Meinecke, D. L. & Peters, A. GABA immunoreactive neurons in rat visual cortex. *J Comp Neurol* **261**, 388-404 (1987).
127. Melzer, S. et al. Long-range-projecting GABAergic neurons modulate inhibition in hippocampus and entorhinal cortex. *Science* **335**, 1506-1510 (2012).
128. Miles, R., Toth, K., Gulyas, A. I., Hajos, N. & Freund, T. F. Differences between somatic and dendritic inhibition in the hippocampus. *Neuron* **16**, 815-823 (1996).
129. Mizuseki, K., Diba, K., Pastalkova, E. & Buzsaki, G. Hippocampal CA1 pyramidal cells form functionally distinct sublayers. *Nat Neurosci* **14**, 1174-1181 (2011).
130. Monier, C., Chavane, F., Baudot, P., Graham, L. J. & Fregnac, Y. Orientation and direction selectivity of synaptic inputs in visual cortical neurons: a diversity of combinations produces spike tuning. *Neuron* **37**, 663-680 (2003).
131. Monory, K. et al. The endocannabinoid system controls key epileptogenic circuits in the hippocampus. *Neuron* **51**, 455-466 (2006).

132. Morris, R. G., Garrud, P., Rawlins, J. N. & O'Keefe, J. Place navigation impaired in rats with hippocampal lesions. *Nature* **297**, 681-683 (1982).
133. Moser, E. I. & Andersen, P. Conserved spatial learning in cooled rats in spite of slowing of dentate field potentials. *J Neurosci* **14**, 4458-4466 (1994).
134. Moser, E. I., Kropff, E. & Moser, M. B. Place cells, grid cells, and the brain's spatial representation system. *Annu Rev Neurosci* **31**, 69-89 (2008).
135. Moser, M. B., Moser, E. I., Forrest, E., Andersen, P. & Morris, R. G. Spatial learning with a minislab in the dorsal hippocampus. *Proc Natl Acad Sci U S A* **92**, 9697-9701 (1995).
136. O'Keefe, J. Place units in the hippocampus of the freely moving rat. *Exp Neurol* **51**, 78-109 (1976).
137. O'Keefe, J. A computational theory of the hippocampal cognitive map. *Prog Brain Res* **83**, 301-312 (1990).
138. O'Keefe, J. & Conway, D. H. Hippocampal place units in the freely moving rat: why they fire where they fire. *Exp Brain Res* **31**, 573-590 (1978).
139. O'Keefe, J. & Dostrovsky, J. The hippocampus as a spatial map. Preliminary evidence from unit activity in the freely-moving rat. *Brain Res* **34**, 171-175 (1971).
140. O'Keefe, J. & Nadel, L. *The Hippocampus as a Cognitive Map* (Oxford University Press, USA, 1978).
141. O'Reilly, R. C. & Rudy, J. W. Computational principles of learning in the neocortex and hippocampus. *Hippocampus* **10**, 389-397 (2000).
142. O'Reilly, R. C. & Rudy, J. W. Conjunctive representations in learning and memory: principles of cortical and hippocampal function. *Psychol Rev* **108**, 311-345 (2001).
143. Ogiwara, I. et al. Nav1.1 localizes to axons of parvalbumin-positive inhibitory interneurons: a circuit basis for epileptic seizures in mice carrying an Scn1a gene mutation. *J Neurosci* **27**, 5903-5914 (2007).
144. Okun, M. & Lampl, I. Instantaneous correlation of excitation and inhibition during ongoing and sensory-evoked activities. *Nat Neurosci* **11**, 535-537 (2008).
145. Papp, E., Leinekugel, X., Henze, D. A., Lee, J. & Buzsaki, G. The apical shaft of CA1 pyramidal cells is under GABAergic interneuronal control. *Neuroscience* **102**, 715-721 (2001).
146. Penttonen, M., Kamondi, A., Acsady, L. & Buzsaki, G. Gamma frequency oscillation in the hippocampus of the rat: intracellular analysis in vivo. *Eur J Neurosci* **10**, 718-728 (1998).
147. Pielage, J., Bulat, V., Zuchero, J. B., Fetter, R. D. & Davis, G. W. Hts/Adducin controls synaptic elaboration and elimination. *Neuron* **69**, 1114-1131 (2011).
148. Pizzorusso, T. et al. Reactivation of ocular dominance plasticity in the adult visual

- cortex. *Science* **298**, 1248-1251 (2002).
149. Pleasure, S. J. et al. Cell migration from the ganglionic eminences is required for the development of hippocampal GABAergic interneurons. *Neuron* **28**, 727-740 (2000).
 150. Poo, C. & Isaacson, J. S. Odor representations in olfactory cortex: "sparse" coding, global inhibition, and oscillations. *Neuron* **62**, 850-861 (2009).
 151. Porter, J. T. et al. Selective excitation of subtypes of neocortical interneurons by nicotinic receptors. *J Neurosci* **19**, 5228-5235 (1999).
 152. Pothuizen, H. H., Zhang, W. N., Jongen-Relo, A. L., Feldon, J. & Yee, B. K. Dissociation of function between the dorsal and the ventral hippocampus in spatial learning abilities of the rat: a within-subject, within-task comparison of reference and working spatial memory. *Eur J Neurosci* **19**, 705-712 (2004).
 153. Pouille, F., Marin-Burgin, A., Adesnik, H., Atallah, B. V. & Scanziani, M. Input normalization by global feedforward inhibition expands cortical dynamic range. *Nat Neurosci* **12**, 1577-1585 (2009).
 154. Quilichini, P., Sirota, A. & Buzsaki, G. Intrinsic circuit organization and theta-gamma oscillation dynamics in the entorhinal cortex of the rat. *J Neurosci* **30**, 11128-11142 (2010).
 155. Roberts, T. F., Tschida, K. A., Klein, M. E. & Mooney, R. Rapid spine stabilization and synaptic enhancement at the onset of behavioural learning. *Nature* **463**, 948-952 (2010).
 156. Rollenhagen, A. et al. Structural determinants of transmission at large hippocampal mossy fiber synapses. *J Neurosci* **27**, 10434-10444 (2007).
 157. Rosenbaum, R. S. et al. Remote spatial memory in an amnesic person with extensive bilateral hippocampal lesions. *Nat Neurosci* **3**, 1044-1048 (2000).
 158. Royer, S., Sirota, A., Patel, J. & Buzsaki, G. Distinct representations and theta dynamics in dorsal and ventral hippocampus. *J Neurosci* **30**, 1777-1787 (2010).
 159. Rudy, J. W. & O'Reilly, R. C. Conjunctive representations, the hippocampus, and contextual fear conditioning. *Cogn Affect Behav Neurosci* **1**, 66-82 (2001).
 160. Ruediger, S., Spirig, D., Donato, F. & Caroni, P. Goal-oriented searching mediated by ventral hippocampus early in trial-and-error learning. *Nat Neurosci* **15**, 1563-1571 (2012).
 161. Ruediger, S. et al. Learning-related feedforward inhibitory connectivity growth required for memory precision. *Nature* **473**, 514-518 (2011).
 162. Sargolini, F. et al. Conjunctive representation of position, direction, and velocity in entorhinal cortex. *Science* **312**, 758-762 (2006).
 163. Saxena, S., Cabuy, E. & Caroni, P. A role for motoneuron subtype-selective ER stress in disease manifestations of FALS mice. *Nat Neurosci* **12**, 627-636 (2009).

164. Saxena, S. & Caroni, P. Selective neuronal vulnerability in neurodegenerative diseases: from stressor thresholds to degeneration. *Neuron* **71**, 35-48 (2011).
165. Shadlen, M. N. & Newsome, W. T. The variable discharge of cortical neurons: implications for connectivity, computation, and information coding. *J Neurosci* **18**, 3870-3896 (1998).
166. Shatz, C. J. & Stryker, M. P. Ocular dominance in layer IV of the cat's visual cortex and the effects of monocular deprivation. *J Physiol* **281**, 267-283 (1978).
167. Smith, D. M. & Mizumori, S. J. Hippocampal place cells, context, and episodic memory. *Hippocampus* **16**, 716-729 (2006).
168. Smith, D. M. & Mizumori, S. J. Learning-related development of context-specific neuronal responses to places and events: the hippocampal role in context processing. *J Neurosci* **26**, 3154-3163 (2006).
169. Sohal, V. S., Zhang, F., Yizhar, O. & Deisseroth, K. Parvalbumin neurons and gamma rhythms enhance cortical circuit performance. *Nature* **459**, 698-702 (2009).
170. Solstad, T., Boccara, C. N., Kropff, E., Moser, M. B. & Moser, E. I. Representation of geometric borders in the entorhinal cortex. *Science* **322**, 1865-1868 (2008).
171. Southwell, D. G., Froemke, R. C., Alvarez-Buylla, A., Stryker, M. P. & Gandhi, S. P. Cortical plasticity induced by inhibitory neuron transplantation. *Science* **327**, 1145-1148 (2010).
172. Squire, L. R. Memory systems of the brain: a brief history and current perspective. *Neurobiol Learn Mem* **82**, 171-177 (2004).
173. Sugiyama, S. et al. Experience-dependent transfer of Otx2 homeoprotein into the visual cortex activates postnatal plasticity. *Cell* **134**, 508-520 (2008).
174. Sutula, T. P. & Dudek, F. E. Unmasking recurrent excitation generated by mossy fiber sprouting in the epileptic dentate gyrus: an emergent property of a complex system. *Prog Brain Res* **163**, 541-563 (2007).
175. Swadlow, H. A. Fast-spike interneurons and feedforward inhibition in awake sensory neocortex. *Cereb Cortex* **13**, 25-32 (2003).
176. Szabadics, J. & Soltesz, I. Functional specificity of mossy fiber innervation of GABAergic cells in the hippocampus. *J Neurosci* **29**, 4239-4251 (2009).
177. Tan, A. Y., Zhang, L. I., Merzenich, M. M. & Schreiner, C. E. Tone-evoked excitatory and inhibitory synaptic conductances of primary auditory cortex neurons. *J Neurophysiol* **92**, 630-643 (2004).
178. Tian, N. et al. The role of the synthetic enzyme GAD65 in the control of neuronal gamma-aminobutyric acid release. *Proc Natl Acad Sci U S A* **96**, 12911-12916 (1999).
179. Tole, S., Christian, C. & Grove, E. A. Early specification and autonomous development of cortical fields in the mouse hippocampus. *Development* **124**, 4959-4970 (1997).

180. Traub, R. D., Bibbig, A., LeBeau, F. E., Buhl, E. H. & Whittington, M. A. Cellular mechanisms of neuronal population oscillations in the hippocampus in vitro. *Annu Rev Neurosci* **27**, 247-278 (2004).
181. Traub, R. D. et al. Single-column thalamocortical network model exhibiting gamma oscillations, sleep spindles, and epileptogenic bursts. *J Neurophysiol* **93**, 2194-2232 (2005).
182. Traub, R. D., Whittington, M. A., Colling, S. B., Buzsaki, G. & Jefferys, J. G. Analysis of gamma rhythms in the rat hippocampus in vitro and in vivo. *J Physiol* **493**, 471-484 (1996).
183. Traub, R. D., Whittington, M. A., Stanford, I. M. & Jefferys, J. G. A mechanism for generation of long-range synchronous fast oscillations in the cortex. *Nature* **383**, 621-624 (1996).
184. Tulving, E. Episodic memory: from mind to brain. *Annu Rev Psychol* **53**, 1-25 (2002).
185. Turrigiano, G. Too many cooks? Intrinsic and synaptic homeostatic mechanisms in cortical circuit refinement. *Annu Rev Neurosci* **34**, 89-103 (2011).
186. Turrigiano, G. Homeostatic synaptic plasticity: local and global mechanisms for stabilizing neuronal function. *Cold Spring Harb Perspect Biol* **4**, a005736 (2012).
187. Volman, V., Behrens, M. M. & Sejnowski, T. J. Downregulation of parvalbumin at cortical GABA synapses reduces network gamma oscillatory activity. *J Neurosci* **31**, 18137-18148 (2011).
188. Vorhees, C. V. & Williams, M. T. Morris water maze: procedures for assessing spatial and related forms of learning and memory. *Nat Protoc* **1**, 848-858 (2006).
189. Wang, X. J. & Buzsaki, G. Gamma oscillation by synaptic inhibition in a hippocampal interneuronal network model. *J Neurosci* **16**, 6402-6413 (1996).
190. Wehr, M. & Zador, A. M. Balanced inhibition underlies tuning and sharpens spike timing in auditory cortex. *Nature* **426**, 442-446 (2003).
191. West, A. E. et al. Calcium regulation of neuronal gene expression. *Proc Natl Acad Sci U S A* **98**, 11024-11031 (2001).
192. Wichterle, H., Turnbull, D. H., Nery, S., Fishell, G. & Alvarez-Buylla, A. In utero fate mapping reveals distinct migratory pathways and fates of neurons born in the mammalian basal forebrain. *Development* **128**, 3759-3771 (2001).
193. WIESEL, T. N. & HUBEL, D. H. SINGLE-CELL RESPONSES IN STRIATE CORTEX OF KITTENS DEPRIVED OF VISION IN ONE EYE. *J Neurophysiol* **26**, 1003-1017 (1963).
194. WIESEL, T. N. & HUBEL, D. H. EFFECTS OF VISUAL DEPRIVATION ON MORPHOLOGY AND PHYSIOLOGY OF CELLS IN THE CATS LATERAL GENICULATE BODY. *J Neurophysiol* **26**, 978-993 (1963).

195. Wilent, W. B. & Contreras, D. Dynamics of excitation and inhibition underlying stimulus selectivity in rat somatosensory cortex. *Nat Neurosci* **8**, 1364-1370 (2005).
196. Wood, E. R., Dudchenko, P. A., Robitsek, R. J. & Eichenbaum, H. Hippocampal neurons encode information about different types of memory episodes occurring in the same location. *Neuron* **27**, 623-633 (2000).
197. Wu, G. K., Arbuckle, R., Liu, B. H., Tao, H. W. & Zhang, L. I. Lateral sharpening of cortical frequency tuning by approximately balanced inhibition. *Neuron* **58**, 132-143 (2008).
198. Yang, G., Pan, F. & Gan, W. B. Stably maintained dendritic spines are associated with lifelong memories. *Nature* **462**, 920-924 (2009).
199. Yang, K. et al. Vasoactive intestinal peptide acts via multiple signal pathways to regulate hippocampal NMDA receptors and synaptic transmission. *Hippocampus* **19**, 779-789 (2009).
200. Zhang, L. I., Tan, A. Y., Schreiner, C. E. & Merzenich, M. M. Topography and synaptic shaping of direction selectivity in primary auditory cortex. *Nature* **424**, 201-205 (2003).

9. Acknowledgements

First, I would like to thank Dr Pico Caroni, who has mentored and allowed me to work in his lab for my PhD thesis. His passion and enthusiasm (for science and else) have supported every one of my projects, experiments and crazy ideas throughout these years, and taught me what being a great scientist should be about. Grazie mille Pico!!!

A special thank you goes to Dr. Silvia Arber, whose suggestions, reagents and heads up about interesting literature came as a big help in many (...many!) occasions; Dr. Botond Roska, who has been always helpful for any experiment or discussion to improve the quality of my research, or challenge interesting observations; to Dr. Filippo Rijli, whose prospective on development was shared in front of many cups of coffee. Grazie!

I would also like to thank Ivan, whose friendship started in front of a slice culture in a cold, dark room, and continues strong today: grazie capo!!

Mike and Yuichi deserve a special mention: apart from humorless jokes, their backing was great, continuous and essential. And, of course, they are awesome.

As my fellows in this journey, I would like to thank Sarah, Claudia, Ewa, Dominique, Smita, Francesco, Smitha, Fernando, Melissa, Maria, Arghya, Anna and in general all the members of the Caroni lab for their useful comments and support.

I probably wouldn't have gone through this if my family were not so supportive. They backed my every decision, no matter what sacrifice was implicated, and helped me throughout. Grazie!!!

And, last but not least, my wife, Maria Grazia. She has been there for every success and every failure; every experiment or long hour at the microscope; and much of what is in these pages would not have been possible without her. I will never thank you enough for being who you are. T.A.T!!!